TAL TECH

DOCTORAL THESIS

Hygrothermal Performance of Masonry Walls Retrofitted with Interior Insulation in Cold Climate

Paul Klõšeiko

Hygrothermal Performance of Masonry Walls Retrofitted with Interior Insulation in Cold Climate

PAUL KLÕŠEIKO

TAL TECH PRESS

TALLINN UNIVERSITY OF TECHNOLOGY
School of Engineering
Department of Civil Engineering and Architecture
This dissertation was accepted for the defence of the degree 05/07/2022

Supervisor: Prof. Targo Kalamees
                         School of Engineering
                         Tallinn University of Technology
                         Tallinn, Estonia

Opponents: Prof Carsten Rode
                         Department of Civil and Mechanical Engineering
                         Technical University of Denmark
                         Kongens Lyngby, Denmark

                         Prof Jan Tywoniak
                         Department of Architectural Engineering
                         Faculty of Civil Engineering
                         Czech Technical University in Prague
                         Praha, Czechia

Defence of the thesis: 09/08/2022, Tallinn

Declaration:
Hereby I declare that this doctoral thesis, my original investigation and achievement, submitted for the doctoral degree at Tallinn University of Technology has not been submitted for doctoral or equivalent academic degree.

Paul Klõšeiko

                                    ----
                                                            signature

European Union
European Regional
Development Fund

Investing
in your future

Kiviseinte seespoolse lisasoojustuse soojus- ja niiskustehniline toimivus külmas kliimas

PAUL KLÕŠEIKO

Contents

List of publications

The list of author's publications, based on which the thesis has been prepared:

I   **Klõšeiko, P**.; Arumägi, E.; Kalamees, T. (2015). Hygrothermal performance of internally insulated brick wall in cold climate: A case study in a historical school building. Journal of Building Physics, 38 (5), 444–464.10.1177/1744259114532609.

II   **Klõšeiko, P.**; Kalamees, T. (2016). Case Study: In-situ Testing and Model Calibration of Interior Insulation Solution for an Office Building in Cold Climate. CESB 2016 - Central Europe Towards Sustainable Building 2016: Innovations for Sustainable Future; Prague; Czech Republic; 22 June 2016 through 24 June 2016. Prague: Czech Technical University in Prague, 159–166.

III   **Klõšeiko, P.**; Kalamees, T. (2018). Long term measurements and HAM modelling of an interior insulation solution for an office building in cold climate. 7th International Building Physics Conference (IBPC2018); Syracuse, NY, USA; September 23-23 2018. Syracuse CoE, 1423–1428.10.14305/ibpc.2018.ps23.

IV   **Klõšeiko, P.**; Varda, K.; Kalamees, T. (2017). Effect of freezing and thawing on the performance of "capillary active" insulation systems: a comparison of results from climate chamber study to HAM modelling. Energy Procedia, 132: 11th Nordic Symposium on Building Physics, NSB2017, 11-14 June 2017, Trondheim, Norway. Ed. Geving, S.; Time, B. Elsevier, 525–530.10.1016/j.egypro.2017.09.714.

V   **Klõšeiko, P.**; Freudenberg, P. (2019). Generative reverse-modelling approach to hygrothermal material characterization. MATEC Web of Conferences, 282: 4th Central European Symposium on Building Physics (CESBP 2019), Prague, Czech Republic, September 2-5, 2019. Ed. Černý, R.; Kočí, V.; Kočí, J. EDP Sciences. 10.1051/matecconf/201928202088.

VI   **Klõšeiko, P.**; Kalamees, T. (2021). Hygrothermal performance of a brick wall with interior insulation in cold climate: vapour open vs vapour tight approach. Journal of Building Physics.10.1177/17442591211056067.

Author's contribution to the publications

Contributions to the papers in this thesis are:

I	**Paul Klõšeiko**	installation of the measurement devices, data collection and analysis, modelling, writing of the paper
	Endrik Arumägi	concept of the study, installation of the measurement devices, data collection, writing of the paper
	Targo Kalamees	concept of the study, writing of the paper, editing, acquisition of funding
II	**Paul Klõšeiko**	concept of the study, installation of the measurement devices, data collection and analysis, modelling, writing of the paper
	Targo Kalamees	concept of the study, material sampling, editing, acquisition of funding
III	**Paul Klõšeiko**	concept of the study, installation of the measurement devices, data collection and analysis, modelling, writing of the paper
	Targo Kalamees	concept of the study, editing, acquisition of funding
IV	**Paul Klõšeiko**	concept of the study, construction of the test setup, data collection and analysis, modelling, writing of the paper
	Kadi Varda	concept of the study, modelling, construction of the test setup, data collection
	Targo Kalamees	concept of the study, editing, acquisition of funding
V	**Paul Klõšeiko**	concept of the study, co-author of the characterization tool, modelling, analysis, writing of the paper
	Peggy Freudenberg	main development of the optimization tool
VI	**Paul Klõšeiko**	concept of the study, scripting, modelling, analysis, writing of the paper
	Targo Kalamees	editing, acquisition of funding

Introduction

Background

Energy performance requirements, better understanding of moisture safety and higher demands by users have created the need to find solutions to upgrade the envelope of heritage brick buildings. If the façade is valuable, the hygrothermally safer exterior insulation is not an acceptable solution (Figure 1). At the same time, traditional interior insulation solutions using mineral wool with or without vapour barrier are risky due to possible mould hazard and moisture accumulation caused by wind driven rain (Häupl et al., 2005; Møller and Hansen, 2013). The latter can lead to deterioration of the façade and structural problems in wooden beam ends which are supported by the wall.

Figure 1   Exterior insulation is the most appropriate solution to reduce heat losses through walls for most of the buildings built during the second half of the 20th century (left). However, it cannot be used if the facades are valuable (right) and one of the alternatives is the hygrothermally risky interior insulation. Source of photo on the right: Wikimedia commons user "Iifar", CC BY-SA 3.0 EE.

During the last 15 years, the so-called "capillary active" insulation systems have been used in Central Europe to mitigate the aforementioned risks. However, as part of the functioning principle of these systems is to tolerate higher moisture content than usual, their performance in colder climate cannot yet be warranted – frost damage risk and effects of moisture loads can be a lot more pronounced there. As the effects of interior insulation can take a long time to manifest themselves, it would be much more efficient to use hygrothermal modelling to predict the performance of different solutions compared to measurements only. On the other hand, relying solely on modelling, can result in underestimation of risks due to some aspects not considered by the user and/or model. By combining both measurements and modelling to mitigate such issues, this thesis aims to study the suitability of vapour open "capillary active" interior insulation solutions to Estonian climate and compare them to the vapour tight approach that has been used thus far.

Research questions and methods

The main research questions of the thesis are:

RQ1   Is heat, air and moisture (HAM) modelling reliable enough to assess the hygrothermal performance of interior insulation in cold climate and high humidity loads?

RQ2   Is the capillary condensation redistribution (CCR) test relevant to material characterization when modelling "capillary active" interior insulation solutions?

RQ3   Are capillary active insulation systems frost sensitive? If yes, what could the suitable performance criterion be?

RQ4   Which interior insulation approaches function properly in Estonian climate and buildings?

The methods to answer these questions are:

- field studies – on-site hygrothermal measurements;
- laboratory studies – freeze-thaw cycling, hygrothermal and tensile strength measurements, measurement of basic material properties;
- hygrothermal modelling – comparisons to measurements; parametric modelling with long term climate dataset for suitability assessment.

The thesis is based on peer-reviewed journal articles and conference papers. **Publication I-III** involved in-situ measurements of different insulation solutions in real buildings. **Publication IV** used a study in a climate chamber to investigate the performance limits of the capillary active insulation systems by subjecting them to freeze-thaw cycles at different moisture content levels.

In **publications I-VI** the measurements are compared to hygrothermal modelling results. As moisture content levels were significantly underestimated when modelling insulation systems near their performance limits during non-isothermal wetting, the method for optimizing the liquid and vapour conductivity curves of the insulation materials based on the CCR test is proposed in **publication V**.

Publication VI presents and employs the improved liquid and vapour conductivity curves for 2 insulation materials (generated using the tool proposed in **publication V**) in parametric modelling with long-term weather data to identify the effect of different insulation solutions and other parameters (bricks, indoor and outdoor humidity loads, etc.) and recommends the approaches that are on the safer side.
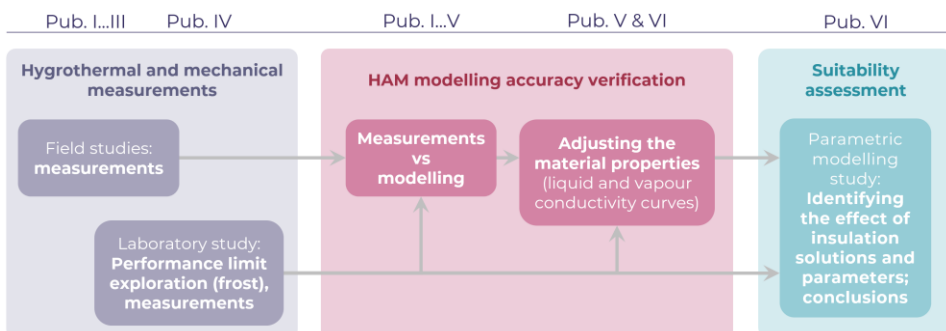

Figure 2   Main structure of the thesis.

Limitations

- The hygrothermal modelling presented in publication VI uses the outdoor climate data from 1970–2019 from Tartu. Future climate and its impact are not considered in this thesis.
- Wooden beam ends or other 2D/3D details have not yet been studied.
- Cost, energy efficiency, ecological footprint, VOC emissions and reaction to fire were not analysed in this work – the focus was on determining the hygrothermal impact of the interior insulation.
- The performance limits of the wall enclosures depend highly on the specific materials. For example, different bricks have different frost resistances. This is still an actively evolving topic with research results suggesting that frost damage is dependent on the degree of moisture saturation and frost temperature (Feng et al., 2019). Furthermore, attempts to derive such data from basic material properties has so far failed. Beside frost resistance, the unknowns also include mould growth inside the structure, exact hygrothermal properties of building materials, etc. Conservative conclusions based on the available data are therefore drawn in this thesis.

Novelty and practical application

New knowledge gained from this research includes:
- Comparisons between **modelling and measurements showed significant underestimation of moisture content levels of "capillary active" insulation materials** in overhygroscopic moisture range when subjected to non-isothermal wetting through vapour diffusion. Relative humidity in hygroscopic range was underestimated during wetting and overestimated during drying periods (hinting at unaccounted for hysteretic effects).
- Modelling with "conventionally" characterized material properties can lead to overly optimistic assumptions of the hygrothermal performance of the "capillary active" interior insulation systems. The results showed that **it makes sense to include the capillary condensation redistribution (CCR) test in material characterization procedures** (publications IV, VI).
- **Insight into frost resistance of the interior insulation systems** (publication IV): autoclaved aerated concrete (AAC), which was presumed to be frost resistant, showed a reduction of its tensile strength after freeze-thaw cycling. Expanded perlite showed a similar performance as AAC, while no statistically significant loss of strength was detected in unsaturated calcium silicate (CaSi) test wall. Frost caused damage in water-saturated CaSi.
- Parametric modelling campaign using a 49-year Estonian climate data and mass brick masonry walls showed the following:
  - CCR-optimized CaSi and AAC exhibited an increased frost risk in the cold side of insulation, interior plaster and glue layer compared to the "conventionally" characterized materials (i.e. those not taking the CCR test into account);
  - frost in the insulation layer can be an issue for both AAC and CaSi insulation systems in certain cases;
  - the exterior layer of masonry must tolerate higher ice saturation levels and freeze-thaw cycles regardless of the insulation type;

- old interior plaster should be removed before applying interior insulation;
- mould indexes behind the insulation were high – emphasis should be put on achieving airtight installation of both vapour tight and vapour open "capillary active" insulation systems to avoid convection behind the insulation and possible contamination of indoor air;
- while the chances of success are good when using interior insulation, a case-by-case approach is necessary to avoid critical combinations.

The applications of the results include:

- **Frost resistance performance criteria** are suggested for AAC, perlite and CaSi insulation systems (maximum ice saturation degree at -15 to -10 °C). They can be **used to assess both HAM modelling and measurement results** (publications IV, VI).
- **AAC and CaSi material data** that take capillary condensation redistribution test into account are created – a **more reliable modelling of those materials** when applied as interior insulation is now possible (publication VI). This is important as material data characterized without the CCR test (as usually found in HAM software databases) results in underestimated moisture content levels especially near performance limits of the insulation systems.
- **The tool to derive the liquid and vapour conductivity functions** through generative inverse modelling (publication V). It can be used for material characterization for hygrothermal modelling while incorporating results from experiments such as CCR, drying, cup tests, water uptake, etc.
- **The decision trees** given in the supplementary material of publication VI can be used to **assess the suitability of interior insulation solutions** and combinations of indoor moisture loads and original brick types.
- **Measurement results** were collected from 3 field studies and 1 laboratory study – in total incorporating 3 wall types and 6 different insulation systems. They can be used as **reference datasets for hygrothermal model validation/calibration** (publications I–III, IV).

Abbreviations

AAC	Autoclaved aerated concrete
avg.	Average
CaSi	Calcium silicate
CCR	Capillary condensation redistribution (test)
CMU	Concrete masonry unit
ET	(Epasit) Epatherm, an insulation system based on a calcium silicate board
EU	European Union
F/T cycle or FTC	Freeze-thaw cycle
HAM	Heat, air and moisture (modelling)
IBK	Institut für Bauklimatik (Technische Universität Dresden)
IBP	(Fraunhofer) Institute for Building Physics
iQ-T	(Remmers) iQ-Therm, an insulation system combining a PUR board with capillary active channels
MC	Moisture content
MP	(Ytong) Multipor, autoclaved aerated concrete insulation board
MRC	Moisture retention curve
MRY	Moisture reference year
MW	Mineral wool
PE	Polyethylene
PIR	Polyisocyanurate
PUR	Polyurethane
RH	Relative humidity
th.	thermal
TT	(Knauf) TecTem, an insulation system based on an expanded perlite board
WDR	Wind-driven rain
WTA	Wissenschaftlich-Technische Arbeitsgemeinschaft für Bauwerkserhaltung und Denkmalpflege / International Association for Science and Technology of Building Maintenance and Monuments Preservation
WWII	The Second World War

Symbols

A_w	Water absorption coefficient, kg/(m²·s$^{0.5}$)
C_{mat}	Relative mould decline coefficient (used in Finnish mould model), -
d	Dimension, mm
D_a	Water vapour diffusivity in still air, m²/s
f_{Rsi}	Temperature factor, -
g	Moisture mass flux, kg/(m²·s)
h_v	Specific enthalpy of water vapor, J/kg
K_g	Gas permeability, s (= kg/(m·s·Pa))
K_l	Liquid water conductivity, s (= kg/(m·s·Pa))
K_v	Water vapour conductivity, s (= kg/(m·s·Pa))
M	Mould index (according to Finnish mould model), -
p_C	Capillary pressure, Pa
p_g	Gas pressure, Pa
p_l	Pressure in liquid phase, Pa
p_v	Water vapour partial pressure, Pa
q	Heat flux, W/m²
R	Thermal resistance, m²·K/W
R_a	Gas constant of air, J/(kg·K)
RH	Relative humidity, %RH
RH_{crit}	Critical relative humidity which should not be exceeded, %RH
R_{if}	Interface resistance, m/s
R_v	Gas constant of water vapour, J/(kg·K)
s	Saturation degree (water or ice volume divided by pore volume), %sat
s_d	Relative water vapour diffusion resistance of a layer (equivalent air layer thickness), m
T	Temperature, K
t	Temperature, °C
U	Thermal transmittance, W/(m²·K)
u_g	Specific internal energy of gas phase, J/kg
u_l	Specific internal energy of liquid phase, J/kg
w	Moisture content, kg/m³
W	Wall factor (used in ISO 15927-3:2009), -
μ	Water vapour diffusion resistance factor, -
Δv	Moisture excess (difference between indoor and outdoor air moisture content), g/m³
λ	Thermal conductivity, W/(m·K)
ρ	Density, kg/m³
ψ	Moisture content by volume, m³/m³

1 Background

1.1 Existing wall structures

While a large share of buildings built before 1950s in Estonia had wooden structure, masonry structures were considered more desirable due to being fire resistant and more "exclusive". Due to higher price, masonry was used for more prominent buildings and today most of them are under heritage protection in one form or another.

In the early 20th century, it was acknowledged that mass-masonry walls had too high thermal transmittance and would also be moist and cause an undesirable indoor climate (Veski, 1935). To overcome that, an air cavity would be added, however, it would be located near the interior surface (see Figure 3 walls 13, 17–18). From today's viewpoint, the exterior cavity is more desirable – the majority of the wall would be protected from driving rain and wooden beam ends lie in drier conditions.

During the era of the first independence period of the Republic of Estonia (1918–1940), the multi-layered walls (see Figure 3 walls 9–11) were promoted as more economically efficient and hygienic than mass masonry walls. 2 cavities were recommended, as the inner one was to be filled with insulation such as peat, flax or saw dust mixed with lime (Grauen, 1935).

Concrete masonry units (CMU) were also a novel technology at that time and products with different shapes and properties appeared (see Figure 3 walls 11, 12, 15, 16, 20). CMU-s with cavities filled with peat were advertised as simpler and cheaper alternative to multi-layered walls made of solid bricks (Tiltsen, 1932).

The wall with an exterior cavity became one of the main masonry structures during the Soviet occupation (1944–1991) – see Figure 4. The introduction of mass-produced standardized apartment houses (Khrushchyovkas) in 1955 marked a sudden drop in the aesthetic quality of new residential buildings. In the latter case, those facades are not mainly considered preservation-worthy (Mändel, 2019) and therefore the use of exterior insulation should be preferred. A decade later, the concrete large panel construction method started to dominate and masonry was again reserved for the more prominent "special" buildings.

In conclusion, for every wall type and construction, there are buildings for which the interior insulation can be the only choice. However, the issue is most pressing for mass masonry structures – thermal transmittance is highest, surface temperatures lowest and wind driven rain flux is not interrupted by a cavity.
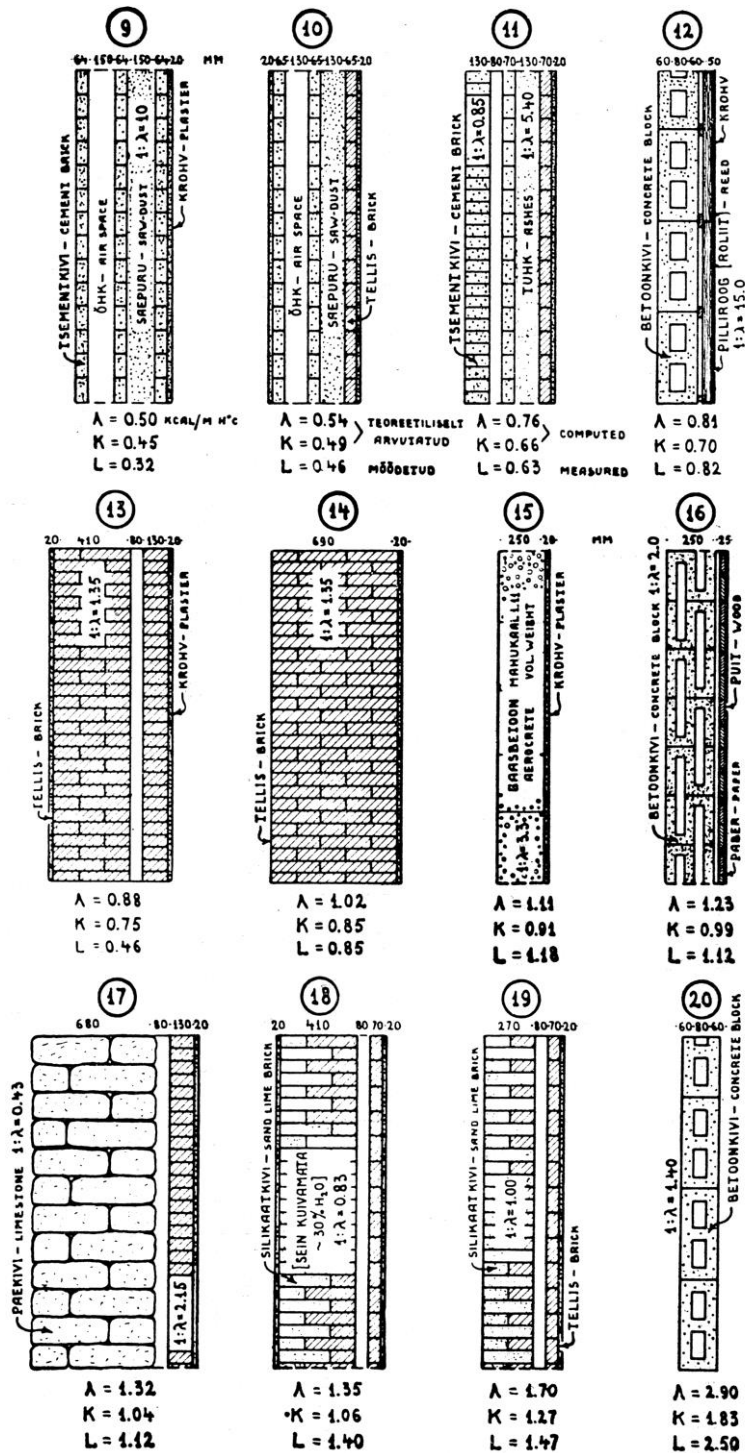
Figure 3   Some masonry structures used in Estonia during pre-WWII era along with calculated (Λ − including surf. resistances; K − w/o surf. resistances) and measured (L− w/o surf. resistances) thermal transmittances (note: right side is interior surface; units: 1 kcal/(m²·h·°C) = 1.163 W/(m²·K)). Reproduced from Jürgenson (1938).
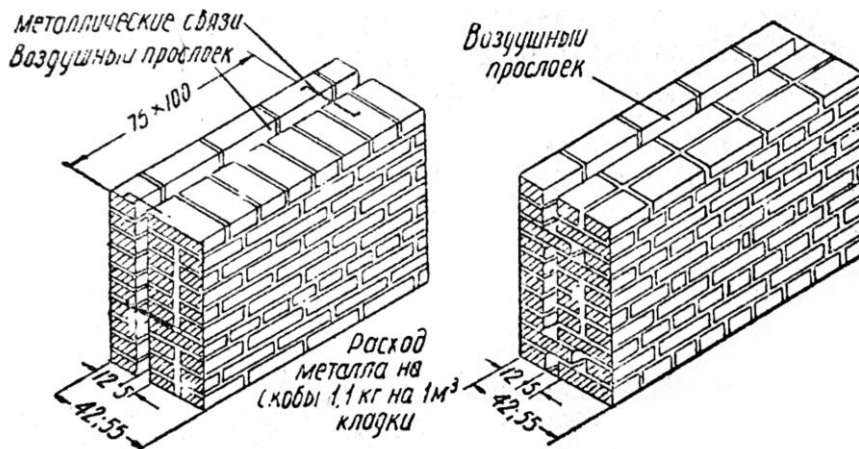
Figure 4   *The Soviet occupation (1944…1991) introduced the 1.5-brick cavity wall as one of the main masonry wall types. Metal wire (left) or bricks (right) were used to tie the leaves together, the cavity could be, but is not always insulated with mineral wool which is covered with bitumen sheet for rain protection. Reproduced from Казачек and Роговин (1953).*

1.2 Main interior insulation approaches

The issues with dampness, mould and low thermal comfort in existing mass masonry in Estonia were recognized back in the 1930s and recommendations to overcome them included:

- to prevent **rising damp**: drainage, slopes on ground, waterproofing of foundation walls (Veski, 1935);
- to prevent **rainwater penetration**: plastering and hydrophobization of the exterior surfaces (Veski, 1935). Jürgenson (1942) claimed that the main means for the rain to wet the masonry are cracks, not necessarily the capillary flow in bricks and recommended repointing the mortar joints;
- to prevent **condensation on interior surfaces**: proper ventilation of the rooms and sufficient insulation of the walls were deemed necessary (Grauen, 1937; Jürgenson, 1942);
- **wooden beam ends** were recommended to be separated from the wall with an air cavity (on the tip and on the sides) to prevent rot (Jürgenson, 1942; Vendach, 1929).

On one hand, Jürgenson (1942) did dew point calculations akin to the later well-known method by Glaser (1958, 1959), which showed condensation in multi-layered brick walls and emphasized that the proper location for vapour tight layers is near the interior surface. On the other hand, he recommended interior insulation of brick walls with vapour-open reed and lime-wood strand boards (which, according to dew point calculations, should cause interstitial condensation).

During the intervening 70 years, the technology and understanding of interior insulation has developed, and today, the main approaches can be split into three (see also Figure 6, where their presumed performance is compared):

- The "traditional" **vapour-tight approach**: reducing the water vapour flux into the wall using vapour barriers or insulation materials with high vapour diffusion resistance.

E.g.: mineral wool insulation with vapour barrier, polyisocyanurate (PIR) insulation boards, foam glass boards, spray foam insulation, etc.

- **Vapour open "capillary active" approach**: the pore structure of the insulation material has fine capillaries, which allows the excess moisture at wall-insulation interface to be redistributed toward the interior surface (see Figure 5). Due to its vapour open nature, wind driven rain can allegedly also dry towards the inside reducing the moisture content of the wall compared to the vapour tight approach.
  E.g.: calcium silicate (CaSi) boards, autoclaved aerated concrete (AAC) boards, wood fiberboards, expanded perlite boards, etc.

- **Hydrophobisation combined with either of the previous approaches.** The approach is based on impregnating and/or coating the exterior surface of the wall to reduce the water uptake while aiming to preserve vapour conductivity. However, the material properties are one of the major unknowns – there are a multitude of producers and products, while the effect of hydrophobization is also dependent on the substrate material (i.e. original masonry) and might degrade over time (Hansen et al., 2018). This is a subject of research on its own is thus not covered in this thesis.
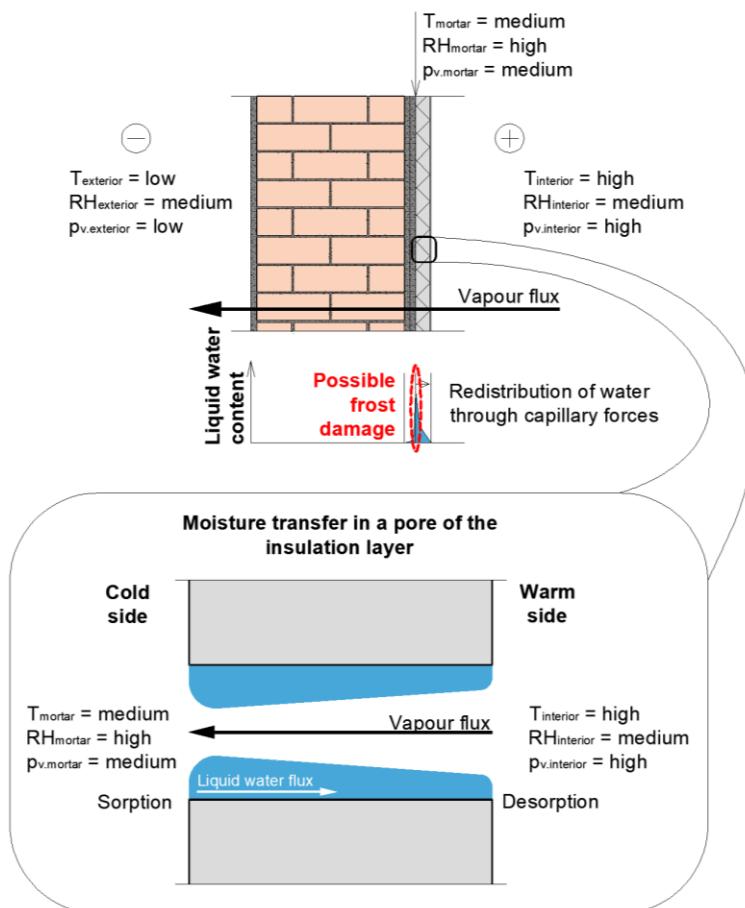

Figure 5   The functioning principle of vapour open "capillary active" insulation system in winter conditions. Based on Zirkelbach et al. (2011) and Plagge (2011).

PRINCIPLE **COLD SEASON** **WARM SEASON** **PROS/CONS**

Vapour open insulation

e.g. mineral wool

+ drying towards interior not restricted

– condensation and mould risk behind insulation

Vapour open insulation + vapour barrier

e.g. min. wool + PE foil

air leak

+ indoor humidity loads mitigated

– air leakages can cause problems
– condensation risk in summer
– moisture accumulation risk

Vapour tight insulation

e.g. PIR, XPS, foam glass

air leak

+ indoor humidity loads mitigated

– air leakages can cause problems
– drying towards interior restricted - moisture accumulation risk

"Capillary active" vapour open insulation

e.g. calcium silicate, aerated concrete

+ drying towards interior not (much) restricted

– indoor humidity loads still affect the wall

LEGEND   Dry   Wet

Figure 6   Comparison of different interior insulation approaches and their impact on a mass masonry wall subjected to wind-driven rain. Based on Zirkelbach and Künzel (2013).

There are also other products and concepts which combine different aspects of these approaches. Examples of them which have been more thoroughly studied include: hydrophilic mineral wool (Pavlík et al., 2005; Toman et al., 2009), mineral wool board wrapped with vapour barrier and a moisture transporting wick (Rode et al., 2020), multi-layered wood fibre board with embedded moisture control layer (Vereecken and Roels, 2014) and a PUR board with capillary active channels (Jensen, Odgaard, et al., 2020).

1.3 Performance criteria

1.3.1 General

Even if most accurate measurement and modelling data is available, there is little to do with them if the performance criteria are missing. WTA Merkblatt E-6-5 (Künzel et al., 2012) shares some guidance to achieve properly functioning interior insulation. Mainly, the following goals can be summarized:

- avoid accumulation of moisture;
- avoid microbial growth (mould, bacteria) on the interior surfaces;
- avoid accelerated degradation of the structure;
- avoid mould and rot.

In addition, several other risks can be summarized, however, they are outside the scope of this study:

- 2D and 3D details/joints – interior insulation also affects neighbouring structures (e.g. exterior-interior wall joints, wooden beam ends supported by the original wall, etc) and the renovation solution has to take into account the possible risks there.
- Reduction of thermal mass of the interior surfaces – as the interior insulation materials have lower density and hence lower thermal inertia, the rooms are quicker to overheat during heat waves. However, it also means that the rooms are easier to heat up if intermittent heating is used. (Vereecken, 2013)
- Salt efflorescence. Beside the original wall, in right conditions the salt crystallization can also damage the interior insulation material calcium silicate (Poupeleer, 2007).
- Higher (hygro)thermal stresses. Larger temperature amplitudes and therefore higher thermal stresses/strains can be expected in the masonry due to the thermal influence of the insulation. (Vereecken, 2013)

1.3.2 Frost

According to Künzel (2011), frost behind an interior insulation system should be avoided. It was suggested that temperature at the insulation-original wall interface should be **above -5 °C** (considering dissolved salts and capillary pressure which reduce the freezing point) and relative humidity **below 95%$_{RH}$**. This very much restricts the thickness of interior insulation that can be applied, especially so in colder climates on walls with high thermal transmittance.

WTA Merkblatt 6-5 (Künzel et al., 2012) recommends taking the saturation degree of the material pores into account, it should stay **below 30%$_{sat}$**. That allows more freedom compared to the previous criterion. Study on Canadian bricks by van Straaten (2014) corroborated that most of the bricks had their critical saturation degree above 30%$_{sat}$.

Scheffler (2013) tested lightweight AAC insulation at 97.4%$_{RH}$, froze it at -15°C for 20 cycles, and detected no loss of compressive or tensile strength. Based on the moisture retention curve in IBK Delphin database, the respective saturation degree at which no damage occurred in AAC insulation is 4%$_{sat}$.

Based on a study by Feng et al. (2019), the **critical saturation degree is a function of temperature** – the lower the frost temperature, the lower the maximum allowable saturation degree. Experiments conducted by Feng et al. (2019) and Al-Omari et al. (2015) suggest that the main damage in the material takes place during the first freeze-thaw

cycles with additional cycles being less significant. Feng et al. (2019) also demonstrated that frost resistance predictions made using two existing models based on simple material parameters (capillary and saturated porosity, water uptake, etc.) did not correlate with the measurement results. Overall, the main issue with the more detailed frost damage models is the lack of experimental data – the results are material-dependent and further studies are required.

1.3.3 Mould

Several models for mould growth assessment exist. Within the scope of this thesis, the Finnish / VTT mould model (Hukka and Viitanen, 1999; Ojanen et al., 2010; Viitanen et al., 2011) is used due to its versatility and applicability to both measurement and modelling results. The model offers two methods to assess the situation – the **critical relative humidity** above which mould growth is possible and **mould index**. The former depends on material sensitivity and temperature (see Figure 7, left), the latter considers the material characteristics, temperature, relative humidity and the duration of conditions favourable for mould growth and returns the mould index value from 0 (no growth) to 6 (extensive mould growth) – see Figure 7, right.

The recommendations by the developers of the mould model suggest that if the analysed surface is in contact with indoor air, the mould index values 1–2 correspond to the upper limits of the safe functioning of the structure (Viitanen et al., 2015).
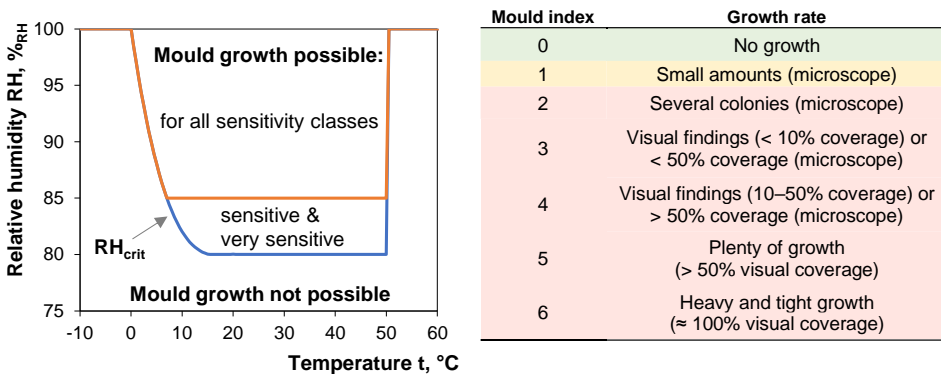

Mould index	Growth rate
0	No growth
1	Small amounts (microscope)
2	Several colonies (microscope)
3	Visual findings (< 10% coverage) or < 50% coverage (microscope)
4	Visual findings (10–50% coverage) or > 50% coverage (microscope)
5	Plenty of growth (> 50% visual coverage)
6	Heavy and tight growth (≈ 100% visual coverage)

Figure 7   *Left: critical relative humidity (RH_{crit}) above which mould growth is possible according to the Finnish mould model. Based on Viitanen et al. (2011). Right: mould indexes along with corresponding descriptions of growth rate and colors denoting acceptability on surfaces in contact with interior air (green – acceptable; yellow – warning; red – unacceptable). Based on Viitanen et al. (2015).*

According to Künzel (2011), mould growth is prevented and contaminants are contained if the whole surface of the insulation board is glued to the wall. However, this depends on the quality of the workmanship, as it is possible to leave air pockets behind the insulation (too dry mortar, uneven subsurface, etc), and unfortunately has occurred in practice (Klõšeiko and Kalamees, 2016; Morelli and MØller, 2019). Therefore, it is still sensible to consider the mould index at least as an indicator of how serious the conditions behind the insulation are and how flawless the workmanship should be.

1.4 Hygrothermal modelling

The dew point / Glaser (1959) / EN ISO 13788 method, which has been widely used since its introduction, has severe limitations. For example, it does not consider liquid conduction, wind driven rain, hygroscopicity, air convection, moisture-dependent material properties and dynamic boundary conditions and is therefore only applicable where these factors are irrelevant. In case of interior insulation of mass masonry walls, neglecting the wind driven rain can result in overly optimistic results and conclusion.

In recent decades the accessibility and use of hygrothermal modelling tools (e.g. IBP Wufi, IBK Delphin, DTU MATCH, Hamtools) has grown noticeably. Compared to the calculations made using the dew point method, complex problems involving dynamic boundary conditions and combined vapour and liquid water transfer can be solved. The premise is, that design decisions can be made without expensive and time-consuming in-situ or laboratory tests.

Numerous studies by different research groups as well as engineers and architects have employed such tools to analyse the impact of interior insulation on the hygrothermal performance of building enclosures. Häupl et al. (2005) modelled the performance of a 600 mm masonry wall in Amsterdam and concluded that the use of vapour tight cellular glass insulation would lead to moisture buildup and the destruction of the structure while the impact of "capillary active" calcium silicate would be much more tolerable. Modelling results of several interior insulation solutions in Norwegian climate by Knarud et al. (2014) show that CaSi has lower relative humidity behind insulation than vapour tight systems. Vereecken et al. (2015) conducted a probablilistic modelling study of a 15–50 cm-thick brick wall using outdoor climate data from Germany. They concluded that of the studied solutions the vapour open calcium silicate is preferable for buildings which are sensitive to frost damage and with wooden beam ends, whilst vapour tight solutions are more appropriate in those buildings where these aspects are not important. A modelling study using Swedish climate data (Abdul Hamid and Wallentén, 2017) exhibits the risk of microbiological growth and an increased corrosion rate of reinforcement if vapour tight solutions are used. At the same time, calcium silicate shows a lower mould risk and can even reduce the corrosion rate and its combination with hydrophobation is reported to perform best. In recent years, the RIBuild project has made valuable contributions to the field through experiments and modelling alike. For example Jensen, Bjarløv, et al. (2020) determined that of the studied solutions, only CaSi and CaSi+PUR systems with hygrophobic treatments would be robust enough to withstand the future climate.

However, the accuracy of hygrothermal modelling is – among correct boundary conditions, proper specifications of the structure, etc. – largely dependent on the reliability of the material properties. The main equations and relationships that govern the hygrothermal processes in the HAM modelling software IBK Delphin (Grunewald, 1997; Nicolai et al., 2009) are given in Figure 8. Compared to the dew point method, which only required thermal conductivity and vapour diffusion resistance factors to describe the materials, the experimental dataset needed to understand the behaviour and interdependence of material properties is now much wider. Furthermore, the processes in over-hygroscopic moisture range are difficult to measure and material properties harder to determine. Unfortunately, this is the moisture content range that mass masonry walls subjected to wind driven rain and "capillary active" insulation systems can also reach.

Conventionally, water uptake and drying tests are used to determine the water vapour and liquid conductivity curves in the higher moisture content range (Krus, 1996; Scheffler

and Plagge, 2010). Assessing the share between the flows in these experiments is based on assumptions as both have the same direction and are subjected to rather extreme conditions (water contact and full saturation).
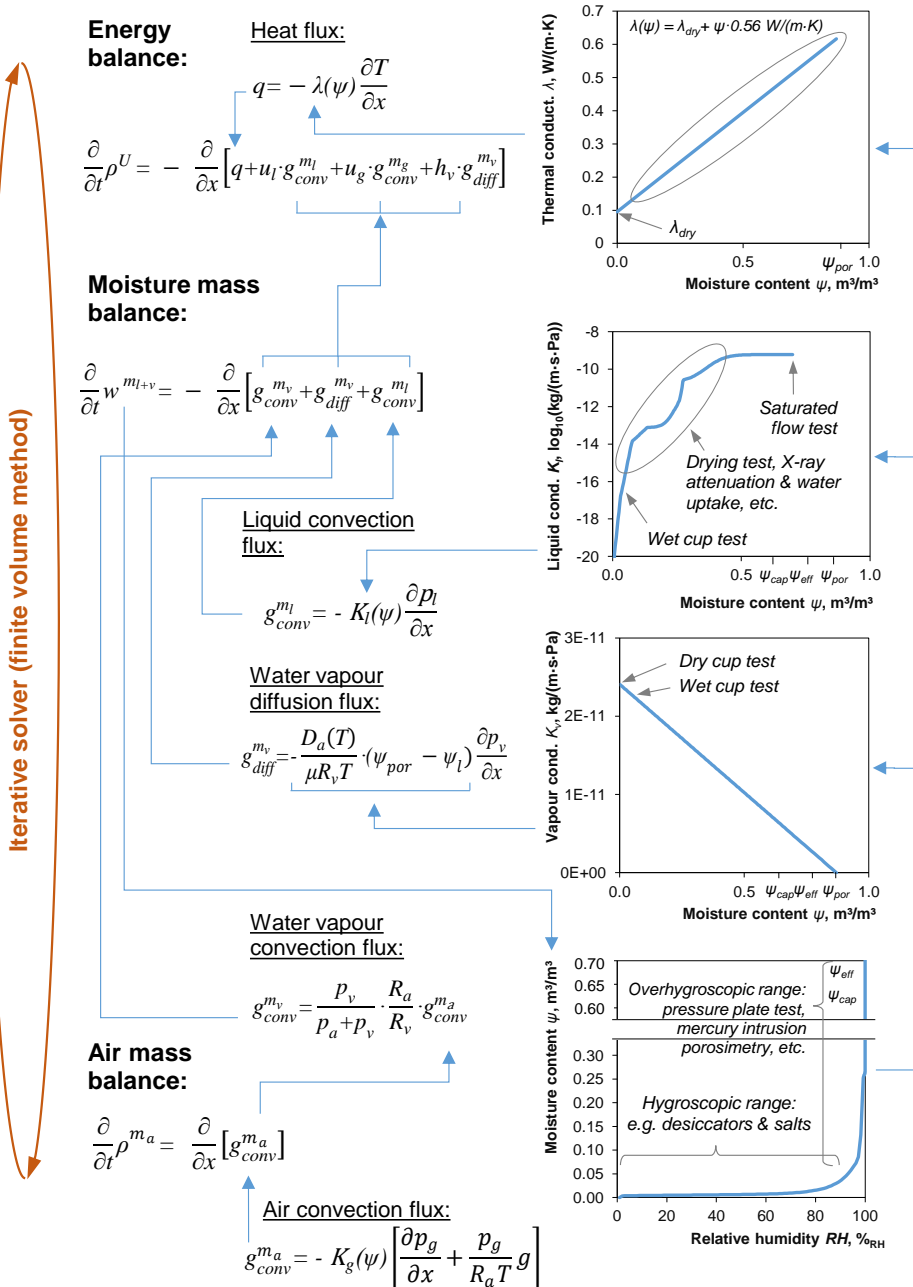

Figure 8   *The main equations and relationships governing the hygrothermal processes in the finite volume mesh of IBK Delphin. Some of the experiments used to create the material property functions (right) are also given. The presented material properties are based on AAC.* (Based on Feng and Janssen, 2021; Nicolai and Grunewald, 2006; Scheffler, 2008; Scheffler and Plagge, 2010)

To gain more information on this, Binder et al. (2010, 2013, 2014) proposed a capillary condensation redistribution (CCR) test, where vapour and liquid flows are in opposite directions. In this test (see Figure 9), a temperature difference causes a condensation plane inside the material sample while the mass change and moisture profile of the sample are monitored.
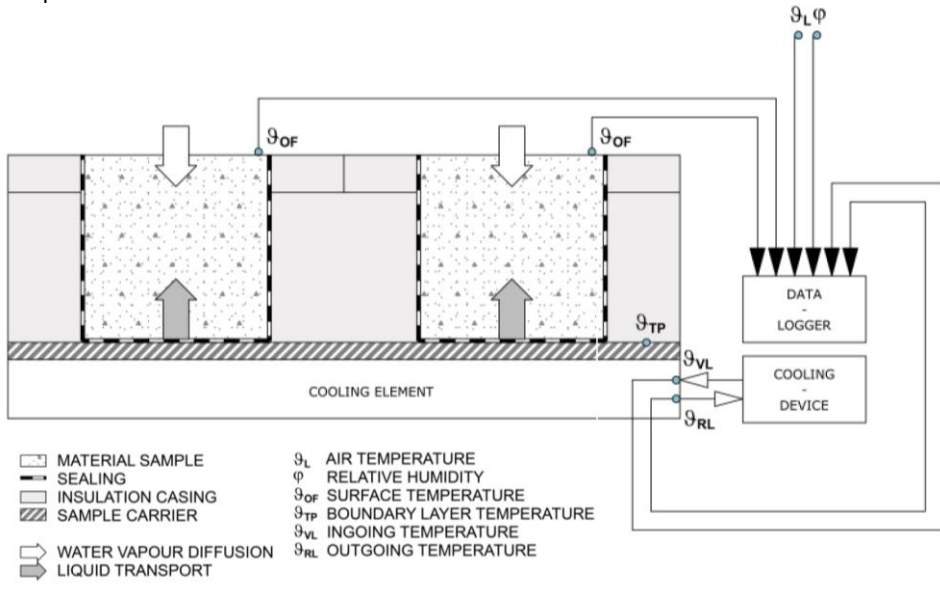

Figure 9   Setup of the capillary condensation redistribution (CCR) test for vapour and liquid conductivity determination. Reproduced from Binder et al. (2013).

In their preliminary example comparisons Binder et al (2014), Publications V and VI (covered in chapter 4 of this thesis) and Hirsch et al. (2020) indicated that modelling with material properties using conventional material characterization (i.e. without taking the CCR test into account) significantly underestimated moisture content in non-isothermal experiments where wetting due to vapour diffusion and possible capillary redistribution were concerned, while CCR-optimized material data managed to better reproduce the measurement results. Furthermore, the conditions in the CCR test are much closer to the real-life application of the "capillary active" insulation materials than a wetting experiment with sudden water contact or an isothermal drying test. Should the performance criterion be a critical moisture content of some kind, then in those conditions the underestimation of moisture content levels using "conventionally" characterized (i.e. without taking the CCR test into account) material data results in a non-conservative error.

However, as of writing this in 2021, only a handful of materials in IBP Wufi and lately also in IBK Delphin database have been characterized based on the CCR test. This raises the question whether the conclusions drawn from previous modelling in high moisture range while using conventional material characterization are still valid. One of the aims of the thesis is to gather further measurement and modelling data to study the impact of the CCR test on the modelling results of interior insulation solutions.

2 Experimental studies

2.1 General

The simplest way to assess the suitability of the interior insulation solutions would be to install the solutions in a building and then wait for the masonry to freeze, wooden beams to rot or mould to grow. However, while the most probable subjects of the interior insulation are valuable buildings and allowing them to be damaged is not acceptable, such processes can also take decades to exhibit themselves. Shorter-term **measurement of hygrothermal conditions inside the walls** can shed the light on the state and trends of temperature and humidity, which can be used to assess the impact of the insulation and help predict the long-term outcome.

At the start of the experiments listed in this thesis (in 2012), in-situ experiments using "capillary active" insulation had only been conducted in Central-European countries. As Estonian colder climate can possibly cause more severe conditions in the insulation and original wall, local measurements were deemed necessary to study the hygrothermal performance of the interior insulation solutions. Acquiring first-hand experience in working with the materials was also vital.

To determine the **frost resistance** of the "capillary active" insulation systems a study of a wall mock-ups was subjected to freeze-thaw cycling in a climate chamber along with **tensile strength and hygrothermal measurements**.

2.2 Methods

2.2.1 Hygrothermal study of 4 different insulation solutions under typical apartment conditions (Spordi 2, Kohtla-Järve)

Figure 10   View of the studied school building.

To compare the hygrothermal performance of different internal insulation materials and to develop an energy renovation solution for historic school building the exterior wall was insulated with four materials, while the fifth section was left uninsulated as a reference (see Figure 11).

Materials were selected so that diffusion open, capillary active, and vapour tight materials were used:

- calcium silicate (CaSi): capillary active material with very high open porosity and low vapour diffusion resistance;
- aerated concrete (AAC) with high open porosity, lower capillary activity and thermal conductivity;
- polyurethane board with capillary active channels (IQ-T) - combines low thermal conductivity and some capillary activity;
- polyisocyanurate board (PIR) with closed pores: low thermal conductivity and relatively high vapour diffusion resistance forming a vapour barrier in itself.

The original brick wall was 73–75 cm thick, composed of three brick layers with air and insulation (peat) layers between them. The thicknesses of the insulation layers were selected to represent typical products and to avoid large thermal transmittance differences between the walls. Figure 12 shows different stages of the insulation and sensor installation.
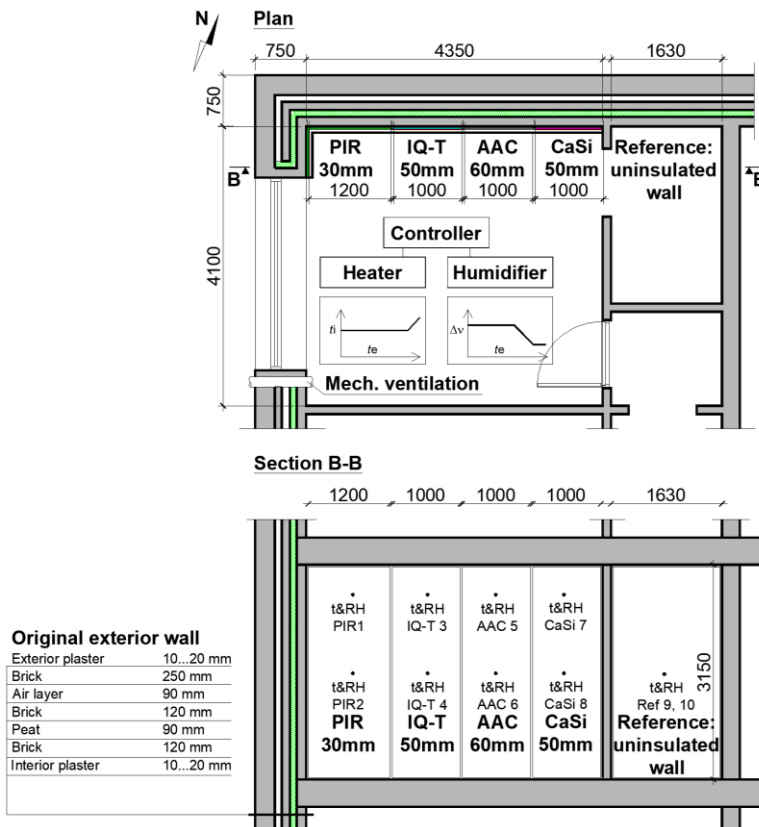

Figure 11   Plan and section/view of the studied test walls.

Figure 12 Top row: test wall before (left) and after (right) the installation of insulation and measurement equipment. Bottom 3 rows: different stages of the process.

Each test wall was equipped with two temperature and relative humidity (RH) sensors between insulation and the original wall (Ø5mm, Rotronic HC2 SC05, accuracy ± 0.3 °C, ± 1%RH) and heat flow plates (Hukseflux HFP01, accuracy ± 5%) on the internal surface of insulation. Internal and external surface temperatures were also measured.

Indoor climate was heated with the set point of thermostat +21 ºC and humidified to keep the moisture excess (Δv difference between indoor and outdoor air moisture content) of 2.3–4.6 g/m³, to represent the average conditions in dwellings with high humidity loads (Kalamees, 2006). Figure 13 shows the values of moisture excess plotted against outdoor temperature.

The climatization of the test room is an attempt to imitate a typical renovation process:

- period 1 (P1): internal insulation works and starting to heat the room: 27.03.2012–4.07.2012; Δv +0.1 g/m³;
- period 2 (P2): starting to humidify ≈ 3 months after installation (4.07.2012–6.08.2012) to represent time period between the renovation and moving back in, high humidity load; Δv +2.3 g/m³ (humidified)
- period 3 (P3): humidifying period to see the influence of different humidity loads on the hygrothermal performance of test walls, medium high humidity load: 6.08.2012–8.10.2012; Δv +2.9 g/m³;
- period 4 (P4): medium humidity load, 8.10.2012–14.12.2012; Δv +4.2 g/m³ (humidified);
- period 5 (P5): with low humidification (from 14.12.2012) to see drying out potential of different walls; Δv +2.5 g/m³ (humidified according to indoor RH).
- period 6 (P6): medium humidity load, 22.01.2013–16.02.2013; Δv +4.6 g/m³ (humidified);
- period 7 (P7): high humidity load, 16.02.2013–17.10.2013; Δv +3.6 g/m³ (humidified);

Indoor and outdoor temperatures as well as temperatures between the insulation and the original wall are shown in Figure 25 (top). Indoor air temperature stayed the same throughout the heating period (+21 ±0.5 °C). Outdoor air temperatures ranged from +17 to +30 °C in July with an average of +19.4 °C. Temperature until December was rather mild, with an average of +5.4 °C in November and minimum temperatures reaching +1 °C on several occasions.
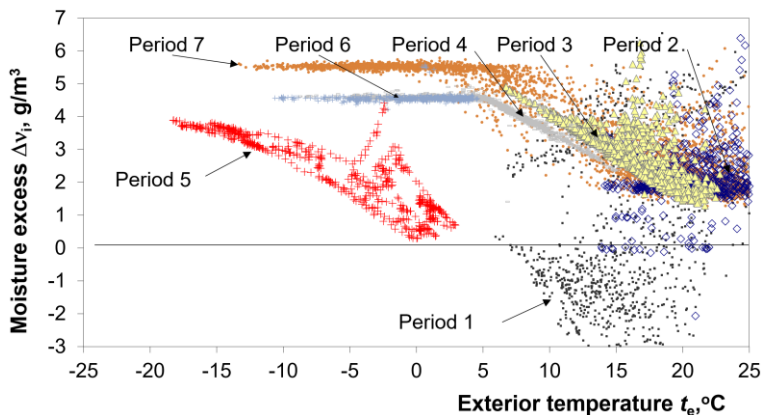

Figure 13 Indoor moisture excess dependent on outdoor temperature during the experiment at Spordi 2, Kohtla-Järve. Combined data from publication I and Klõšeiko et al. (2013a).

2.2.2 Hygrothermal study of AAC insulation in an office building (Vabaduse väljak 7, Tallinn)

Vabaduse väljak 7 is a 7-storey office building built in 1932 (Figure 14 left). As it is heritage protection listed, alterations to the façade are forbidden. During preliminary studies, the wall structure was opened, its dimensions and materials were specified and material samples were collected (Figure 15 and Figure 16). Due to the wall structure being complex and previous experience showing the need for caution, a field study was carried out.
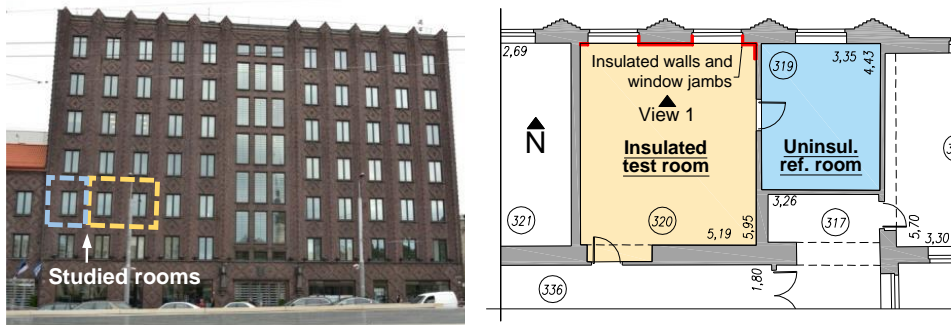

Figure 14   Façade of the studied building (left) and plan of the test rooms (right).

The field study consists of monitoring an insulated test room (Figure 14) and its neighbouring uninsulated reference room. Both are situated on the 3rd floor and are north-facing.

Based on initial hygrothermal simulations a 50mm layer of autoclaved aerated concrete (AAC) insulation Ytong Multipor was chosen to cover the walls and one of the two radiator niches. Due to space restrictions, window jambs were insulated with d = 12.5 mm and 20 mm XPS insulation boards (Tycroc TWP). Figure 15 shows the insulation and measurement setup. Insulation and monitoring equipment were installed during the period of 2–8.07.2014 (Figure 16 bottom row). The following measurement devices were used in monitoring of the hygrothermal performance of the building: *t&RH* probes: Rotronic HygroClip HC2-C05 (accuracy ± 0.3 °C, ± 1%$_{RH}$); heat flux plates: Hukseflux HFP01 (accuracy ± 5%); data logger Grant Squirrel SQ2020 1F8 (accuracy ± 0.05% of readings ± 0.025% of range); data logger Grant Squirrel SQ2010 (accuracy ± 0.1% of readings ± 0.1% of range); temperature probes: Onset Hobo TMC6-HD (accuracy ± 0.15 °C); *t&RH* data loggers: Onset Hobo U12 and UX100 (accuracy ± 0.21 °C, ± 2.5–3.5%$_{RH}$). Measurement and logging interval of 1h was used.
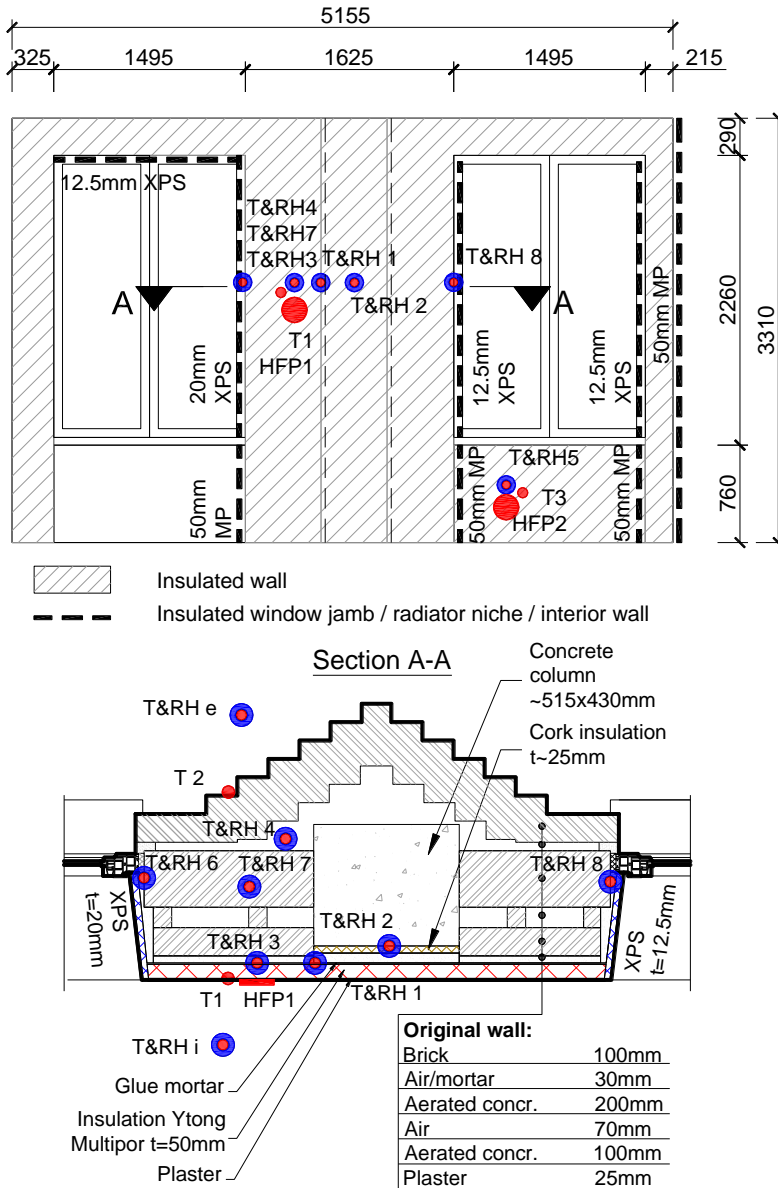
Figure 15   View at the insulated test wall from the inside – placement of sensors and insulation scheme (top). Middle part of the test wall – wall structure, placement of sensors (bottom).

Figure 16   Sampling of the original wall to specify its structure (top left). Original wall after sampling (top right). It is relatively easy to leave air channels behind the insulation due to bad workmanship, wrong tools, too stiff mortar etc. (bottom left). Installation of insulation boards (bottom right).

Figure 17 (left) gives the indoor and outdoor temperatures as measured on site. Minimum outdoor temperature during the winter of 2014/2015 was -11.1 °C with an average of +1.5 °C (1.11.2014–1.03.2015), which is higher than usual. The winter of 2016/17 was similarly mild, while 2015/2016 and 2017/18 also showed lower temperatures (minimum -17.9 °C and -14.8 °C respectively). Average indoor temperature in the measured rooms was 21.5 °C. Due to an intermittent heating scheme the indoor temperature had a daily amplitude of < 4 °C. Figure 17 (right) gives the moisture excess in the studied rooms and shows that moisture loads during the measurement period were relatively low.
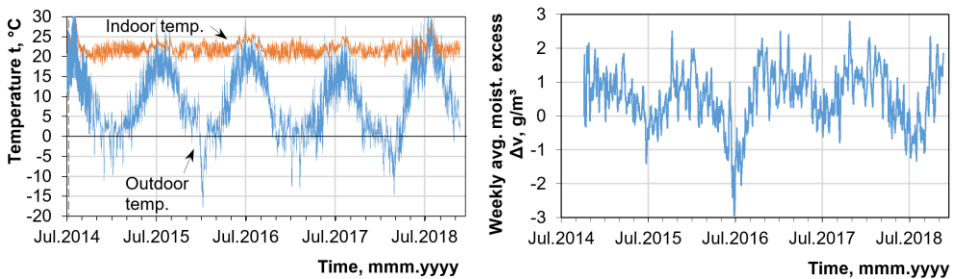

Figure 17   Indoor and outdoor temperatures (left) and indoor air moisture excess during the measurement period. Figures initially published in Publication II are updated to show the whole duration of measurements.

2.2.3 Long-term hygrothermal study of PUR foam and CaSi boards in an office (Vabaduse väljak 10, Tallinn)

This study took place on the last floor of an 8-storey office building (built in 1936; cultural heritage; see Figure 20). Existing interior insulation (gypsum board, PE foil, min. wool) exhibited excessive mould damage and a renovation solution had to be found. The main challenges were: low surface temperatures, high thermal transmittance and avoidance of future biological decay. Preliminary HAM modelling showed that "closed cell" PUR foam injected into air cavities of the masonry and "capillary active" CaSi on the surface of the wall could perform well.

Figure 18   Façade of the studied building; test room is designated with the dashed red line.

Vertical and horizontal sections of the studied wall are given in Figure 20. The wall structure, renovation solution and sensor placement are also shown. Sensors and their positions were selected both to assess the hygrothermal situation after the insulation and to have enough reference points to calibrate the HAM models. Figure 19 shows different stages of the insulation and sensor installation.

The following measurement devices were used: *t&RH* probes: Rotronic HygroClip HC2-C05 (accuracy ± 0.3 °C, ± 1%$_{RH}$); heat flux plates: Hukseflux HFP01 (accuracy ± 5%); data logger Grant Squirrel SQ2020 1F8 (accuracy ± 0.05% of readings ± 0.025% of range); temp. probes & logger: Onset Hobo UX120-006M & TMC6-HD (accuracy ± 0.15 °C); *t&RH* data loggers: Onset Hobo U12 and UX100 (accuracy ± 0.21 °C, ± 2.5–3.5%$_{RH}$). Measurement and logging interval: 1 h.
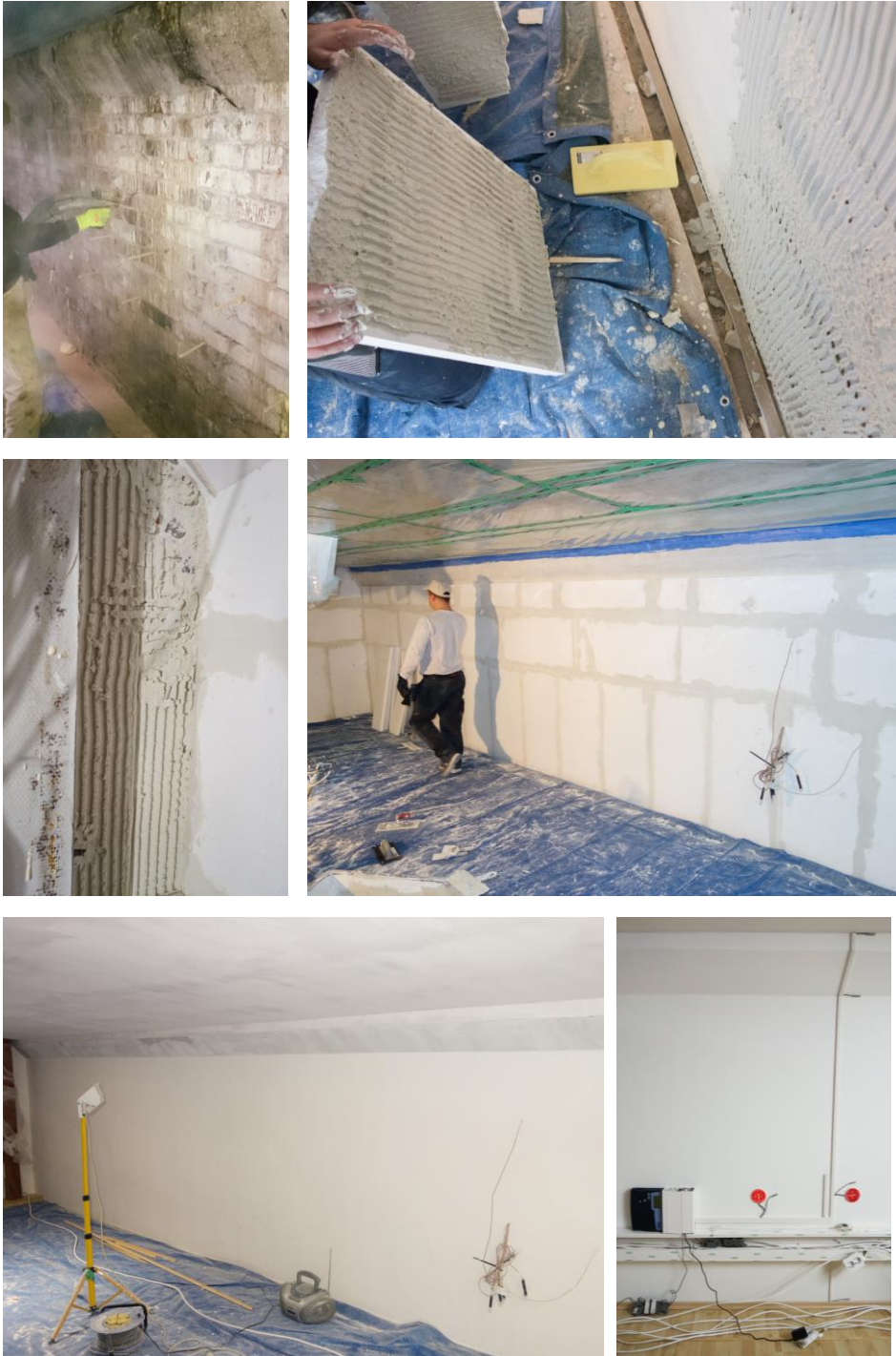
Figure 19   Installation of PUR foam (top left). Air channels can exist in the glue mortar due to bad workmanship, wrong tools, too stiff mortar, uneven subsurface, etc. (top right, middle left). CaSi insulation before (middle right) and after plastering (bottom left). Measurement devices on the interior surface (bottom right).
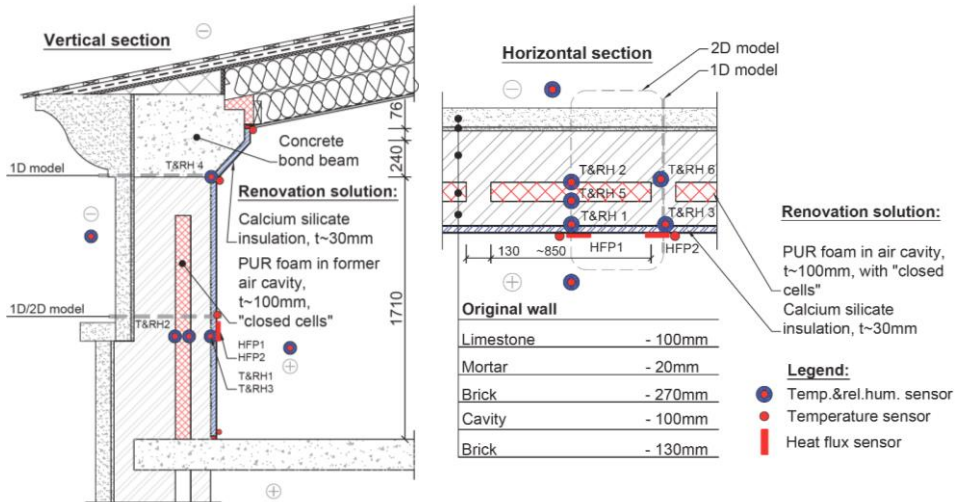
Figure 20   Vertical and horizontal sections of the wall showing sensor placement and wall layers.

The measurements took place from March 2015 til March 2018 and included installation, dryout and use phases. Indoor and outdoor temperatures are given in Figure 28. Moisture excess during the measurement period in the test room was very low (close to moisture class 1 according to EN-ISO 13788 A.2), as a well-functioning HVAC system was installed.

2.2.4 Hygrothermal and mechanical study of AAC, CaSi and expanded perlite systems in climate chamber

2.2.4.1 Test setup
In this study 3 different vapour open "capillary active" insulation systems were tested: Ytong Multipor autoclaved aerated concrete (AAC) in 50mm and 60mm thicknesses (designated as MP50 and MP60 respectively), 50mm Knauf Tectem expanded perlite (TT) and 50mm Epasit Epatherm calcium silicate (ET). All the insulation boards were attached to the base structure using system-specific glue mortar and covered with plaster and paint. The goal of the study was not to imitate the exterior wall exactly as it would appear in real life but to achieve similar moisture content in the insulation systems and to test them for frost resistance. Thus, to shorten the duration of the cycle, a base structure with low thermal mass was selected. This consisted of timber framing, wood particleboard, PE foil and Knauf Aquapanel cement fibreboard. The view and section of the wall are given in Figure 21. The materials in the test wall were selected so that the majority of them would be represented in HAM software IBK Delphin database to reduce uncertainties. Figure 22 shows different stages of the study.

Temperature, relative humidity, moisture content and heat flux sensors were installed in the wall (Figure 21 top and bottom). The following sensors and devices were used:
1) temperature sensors (inside the wall and on surfaces): Onset Hobo TMC15-HD & logger UX120-006M (accuracy ± 0.15 °C);
2) *t&RH* sensors (boundary conditions in chambers and inside the wall): Rotronic HygroClip HC2-C05 (accuracy ± 0.3 °C, ± 1%RH) & A/D converter: Siemens SM331 6ES7331-1kf02-0ab0 (accuracy ± 0.004 V);

3) heat flux sensors: Hukseflux HFP01 (accuracy ± 5%), logger: Grant Squirrel SQ2020 1F8 (accuracy ± 0.05% of readings, ± 0.025% of range);
4) backup *t&RH* sensors for int. and ext. chamber climate: Onset Hobo UX100-023;
5) balance: Vibra AJH-2200CE (e = 0.1 g, d = 0.01 g);
6) oven Venticell 111.

Also, gravimetric measurement of moisture content from different drill core layers were used (see Figure 23). Samples were dried at 70 °C until constant mass had been achieved.
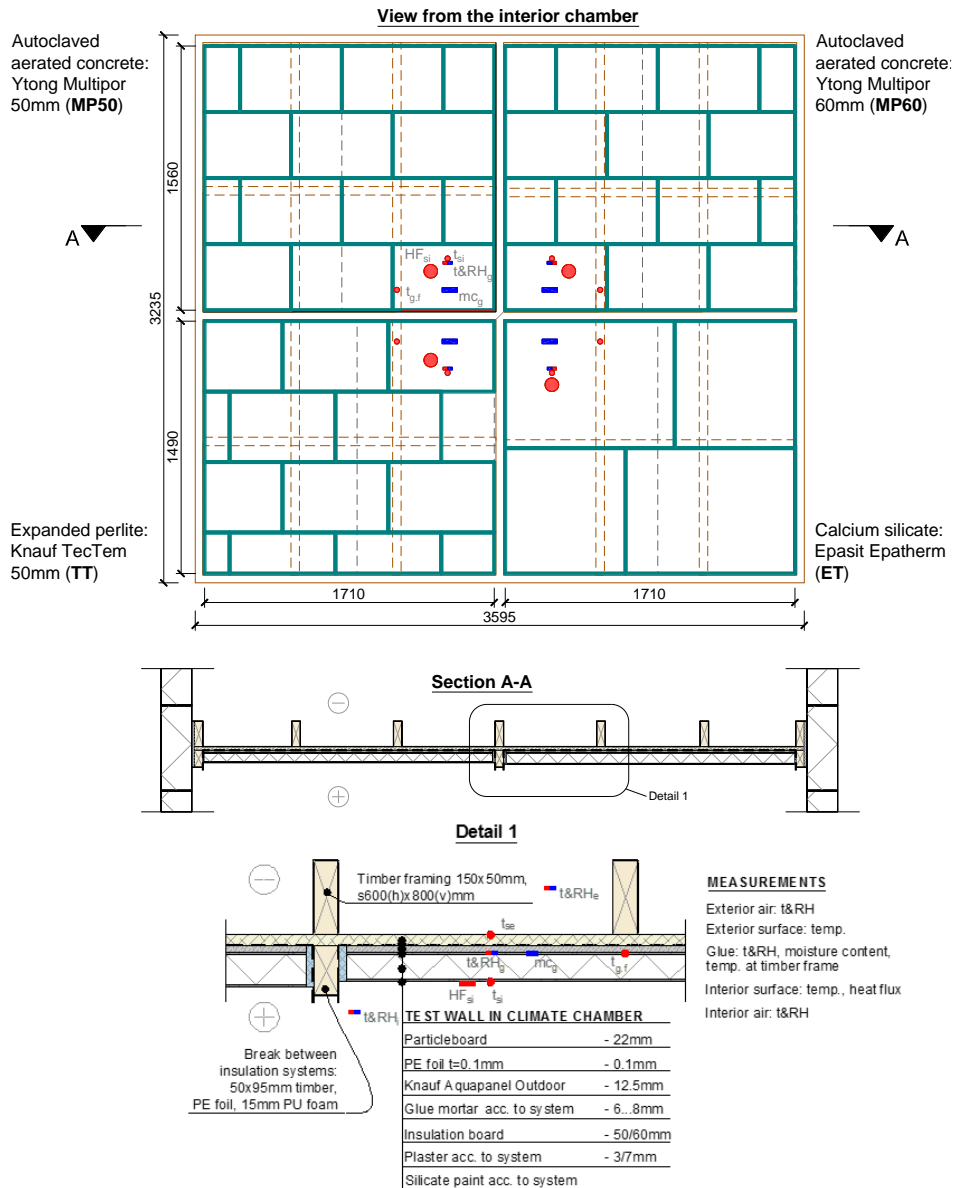
Figure 21   View to the test wall from the interior chamber (top), horizontal section (middle), detail of the layers (bottom).
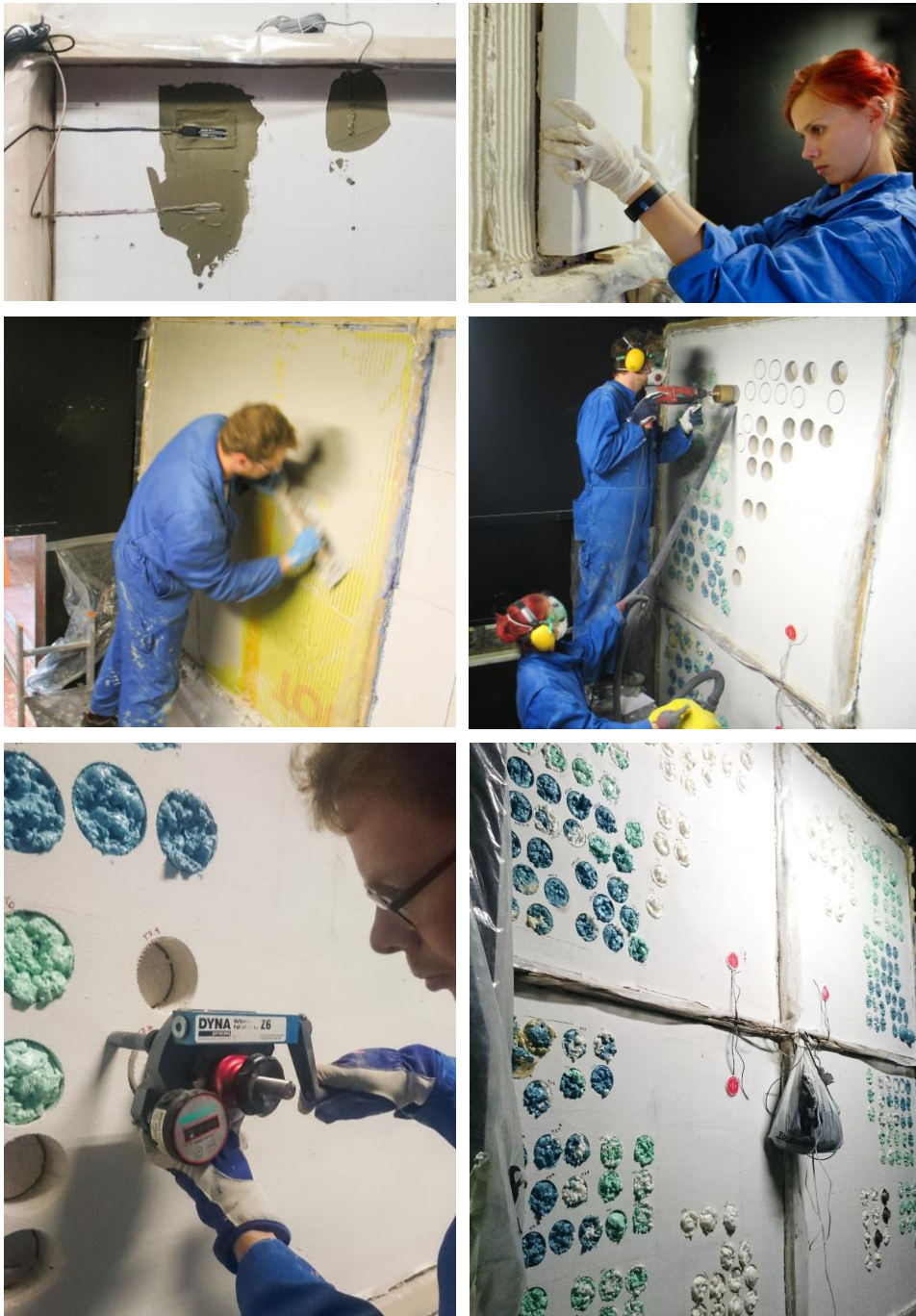
Figure 22 Top left: sensors behind an insulation system. Top right: installation of an insulation board. Middle left: smoothing the interior plaster and the reinforcement mesh. Middle right: cutting the insulation systems in preparation for pull-off testing and gravimetric moisture measurements. Bottom left: pull-off testing of the insulation system. Bottom right: view at the test wall after the final series of sampling.

Figure 23   A typical drill core and layers from which moisture content was gravimetrically measured.

2.2.4.2 Boundary conditions

Temperature and relative humidity in the indoor and outdoor chambers had 5 main periods (see Figure 24):

1) dry-out without artificial climate control;
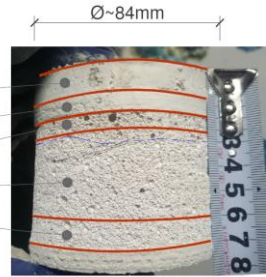2) humidification in the indoor chamber and cooling in the outdoor chamber. The boundary conditions were chose so that the insulation systems would achieve similar moisture content as a 380mm brick wall with 100mm autoclaved aerated concrete or calcium silicate interior insulation according to modelling with a 43-year climatic dataset obtained from Tartu, Estonia;
3) drying – the measured moisture content levels were far higher than the hygrothermal models predicted and it was decided to reduce them;
4) second humidification period;
5) freeze-thaw cycles. A typical freeze-thaw cycle in the exterior chamber consisted of a freezing period ($t \approx$ -29 °C, duration ca. 25 h) and a thawing period ($t \approx$ 20 °C, duration ca. 11 h), while the interior chamber temperature was kept at a constant 20 °C. During the freezing cycle, temperatures in the insulation glue layer dropped to ca -15 – -7 °C depending on the insulation system and moisture content.
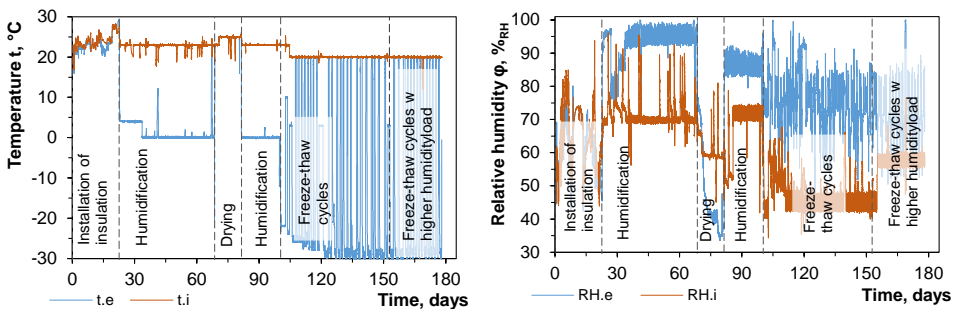
Figure 24   Temperature and relative humidity in indoor and outdoor chambers.

2.2.4.3 Freeze-thaw resistance assessment

At 0, 11, 26 and 53 freeze-thaw cycles 10 test samples of each insulation system were tested for adhesion/tensile strength. A Ø92 mm core-drill was used for the separation of the samples (resulting in Ø85mm specimens) and these were tested with a Proceq DYNA Z Pull-Off tester. Moisture content was sampled initially from 1 and later 2 drill cores per system per series. Although other methods have also been used for frost resistance assessment (e.g. compressive strength (Scheffler, 2013), dilatometry (Mensinga et al.,

2014), dynamic elasticity modulus as used in EVS-EN 14146 (2004), mass loss, visual inspection etc), tensile strength was deemed suitable as the whole system was under study and changes to any layer would become apparent.

2.3 Results and discussion

2.3.1 Hygrothermal performance of the interior insulation solutions

2.3.1.1 4 different insulation solutions under typical apartment conditions (Spordi 2, Kohtla-Järve)

Measured temperature and relative humidity between the insulation and original wall are given in Figure 25. Although the outdoor air temperature stayed under -10 °C for 8 days in December, none of the sensors detected temperatures below 0 °C directly behind the insulation.

Drying finished fastest in the case of CaSi (24 days), AAC section dried to the same level in 38 days, whereas iQ-T reached the lowest *RH* of 86% at the start of humidification (3 months after the installation).

In the case of PIR the critical *RH* from Finnish mould growth model (Ojanen et al., 2010; Viitanen and Ojanen, 2007) was used to assess the possibility of mould growth, as the side which was in contact with the original wall was covered with paper. The limit is given in Figure 25 as "*RH*$_{crit}$ *"80%""*". Measured relative humidity values behind PIR insulation exceeded this critical limit from August to October in 2012 and from June to the end of measurements in October 2013.

After the initial dryout, the relative humidity in the iQ-T section stayed around the limit of 95% which is also the range where the capillary transport of humidity increases significantly. The *RH* sensor malfunctioned after ca 5 months of use and measured values between Oct. 2012 and Jan. 2013 are missing.

Due to the lower vapour resistance of AAC and CaSi, relative humidity between insulation and the original wall reacted more quickly and drastically to the changes of indoor humidity. While the absolute humidity levels stay practically the same, the lower thermal resistance of CaSi layer causes higher temperatures and lower relative humidity levels compared to AAC. In case of AAC, the 95%$_{RH}$ limit is occasionally exceeded.

Figure 25   Measured temperature (top) and relative humidity (bottom) between insulation and original wall. Combined data from Publication I and Klõšeiko et al. (2013b).

Thermal transmittances were calculated based on heat flow and surface temperature measurements for the period of 1.09.2012–28.12.2012. The period was chosen because of its low temperature fluctuations and solar radiation. The average values for thermal transmittance are given in Figure 26. The thermal transmittances of all systems dropped ≈ 3% during the period without humidification.

The average values of surface temperature in November stayed within 19.2–19.8 °C and the average for the uninsulated reference wall was 17.3 °C (the average indoor temperature was 20.9 °C). During the cold period in December, the surface temperature of the reference wall dropped to an average of 13.1 °C, while the sections with insulation stayed 3–4 °C higher (the average indoor temperature was 19.0 °C) depending on the material. A potential issue were low surface temperatures at the metal fasteners of PIR: the temperature factor f_{Rsi} measured at the fastener was 0.72, while the respective value at PIR surface was 0.92 and on the reference wall 0.82.
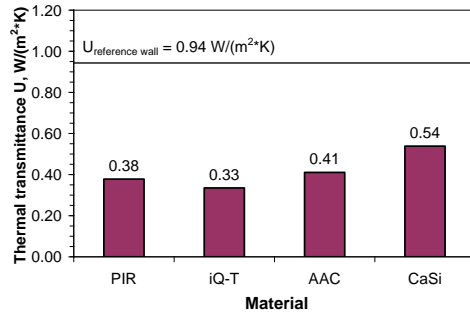
Figure 26   Average thermal transmittances calculated from measured heat fluxes and surfaces temperatures during the period of 1.09.2012–28.12.2012.

2.3.1.2 AAC insulation in an office building (Vabaduse väljak 7, Tallinn)

The measured temperature and relative humidity values at various points in the test wall are given in Figure 27. The dryout to stable relative humidity levels took ca. 1.5 months. Data from all sensors show that hygrothermal conditions during the measurement period stayed well below the safe performance limits of the system. On one hand this can be attributed to relatively low thermal conductivity of the historic aerated concrete (when compared to other masonry structures) and the air cavity between outer brick leaf and interior layers, which reduces the ingress of driving rain. However, it must be noted that indoor humidity load in the test room was low. Comparison of heat flux data from HFP1 (on insulated wall) and a similarly placed sensor on the reference wall revealed over two-fold reduction of thermal transmittance (U_{HFP1} = 0.50 W/(m²·K) vs U_{ref} = 1.13 W/(m²·K)).
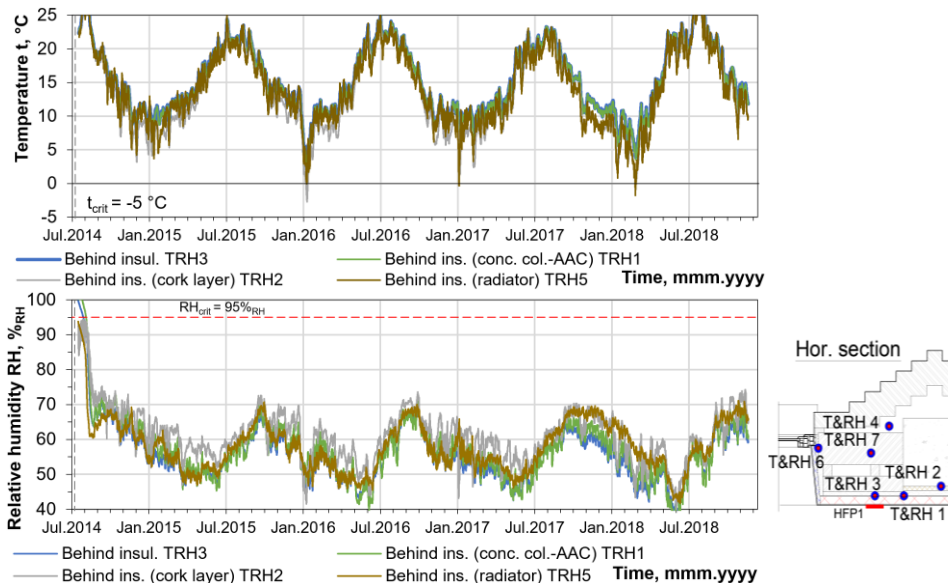
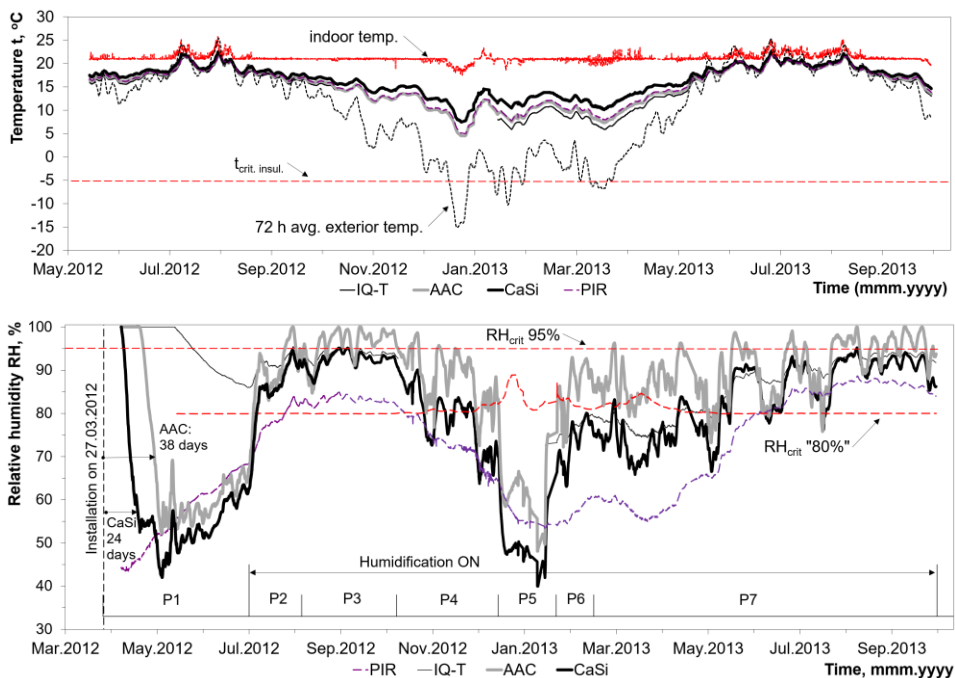*Figure 27   Temperature (top) and relative humidity (bottom) behind insulation layer. Combined data from Publication II and Klõšeiko and Kalamees (2015), extended measurement period is now also shown.*

40

2.3.1.3 Long-term study of PUR foam and CaSi insulation in an office (Vabaduse väljak 10, Tallinn)

The temperatures behind CaSi (Figure 28 top, sensors TRH1, 3, 4) were closest to limits during the winter of the first year. At sensor TRH4 (concrete section) they fell to as low as -2.5 °C, but not reaching the critical -5 °C. In the masonry section the temperatures were higher due to PUR insulation adding further thermal resistance. Consequently, sensors on the exterior side of PUR (TRH2 shown here) measured far lower temperatures than between CaSi and the concrete bond beam. Figure 28 (bottom) gives the measured relative humidity levels. Dryout of the built-in moisture to stable levels took about 2.5–3 months. *RH* values between exterior brick leaf and PUR (sensor TRH2) were quite stable (fluctuating about 5%$_{RH}$ throughout the year) after the dryout of the CaSi built-in moisture.

Analysis of measured data hints that vapour concentration of air in the pores of exterior masonry leaf are governed by the outdoor climate while lagging behind by about half a week. A ≈ 4 g/m³ rise in vapour concentration compared to indoor and outdoor air in autumn (mid-Aug to Oct.) is pronounced, possibly due to rain. However, moisture does not seem to be accumulating in the wall over time, which could be the case with vapour tight interior insulation and heavy wind driven rain loads. Sensors behind CaSi insulation measured vapour concentration quite close to that of the indoor air throughout the year. A lag of a couple of days was detected.
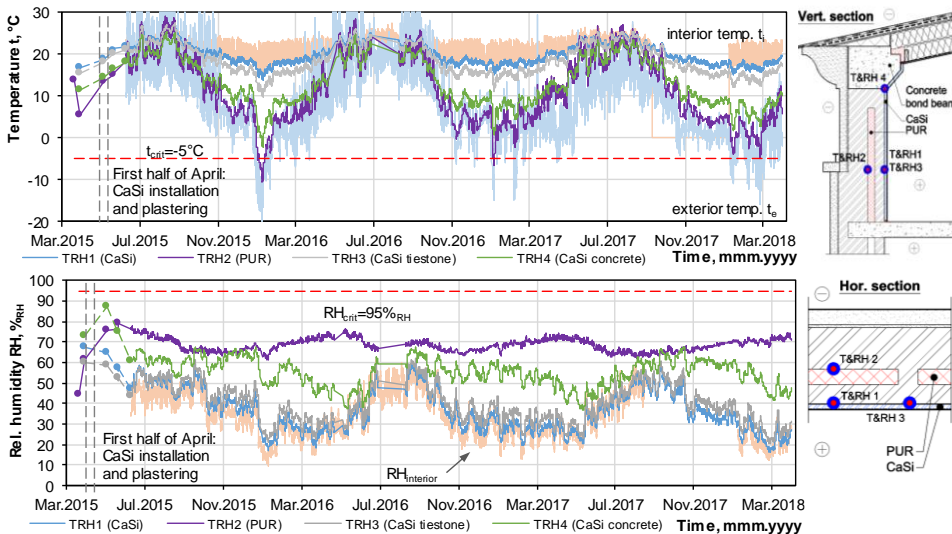
Figure 28   Vabaduse väljak 10: measured temperatures (top) and relative humidity levels (bottom) throughout the monitoring period.

Temperature indexes/factors (f_{Rsi}) were calculated from surface temperatures to assess mould and condensation risk on the wall's surface. The worst situation was detected at the wall-floor intersection (f_{Rsi} = 0.79) and at the concrete bond beam (f_{Rsi} = 0.83). None of those results should indicate a risk, however, as indoor moisture load was low. f_{Rsi} values at the rest of the intersections were also considerably higher (i.e. safer).

Average heat flux and temperature data from 1. Nov. 2015–29. Feb. 2016 were used to calculate the thermal transmittances (*U*) of the insulated wall (see Figure 20 for

placement of the sensors). At tie bricks (HFP2) U = 0.52 W/(m²·K) was measured and between tie bricks (HFP1) the value was U = 0.31 W/(m²·K). 2D thermal transfer modelling of the insulated structure results in an average thermal transmittance of U = 0.39 W/(m²·K), which is ≈ 3-fold reduction compared to the uninsulated case (U = 1.14 W/(m²·K)).

2.3.1.4 Study on freeze-thaw cycling of 3 interior insulation systems in a climate chamber
A typical freeze-thaw cycle in the exterior chamber consisted of freezing (t ≈ -29°C, duration ~25h) and thawing periods (t ≈ 20°C, duration ~11h), while the interior chamber temperature was kept at a constant 20°C. During the freezing period, the temperature inside the glue layer dropped to as low as -15 to -10 °C depending on the insulation system (see Figure 29). Due to relatively high moisture content of the insulation systems, the effect of freezing and thawing is evident on the temperature chart. It can be said that freezing starts at nearly 0°C for MP50 and MP60 (AAC) and at around -1…-2°C for TT and ET (CaSi) systems. This is higher than the ≥ -5°C temperature limit for frost avoidance derived from thermodynamics by Künzel (2011) and suggests that larger pores are filled with water. Using porosities from the Delphin database and measured densities, the saturation degrees were calculated from the measured moisture content at the end of each pull-off test cycle (Figure 36). The saturation degree in insulation reached the highest in ET (CaSi; 20%$_{sat}$) and stayed the lowest in MP (AAC) and TT insulations (10…11%$_{sat}$). In the case of the substrate (cement fiberboard), the trend was reversed – the lowest saturation degree was in the ET (CaSi) and TT sections (27…29%$_{sat}$) vs MP (AAC; 36…37%$_{sat}$). The highest saturation degree in the glue was in the TT (41%$_{sat}$) and lower in the MP (AAC) and ET sections (CaSi; 25…32%$_{sat}$).

Figure 30 compares the moisture content of the cold layer and the mean of the whole insulation layer to the mean thermal conductivity of the insulation layer. As the moisture content is not uniform along the thickness and between the insulation systems, the correlation between the mean thermal conductivity and the moisture content levels is different. Also, it should be considered that ice has higher thermal conductivity than water and the insulation was partly frozen during some stages of the study. The ET (CaSi) was better at redistributing moisture towards the warm side than e.g. MP (AAC) and also continued to accumulate moisture throughout the test – the former had a more notable increase (ca 30%) in the mean thermal conductivity than the latter (ca 10%).
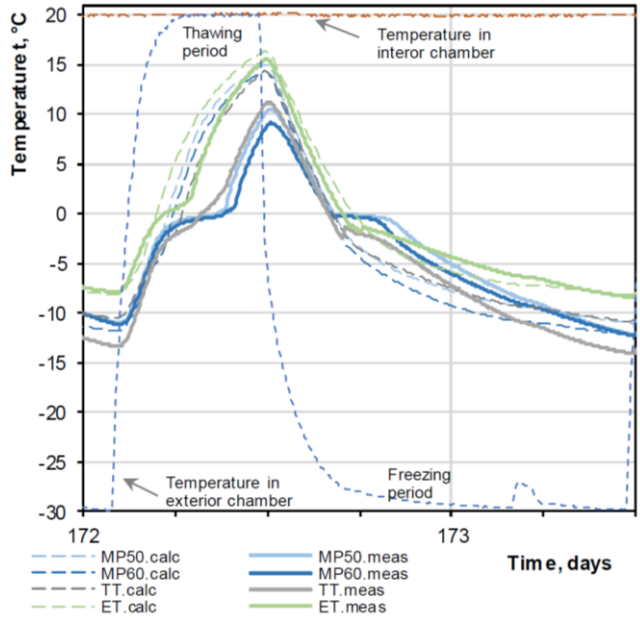
Figure 29   Measured and modelled temperatures behind the insulation layer during a typical freezing
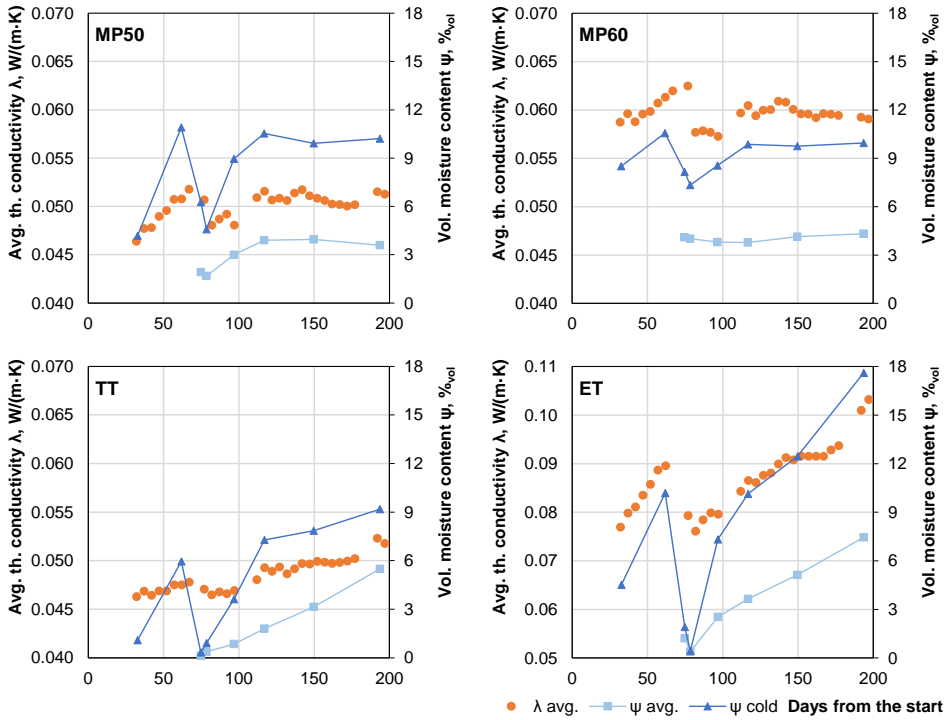cycle.

Figure 30   Mean thermal conductivities of the insulation layer and moisture content levels (mean and
cold side of the insulation) measured during the climate chamber experiment. Combined data
from Publication IV, Varda (2017) and Publication VI.

2.3.1.5 Discussion

A factor influencing the accuracy of direct comparison between the Spordi 2a and Vabaduse väljak 7 reference and insulated wall sections could be air flows in cavities and non-uniform distribution of insulation in the existing wall (in Spordi 2a case). In Spordi 2a, the total thickness of the multi layered wall was high (ca 700 mm) and 1000 mm-wide test wall sections are probably not wide enough to give a complete comparison on the effect on the exterior layers between the systems that aim to be vapour tight and those that are more vapour open. However, the impact on the insulation-original wall interface can still be judged.

As all systems using "wet installation" had a ≈ 5 mm layer of glue mortar according to installation instructions, the amount of water added inside the wall was largely the same. On IQ-T, the topmost plaster level was thicker than on the other systems (10-15 mm vs 2 mm on CaSi and 5 mm on AAC).

The moisture added during the retrofit works can cause long periods of high *RH*, if the renovation works are done during the period when the outdoor and indoor conditions are not suitable for the drying out or the moisture is not dried out before the rooms are taken into use again. The results show that the timing of the renovation works or when the rooms are put into use again need to be considered. The length of time after the renovation works is most critical for the IQ-T, while for CaSi and AAC it is considerably shorter. Beside specific insulation material, the dryout time is dependent on the indoor and outdoor conditions and the original wall too, as shown by a 3-fold difference in its length when comparing CaSi systems in different case studies. Even longer dryout time was measured by Jensen, Bjarløv, et al. (2021) when cork insulation plaster was used – in that case, the whole insulation layer was initially nearly saturated with water.

In general, direct comparison with works by other researchers is difficult as the indoor and outdoor climate loads, insulation thicknesses, material properties, wall structures and studied details (some concentrated on wooden beam ends) are different. However, like in current case studies, if the indoor humidity load is governed by the users naturally, the performance of the interior insulation systems is good (Häupl et al., 2004; Ruisinger, 2013) and if artificial humidification is used, the measured relative humidity is higher (De Mets et al., 2017; Jensen, Bjarløv, et al. 2021; Jensen, Odgaard, et al., 2020) and might exceed the basic 95%$_{RH}$ criterion.

2.3.2 The effect of freezing and thawing on the tensile strength of the insulation systems

The tensile strength levels of the insulation systems before and after freeze-thaw cycling are given in Figure 31. Testing showed quite a high spread. In TT & ET (CaSi) systems the rupture appeared in insulation layer near the glue in all cases. With MP50 and MP60 (AAC) it occurred in the middle of the insulation layer during the base (0 cycles) and 11 cycle cases. However, after 26 and 53 cycles (especially with MP50), the drill cores mostly separated from the base structure (cement fiberboard) and the glue layer interface.

Comparing the base cases to the tensile strengths at 53 cycles, independent samples 1-tailed t-tests showed a statistically significant drop in tensile strengths for all insulation systems (p < 0.05) except for ET (CaSi). In case of MP50 and MP60 (AAC), the deterioration was significant already at 26 cycles. However, as statistical equivalence of the results from different cycles was not tested for, it cannot be said that ET (CaSi) is frost resistant.
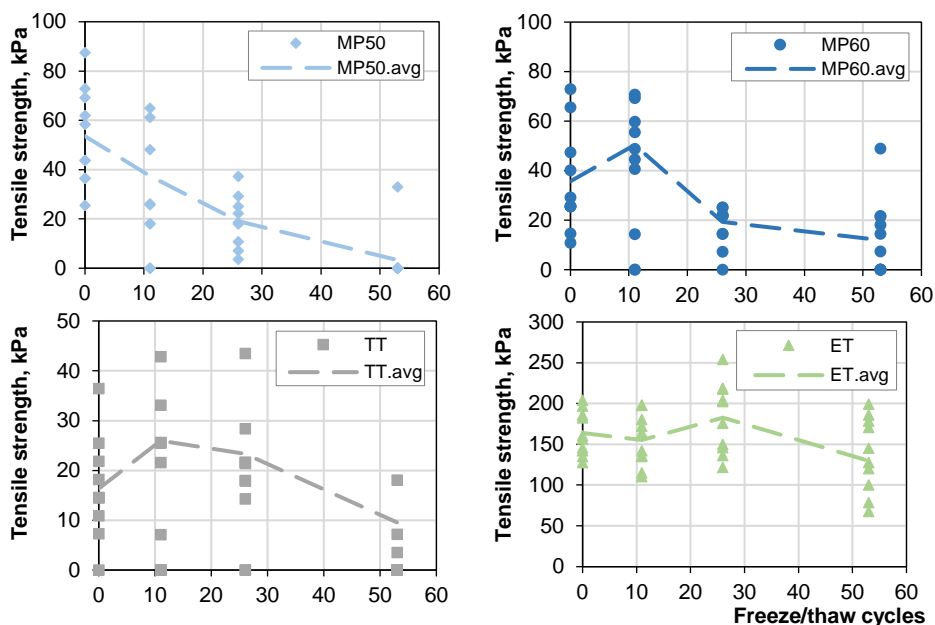
Figure 31   Tensile strengths of drill cores: sample and mean values of 50 mm Multipor (MP50, top left), 60 mm Multipor (MP60, top right), 50 mm Tectem (TT, bottom left) and 50mm Epatherm (ET, bottom right).

2.4 Chapter conclusions

The interior insulation had the expected positive effect: **thermal transmittances were reduced and interior surface temperatures increased**. The studied solutions cut the thermal transmittances 2-3-fold, which shows potential for energy savings. The surface temperatures on the insulation systems were considerably higher than those on the uninsulated reference walls thus improving thermal comfort. However, the metal fasteners penetrating the PIR insulation system had an even lower interior surface temperature than that of the reference wall and they could become a problem in high indoor humidity loads. The fact that in none of the case studies the temperature behind "capillary active" insulation systems dropped below the -5 °C threshold should not be taken for granted and can be attributed to mild winters and favourable wall structures.

In **dryout time of built-in moisture** inherent to the "capillary active" insulation systems is considerable (especially in the case of more vapour tight iQ-T system) and should be accounted for when planning the retrofit. On the other hand, installation works of PIR insulation did not introduce additional moisture to the wall.

In **low indoor humidity loads** (office setting; Vabaduse väljak 7 and 10, Tallinn; moisture excess Δv ≈ 1.5 and 1 g/m³ respectively), the tested solutions performed well and were not close to exceeding the 95%RH performance criteria.

The results from the test with **humidity loads similar to high population density apartments** (Spordi 2a, Kohtla-Järve; moisture excess Δv ≈ 2 to 6 g/m³) showed that 95%RH performance criterion of "capillary active" insulation materials can be exceeded even in a rather mild winter by insulating a favourable masonry wall (2 cavities, one of them insulated) with modest interior insulation thicknesses (60 mm AAC exceeded the criterion, 50 mm CaSi was on the limit). Considering that the outdoor weather can be

colder, wind driven rain more pronounced and thermal resistance of the original wall lower, the 95%$_{RH}$ limit is probably quite hard to fulfil. Therefore, higher allowable humidity/moisture content levels behind the insulation are needed. According to the Finnish mould model, the relative humidity behind all insulation systems was high enough for mould growth initiation, however, the "capillary active" systems are marketed as mould resistant and their glue layer should not leave any space for the mould to grow. Still, it is questionable if using a paper-covered insulation (PIR system) in contact with the original wall is a wise choice.

Climate during the measurement periods was quite mild and all tested walls had some favourable properties. Thus, far reaching conclusions cannot be drawn from these measurements only. To assess the performance in more severe climatic conditions, modelling could be used. However, its results should have to be accurate or at least conservative in its errors – also in the overhygroscopic range.

Freeze-thaw cycling of the insulation systems in the climate chamber study at ca 10%$_{sat}$ and ca -10 °C revealed that the tensile strength of AAC and the expanded perlite insulation systems are reduced. These results show that damage can possibly occur much earlier than the maximum allowable 30%$_{sat}$ saturation degree recommended by WTA Merkblatt 6-5 (Künzel et al., 2012). In the CaSi system, damage occurred in saturated samples. This means that the insulation materials cannot be considered as "frost resistant" by default.

3 Comparison of hygrothermal modelling and measurement results

3.1 General

While the results of previous chapter demonstrated that in case studies in real buildings the insulation solutions performed rather well, they probably did not yet have to endure the most severe climatic loads of their lifetime. Also, the results do not automatically reflect on other masonry structures. To overcome these limitations, hygrothermal modelling can help rapidly test the solutions in different conditions. In this chapter, the measurements are compared to modelling results to check the accuracy of these predictions. There were two main reasons for that comparison:

- to acquire a better understanding of the hygrothermal performance of the internally insulated brick walls;
- to validate the simulation model for future simulations with different initial and climatic conditions as well as with different dimensions of the building envelope.

3.2 Methods

3.2.1 Model setup

Hygrothermal simulation software IBK DELPHIN (Grunewald, 1997; Nicolai, 2008) versions 5.8.1–5.9.6 were used for hygrothermal modelling. To take the phase change enthalpies and freezing point depression into account, the ice modelling (model by Häupl and Xu (2001), implementation by Nicolai and Sontag (2013)) was turned "on" in Vabaduse väljak 10 and climate chamber studies. 2D models were used where appropriate (Vabaduse väljak 7: from the window to the center axis of the column, see Figure 15; Vabaduse väljak 10: from the tie brick to the center of the cavity, see Figure 20) and were also compared to respective 1D models.

3.2.2 Material properties

Material properties from IBK Delphin database were used as much as possible due to them being comprehensively studied and calibrated at TU Dresden. If the specific materials were not present (historic bricks, plasters, mortars, insulation materials etc), best of the matches based on basic material properties (open porosity, absorption coefficient of water, and density that were measured in the laboratory) were selected. The material properties of the unknown materials (e.g. brick) were calibrated against measured temperature, relative humidity and heat flux data within the range of measurement results of the basic parameters.

The main properties of materials used in **Spordi 2a**, Kohtla-Järve study are shown in Table 1. The properties of the peat layer in the interior cavity were based on literature (Jürgenson, 1942; Kuts and Sheiman, 1965; Mikk, 1977; Vinha et al., 2005) and the "blown in cellulose" material in the database. Table 2 gives the respective materials in the Delphin database for **Vabaduse väljak 7**, Tallinn study. At **Vabaduse väljak 10**, Tallinn the Delphin database ID 543 and 569 were used for brick and concrete respectively), PUR foam properties were fine-tuned according to the limits given in its datasheet (based on ID 195; following changes were made: ρ = 39 kg/m³, μ = 39, λ = 0.022 W/(m·K)). The rest of the material IDs from the Delphin database used in models were 464, 143, 424, 21, 230.

Table 1   Spordi 2a, Kohtla-Järve: material properties used for HAM modelling.

Property	RH	Original wall materials				Insulation materials			
		Exterior plaster	Brick	Peat	Interior plaster	PIR	iQ-T	AAC	CaSi
Material ID		145	531	580	148	193	438	596	424
Dry density ρ, kg/m³		1270	1800	150	1800	35	49	126	297
Thermal conductivity λ, W/(m·K)	0%	0.55	0.70	0.07-0.09	0.82	0.020	0.029	0.045	0.067
	33%	0.56	0.70	0.07-0.09	0.82	0.020	0.029	0.046	0.071
	75%	0.58	0.70	0.07-0.09	0.83	0.021	0.029	0.047	0.075
	≥93%	0.59	0.71	0.07-0.09	0.83	0.022	0.030	0.054	0.077
Moisture content w, kg/m³	33%	11	4.8	9.1	2.3	0.49	0.27	1.3	16
	75%	57	6.4	18	9.2	0.96	0.35	3.4	21
	≥93%	75	13	42	25	4.4	1.4	16	26
Vapor diffusion resistance coefficient μ, -	0%	12	25	2	12	400	51	6	11
	33%	12	25	2	12	400	51	6	11
	75%	14	25	2	13	400	51	6	11
	≥93%	14	26	2	13	400	51	6	11
Water absorption coefficient A_w, kg/(m²·h$^{0.5}$)		0.0093	0.055	0.15	0.127	$1.0 \cdot 10^{-7}$	0.013	0.0036	0.39

Table 2   Vabaduse väljak 7, Tallinn: material properties used for HAM modelling.

Material	Equivalent in Delphin database
Brick	Old Building Clinker Hamburg Holstenkamp (ID528)
Aerated concrete	Based on "Lightweight concrete" (ID159) and "Blast furnace slag concrete" (ID29)
Plaster	Lime plaster (ID629)
AAC insulation board (Ytong Multipor)	Mineral Foam Multipor (from 2011), ID595
Glue mortar/plaster for AAC insulation (Ytong Leichtmörtel)	Glue Mortar (For Mineral Insulation Board), ID77
Glue foam for XPS (Ceresit CT84)	Polyurethane-foam, ID195
XPS insulation board (Tycroc TWP)	Polystyrene Board – Extruded (ID189)
Wood	Spruce SW Radial (ID460)
Concrete	Concrete (ID569)
Cork	Insulation-Clay-Cork-FW (ID801)

The models of test walls in the **climate chamber** use material properties from the Delphin database. Exact matches existed for all materials except for the Epasit Epatherm glue and plaster layers, which were selected based on their basic parameters (ρ, ψ, λ, μ, A_w). Also, the definite properties of 0.1 mm PE foil and 22 mm particleboard are not yet known. The effect of particleboard on the insulation systems is largely thermal and its properties in the models were adjusted using the heat fluxes and temperatures.

The thicknesses of the layers were based on measurements of the drill cores. Based on the manufacturer's data, an additional vapour resistance of s_d = 0.18 m was added to the interior surface to take the silicate paint into account.

3.2.3 Boundary conditions

The following climatic boundary conditions were used: indoor and outdoor temperature and relative humidity – measured on site; precipitation, wind speed, wind direction – measured ca 10 km away (at Jõhvi and Tallinn-Harku weather stations of Estonian Weather Service); diffuse and direct radiation – measured ca 150 km away (at Tõravere weather station of Estonian Weather Service). The time step for the data was 1 hour.

In the case of the climate chamber study, the boundary conditions comprised of temperature and relative humidity measured in indoor and outdoor chambers and surface temperatures measured at 5-minute time steps.

3.3 Results and discussion

3.3.1 Hygrothermal study of 4 different insulation solutions under typical apartment conditions (Spordi 2, Kohtla-Järve)

Modelled and measured relative humidity values (which include both thermal and moisture modelling errors) behind the insulation are given in Figure 32 and Figure 33. Further comparisons (temperature, vapour pressure and relative humidity for the whole measurement period) can be seen in Klõšeiko (2014). While modelled and measured temperatures correlated well, discrepancies were found when looking at humidity data. Satisfactory agreement was achieved with the more vapour tight solutions PIR and iQ-T. However, as the simulated RH levels for both CaSi and AAC were considerably lower than measured values during the wetting period, a safety margin of 5-10%$_{RH}$ should be used when analysing future simulation results. Possible sources of deviations include ventilation in the air cavity (air could mix between different wall sections), evenness of peat layer and material properties. As the humidity levels are underestimated during wetting and overestimated during the drying period, hysteresis of materials (which IBK Delphin does not currently account for) is also an apparent culprit.
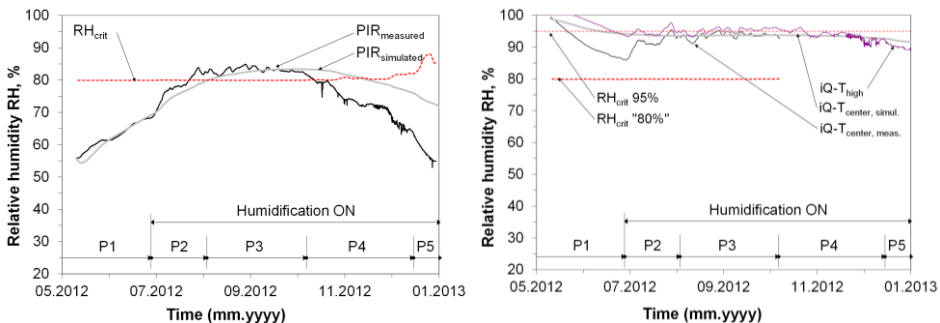

Figure 32   Relative humidity between the insulation and original wall: PIR board (left) and iQ-T (right); periods of humidification.
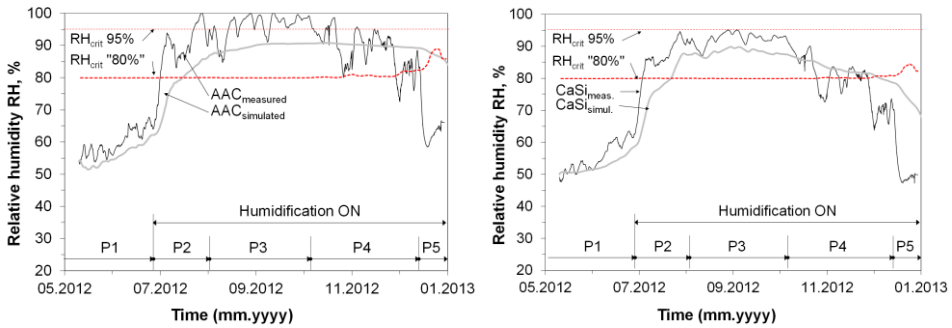
Figure 33 *Relative humidity between the insulation and original wall: AAC (left) and CaSi (right); periods of humidification.*

3.3.2 Hygrothermal study of AAC insulation in an office building (Vabaduse väljak 7, Tallinn)

Because monitoring sensors cover the axis HFP1-TRH3-THR7 best, the measurement and simulation results (Figure 34) from the position of TRH3 are compared here. Different types (temperature, relative humidity, heat flux, water vapour pressure) of data allow for finer assessment of the simulation accuracy.
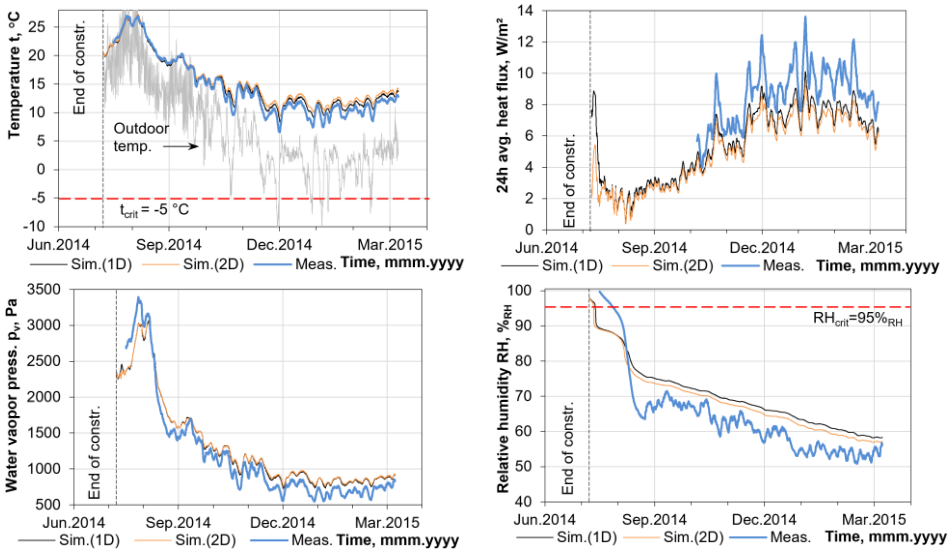
Figure 34 *Measurements compared to modelling results at TRH3 (between interior insulation and original AAC masonry). Reformatted figures from Publication II (changed the axis limits of top left fig.; removed erroneous modelling results starting from 11. March 2015).*

The models were calibrated by iteratively fine-tuning the properties of the historic aerated concrete while comparing simulation results with measurements from all relevant sensors. While good agreement was mostly found, larger discrepancies exist in measured and modelled heat flux data. Although opening of the structure and data from TRH4 gives ground to belief that some ventilation took place in the air cavities, they were modelled as unventilated. This and uncertainties concerning the original wall material properties could cause the differences. Comparison of 2D and 1D models showed that in this position (TRH3) the results from the models differed only slightly. Temperature error of

both models at TRH3 was non-conservative (i.e. the modelled temperatures were ca 3 °C higher at indoor-outdoor $\Delta T \approx 30$ K) and should be considered when doing frost avoidance assessment. Water vapour pressure and relative humidity errors were conservative (lower than measured).

At a hygrothermally more critical position TRH1 (behind insulation at the edge of a concrete column) humidity and temperature coincided better with measurement results and both errors were found to be conservative (i.e modelled humidity higher and temperature lower than measured). Between the old cork insulation and the concrete column (TRH2) an underestimation of temperature and overestimation of water vapour pressures occurred. This resulted in an RH modelling error of +10%RH during the winter period making calculation in this position conservative. Unreliable material data for existing cork insulation could be the possible cause for errors there.

3.3.3 Hygrothermal study of PUR foam and CaSi boards in an office (Vabaduse väljak 10, Tallinn)

Results from the models which achieved the best fit and positions that are most relevant to the assessment criteria are presented here. Figure 35 shows data from TRH2 (between CaSi and tie brick) and TRH4 (between CaSi concrete bond beam). Relative humidity is given as it integrates the errors in thermal and moisture calculations.

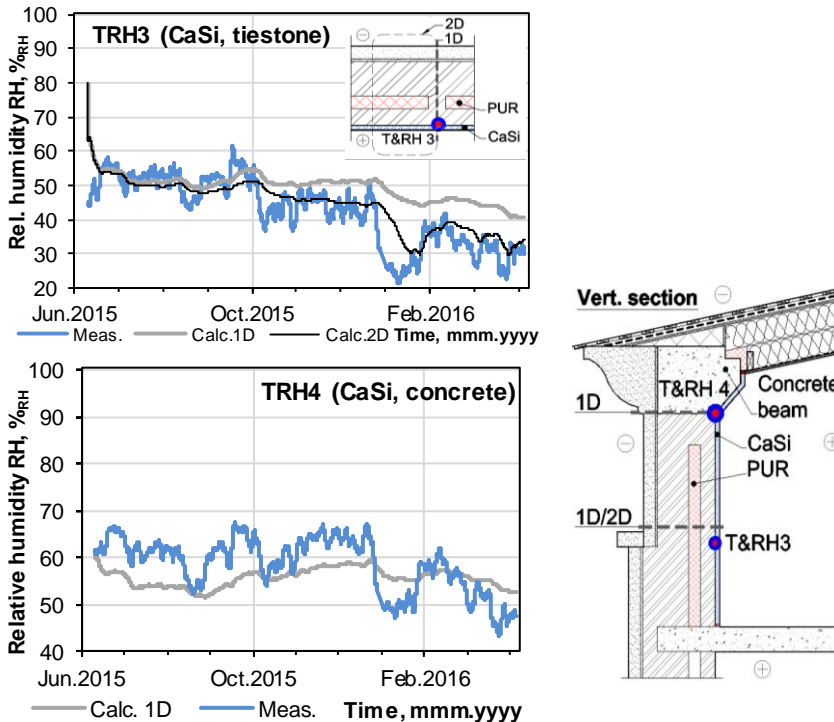Figure 35   *Comparison of measured and modelled relative humidity levels at TRH3 (between CaSi and tie brick; top right) and TRH4 (CaSi insulation on top of concrete; bottom left).*

The agreement of calculated and measured temperatures (TRH3 2D model; TRH4 1D model) was within ± 1 °C for most of the year with an overestimation of temperatures by 2 to 3 °C in summer (possibly due to deficiencies in solar modelling of the south facing

wall). TRH3 1D model exhibits too low temperatures which results in higher than measured RH. Like in previously described studies, the modelled RH values exhibit less fluctuation in all cases – again, as wetting periods are underestimated and drying periods overestimated, this could point at hysteretic effects currently not considered by the modelling tool. 24h avg. heat fluxes in masonry section achieved less than ±1 W/m² (ca. 5–10%) difference for most of the heating period using 2D model; in case of 1D models, the errors were 4–8 times higher.

Beside the lack of hysteretic modelling other possible sources of errors could be: the material data (limestone as a location specific and inhomogeneous material; only basic parameters were measured for brick), unknowns concerning the actual wall structure, wind driven rain modelling, solar radiation modelling. At concrete beam (TRH4) only 1D model through concrete was used, while the location also has interaction with the brick layer and the exact dimensions of the cornice could not be determined.

The correlation between measurements and modelling was deemed satisfactory. For performance assessment of the CaSi insulation the 1D model of the masonry section might be good enough as the relative humidity was generally overestimated during the comparison period. However, as wind driven rain could cause the accumulation of moisture in the exterior masonry leaf, a 2D model is also necessary.

3.3.4 Hygrothermal and mechanical study of AAC, CaSi and expanded perlite systems in climate chamber

As the relative humidity inside the glue layer was over the measurement range of *RH* sensors for most of the study, the comparison can be given for the initial phases (Figure 36 bottom right). The trend coincides with previous studies where measured relative humidity levels exceeded the modelled values in higher hygroscopic range and when sharp rises were concerned – again, this can point at hysteretic effects which the modelling tool currently does not account for.

Gravimetric measurements give a more accurate indication of moisture content of the material compared to RH measurements. Almost all hygrothermal models underestimated the moisture content during humidification periods. Typically, 1.5–3-fold differences occurred in the glue and exterior parts of the insulation layers. The exception was cement fiberboard (Figure 36 top left), where TT and ET models achieved best correlations. Theory of underestimated moisture content is asserted by freeze thaw-cycling where the delay in temperature drops and rises is not apparent in modelled data (see Figure 29). It has to be born in mind that the detailed glue and plaster material data of ET system was not available and it influences the modelling results.
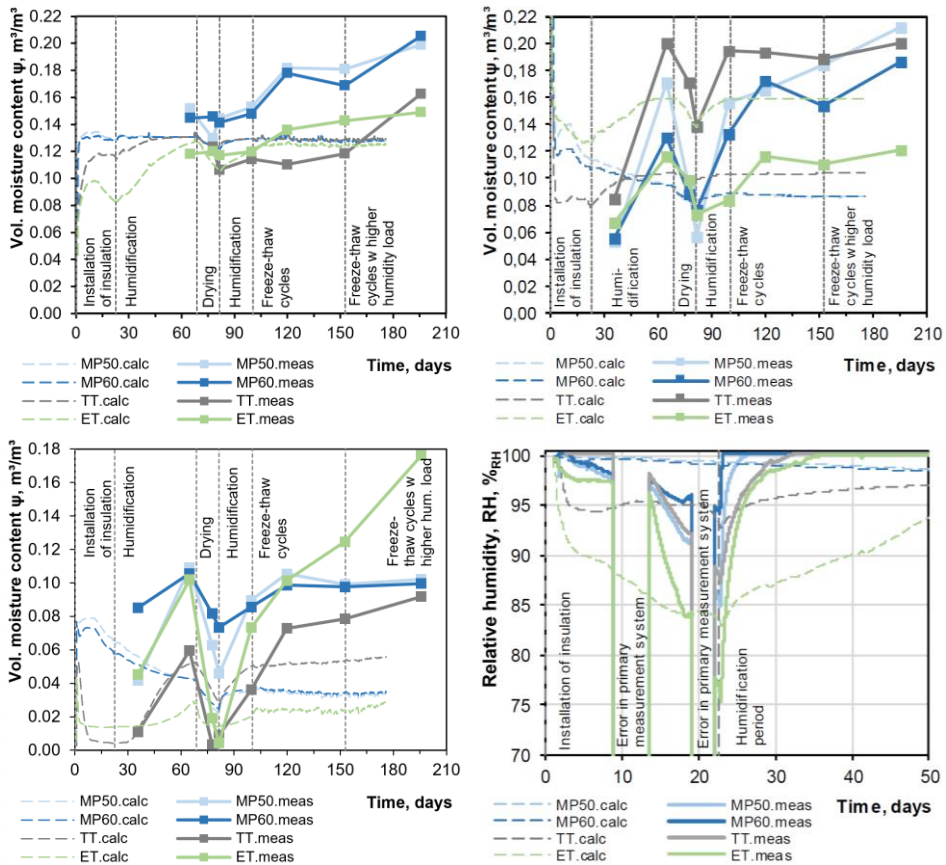
Figure 36   *Gravimetrically measured volumetric moisture contents in different parts of drill cores and comparison to modelling results: cement fiberboard (top left), glue mortar (top right) and exterior part of insulation (bottom left). Bottom right: measured and modelled relative humidity levels inside the wall (glue layer) during the first stages of the test (readings were over range for the rest of the study).*

NB1: measured vol. moisture content of glue layers was calculated using respective densities from the Delphin database; NB2: detailed hygrothermal material data for ET glue and plaster layers was not available and their modelling results should be treated with caution. NB3: compared to Publication IV the measured vol. moisture content of cement fiberboard and exterior part of insulation have been recalculated according to measured dry densities as in Publication VI instead of using Delphin database values.

It is certain that errors were made sampling the data during this study (sensor accuracy, flaws in cutting, weighing, drying, etc). However, as large deviations, repeated sampling, duplicated sensors and previous studies show, the trend is probably still the same. Beside measurement errors, the other possibility is that the model might have its weaknesses. Deviations in material production might induce errors. Janssen et al. (2015) raised doubts about the Delphin's approach to over-capillary moisture range, according to which, the slow secondary phase in capillary absorption experiments is caused by low capillarity instead of the widely accepted concept of air entrapment. The latter held true in experiments by Janssen et al. (2015). However, in this study, only AAC (MP50 & 60) reached such moisture content, while the issues with correlation are present with other

materials too – thus, it cannot be the reason for deviations between modelling and measurements. Dynamic effects too have been identified influencing the hygrothermal processes (Janssen et al., 2016), but are not yet reliably described by the models. Finally, the methods and experimental dataset for deriving the moisture dependent liquid conductivity (K_l) function might be the cause of inconsistencies as indicated by Binder et al. (2010, 2013, 2014).

3.4 Chapter conclusions

The modelling accuracy of the "capillary active" insulation materials was deemed satisfactory in the lower hygroscopic range, however, above ca 90%$_{RH}$, the modelling results begin to underestimate humidity levels. Similar discrepancies are also apparent in a studies by De Mets et al. (2017) and Jensen, Bjarløv, et al. (2020). In the latter case an automated script was used to calibrate the models to the measurements, but RH between CaSi and original wall was still underestimated by ca 10%$_{RH}$ (while measurements indicated ≈ 100%$_{RH}$).

Busser et al. (2019) analysed dozens of studies comparing numerical predictions to experimental data and found that especially if hygroscopic materials (including calcium silicate and aerated concrete) are used, current models have issues with predicting mass transfer kinetics, especially with varying load. The results also showed that models which take hysteresis effects and temperature dependency of the moisture storage capacity into account agree better with measured values. Hysteresis in this context means that the equilibrium moisture content depends not only on the ambient conditions (temperature and relative humidity), but also on the history – desorption processes have higher equilibrium moisture content than adsorption. For example, Mualem (1984) and Pedersen (1990) proposed and applied methods to account for the phenomenon in HAM modelling. Busser et al. (2019) also suggested that some other phenomena (advection of air, nonequilibrium state and microscopic effects) are currently not considered and could explain the discrepancies.

In the climate chamber study – while having the most reliable material data, controlled boundary conditions and various measurement methods – the discrepancies are most apparent, as the overhygroscopic moisture range is concerned. There, the moisture content levels in the insulation glue and cold side of the insulation board are underestimated roughly 2-fold. The latter becomes a reason for concern when freezing temperatures are allowed – the modelling results can leave an impression that the maximum relative humidity or moisture saturation degree is not exceeded, while in reality it might be. It will also affect the accuracy of how the performance of neighbouring layers and components are modelled – for example, the rate of wood decay in beam ends can be underestimated too.

4 Optimizing the liquid and vapour conductivity curves based on an experimental dataset which includes CCR test results

4.1 General

Previous research by Binder et al. (2010) and results in chapter 3 indicated that in over-hygroscopic moisture content range, the modelling results can show much lower moisture content than there actually is – should such modelled values be used to assess e.g. frost resistance, the errors would be non-conservative. Usually, water uptake and drying test are used to determine the water vapour and liquid conductivity curves in the higher moisture content range (Krus, 1996; Scheffler and Plagge, 2010). Assessing the share between the flows in these cases is based on assumptions as both have the same direction and are subjected to rather extreme conditions (water contact and full saturation). To gain more information on this, Binder et al (2010, 2013, 2014) proposed a capillary condensation redistribution (CCR) test. There, a condensation plane inside a material sample is caused by a temperature difference while the mass change and moisture profile are monitored (see Figure 9).

Taking the CCR test results into account has so far been a step-by-step iterative process (Binder et al., 2014), which adds to the already existing high work load when conducting the material characterization. This chapter investigates the application of a generative optimization tool GenOpt to counter that and to increase the reliability of the modelling results.

This chapter presents the optimization tool from Publication V and updated methods, reference data and results from Publication VI. The main changes compared to Publication V are the use of monotonically decreasing vapour conductivity functions and the inclusion of CCR data for CaSi from Hirsch et al (2020) (now the whole CaSi dataset is measured from the same material). To show the effect of including the CCR-test in the reference dataset, the "CCR-optimized" material data is now compared to the functions optimized without the CCR test instead of the properties from the Delphin database (to exclude the influence of different users and tools and which created them). The material functions optimized without the CCR test presented in this chapter still exhibited similar hygrothermal performance as the respective files in the Delphin database.

4.2 Methods

The proposed workflow incorporates optimization tool GenOpt (Wetter, 2001) and hygrothermal modelling software IBK Delphin (Grunewald, 1997; Nicolai et al., 2009) to search for the best fit of the water vapour and liquid conductivity curves of interior insulation materials based on experimental data from material tests. This work is a further development of the tool by Freudenberg et al. (2017) used to calibrate hygrothermal simulations according to measurements.

The operating principle of the optimization tool is given in Figure 37. Moisture dependent water vapour ($\log(K_v(\psi))$) and liquid water conductivity ($\log(K_l(\psi))$) curves are defined by having a certain number of points at fixed moisture content values while GenOpt varies their conductivities. As GenOpt handles all optimizable variables independently, the Python script checks if the liquid conductivity curve is monotonically increasing. In the case of vapour conductivity, the curve should increase until point i and is expected to fall from point j (both can be defined). Penalties are applied if previous conditions are not met.
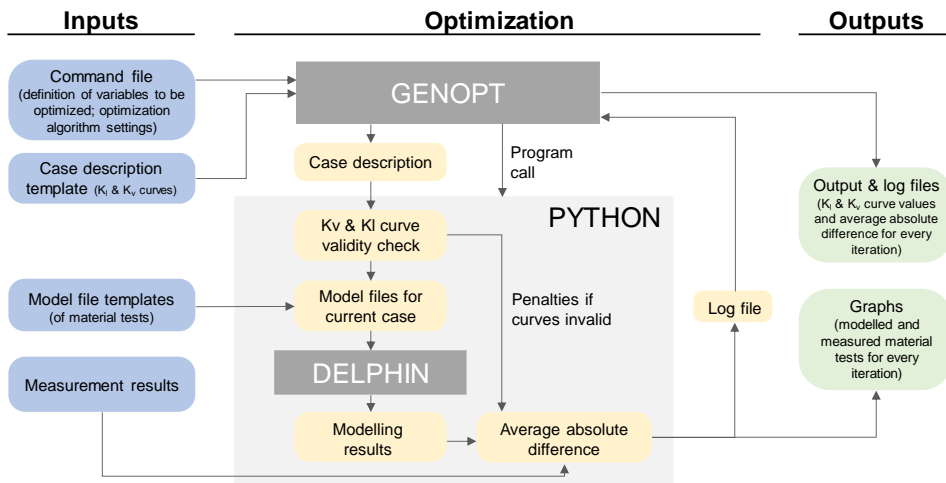
Figure 37   Operating principle of the optimization tool based on GenOpt, Python and Delphin 5.9.

This chapter presents optimization cases with autoclaved aerated concrete (AAC; mostly large macropores and fine capillaries) and calcium silicate (CaSi; mostly fine capillaries) insulation materials as examples. The tests currently incorporated in the optimization tool are: capillary condensation redistribution (CCR; moisture content profile at the end of the experiment; avg. moisture content over time), drying (avg. moisture content over time), wet cup (moisture flux at wet cup boundary conditions) and water uptake tests (the latter was currently used for CaSi). Table 3 summarizes the sources of material test data that were used to characterize the materials described in this chapter. The first point of the K_v curve was fixed to conductivity determined from dry cup measurements. The vapour conductivity curve was forced to be monotonically decreasing and vice versa for the liquid conductivity curve. The end of the liquid conductivity curve was set according to the saturated flow test. Optimization limits were selected wide enough to keep the process unbiased. The average absolute difference between the measured and modelled data is used as a cost function that GenOpt tries to minimize using Particle Swarm Optimization combined with the Generalized Pattern Search method implementation of the Hooke-Jeeves algorithm (GPSPSOOCCHJ)(Wetter, 2016). Weighting factors were applied to the tests to take different scales into account and to keep the optimization balanced. Another set of material functions was optimized without the CCR test, which resulted in a similar hygrothermal performance as the respective files in the Delphin database.

Finally, the CCR-optimized and "conventional" material files were used to model two different studies (Spordi 2a, Kohtla-Järve, see section 2.2.1 and the climate chamber study, see section 2.2.4) and are compared to the respective measurement results.

Table 3   Source of material test data for conductivity function optimization.

Test	Usage	Source	
		AAC	**CaSi**
Desiccator test, pressure plate test	Moisture retention curve of the material	TU Dresden IBK lab data for material ID595	TU Dresden IBK lab data for material ID571
Drying test	Reference for liquid and vapour conductivity optimization		
Water uptake test*	Reference for liquid and vapour cond. optimization (high moist. cont.)		
Saturated flow test	Liquid conductivity near saturation		
Dry cup test	Vapour conductivity of dry material	In-house measurements, TU Dresden IBK lab data for ID595	In-house measurements, TU Dresden IBK lab data for ID571
Wet cup test	Reference for liquid and vapour conductivity optimization		
CCR test	Reference for liquid and vapour conductivity optimization	Binder et al. (2014)	Hirsch et al (2020)

* – water uptake test was used for optimization of CaSi

4.3 Results and discussion

4.3.1 Optimization results

The optimized material data (Figure 38 row 1) shows notably reduced liquid conductivity in the moisture content range of 0.01–0.15 m³/m³ compared to the curves optimized based on a conventional experimental dataset. Similarly to Binder et al. (2014) and Hirsch et al. (2020) an ideal combination of material functions that would fit all the reference tests (Figure 38 rows 2–4) could not be found – the main contradiction being between the CCR and drying tests and, in the case of the slightly hydrophobic dry AAC, water uptake too. Moisture content levels in the drying test are overestimated by the CCR-optimized material functions once the moisture content levels reach those described by the CCR test. This could be due to vapour conductivity actually being higher, but being restricted to be monotonically decreasing by the optimization tool.

As described by Scheffler (2008), the drying test helps to describe the conductivity curves after transitioning from the initial linear mass decrease phase (which is characterized by surface mass transfer coefficient and boundary conditions). The results are thus presumed to be more reliable in the range between 0–0.2 m³/m³ and near saturation, where reference data is available. The decrease in mass change rate during the drying test indicates the critical moisture content where a significant change in liquid conductivity takes place (Vos and van Minnen, 1966). Based on the drying test, the approximate values are 0.3 m³/m³ and 0.2 m³/m³ for AAC and CaSi respectively (although high air velocity exaggerates them). Moisture content at the end of the CCR test for both AAC and CaSi are below these values, which agrees with the shape of the moisture content profiles provided in the literature too (Binder et al., 2010, 2013, 2014; Hirsch et al., 2020) – a more uniform distribution would be expected should the opposite be true.

Here – while not being a universally applicable approach – more preference was placed on achieving better correlation with the CCR test than the drying experiment, as the former describes the behaviour of "capillary active" insulation in actual usage scenarios and at performance limits better. Furthermore, in sense of possible moisture and frost damage in the interior insulation system, the error caused by failing to reproduce faster drying would overestimate the risk, while failure to capture the wetting processes (akin to the CCR test) would leave possible risks unnoticed.
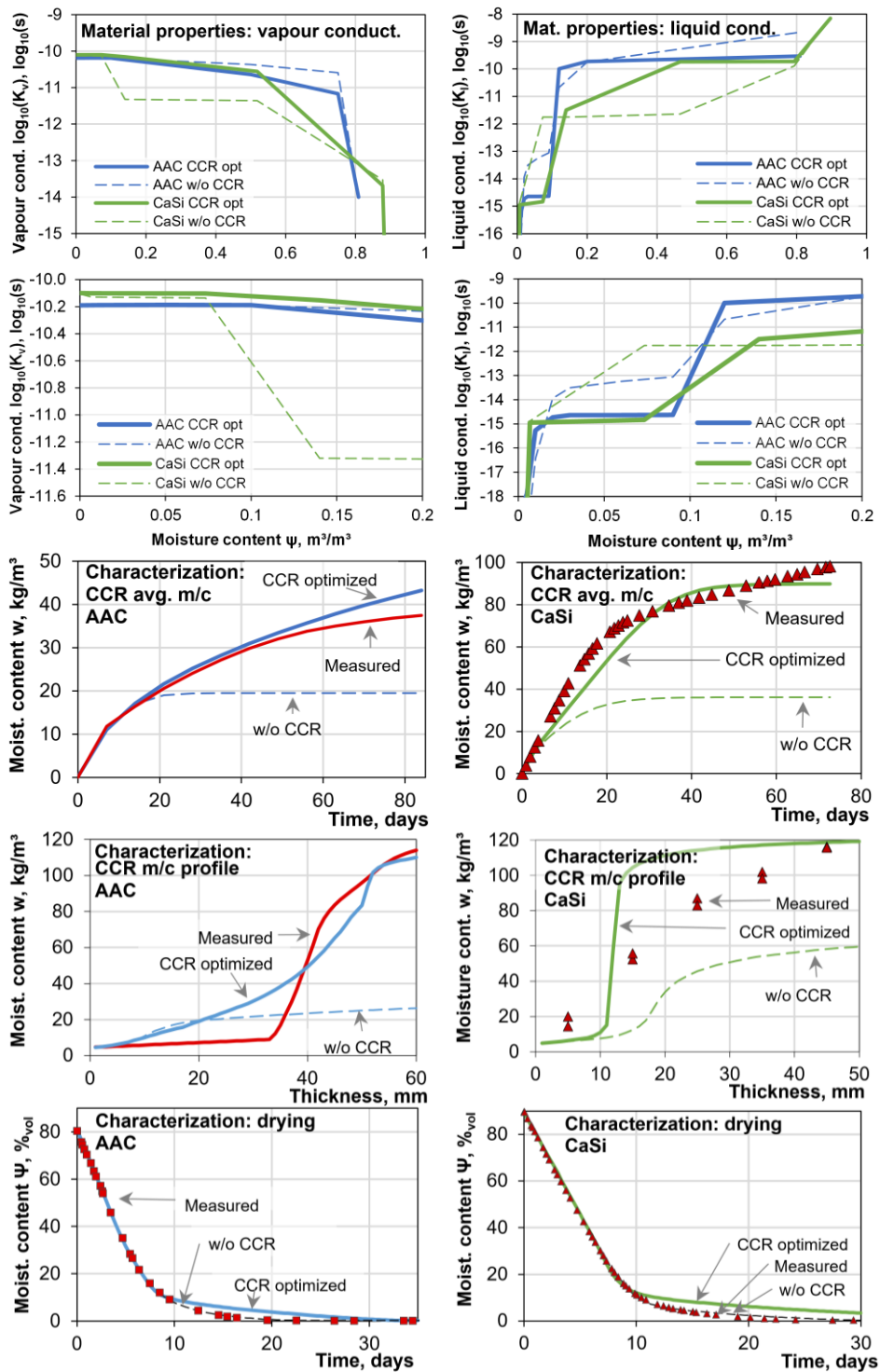
Figure 38   CCR-optimized and conventionally characterized material properties ("w/o CCR") used in this study (top 2 rows) and some of the material tests used as a reference for optimization (bottom 3 rows). Figures and data from Publication VI.

4.3.2 Comparison to measurements

In a laboratory study with a high moisture load (as described in section 2.2.4), the moisture content in the cold (exterior) part of the AAC and CaSi insulation boards increased about 2.5–3 times and therefore dramatically improved the correlation with measurement data (see Figure 39). Similarly to the drying test described in section 4.3.1, the moisture content levels during the dryout phases are overestimated using the CCR-optimized material files. The deviations in the courses of modelled and measured m/c of the whole AAC layer (Figure 39 bottom left) at the final phases of the experiment can be explained by the loss of capillary contact between the insulation and base layers (also shown by the loss of tensile strength in Figure 31). It should be noted that while CaSi achieves quite good correlation with measured average moisture content of the whole insulation layer (Figure 39, bottom right) and during the initial wetting phases in the cold layer (Figure 39, top right), it still fails to capture the increasing trend during the second wetting phase. This probably hints at overestimated capillary conductivity at those moisture content levels and redistribution of moisture within the insulation layer (similarly to Figure 38, row 3 right). This implies a risk of underestimating the moisture content in further modelling at similar conditions.

In the case of more realistic moisture loads in a real building (as described in section 2.2.1), the difference of RH on the cold side of the insulation was small (conventional vs CCR-optimized properties) and did not improve nor worsen the correlation between measured and modelled data noticeably (see Figure 40). The discrepancies in the second study can be attributed to a lack of detailed material data, but also to hysteresis and dynamic effects (Bianchi Janetti and Janssen, 2020; Janssen et al., 2016) in ad- and desorption processes.

Figure 39   Comparison of measurement results to modelling with CCR-optimized and conventionally characterized material properties ("w/o CCR"). Study 1 (high moisture content; climate chamber), avg. moisture content of cold side of insulation (top row) and avg. of the whole insulation layer (bottom row). The CCR-optimized material shows about 2–3-fold increase in max. moisture content and coincides better with measurement data. Measurements from Pub. IV, modelling from VI.

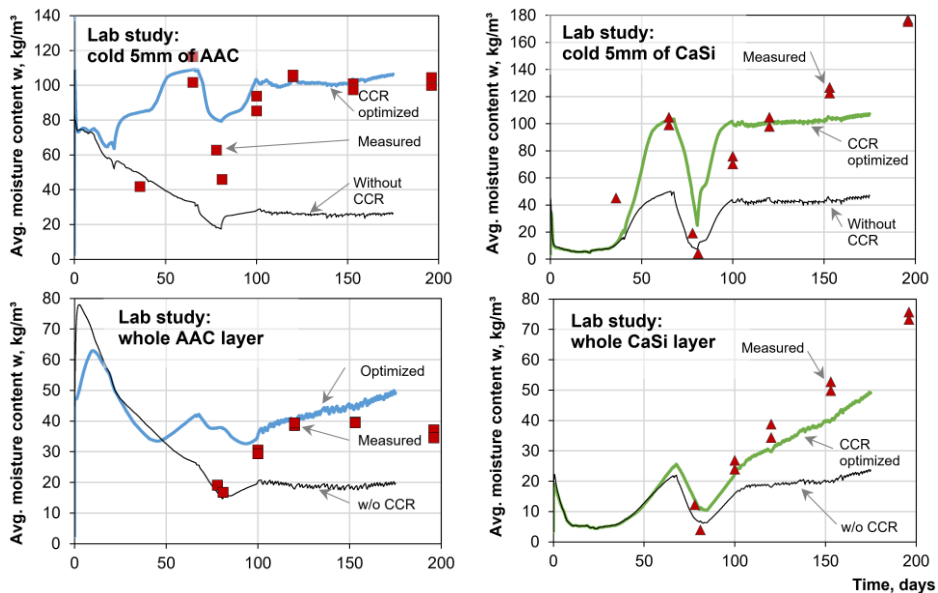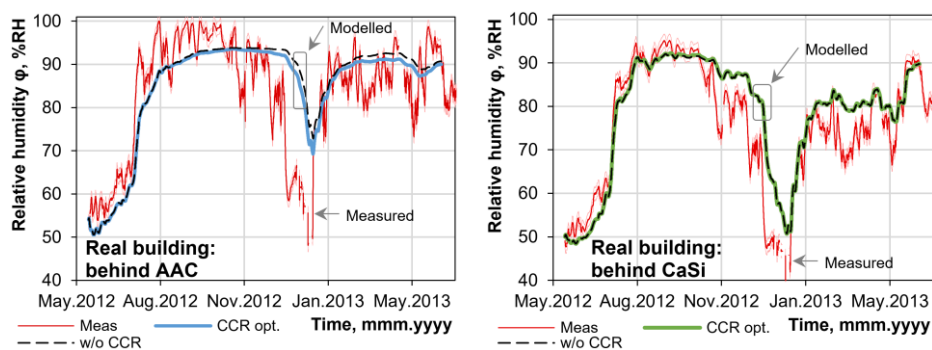*Figure 40   Study 2 (medium moisture content; real building), relative humidity in cold side of insulation: comparison of measurement results to modelling with optimized and conventionally characterized material properties. No notable differences between modelling results. Measurement data from Publication I, modelling from VI.*

It is worth bearing in mind that the CaSi materials used in the studies were not the same specific product as optimized in this chapter, while the CCR-test data for the AAC material could have been measured using a different product. However, they all belonged to their respective families of similar products and the improvement to the modelling ability to reproduce higher moisture contents in study 1 outweighs the possible uncertainties in their intended use in this thesis – to model the materials as interior insulation solutions where higher moisture content levels can also occur.

4.4 Chapter conclusions

The proposed material characterization tool proved capable of creating the conductivity curves using different experimental datasets for two "capillary active" insulation materials. Although the variation limit boundaries were kept large and different initial values and curve resolutions were used for optimization, the resulting optimized curves were in a relatively similar range.

Still, as the CCR test data for AAC was taken from literature and the exact tested products and boundary conditions were not disclosed, it is quite possible that the CCR and the rest of material data were measured from different products. This may introduce mismatches in moisture retention curves and the optimization algorithm trying to compensate for it through conductivity curves.

Comparison with case study results show that for both AAC and CaSi, the optimized materials show better correlation to measured data in the high moisture content range (especially so for AAC; CaSi still underestimated the moisture content at the cold side), hinting at the value of the CCR test. The improvements in better reproducing non-isothermal wetting phase come at a cost though – the moisture content levels in lower overhygroscopic drying phases are now overestimated. It is acceptable in current intended use but should be kept in mind when interpreting the modelling results. In hygroscopic range, the optimized properties perform similarly to their default counterparts – as Delphin has shown to be quite reliable in that range, it could be considered a good result for the algorithm.

These results underline that there are still many unknowns when dealing with overhygroscopic moisture contents – caution is advised when drawing far-reaching conclusions from the modelling results in that range. As the CCR and drying experiments

follow different moisture retention curves (ad- and desorption respectively) but are currently modelled and optimized according to desorption curve only, there are bound to be inherent errors introduced by that approach.

Future work could include applying it to a modelling tool which incorporates hysteretic modelling, developing a better user interface, a wider experimental base for optimization and defining stricter rules/boundaries for the conductivity curves. Currently, the results are less reliable above moisture content levels reached in the CCR test – the share of liquid and vapour transfer is hard to determine due to the drying test having both fluxes in the same direction and being useful as a reference after first drying phase. Also, the CCR test could be enhanced with relative humidity sensors in the samples to gain more reference data from the hygroscopic range.

5 Parametric modelling with long-term dataset

5.1 General

In their preliminary example comparisons Binder et al (2014) and Hirsch et al. (2020) along with results in chapter 4 indicated that the modelling using conventional material characterization underestimated moisture content levels, especially near the performance limits which might not be reached in laboratory or in-situ tests that have been used to calibrate the HAM models. This could mean that frost or moisture damage risks might be left unnoticed and raises the question whether the conclusions drawn from previous modelling in the high moisture range while using a conventional material characterization are still valid.

By using a parametric study of different interior insulation solutions and a long-term real weather dataset (a preferable choice over Reference Years or mean years that have been typically used in previous studies), this chapter has two main aims:

- To quantify the difference in the modelling results caused by conventional and CCR-optimized material characterization processes.
- To assess the suitability of vapour open and vapour tight insulation approaches in cold climate and to determine if the "capillary active" vapour open materials with corrected liquid conductivity curves still have the advantages as described in the literature.

5.2 Methods

5.2.1 Calculation models

IBK Delphin 5.9.6 (Grunewald, 1997; Nicolai et al., 2009) was used for HAM modelling. Delphin uses the implementation of the ice model by Nicolai and Sontag (2013) to take the phase change enthalpies and freezing point depression (model by Häupl and Xu (2001)) into account.

A 51 cm thick masonry wall was selected to represent a typical Estonian mass masonry structure. Thinner walls would have a lower thermal resistance and moisture capacity (hence making them more critical), however, they are not common. Thicker walls, in contrast, are less critical and usually have an air cavity, which further reduces the effect of wind driven rain.

Figure 41 describes the structure of models used in the current study as modelled in IBK Delphin. Two 1-dimensional base models were created: a section through brick layer, intersected with a vertical mortar joint (base model B), and a section through a horizontal mortar joint itself (base model M). Two 1-dimensional models were chosen instead of a single 2D model due to modelling speed, which also allowed more variations in parameters to be included. Preliminary modelling showed that the difference in results between the 1D and 2D models was small, which corroborates the findings of Vereecken and Roels (2013).

Two different insulation approaches were considered – vapour open capillary active autoclaved aerated concrete (AAC) & calcium silicate (CaSi) and a more vapour tight polyisocyanurate (PIR) insulation with a 9 mm gypsum board on top of it as a finishing layer. The vapour open systems were presumed to have hydraulic contact with the original wall as glue mortar is used for installation, while a 3 mm air cavity was assigned between the original wall and the PIR insulation system (to account for unevenness of

the original wall). According to the manufacturer's guidelines (Heße et al., 2018), the old interior plaster was retained under the insulation layer.

The thicknesses of the insulation layers (30 mm PIR, 60 mm AAC and 90 mm CaSi) were selected to represent real products available on the market while achieving similar thermal resistance. The largest differences were between the CaSi and PIR: the thermal resistance of the PIR system was ca 1/10 higher than that of the CaSi one, while thermal transmittances of the whole walls differed by ca. 5%. To minimize the frost risks in cold climates, the layers were intentionally thin.
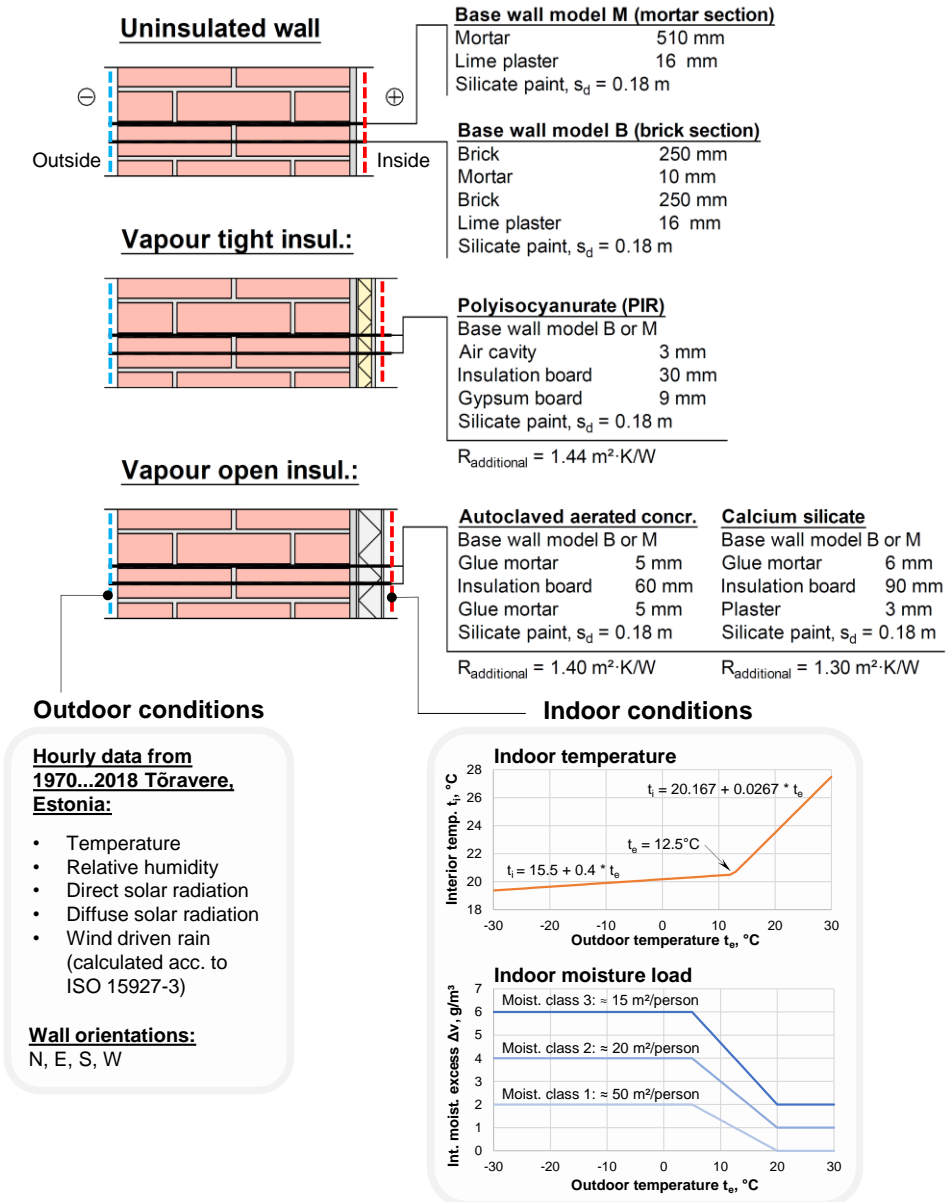

Figure 41   Schematic of the 1D wall models and their boundary conditions used in IBK Delphin.

5.2.2 Material properties

Table 4 gives the overview of basic material properties used for modelling in different combinations. Three different bricks were selected from the Delphin database to represent historic Estonian bricks based on in-house measurements of their basic parameters (type, porosity, vapour conductivity and water uptake coefficient). The selection of 3 lime-cement mortars covered different historic mortars in the Delphin database.

Three interior insulation solutions with different approaches were selected:

- 2 vapour open solutions advertised as "capillary active":
  - Autoclaved aerated concrete (based on data for IBK Delphin material ID 643/595).
  - Calcium silicate (based on data for IBK Delphin material ID 571).

  Both had 2 versions: one being the result of conventional material characterization and another which included the capillary condensation redistribution test in the calibration of its liquid and vapour conductivity functions. The curves were created using the tool described in chapter 4 and are given in Figure 38 (top row).

- "Vapour tight" material without liquid conductivity: polyisocyanurate (PIR) board (without diffusion tight coatings) with a gypsum board applied on top (id 599). The insulation material was based on material ID 194 with a modified vapour diffusion resistance coefficient μ = 60 and a thermal conductivity of λ_{dry} = 0.023 W/(m·K).

Table 4 Basic material properties of materials used in modelling.

Material name	ID in Delphin	Density ρ, kg/m³	Thermal conductivity λ_{dry}, W/(m·K)	Porosity ψ_{por}, m³/m³	Water vap. diffusion resistance factor μ, -	Water uptake A_w, kg/(m²·s$^{0.5}$)
Brick Bernhard	97	2060	1.00	0.25	19	0.100
Historical Brick (Cluster 4)	33	1710	0.80	0.33	8.3	0.278
Lime Sand Brick (traditional)	153	1810	1.00	0.34	40	0.052
Lime cement mortar	143	1570	0.70	0.41	11	0.176
Lime cement mortar	717	1878	0.80	0.29	37	0.036
Lime cement mortar (low cement ratio)	718	1739	1.05	0.34	28	0.494
Lime Plaster (historical)	148	1800	0.82	0.30	12	0.127
Glue Mortar	407	1472	0.92	0.44	38	0.008
Inside Plaster	656	1279	0.31	0.52	10	0.082
CaSi insulation		270	0.069	0.91	2.5	1.13
Glue Mortar	77	830	0.16	0.69	13	0.003
AAC insulation		99	0.044	0.96	3	0.006
PIR insulation		32	0.023	0.95	60	-
Gypsum Board	599	745	0.18	0.72	11	0.179
Air gap (3 mm)	13	1.3	0.03	1	1	-

5.2.3 Interface contact resistances

Derluyn et al. (2011) obtained the interface resistances R_{if} of $1.25 \cdot 10^{10}$ m/s (dry cured mortar) and $2.5 \cdot 10^{10}$ m/s (wet cured mortar), while Vereecken & Roels (2013) used $2.5 \cdot 10^{10}$ m/s and $5 \cdot 10^{10}$ m/s respectively in their simulations. Later, Vereecken and Roels (2015a) studied the hydraulic contact resistances in the case of capillary active insulation glue and concluded that constant resistances do not represent measurements very well and recommended values depending on moisture content. Calle et al. (2019) determined that hydraulic lime-brick interface resistances are an order of magnitude lower than the cement mortar-brick ones available in literature. Zhou et al. (2020) conducted an experiment on the water uptake of a masonry section and determined that the interface resistances between brick and mortar were in the range of $3.5 \cdot 10^{9}$ to $8 \cdot 10^{10}$ m/s – this shows that the interface resistances can vary by several orders of magnitude even on different interfaces of the same masonry.

In this study, in order to simplify the modelling, interface resistance of R_{if} = $2.5 \cdot 10^{10}$ m/s is compared to the perfect hydraulic contact (R_{if} = 0 m/s). Resistances are applied to brick-mortar and brick-plaster interfaces. The choices made here are meant to reflect the impact of different parts of the interface resistance spectrum and should not be considered as the only possibilities.

5.2.4 Boundary conditions

A 49-year period of historical weather data from Tõravere, Estonia was used as **outdoor climate**. According to the Köppen-Geiger classification, Estonia belongs to humid continental climatic zone (Dfb). Outdoor temperature, relative humidity, wind speed, wind direction, short-wave radiation and wind driven rain were assigned as climate conditions. The overview of them is given in Figure 42 and Figure 43.

Hourly values of wind driven rain (WDR) imposed on the wall were calculated according to ISO 15927-3 (2009). The parameters for WDR calculations were mostly fixed: height: 7 m, terrain category: III (suburban and industrial areas), topography coefficient CT: 1 (building not on an uphill slope), obstruction factor O: 0.8 (obstacles of similar size 80–100 m from the building, no wind funnelling). Wall factor W was varied as 0.5 (top part of a multi-storey building without eaves) and 0.75 (local maxima). Yearly mean wind driven rain rose (W = 0.5) is given in Figure 43 (center). If the air temperature was below -2 °C, the precipitation was deemed as snow and discarded.

The climate data used for the modelling starts on the 1st of January 1970. The initial temperature of the wall was 12 °C and 80%$_{RH}$ was assigned on all layers.

The **indoor climate** model was based on the analysis of 190 apartments with central heating (Ilomets et al., 2018). The indoor temperature model was based on the indoor climate of Estonian brick apartments and it corresponds to the lower limit of Fig. 7 in Ilomets et al. (2018). The indoor temperature and moisture excess dependence on outdoor temperature is given in Figure 41 (bottom right). The different moisture excess (moisture load) levels based on Figure NA.3 from EVS EN ISO 13788 (2012) were varied and are shown in Figure 41 (bottom right). Figure 41 (bottom right) also gives the corresponding average occupancy rates based on Fig. 9 in Ilomets et al. (2018).
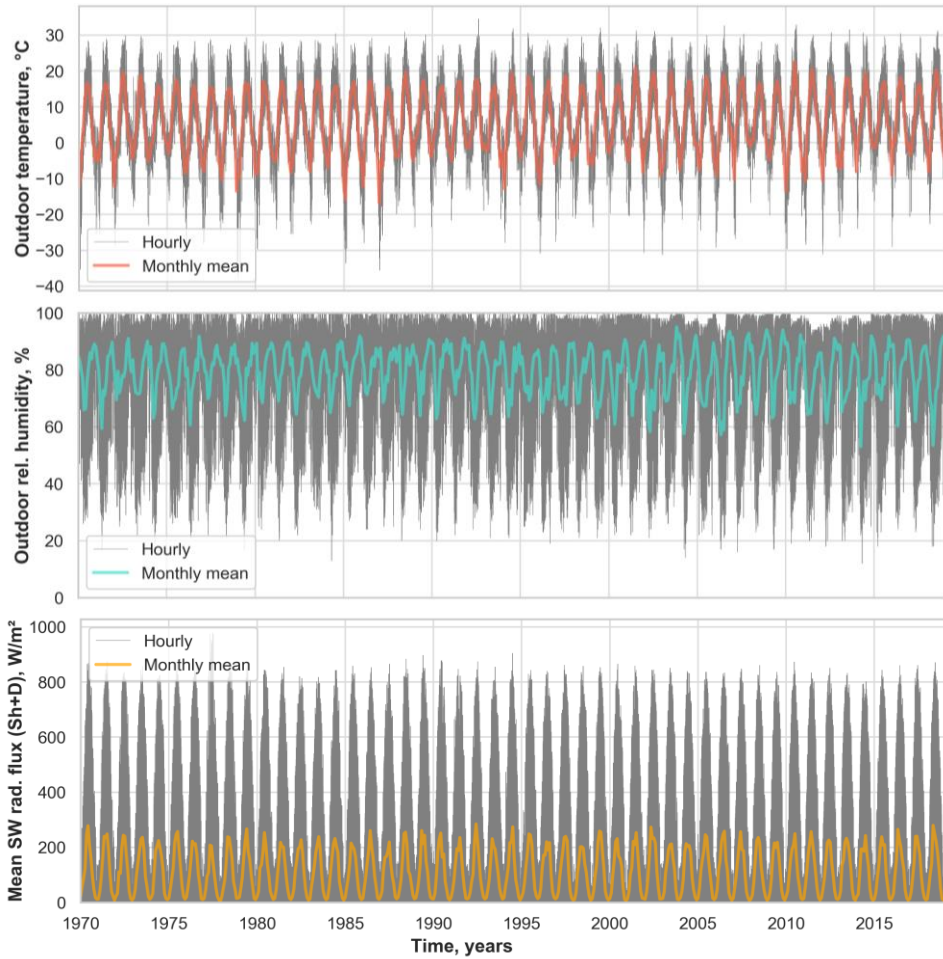
Figure 42   Outdoor boundary conditions: hourly and monthly mean temperature (top), relative humidity (middle) and total shortwave (direct + diffuse) radiation on a horizontal surface (bottom).
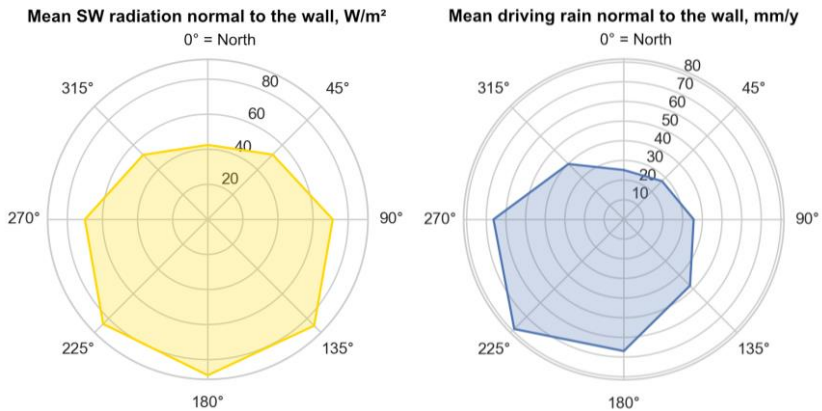

Figure 43   Mean shortwave radiation (direct + diffuse; left) and yearly mean wind driven rain roses (calculated according to ISO 15927-3:2009, wall factor W = 0.5; right).

5.2.5 Summary of variations

The summary of all varied parameters is given in Table 5. Combinations of them resulted in 3455 different models. No weighting of the variations was done as the distribution of the parameters in real life is not known.

Table 5   Variations of parameters used in the parametric study.

Parameter	Variations
Brick	• Historical brick (ID 97) • Brick Bernhard (ID 33) • Lime sand brick (ID 153)
Lime-cement mortar	• Lime cement mortar (ID 143) • High cement ratio (ID 717) • Low cement ratio (ID 718)
Interface resistances (brick-mortar and mortar-insulation)	• Perfect hydraulic contact • $2.5 \cdot 10^{10}$ m/s
Wall factor *W* in ISO 15927-3 (rain exposure)	• 0.5 • 0.75
Wall orientations	• North • East • South • West
Indoor air moisture excess	• Moisture class 1 (≈ 50 m²/person) • Moisture class 2 (≈ 20 m²/person) • Moisture class 3 (≈ 15 m²/person)
Interior insulation solution	• Uninsulated • AAC (CCR-optimized) • AAC (without CCR) • CaSi (CCR-optimized) • CaSi (without CCR) • PIR on paper backing + gypsum board

5.2.6 Performance assessment

The performance assessment is based on the criteria described in section 1.3. Figure 44 shows the sections and parameters checked in these locations. The greatest number of freeze-thaw cycles and the highest ice content occurs near the exterior surface. The exact location of the critical section depends on the combination of the material properties, insulation solution and saturation degree used to count the freeze-thaw cycles, etc., all of which varied from case to case. Based on preliminary modelling, the layers between

5–135 mm from the exterior surface were used to judge the magnitude of changes caused by different parameters and the result from the most critical layer of each case is presented as "exterior masonry".
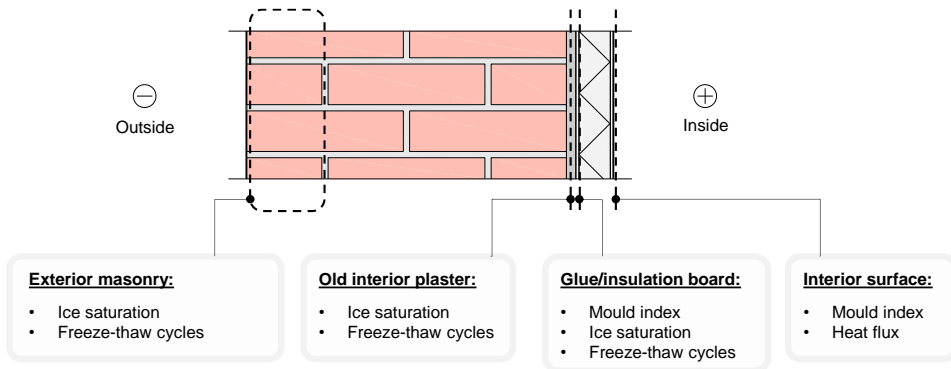

Figure 44   Sections and parameters used for performance assessment.

The **freeze-thaw cycles** were counted if ice saturation (ratio between ice and pore volumes) rose above a certain level and was then reduced to zero. Unfortunately, the exact damage criteria for used materials were unknown. To overcome this, the freeze-thaw cycles are presented as curves of freeze thaw cycles as a function of different ice saturation threshold levels. This allows to get an overview of the cycle counts independent of a specific saturation degree criterion.

Based on the assumption that the main damage takes place during the first cycles (Al-Omari et al., 2015; Feng et al., 2019) and that critical saturation degree is a function of temperature (the lower the frost temperature, the lower the maximum allowable saturation degree), the results are also assessed based on curves of **maximum ice saturation as a function of temperature**.

Mould growth was analysed using the Finnish mould model (Hukka and Viitanen, 1999; Ojanen et al., 2010; Viitanen et al., 2011). The interior surface and surfaces behind the insulation layer were concentrated on (due to the possibility of air gaps). The parameters for mould index calculation are given in Table 6, the choice of which was based on the documentation of the Finnish mould model calculation file (VTT and TTY, 2018). According to that, the AAC has separate sensitivities for mould growth and M_{max}.

Changes in **heat fluxes** were assessed based on the modelling results on the interior surface. As the thermal boundary conditions were the same for different insulation solutions, the heat flux also reflected the thermal transmittance.

Table 6   Surface properties used for mould index calculation according to the Finnish mould model.

Surface	Parameter	Surface properties			
		Uninsul.	AAC	CaSi	PIR (paper coated)
Interior surface	Material	wallpaper	plaster + paint	plaster + paint	gypsum board + paint
	Sensitivity	sensitive	medium resistant	medium resistant	sensitive
	C_{mat}	0.25	0.25	0.25	0.25
Behind insulation	Material		AAC	CaSi	paper coated PUR
	Sensitivity		sensitive (mould growth), med. resistant (M_{max})	medium resistant	sensitive
	C_{mat}		0.25	0.25	0.25

5.3 Results and discussion

5.3.1 Frost and moisture in exterior layers of masonry

The depth of the harshest location in the exterior masonry varies between models and observed quantities. For each case, the layers between 5–135 mm from the exterior surface are analysed and the most critical result is presented.

The maximum ice saturations of insulated cases are nearly all higher than the uninsulated ones (median relative increase ranged between 7–8%, maximum up to 93% – see Annex 2.1 (Klõšeiko and Kalamees, 2021)). However, the difference between the studied insulation solutions (vapour tight and vapour open both in CCR-optimized and conventional form) is small.

Figure 45 (left) helps to analyse the modelling results based on the concept that the combination of high ice saturation levels and low temperatures contribute to the destruction of the material (Feng et al., 2019). In general, the insulated models were colder and more saturated with ice, but the difference between insulation types, and optimized and conventional material characterization is negligible.
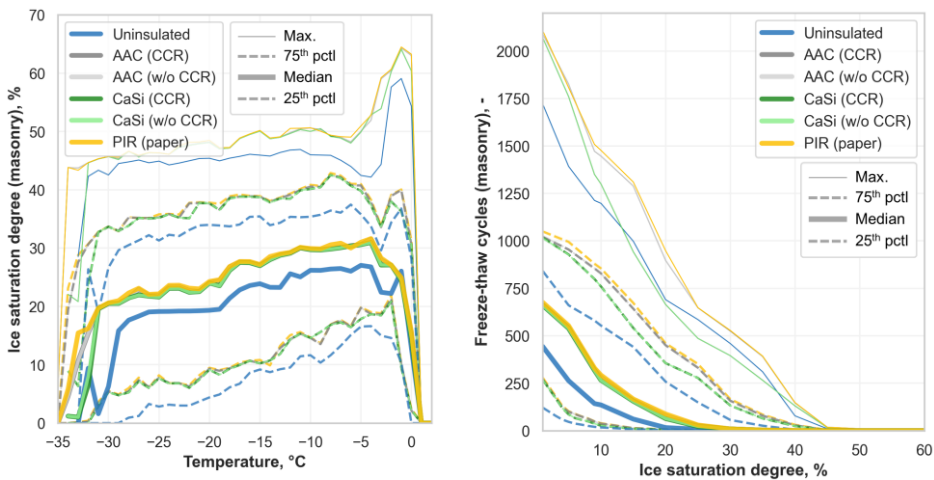

Figure 45   The most critical results from exterior layers of masonry: maximum ice saturation at different temperatures (left) and freeze thaw cycles dependent on the ice saturation degree limit (right).

Regardless of the insulation solution, the number of **freeze-thaw cycles** increased significantly, with a median relative increase of ≈ 55% compared to uninsulated walls. Figure 45 (right) shows the number of freeze thaw cycles dependent on the ice saturation limit that is used to count them. The relative increase in FTC caused by interior insulation was greater at higher limiting saturation degrees, while CaSi performed slightly better than AAC and PIR in the top quartile if medium ice saturations were used as the FTC threshold.

The main factors contributing to both maximum ice saturation and freeze thaw cycles (see Annexes 1.1–1.3, 2.1 and 3.1 in Klõšeiko and Kalamees, 2021) in the exterior layer were the brick type and wind driven rain load (dependent on orientation and rain exposure coefficient). Compared to them, the effects of indoor moisture load, hydraulic contact resistances and even the type of insulation (whether it is "capillary active" or "vapour tight", and the specifics of material characterization) are minute. This means that the impact of interior insulation probably stems mainly from its additional thermal resistance.

Unfortunately, the performance limits of the modelled bricks are not known. The conservative 30%$_{sat}$ ice saturation limit was exceeded in about half of the uninsulated cases and in 2/3 of the insulated cases (regardless of the insulation solution; see Annex 3.1 in (Klõšeiko and Kalamees, 2021)). Should the 30%$_{sat}$ limit prove to be true, the bricks of a historic building would probably be damaged even before any thermal upgrade and the insulation works would only worsen the situation.

The critical saturation degrees (tested at -15 °C) of various bricks from North America were presented in Figure 5 in a paper by van Straaten (2014). Most of the bricks tested there were able to endure higher saturation degrees than those reached in this study. However, as Figure 45 (left) shows, the temperature in this study can be far lower and thus more critical.

On one hand, increase in ice saturation due to insulation is not very dramatic and if the results about the North American bricks are representative of Estonian ones too, it could be deduced that if the façade has survived until now without frost damage, the interior insulation should not be a major problem. On the other hand, if the main cause of the damage is the high number of freeze-thaw cycles at higher ice saturation degrees, the distinction is clear – insulation causes higher cycle counts and hence accelerated degradation.

5.3.2 Frost between interior insulation and original wall

Maximum **ice saturation** levels in the plaster on the interior surface of the original wall behind the insulation are given in Figure 46 (left).

The lower 3 quartiles perform similarly in vapour open solutions. As Annex 2.3 (Klõšeiko and Kalamees, 2021) shows, the PIR insulation is mostly more critical and can cause up to 75%$_{sat}$ higher ice saturation than a similar case using the vapour open approach. The tentative 30% ice ratio threshold was exceeded in 31% of PIR cases, while when using CaSi and AAC insulation the rate was much lower at 2% and 8% respectively (also see Annex 3.2 in (Klõšeiko and Kalamees, 2021)). The CCR optimization caused more severe conditions in the majority of the cases compared to material characterization without the CCR data. Furthermore, the number of cases exceeding the tentative 30% ice ratio increased by ≈ 2 times when using optimized material properties.

The outcome was mainly determined by the wind-driven rain load (wall orientation and exposure coefficient) and the material of the original wall – see Annex 1.1–1.3 and 3.2

in (Klõšeiko and Kalamees, 2021). Of the walls with optimized material characterization exceeding the 30% ice saturation ca 1/10 were oriented to the west. Walls made of sand-lime bricks fared best: they did not exceed the limit in vapour open cases and had a 2% failure rate when PIR insulation was used. The other two brick types were more susceptible to higher ice saturations.

The trend and the contributing factors were similar when **freeze-thaw cycles** were considered (Figure 46, right). In lower ice saturation degrees, the top quartile of FTC was roughly 1.5–2 times higher using PIR insulation compared to vapour open insulation. If higher ice limits are used, the number of freeze-thaw cycles in PIR's top quartile is vastly higher than in vapour open materials.
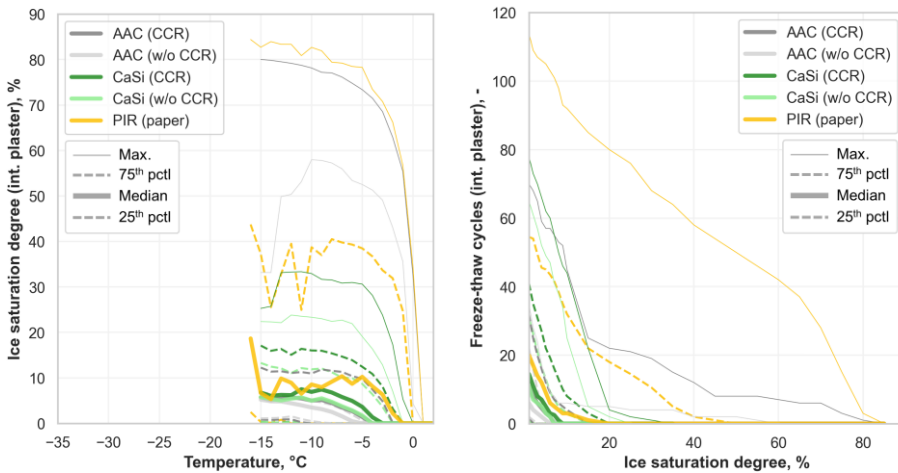

Figure 46   The old interior plaster layer behind the insulation: maximum ice saturation at different temperatures (left) and freeze thaw cycles dependent on the ice saturation degree limit (right).

Vereecken and Roels (2016) suggested that in severe climate conditions, the insulation material and glue mortar should be able to handle the freezing and thawing; according to the current study, this applies to the old interior plaster too.

High ice ratio and the number of freeze-thaw cycles imply that if PIR insulation is applied on top of existing interior plaster, gluing the insulation to the plaster may not be enough and a mechanical fastening to the masonry layer should also be used. This will possibly cause issues with high surface humidity at the fasteners and is further discussed in section 5.3.4.2.

While the number of freeze-thaw cycles using vapour open materials was lower compared to PIR, the extreme cases of AAC still caused ice saturation well above the 30%$_{sat}$ limit – some even on par with PIR (albeit subjected to fewer cycles). Should the damage occur, it would have an impact on the hydraulic contact with the original wall and possibly hamper the intended functioning of the capillary active insulation (Vereecken and Roels, 2015a).

It must be noted that only one plaster type was modelled in this study, however, it is doubtful that the interior plasters would have been designed to endure repeated high ice saturation levels that the extreme cases of the AAC and PIR insulation solutions cause. Therefore, the safe option would be the removal of the existing interior plaster.

5.3.3 Frost in the cold side of the insulation

Due to a more realistic moisture distribution (higher moisture content on the cold side of insulation), the CCR-optimized materials showed an increase in both the maximum ice saturation and in freeze-thaw cycles (Figure 47). While the median increase was rather low at 0.2%$_{sat}$ and 1 cycle for both AAC and CaSi, the change was greater in the top quartile as the increase could reach 5%$_{sat}$ and 7%$_{sat}$ and 45 and 28 cycles respectively in some cases (see Annex 2.2 in (Klõšeiko and Kalamees, 2021)).

Similarly to the interior plaster layer, the high values were caused by a high indoor moisture load and a wind-driven rain load (orientation and rain exposure) – see Annexes 1.1 and 3.4 (Klõšeiko and Kalamees, 2021). The type of brick also had an impact here. While maximum moisture saturation degrees in the exterior layer of PIR insulation reached over 80%$_{sat}$ in extreme cases, no ice was detected there due to high moisture content coinciding with warm temperatures.
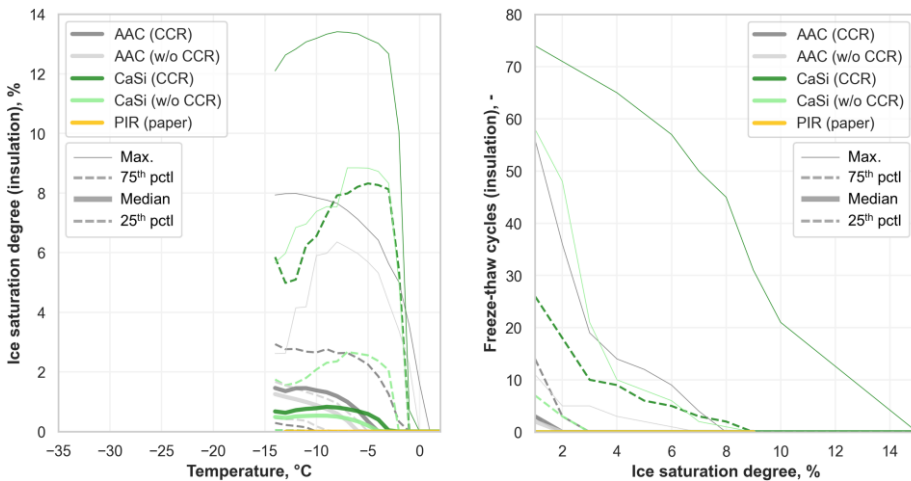

Figure 47 The cold side of the interior insulation: maximum ice saturation at different temperatures (left) and freeze thaw cycles dependent on the ice saturation degree limit (right).

Although the maximum ice saturation in the insulation layer was well below the tentative 30%$_{sat}$ limit, section 2.3.1.4 of the thesis and Publication IV suggested that the AAC insulation system can still fail below that level. Significant reduction of tensile strength of the AAC insulation system was detected at glue saturation of 15–20%$_{sat}$ and insulation saturation of ≈ 10%$_{sat}$. The rupture occurred in either the cold side of the insulation, at the glue-insulation interface or the glue-substrate interface. The loss of strength progressed over the duration of the experiment (concluding at 53 freeze-thaw cycles). In the current study, similar ice saturation levels were modelled in extreme cases in the glue layer using CCR-optimized AAC material, suggesting that damage could occur. In the same study (section 2.3.1.4 / Publication IV) CaSi fared better, as damage occurred in saturated samples, while no statistically significant changes in tensile strength were detected during the test at 10-20%$_{sat}$.

Scheffler (2013) also tested AAC for frost damage and found that no loss of strength occurred in samples conditioned at 97.4%$_{RH}$ and frozen at -15°C for 20 cycles. This humidity corresponds to ≈ 4%$_{sat}$ and the minimum temperatures in the insulation in current study were ≈ -15°C too. Stemming from the moisture content where damage did *not* occur, the ice saturation limits of 4%$_{sat}$ (AAC) and 10%$_{sat}$ (CaSi) can be conservatively used to

compare the results of optimized and conventionally characterized materials (see Annex 3.4 (Klõšeiko and Kalamees, 2021)). The failure rate of the optimized AAC models was about 7 times higher than the conventional ones (9.5% vs 1.5% of all models using the respective material data), while 16% of the optimized CaSi cases failed in contrast to 0% without CCR. According to these results, keeping the indoor humidity within Moisture class 1, and reducing the wind driven rain wall factor to 0.5 will mitigate frost damage risks in the insulation layer.

5.3.4 Mould indexes behind the insulation and on the interior surface

5.3.4.1 Results

The risk of mould growth is assessed using mould indexes with values above 1 being undesirable and indicating mould growth. The surface parameters used for mould index calculation and the choice of the performance criterion are discussed in sections 5.2.6 and 5.3.4.2.

Figure 48 (left) gives the **maximum mould indexes** over the whole modelling period for the surface **between the insulation and the original wall**. The median maximum mould indexes were well above the safe threshold of 1 for all insulation solutions except the CaSi without CCR optimization (also see Annex 3.3 in (Klõšeiko and Kalamees, 2021)). Median maximum mould indexes for both AAC materials were ca 2, which corresponds to "several local mould growth colonies" that are detectable using a microscope. The median levels were lower in CaSi walls, however, similarly to AAC, the top quartile was at the maximum possible value according to their sensitivity class (mould index = 3). Paper-coated PIR performed far worse as the majority of models indicated moderate to plenty of visually detectable growth, the median increase compared to vapour open insulation solutions was ca. 2 units on the mould index scale (see Annex 2.3 in (Klõšeiko and Kalamees, 2021)).

Based on Annexes 1.2 and 3.3 (Klõšeiko and Kalamees, 2021), the mould index behind insulation is mainly determined by the indoor humidity load. About 15% of the optimized CaSi cases in the mildest indoor moisture class 1 ($\Delta v_{t_e < 5℃}$ = 2 g/m³, 53 m² / person) had a maximum mould index above the acceptable threshold of 1, while in the case of AAC, it was roughly twice of that. The failure rate of the PIR models at a low humidity load was a further ≈ 2 times higher than those of the AAC ones (ca 70% of the cases). Virtually all cases with indoor humidity loads in moisture classes 2 ($\Delta v_{t_e < 5℃}$ = 4 g/m³, 20 m² / person) and 3 ($\Delta v_{t_e < 5℃}$ = 6 g/m³, 15 m² / person) failed regardless of the insulation solution, with the exception being CaSi, where in moisture class 2, the failure rate was 43%. Wind driven rain load was also important with northerly and easterly walls faring better than others.

The higher mould index of PIR insulation can be explained by its higher sensitivity to mould growth and by higher humidity occurring also in warm periods, which is more favourable for mould growth. The opposite is true for the AAC and CaSi – their sensitivity class is lower and their higher vapour conductivity allows for drying out during the summer, while the indoor moisture load causes wetting during cold periods.
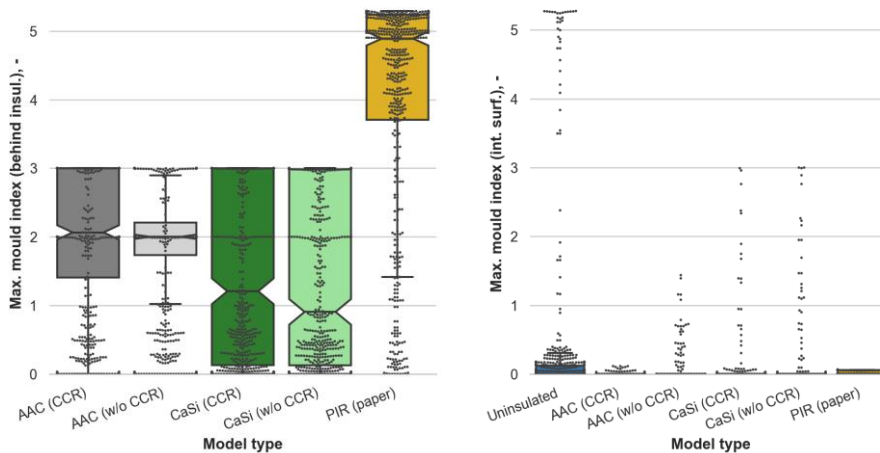
Figure 48   Maximum mould indexes behind the insulation (left) and on the interior surface (right).

The maximum **mould indexes on the interior surface** are given in Figure 48 (right) and the failure decision tree in Annex 3.5 in (Klõšeiko and Kalamees, 2021). Uninsulated walls are most at risk with 9% of the cases failing to stay below the critical threshold of mould index 1 and at some combinations showing serious mould growth. All the failed walls were oriented to the west with a high rain exposure coefficient, a high indoor moisture load and good hydraulic contact in masonry further contributing to the failure. The majority ($\approx$ 95%) of the failures occurred in walls made of burnt bricks (id 33 and 97) while sand-lime brick (id 153) walls fared better – the latter had a lower water uptake coefficient A_w, which caused less wind driven rain to be absorbed into the masonry.

The PIR insulation did not cause problems with mould index on the interior surface, while in the CaSi and unoptimized AAC walls some combinations existed above the mould index 1. None of the AAC walls with CCR-optimized material data failed and the failure rate was reduced 2-fold in the CCR-optimized CaSi – this can be attributed to their lower liquid conductivity and reduced redistribution of moisture towards the interior surface.

5.3.4.2 Discussion

The modelled mould indexes behind the insulation were high for all insulation solutions. However, the VTT mould model was developed to predict mould growth on exposed surfaces, while by design, the AAC and CaSi systems should be glued in whole plane, and the PIR boards sealed around the board perimeter. According to Künzel (2011) gluing on the whole surface of the insulation should prevent mould growth and contaminants reaching the indoor air. This depends on the quality of the workmanship, as it is possible to leave air pockets behind the insulation (too dry mortar, uneven subsurface, etc), and unfortunately has occurred in practice (Klõšeiko and Kalamees, 2016; Morelli and MØller, 2019). The instructions of one AAC producer (Heße et al., 2018) state that "the high alkalinity of the product effectively inhibits mould growth.", which (at least to some degree) is taken into account in the mould index calculation by a lower sensitivity parameter. The producer also suggests filling the joints between the insulation and floors/ceilings/interior walls with hemp felt – creating an air cavity and introducing biodegradable material into the moist zone. The latter, in light of the current modelling results, is a very questionable recommendation.

In a recent field study Jensen et al. (2020) detected mould growth on the masonry-AAC insulation interface and inside the AAC material itself too. The growth inside the AAC was even higher than on the interface and the authors presume it to be due to the lower pH than on the glue mortar. In contrast, mould growth in CaSi systems stayed below the detection levels both on the interface and inside the material, although subjected to similar conditions and pH values, and the Finnish/VTT mould model predicting growth for both CaSi and AAC.

In a laboratory study Jensen et al. (2021) further tested the mould growth on the masonry-insulation interface. It was determined that when the pH of the surface is high, the existing mould growth is inactivated. However, 12 months from the start of the experiment, the spores on the interface were still viable and could become active as the pH declines over time.

A RIBuild project report (Johansson et al., 2019) compared the VTT mould modelling results to measurements and detected a high number (61%) of false-negatives (i.e. mould was observed although model predicted no growth) in borderline cases, while in low humidity and extreme cases the model agreed with the results.

Also, questions can be raised about the PIR insulation. According to the installation instructions of one product (Kingspan Insulation OÜ, 2017), PU foam caulk is applied around the perimeter of the boards, probably leaving an air gap behind the insulation. The insulation is also penetrated by mechanical fasteners. Metal screws or wall plugs are usually used to affix the PIR + a gypsum board system to the wall causing surface temperatures much lower than the 1D models in this article predict. This was also demonstrated in-situ in a previous study (Publication I), where condensation and rust occurred on the fasteners. This means that the mould index when using PIR insulation could actually be higher in both studied sections – behind the insulation and on the interior surface.

Overall, while the mould index calculated here does not directly describe the exact situation behind the insulation in 1D wall (as the air cavities should not be a rule, but an exception to be avoided), it can reveal what happens in borderline cases (bad workmanship, air leakages, joints tightened with biodegradable hemp wool etc). Due to the higher modelled mould indexes it also shows that risks associated with such cases in the PIR insulation are much higher than those of the AAC insulation.

5.3.5 Heat flux on the interior side

Figure 49 (left) gives the mean heat fluxes for main model types. All insulation solutions present a ≈ 65% median reduction of mean heat fluxes compared to the uninsulated cases. In case of the vapour open insulation, the spread of the results is larger due to the higher variability of the moisture content of the insulation (Figure 49, right).

Leaving aside the differences in thermal conductivities of the original wall, moisture content and heat flux in the vapour open systems are primarily dependent on the indoor moisture load and wind driven rain (see Annex 1.3 in Klõšeiko and Kalamees, 2021). As the PIR insulation itself is fairly vapour tight, the variations in its heat flux are caused by changes in the moisture content of the original wall and its thermal resistance. As long as the thermal resistances are similar, the authors do not see a reason to prefer one system to another based on their slightly different thermal behaviour alone.
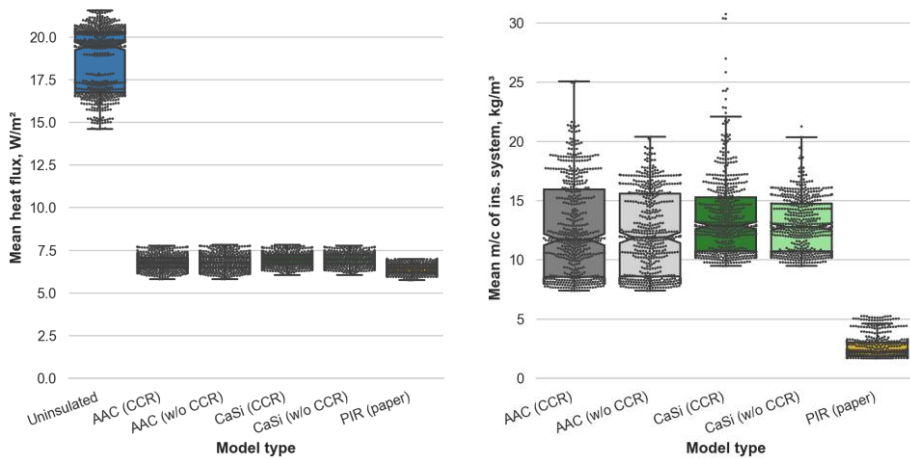
Figure 49   Mean heat fluxes on the interior surface (left) and mean moisture content of the whole insulation system (left).

5.4 Chapter conclusions

Based on the modelling done with AAC and CaSi in this study it can be stated that the material characterization process using a capillary condensation redistribution test causes more critical results. The **CCR-optimized material data** resulted in the following changes **compared to the result of the conventional material characterization**:

- increased moisture content, maximum ice ratios and freeze-thaw cycles in the cold side of the insulation;
- higher maximum ice ratios and more freeze-thaw cycles in the interior plaster and glue mortar;
- the increases coincide with high indoor (moisture class 3) and outdoor moisture loads (West-oriented walls, higher rain exposure coefficient), which cause more critical conditions.

The CCR-optimized materials performed worse especially near their tentative performance limits, which, for example, in the cold side of the insulation layer resulted in a 7-fold increase in failure rate due to frost in the case of AAC, and caused previously unexpected failures when using CaSi. Although not studied here, the damper conditions behind the insulation would also have an impact on mould and rot risks of wooden beam ends. While the results only describe the effect of CCR-optimization on specific CaSi and AAC materials, it is probable that similar results also occur when other insulation materials with notable liquid conductivity are accounted for and it makes sense to incorporate the CCR test into the material characterization procedures.

When **comparing the "capillary active" vapour open insulation to "vapour tight" PIR insulation**, no significant differences were found in freeze-thaw cycles and in the maximum ice saturation of the exterior part of the masonry, however, the increase of mean moisture content of the whole wall was ca. 1.4 times higher using PIR than vapour open solutions. Nevertheless, AAC and CaSi insulations bring some benefits over PIR: maximum ice volumes and freeze-thaw cycles and mould indexes behind the insulation are significantly reduced. The results suggest that PIR insulation would require mechanical

fastening to the underlying structure as the original interior plaster will be at risk of frost damage. The mould risk on top of those fasteners will probably be higher than the current 1D modelling suggests. Still, in extreme cases AAC insulation can also cause the ice saturations in the original interior plaster to reach ≈ 70% – thereby hinting at frost damage risk. This would have an impact on the hydraulic contact with the original wall and possibly hamper the intended functioning of the capillary active insulation (Vereecken and Roels, 2015a). It is therefore necessary to detect and avoid those extreme cases in the design process. Calculated mould indexes behind the insulation using the paper-backed PIR product were very high and in 89% of the cases above the safe threshold. Therefore, until further research into actual mould growth inside such structures has been conducted or gapless installation can be absolutely assured, the application of such products on mass masonry walls open to wind driven rain cannot be recommended.

In general, the vapour open materials with CCR-optimized data still have their specific advantages over the vapour tight solution, although the gap is smaller than before. Furthermore, the mass masonry wall is probably the best showcase for the vapour open approach – for example, should the original wall have air cavities, the wind driven rain loads would be reduced and the vapour tight approach might become more favourable (presuming the issues with fasteners and unintentional defects can be mitigated).

The overall impact of interior insulation can be summarized by the following:
- a 65% median reduction of mean heat fluxes (30 mm PIR, 60 mm AAC or 90 mm CaSi on top of a 52 cm-thick mass masonry wall);
- a reduction of interior surface mould indexes: 7% of the uninsulated walls failed to stay below the threshold value, while the failure rate was 1.9% of all CaSi cases and 0 when using AAC or PIR;
- maximum mould indexes between masonry and insulation ranged from high using CaSi (median ≈ 1.2) and AAC (median ≈ 2.1) to very high using PIR (median ≈ 4.9). This hints that whole-surface gluing is required for AAC & CaSi and an airtight installation for all insulation solutions;
- the exterior layer of the original wall must tolerate higher ice saturation levels (median relative increase ≈ 8%) and freeze-thaw cycles (median relative increase ≈ 50%) regardless of the type of insulation;
- the old interior plaster will become moist and susceptible to frost damage – unless it is certain that the plaster can endure that, its removal is recommended.

Nonetheless, a criterion with high failure rate could be found for all systems. As the real distribution of currently varied parameters was not exactly known, even the outlier cases should be considered carefully. Thus, as Vereecken and Roels (2015b, 2016) have also stated, the "capillary active" interior insulation is no miracle cure and still needs case-specific approach.

Frost and mould risk inside and directly behind vapour open and vapour tight insulation approaches are governed by the indoor air moisture load and can be at least to some degree mitigated by lowering it. The hygrothermal conditions in the exterior layer of the original wall can be mainly improved by reducing the wind driven rain loads. Hydrophobization can help here (Jensen, Bjarløv, et al., 2020) but accounting for it in modelling also depends on the availability of material data and literature shows that the treatment can also worsen the situation (Calle and Van Den Bossche, 2021; Janssen et al., 2020; Metavitsiadis et al., 2017).

6 Conclusions

6.1 The main outcomes

The solutions studied in this thesis offered a 2–3-fold reduction in thermal transmittances compared to the original walls, while also considerably increasing interior surface temperatures. This shows the potential for energy savings, improved thermal comfort and reduced risk of mould growth on interior surfaces.

Field measurements gave the first indications of the **suitability of interior insulation solutions (RQ4)**. They showed that in low indoor humidity loads, the selected solutions worked well and no performance criteria were exceeded. However, the test wall with humidity loads similar to high inhabitant density apartments hinted that the basic 95%$_{RH}$ performance criterion of "capillary active" insulation materials can be exceeded even if climate, original wall and insulation thicknesses were all favourable. This means that more sophisticated criteria – perhaps based on saturation degree and temperature – are required. The measurements also demonstrated that the dryout time of built-in moisture inherent to the "capillary active" insulation systems is considerable and should be accounted for when planning the retrofit.

Insight was gained into the **frost resistance of the interior insulation systems (RQ3)**: AAC, which was presumed to be frost resistant, showed a reduction of its tensile strength after freeze-thaw cycling at ca 10%$_{sat}$ and ca -10 °C. Expanded perlite showed similar performance as AAC. It is important to note that damage occurred below the ≈ 30%$_{sat}$ limit that is sometimes also used to assess frost risk. While no statistically significant loss of strength was detected in the unsaturated CaSi test wall, water-saturated CaSi still suffered damage. These results can be used as a performance criterion.

Comparisons between modelling and measurements (RQ1) showed good agreement in thermal performance, while modelling underestimated relative humidity levels during wetting and overestimated them during drying periods hinting at hysteretic effects that are not considered by the model. Worryingly, the "conventionally characterized" material properties (as currently mostly found in modelling software databases) severely underestimated overhygroscopic moisture content levels in "capillary active" insulation materials when subjected to non-isothermal wetting through vapour diffusion. Unfortunately, it is one of the standard use cases for such materials.

The inclusion of the **capillary condensation redistribution (CCR) test (RQ2)** into the dataset that liquid and vapour conductivity curves were derived from improved the correlation in the overhygroscopic moisture range during non-isothermal wetting, while conservatively reducing agreement with the drying experiment (i.e. overestimated the moisture content). Still, when avoiding frost and moisture damage is the aim with the currently widely used HAM-modelling software, modelling with "conventionally characterized" material data can lead to overly optimistic assumptions of the hygrothermal performance of the "capillary active" interior insulation systems. Thus, it makes sense to include the CCR test in material characterization procedures to overcome that.

Parametric modelling using a 52 cm-thick brick wall and a long-term climate dataset gave further insights to the **suitability of interior insulation to Estonian conditions (RQ4)**. It showed that the exterior layer of masonry must tolerate higher ice saturation levels and freeze-thaw cycles regardless of the insulation type (vapour open or tight). The "capillary active" insulation systems had advantages compared to the vapour tight PIR: moisture content, mould indexes and frost risk behind the insulation were lower.

However, these benefits were not as pronounced if the CCR-optimized material data were used (opposed to "conventional" material data that has been used so far and is mostly found in HAM software databases). Furthermore, frost in "capillary active" insulation layer can be an issue for both AAC and CaSi insulation systems in certain cases. To avoid frost damage in old interior plaster and preserve capillary contact (which is essential for "capillary active" insulation), the layer should be removed before applying interior insulation. Mould indexes behind the insulation were high – emphasis should be put on achieving airtight installation of both vapour tight and vapour open "capillary active" insulation systems. While the chances of success are high when using interior insulation, a case-by-case approach is necessary to avoid the critical combinations.

6.2 Further studies

While it can be currently stated that the exterior brick layer will be at a worse state after the insulation, the question whether the risks of accelerated frost damage would be realized needs to be answered based on further material studies, for example, by determining the critical saturation degrees and their temperature dependencies of these materials. Further determination of the exact frost damage limits of the CaSi and AAC systems themselves will probably show the results of current thesis in better light as the current limiting criteria were selected rather conservatively.

The failure to acquire good reproduction of both CCR and drying experiments at the same time using modelling methods employed in this thesis deserves further attention. Possible avenues worth exploring are: including hysteretic and dynamic effects in the models, widening the experimental dataset and improving the optimization methods.

This thesis mainly dealt with 1D modelling, however, 2D and 3D modelling are also required, as corners, exterior wall - interior wall details, wooden beam ends, etc. – also in future climate – can result in more critical situations.

The parametric modelling in chapter 5 assessed a 52 cm-thick mass masonry wall, which is on the critical end of the spectrum of existing structures. For more favourable cavity walls, the preferrable solutions and allowable insulation thicknesses can be quite different. Beside the hygrothermal performance, cost and energy performance along with ecological footprint should also be investigated.

References

Abdul Hamid A and Wallentén P (2017) Hygrothermal assessment of internally added thermal insulation on external brick walls in Swedish multifamily buildings. *Building and Environment* 123: 351–362.

Al-Omari A, Beck K, Brunetaud X, et al. (2015) Critical degree of saturation: A control factor of freeze-thaw damage of porous limestones at Castle of Chambord, France. *Engineering Geology* 185: 71–80.

Bianchi Janetti M and Janssen H (2020) Impact of the drying rate on the moisture retention curve of porous building materials. *Construction and Building Materials* 258: 119451.

Binder AB, Zirkelbach DM and Künzel HM (2010) Test Method to Quantify the Wicking Properties of Insulation Materials Designed to Prevent Interstitial Condensation. In: *Thermal Performance of the Exterior Envelopes of Whole Buildings XI*, Clearwater Beach, Florida, 2010, pp. 1–12. ASHRAE.

Binder AB, Künzel HM and Zirkelbach DM (2013) A new approach to measure liquid transport in capillary active interior insulation. In: *Proceedings of 2nd Central European Symposium on Building Physics (CESBP2013)* (eds A Mahdavi and B Martens), Vienna, 2013, pp. 393–400. ÖKK-Editions.

Binder AB, Zirkelbach DM and Künzel HM (2014) Keeping risks at bay – improving a test method to reliably quantify the capability of capillary active interior insulation. In: *Proceedings of 10th Nordic Symposium on Building Physics (NSB2014)* (eds J Arfvidsson, L-E Harderup, A Kumlin, et al.), Lund, 2014, pp. 1061–1068. Building Physics, LTH, Lund University.

Busser T, Berger J, Piot A, et al. (2019) Comparison of model numerical predictions of heat and moisture transfer in porous media with experimental observations at material and wall scales: An analysis of recent trends. *Drying Technology* 37(11): 1363–1395.

Calle K and Van Den Bossche N (2021) Sensitivity analysis of the hygrothermal behaviour of homogeneous masonry constructions: Interior insulation, rainwater infiltration and hydrophobic treatment. *Journal of Building Physics* 44(6): 510–538.

Calle K, De Kock T, Cnudde V, et al. (2019) Liquid moisture transport in combined ceramic brick and natural hydraulic lime mortar samples: Does the hygric interface resistance dominate the moisture transport? *Journal of Building Physics* 43(3): 208–228.

De Mets T, Tilmans A and Loncour X (2017) Hygrothermal assessment of internal insulation systems of brick walls through numerical simulation and full-scale laboratory testing. *Energy Procedia* 132: 753–758.

Derluyn H, Janssen H and Carmeliet J (2011) Influence of the nature of interfaces on the capillary transport in layered materials. *Construction and Building Materials* 25(9): 3685–3693.

EVS and CEN (2004) EVS-EN 14146:2004 Natural stone test methods - Determination of the dynamic modulus of elasticity (by measuring the fundamental resonance frequency).

EVS, CEN and ISO (2009) EVS-EN ISO 15927-3:2009 Hygrothermal performance of buildings - Calculation and presentation of climatic data — Part 3: Calculation of a driving rain index for vertical surfaces from hourly wind and rain data.

EVS, CEN and ISO (2012) EVS-EN ISO 13788:2012 Hygrothermal performance of building components and building elements - Internal surface temperature to avoid critical surface humidity and interstitial condensation - Calculation methods.

Feng C and Janssen H (2021) Hygric properties of porous building materials (VII): Full-range benchmark characterizations of three materials. *Building and Environment*: 107727.

Feng C, Roels S and Janssen H (2019) Towards a more representative assessment of frost damage to porous building materials. *Building and Environment*: 106343.

Freudenberg P, Ruisinger U and Stöcker E (2017) Calibration of Hygrothermal Simulations by the Help of a Generic Optimization Tool. *Energy Procedia* 132(November): 405–410.

Glaser H (1958) Temperatur- und Dampfdruckverlauf in einer homogenen Wand bei Feuchtigkeitsausscheidung. *Kältetechnik* 10(6): 174–179.

Glaser H (1959) Grafisches Verfahren zur Untersuchung von Diffusionsvorgénge. *Kältetechnik* 11(10): 345–349.

Grauen A (1935) Õõnesseinte konstruktsioonist. *Tehnika Ajakiri* 14(4): 61.

Grauen A (1937) Hoonete niiskusest ja abinõudest selle vastu. *Tehnika Kõigile* (6).

Grunewald J (1997) *Diffusiver und konvektiver Stoff- und Energietransport in kapillarporösen Baustoffen*. Technische Universität Dresden.

Hansen TK, Bjarløv SP, Peuhkuri RH, et al. (2018) Performance of hydrophobized historic solid masonry – Experimental approach. *Construction and Building Materials* 188: 695–708.

Häupl P and Xu Y (2001) Numerical Simulation of Freezing and Melting in Porous Materials under the Consideration of the Coupled Heat and Moisture Transport. *Journal of Thermal Envelope and Building Science* 25(1): 4–31.

Häupl P, Grunewald J and Petzold H (2004) Energetische Sanierung des Herrenschießhauses Nürnberg mit kapillaraktiver Innendämmung. *Bauphysik* 26(1): 43–48.

Häupl P, Grunewald J and Ruisinger U (2005) Hygrothermal analysis of external walls within the reconstruction of the Rijksmuseum Amsterdam. In: *Proceedings of Structural Studies, Repairs and Maintenance of Heritage Architecture IX* (eds CA Brebbia and A Torpiano), Southampton, 2005, pp. 345–354. WIT Press.

Heße M, Griebel H, Georgi F, et al. (2018) Multipor Insulation Guide. 1st ed. Duisburg: Xella Baustoffe GmbH.

Hirsch H, Heyn R and Klõšeiko P (2020) Capillary condensation experiment for inverse modelling of porous building materials. Kurnitski J and Kalamees T (eds) *E3S Web of Conferences* 172: 17003.

Hukka A and Viitanen H (1999) A mathematical model of mould growth on wooden material. *Wood Science and Technology* 33(6): 475–485.

Ilomets S, Kalamees T and Vinha J (2018) Indoor hygrothermal loads for the deterministic and stochastic design of the building envelope for dwellings in cold climates. *Journal of Building Physics* 41(6): 547–577.

Janssen H, Vereecken E and Holúbek M (2015) A confrontation of two concepts for the description of the over-capillary moisture range: Air entrapment versus low capillarity. *Energy Procedia* 78: 1490–1494.

Janssen H, Scheffler GA and Plagge R (2016) Experimental study of dynamic effects in moisture transfer in building materials. *International Journal of Heat and Mass Transfer* 98: 141–149.

Janssen H, Deckers D, Vereecken E, et al. (2020) *RIBuild D2.3: Impact of water repellent agents on hygric properties of porous building materials*. Available at: https://www.ribuild.eu/s/RIBuild_D23_final.pdf.

Jensen NF, Odgaard T, Bjarløv SP, et al. (2020) Hygrothermal assessment of diffusion open insulation systems for interior retrofitting of solid masonry walls. *Building and Environment* 182(107011): 1–17.

Jensen NF, Bjarløv SP, Rode C, et al. (2020) Hygrothermal assessment of four insulation systems for interior retrofitting of solid masonry walls through calibrated numerical simulations. *Building and Environment* 180(107031): 1–15.

Jensen NF, Bjarløv SP, Rode C, Andersen B and Møller Eva B (2021) Hygrothermal performance of six insulation systems for internal retrofitting solid masonry walls. *Journal of Building Physics*: 174425912098874.

Jensen NF, Bjarløv SP, Rode C, Andersen B and Møller Eva B. (2021) Laboratory-based investigation of the materials' water activity and pH relative to fungal growth in internally insulated solid masonry walls. *Indoor Air*: ina.12796.

Johansson P, Lång L, Capener C-M, et al. (2019) *RIBuild D2.2: Threshold values for failure, linked to types of building structures and failure modes*. Available at: https://www.ribuild.eu/s/RIBuild_D22_v10_1.pdf.

Jürgenson L (1938) Talvel 1937/1938 teostatud välisseinte soojajuhtivuse mõõtmistest. *Tehnika Ajakiri* 17(9): 184–191.

Jürgenson L (1942) *Elamu Soojapidavus*. Tartu: Tartu Eesti kirjastus.

Kalamees T (2006) *Hygrothermal criteria for design and simulation of buildings*. Tallinn University of Technology.

Kingspan Insulation OÜ (2017) Kingspan Therma TW56 Anselmi paigaldusjuhised / installation instructions. Available at: https://www.kingspan.com/ee/et-ee/tooted/soojustus/materjalid/projekteerimisjuhendid/kingspan-therma-tw56-anselmi-illustreeritud-paigal (accessed 14 January 2020).

Klõšeiko P (2014) *Seespoolse lisasoojustusega tellisseina soojus- ja niiskustehniline toimivus Kohtla-Järve koolimaja näitel / Hygrothermal performance of a brick wall with interior thermal insulation: a case study in Kohtla-Järve school building*. Tallinna Tehnikaülikool / Tallinn University of Technology.

Klõšeiko P and Kalamees T (2015) *Vabaduse väljak 7 seespoolse lisasoojustuse niiskustehnilise toimivuse uuringu lõpparuanne*. Tallinn.

Klõšeiko P and Kalamees T (2016) *Vabaduse väljak 10 seespoolse lisasoojustus konsultatsioon, lahenduste väljatöötamine ja niiskustehnilise toimivuse uuring. Lõpparuanne / Consultation, design and performance an interior insulation solution of Vabaduse väljak 10 office building*. Tallinn. Available at: https://uuringud.tallinn.ee/uuring/vaata/2016/Vabaduse-valjak-10-seespoolse-lisasoojustuse-lahenduse-valjatootamine-ja-niiskustehnilise-toimivuse-uuring.

Klõšeiko P and Kalamees T (2021) Supplementary material to article 'Hygrothermal performance of a brick wall with interior insulation in cold climate: vapour open vs vapour tight approach'. Zenodo. DOI: 10.5281/zenodo.5078138.

Klõšeiko P, Arumägi E and Kalamees T (2013a) Hygrothermal performance of internally insulated brick wall in cold climate: field measurement and model calibration. In: *Proceedings of 2nd Central European Symposium on Building Physics (CESBP2013)* (eds A Mahdavi and B Martens), Vienna, 2013, pp. 185–192. ÖKK-Editions.

Klõšeiko P, Arumägi E and Kalamees T (2013b) *Muinsuskaitse all oleva koolimaja tellistest välisseina seespoolse lisasoojustuse soojus- ja niiskustehnilise toimivuse uuring*. Available at: http://www.kredex.ee/public/Uuringud/COOLBRICKS_raport_030314.pdf (accessed 27 March 2014).

Knarud JIB, Geving S and Kvande T (2014) Hygrothermal simulations of internally insulated massive masonry walls exposed to driving rain in cold climate. In: *Proceedings of the 10th Nordic Symposium on Building Physics (NSB 2014)* (eds J Arfvidsson, L-E Harderup, A Kumlin, et al.), Lund, 2014, pp. 1141–1148.

Krus M (1996) *Moisture Transport and Storage Coefficients of Porous Mineral Building Materials. Theoretical Principles and New Test Methods*. Stuttgart: Fraunhofer IRB Verlag.

Künzel H, Worch A, Bäumler S, et al. (2012) Innendämmung nach WTA II: Nachweis von Innendämmsystemen mittels numerischer Berechnungsverfahren (Merkblatt 6-5).

Künzel HM (2011) Bauphysik der Innendämmung und Bewertungsverfahren. In: *1. Internationaler Innendämmkongress 2011*, Dresden, 2011, pp. 9–16. TU Dresden.

Kuts PS and Sheiman VA (1965) Investigation of the hygroscopic properties of peat insulating slabs. *Journal of Engineering Physics* 9(5): 394–396.

Mändel M (2019) *Tehiskivimaterjalid Eesti 20. sajandi arhitektuuris*. Estonian Academy of Arts.

Mensinga P, De Rose D, Straube J, et al. (2014) A Test Method to Identify the Onset of Freeze-Thaw Deterioration in Masonry. *Selected Technical Papers STP 1577* 2014(1577): 197–217.

Metavitsiadis V, Soulios V, Janssen H, et al. (2017) Wall hydrophobization and internal insulation: the impact of impregnation strength and depth on moisture levels and moisture damages. In: *Proceedings of Hydrophobe VIII* (eds J-G Dai, H Yokota, TJ Zhao, et al.), Hong Kong, 2017, pp. 69–76. The Hong Kong Polytechnic University.

Mikk I (1977) *Soojustehnika Käsiraamat*. Tallinn: Valgus.

Møller EB and Hansen EJ de P (2013) Risk assessment on interior insulation: Where do we need more knowledge? In: *2. Internationaler Innendämmkongress. Tagungsunterlage* (eds J Grunewald, R Plagge, and J Gerdes), Dresden, 2013, pp. 52–61. Dresden Technische Universität.

Morelli M and Møller EB (2019) Energy savings and risk of mold growth in apartments renovated with internal insulation. *Science and Technology for the Built Environment* 25(9): 1199–1211.

Mualem Y (1984) A modified dependent-domain theory of hysteresis. *Soil Science* 137(5): 283–291.

Nicolai A (2008) *Modeling and Numerical Simulation of Salt Transport and Phase Transitions in Unsaturated Porous Building Materials*. ProQuest, Syracuse University. Graduate School.

Nicolai A and Grunewald J (2006) Delphin 5 Manual. 5.2. Dresden.

Nicolai A and Sontag L (2013) Implementation of an efficient numerical solution method to simulate freezing processes in porous media. In: *Proceedings of 2nd Central European Symposium on Building Physics (CESBP2013)* (eds A Mahdavi and B Martens), Vienna, 2013. ÖKK-Editions.

Nicolai A, Scheffler GA, Grunewald J, et al. (2009) An efficient numerical solution method and implementation for coupled heat, moisture and salt transport: The Delphin Simulation Program. In: Franke L, Deckelmann G, and Espinosa-Marzal R (eds) *Simulation of Time Dependent Degradation of Porous Materials*. Göttingen: Cuvillier Verlag, pp. 85–100.

Ojanen T, Viitanen H, Peuhkuri R, et al. (2010) Mold Growth Modeling of Building Structures Using Sensitivity Classes of Materials. In: *Proceedings of Thermal Performance of the Exterior Envelopes of Buildings XI*, Clearwater Beach, Florida, 2010. ASHRAE.

Pavlík Z, Jiřičková M, Pavlík J, et al. (2005) Interior Thermal Insulation System Based on Hydrophilic Mineral Wool. *Journal of Building Physics* 29(1): 21–35.

Pedersen CR (1990) *Combined heat and moisture transfer in building constructions*. Technical University of Denmark.

Plagge R (2011) Energetic Refurbishment of Brick Buildings. Malmö: TU Dresden.

Poupeleer A-S (2007) *Transport and Crystallization of Dissolved Salts in Cracked Porous Building Materials. Ph.D Thesis*.

Rode C, Friis NK, Pedersen C, et al. (2020) Moisture performance of a new thermal insulation composite for interior application. Kurnitski J and Kalamees T (eds) *E3S Web of Conferences* 172: 01001.

Ruisinger U (2013) Long-term measurements and simulations of five internal insulation systems and their impact on wooden beam heads. In: *Proceedings of 2nd Central European Symposium on Building Physics*, Vienna, 2013.

Scheffler GA (2008) *Validation of Hygrothermal Material Modelling Under Consideration of the Hysteresis of Moisture Storage*. Dresden University of Technology.

Scheffler GA (2013) Frostempfindlichkeit kapillaraktiver Innendämmung. In: *2. Internationaler Innendämmkongress. Tagungsunterlage* (eds J Grunewald and R Plagge), Dresden, 2013. TU Dresden.

Scheffler GA and Plagge R (2010) A whole range hygric material model: Modelling liquid and vapour transport properties in porous media. *International Journal of Heat and Mass Transfer* 53(1–3): 286–296.

Tiltsen E (1932) Tsementkiviehitistest. *Tehnika Ajakiri ja Auto* 11(4): 60–61.

Toman J, Vimmrová A and Černý R (2009) Long-term on-site assessment of hygrothermal performance of interior thermal insulation system without water vapour barrier. *Energy and Buildings* 41(1): 51–55.

van Straaten R (2014) Improving Access to the Frost Dilatometry Methodology for Assessing Brick Masonry Freeze Thaw Degradation Risk. In: *Proceedings of the 14th Canadian Conference on Building Science and Technology*, Toronto, 2014, pp. 79–88.

Varda K (2017) *Külmumistsüklite mõju kapillaaraktiivsetele seespoolse lisasoojustuse süsteemidele*. Tallinn University of Technology.

Vendach F (1929) Kuidas asetada laetalad kiviseinale. *Tehnika Põllumajanduses* (4): 118–119.

Vereecken E (2013) *Hygrothermal analysis of interior insulation for renovation projects*. KU Leuven.

Vereecken E and Roels S (2013) Hygric performance of a massive masonry wall: How do the mortar joints influence the moisture flux? *Construction and Building Materials* 41: 697–707.

Vereecken E and Roels S (2014) A comparison of the hygric performance of interior insulation systems: A hot box–cold box experiment. *Energy and Buildings* 80: 37–44.

Vereecken E and Roels S (2015a) A numerical study of the influence of the hydraulic interface contact on the hygric performance of a multi-layered system. In: *XIII Conference on Durability of Building Materials and Components - XIII DBMC* (eds M Quattrone and VM John), 2015, pp. 512–519. RILEM Publications SARL.

Vereecken E and Roels S (2015b) Capillary active interior insulation: do the advantages really offset potential disadvantages? *Materials and Structures* 48(9): 3009–3021.

Vereecken E and Roels S (2016) Capillary Active Interior Insulation Systems for Wall Retrofitting: A More Nuanced Story. *International Journal of Architectural Heritage* 10(5): 558–569.

Vereecken E, Van Gelder L, Janssen H, et al. (2015) Interior insulation for wall retrofitting – A probabilistic analysis of energy savings and hygrothermal risks. *Energy and Buildings* 89: 231–244.

Veski A (1935) Uuemaid uurimisi niiskuse vastu võitlemiseks elukorterites ja keldrites Eestis. *Majaomanik* (12): 7.

Viitanen H and Ojanen T (2007) Improved Model to Predict Mold Growth in Building Materials. In: *Thermal Performance of the Exterior Envelopes of Buildings X*, 2007, p. 8.

Viitanen H, Ojanen T and Peuhkuri R (2011) Mould growth modelling to evaluate durability of materials. In: *Proceedings of the XII DBMC: 12th International Conference on Durability of Building Materials and Components* (eds VP de Freitas, MH Corvacho, and M Lacasse), Porto, 2011. FEUP Edições.

Viitanen H, Krus M, Ojanen T, et al. (2015) Mold Risk Classification Based on Comparative Evaluation of Two Established Growth Models. *Energy Procedia* 78: 1425–1430.

Vinha J, Valovirta I, Korpi M, et al. (2005) Rakennusmateriaalien rakennusfysikaaliset ominaisuudet lämpötilan ja suhteellisen kosteuden funktiona.

Vos BH and van Minnen J (1966) *Report no. II-11/23 n5: Moisture transport in porous materials*. Delft.

VTT and TTY (2018) Suomalainen homemalli / Finnish mould model calculation file (version 11.05.2018). Available at: https://research.tuni.fi/uploads/2019/01/suomalainen_homemalli_11052018.xlsx (accessed 14 January 2020).

Wetter M (2001) GenOpt-A generic optimization program. In: *Seventh International IBPSA Conference*, Rio de Janeiro, Brazil, 2001.

Wetter M (2016) *GenOpt® User Manual v3.1.1*. Berkeley: LBNL.

Zhou X, Desmarais G, Vontobel P, et al. (2020) Masonry brick–cement mortar interface resistance to water transport determined with neutron radiography and numerical modeling. *Journal of Building Physics* 44(3): 251–271.

Zirkelbach D and Künzel H (2013) Innendämmung von Außenwänden : Planungshinweise und Systemauswahl Design recommendations and system selection. *Detail Green*. München: Institut für Internationale Architektur-Dokumentation GmbH & Co. KG.

Zirkelbach D, Binder A and Künzel HM (2011) Kapillaraktive Innendämmungen - Wirkung und Beurteilung. In: *1. Internationaler Innendämmkongress 2011* (eds J Grunewald and R Plagge), Dresden, 2011, pp. 43–51. TU Dresden.

Казачек ГА and Роговин ЯА (eds) (1953) *Справочник Мастера-Строителя*. 2nd ed. Minsk: Государственное издательство БССР.

Acknowledgements

I would like to express my sincere gratitude to Targo Kalamees for being an inspiring and understanding supervisor and making the PhD project with its interesting on-site and laboratory measurements, conferences, meetings, and wonderful colleagues possible.

Thank you, Eleriin, for supporting me along the journey during weekdays and helping to drill out bricks and plaster the test walls in the weekend.

Thank you, Endrik Arumägi, for guiding me along the first steps of conducting research in the Wild East of Estonia and for being a jolly good roommate for the rest of the journey.

Thank you, Kadi Varda, for spending countless hours with me in the climate chamber constructing, drilling, pulling, cutting, weighing, drying, weighing, drying, weighing, drying, and weighing again the absurd number of samples for nearly too many times.

Thank you, Institute of Building Climatology team at TU Dresden, for enabling the fruitful visit in 2018 and co-operation. Namely John Grunewald, Peggy Freudenberg and Hauke Hirsch for helping me to take the dive into the magical world of material characterization and sharing material measurement data, and Uli Ruisinger & Heiko Fechner for relentlessly answering my questions about Delphin.

Thank you, Peeter Linnas, for introducing me to the inner workings of the climate chamber, making things happen and then keeping them going in the physical world.

Thank you, Kaia Koitmäe, Mattias Põldaru, Eneli Liisma, Tanel Tuisk, for the help measuring the material properties.

Thank you, Tuule-Mall Parts and Jaanus Hallik, for discussions about statistical testing and showing the shortcuts in Python wizardry.

Thank you, Kalle Kuusk, Raimo Simson, Simo Ilomets, Karl-Villem Võsa, Laura Kadaru, Kristo Kalbe, Villu Kukk, Martin Thalfeldt, Mikk Maivel and Peep Pihelo, for keeping the spirits high.

Thank you, Maris Mändel, for sharing thoughts on the historical background and values of the masonry structures both in-person and through your excellent PhD thesis.

Thank you, Piret Bossack, for ensuring the articles and prepositions are in right places.

Abstract

Hygrothermal Performance of Masonry Walls Retrofitted with Interior Insulation in Cold Climate

Background

Energy efficiency requirements, a better understanding of moisture safety and higher demands by users have created the need to find solutions to upgrade the envelope of heritage brick buildings. If the façades are valuable, the hygrothermally safer exterior insulation is not an acceptable solution. At the same time, traditional interior insulation solutions using mineral wool with or without a vapour barrier are risky due to possible mould hazard and moisture accumulation caused by wind driven rain. The latter can lead to the deterioration of the façade and structural problems in wooden beam ends which are supported by the wall.

During the last 15 years, the so-called "capillary active" insulation systems have been used in Central Europe to mitigate these risks. However, as part of the functioning principle of these systems is to tolerate higher moisture content than usual, their performance in colder climate cannot be warranted – frost damage risk and the effects of moisture loads can be a lot more pronounced there.

Methods

To assess the suitability of vapour open "capillary active" and "traditional" vapour tight solutions to Estonian climate, experimental and theoretical studies were carried out. Hygrothermal conditions of 6 different insulation systems in 3 real buildings were monitored. A study in a climate chamber investigated the effect of freezing and thawing on 3 "capillary active" interior insulation systems while monitoring the hygrothermal conditions too. To judge the accuracy of hygrothermal modelling in predicting the performance of the insulated walls, modelling results were compared to the measurements. A tool for liquid and vapour conductivity curve optimization was developed to take the capillary condensation redistribution test results into account and improve the accuracy of the modelling during non-isothermal wetting. Finally, a parametric modelling study using a 49-year real climate dataset aims to identify the effect of different insulation solutions and other parameters (bricks, indoor and outdoor humidity loads, etc.) and recommends the approaches that are on the safer side.

Results and conclusions

The solutions studied in this thesis offered a 2–3-fold reduction in thermal transmittances compared to the original walls, while also considerably increasing the interior surface temperatures. This shows the potential for energy savings, improved thermal comfort and reduced risk of mould growth on interior surfaces.

Field measurements showed that while in low indoor humidity loads, the selected solutions worked well and no performance criteria were exceeded. However, the test wall with humidity loads similar to high inhabitant density apartments hinted that the basic 95%$_{RH}$ performance criterion of "capillary active" insulation materials can be exceeded even if climate, original wall and insulation thicknesses were all favourable. This means that more sophisticated criteria – perhaps based on saturation degree and temperature – are required. The measurements also demonstrated that the dryout time of built-in moisture inherent to the "capillary active" insulation systems is considerable and should be accounted for when planning the retrofit.

Insight was gained into the frost resistance of the interior insulation systems: AAC, which was presumed to be frost resistant, showed a reduction of its tensile strength after freeze-thaw cycling (at ca 10%$_{sat}$ and ca -10°C). Expanded perlite showed similar performance as AAC, while no statistically significant loss of strength was detected in the unsaturated CaSi test wall. Frost caused damage in water-saturated CaSi. These results can be used as performance criterion.

Comparisons between modelling and measurements showed good agreement in thermal performance, while modelling underestimated relative humidity levels during wetting and overestimated them during drying periods hinting at hysteretic effects that are not considered by the model. Worryingly, the "conventionally characterized" material properties (as currently mostly found in modelling software databases) severely underestimated overhygroscopic moisture content levels in "capillary active" insulation materials when subjected to non-isothermal wetting through vapour diffusion. Unfortunately, it is one of the standard use cases for such materials.

The inclusion of the capillary condensation redistribution (CCR) test into the dataset that liquid and vapour conductivity curves were derived from improved the correlation in the overhygroscopic moisture range during non-isothermal wetting, while conservatively reducing agreement with the drying experiment (i.e. overestimated the moisture content). Still, when avoiding frost and moisture damage is the aim with the currently widely used HAM-modelling software, using "conventionally characterized" material data can lead to overly optimistic assumptions of the hygrothermal performance of the "capillary active" interior insulation systems. Thus, it makes sense to include the CCR test in material characterization procedures to overcome that.

Parametric modelling using a 52 cm-thick brick wall and long-term dataset showed that the exterior layer of masonry must tolerate higher ice saturation levels and freeze-thaw cycles regardless of the insulation type (vapour open or tight). Also, frost in the insulation layer can be an issue for both AAC and CaSi insulation systems in certain cases. To avoid frost damage in old interior plaster and preserve capillary contact (which is essential for "capillary active" insulation), the layer should be removed before applying interior insulation. Mould indexes behind the insulation were high – emphasis should be put on achieving airtight installation of both vapour tight and vapour open "capillary active" insulation systems. While the chances of success are high when using interior insulation, case-by-case approach is necessary to avoid the critical combinations.

Keywords: interior insulation, hygrothermal modelling, historic masonry, measurements

Lühikokkuvõte

Kivikonstruktsioonide seespoolse lisasoojustuse soojus- ja niiskustehniline toimivus külmas kliimas

Taust

Energiatõhususe nõuded, parem arusaam niiskusturvalisusest ning varasemast kõrgemad ootused soojuslikule mugavusele on loonud vajaduse kultuuriväärtuslikele hoonetele sobivate soojustuslahenduste järgi. Kuigi väljast soojustamine on niiskustehniliselt turvaline, pole see väärtuslike fassaadide puhul aktsepteeritav lahendus. Seespoolselt mineraalvillaga soojustades kaasnevad samas hallituserisk ning aurutõket kasutades kaldvihmast tingitud niiskuse akumulatsioon. Viimane kiirendab omakorda fassaadide lagunemist ning müüritisele toetuvate vahelaetalaotste mädanemist.

Viimase 15 aasta jooksul on Kesk-Euroopas hakanud levima "kapillaaraktiivsete" soojustusmaterjalide kasutamine, mis peaksid mainitud riske maandama. Paraku, kuna osaks nende materjalide toimimispõhimõttest on taluda tavalisest kõrgemaid niiskussisaldusi, ei saa eeldada, et nende toimivus on lisaks Kesk-Euroopale ka külmemas kliimas tagatud – niiskuskoormuste mõju ja külmakahjustused võivad siin olla palju rõhutatumad.

Meetodid

Hindamaks "kapillaaraktiivsete" ja "traditsiooniliste" seespoolse lisasoojustuslahenduste sobivust Eesti kliimasse kasutati katselisi ja arvutuslikke meetodeid. 6 erineva soojustussüsteemi soojuslikku ja niiskuslikku toimivust jälgiti kolmes hoones. Uuringuga kliimakambris hinnati 3 "kapillaaraktiivse" soojustussüsteemi külmakindlust ning samal ajal jälgiti ka soojuslikke ja niiskuslikke tingimusi.

Et pelgalt mõõtmiste põhjal hinnangute andmine oleks liialt töö- ja ajamahukas, on suureks abiks soojuse, õhu ja niiskuse (SÕN) modelleerimine. Esmalt võrreldi katseliselt kogutud mõõtmistulemusi samade olukordade modelleerimistulemustega. Seejärel arendati välja tööriist soojustusmaterjalide vedeliku- ja aurujuhtivuskõverate optimeerimiseks ning seeläbi modelleerimistäpsuse tõstmiseks. Laiema ülevaate saamiseks ning soovituste andmiseks modelleeriti lõpuks 49 aasta Tõravere väliskliima abil parameetriliselt nii aurutihedat kui "kapillaaraktiivseid" lahendusi varieerides nt tellise- ja mörditüüpe, sise- ja väliskliimakoormusi, seina asendit jpm.

Tulemused ja järeldused

Töös uuritud lahenduste abil saavutati 2–3 korda madalam soojusläbivus kui esialgsetel soojustamata seintel ning tõusid ka sisepinnatemperatuurid. See tähendab energiasäästupotentsiaali, kõrgemat soojuslikku mugavust ning välispiirete sisepindade madalamat hallitusriski.

Välimõõtmiste tulemused näitasid, et madalates siseõhu niiskuskoormustes toimisid uuritud lahendused hästi ning toimivuskriteeriume ei ületatud. Kui siseõhu niiskuskoormus oli võrreldav kõrge elaniketihedusega korteritega, ületati perioodiliselt kapillaaraktiivsete soojustusmaterjalide lihtsustatud 95%$_{RH}$ toimivuskriteeriumi – seda isegi juhul, kui esialgne sein, kliima ning soojustuse paksused olid toimivuse jaoks soodsad. Et selliseid tingimusi lubada, on vaja põhjalikumatele uuringutele tuginevaid toimivuskriteeriume (nt materjali küllastustasemest ning temperatuurist sõltuv külmakindluse piir). Mõõtmised näitasid veel, et märgpaigaldusega "kapillaaraktiivsete"

süsteemide ehitusniiskuse väljakuivamise kestus on märkimisväärne ning sellega tuleks ehitustöid planeerides arvestada.

"Kapillaaraktiivste" soojustussüsteemide külmakindluse uuring näitas, et eelduslikult külmakindla poorbetooni tõmbetugevus siiski pärast külmumis-sulamistsükleid (≈ 10%$_{sat}$ küllastustaseme ja ≈ -10 °C temperatuuri juures) langes ning ka paisutatud perliit käitus analoogselt poorbetoonsüsteemile. Kaltsiumsilikaatsoojustusega testseinas tõmbetugevuse langust 10-20%$_{sat}$ küllastustaseme ja ≈ -8 °C juures ei tuvastatud, küll aga ilmnesid kahjustused veega küllastatud katsekehades. Need andmed on koos kirjandusest leitud andmetega kasutatavad külmakindluse toimivuskriteeriumina.

Mõõtmis- ja arvutustulemuste võrdlus näitas, et soojuslikult on korrelatsioon hea, samas kui modelleeritud suhteline niiskus oli märgumisel alahinnatud ning kuivamisel ülehinnatud, mis vihjab mudeli poolt arvestamata hüstereesi mõjule. Paraku alahindas "traditsiooniliselt" määratud auru- ja veejuhtivusfunktsioonidega modelleerimine ülehügroskoopses piirkonnas märgumisprotsesside niiskussisaldusi. Viimane on aga tüüpiline "kapillaaraktiivse" seespoolse lisasoojustuse kasutamisjuhtum.

Kui materjalide auru- ja vedelikujuhtivuse kõverad määrata lisaks varasemale ka kapillaarkondensaadi ümberjaotuskatse (*capillary condensation redistribution* ehk CCR ehk *kapi-test*) põhjal, paranes oluliselt mitteisotermilise märgumisprotsessi korrelatsioon mõõtmistega ülehügroskoopses piirkonnas, aga suurenes kuivamiskatses tehtav viga (niiskussisaldus ja kuivamise kestus on ülehinnatud). Kuna kuivamiskatsel tehtav viga on tagavara kasuks, aga märgumisel saavad tuvastatud varem ehk märkamata jäänud külma- ja niiskuskahjustused, siis tulevikus on mõistlik kapillaarkondensaadi katse analoogsete materjalide omaduste määramisel siiski kohe sooritada.

Parameetrilised arvutused 52 cm-paksuse tellisseinaga 49 aasta Tõravere väliskliima tingimustes näitasid, et nii aurutiheda kui "kapillaaraktiivse" auru juhtiva soojustuslahenduse puhul peab müüritise väliskiht taluma varasemast kõrgemaid jääküllastuse tasemeid ning rohkem külmumistsükleid. Soojustuskihis võib külmumine teatud kombinatsioonide puhul probleeme valmistada nii poorbetoon- kui kaltsiumsilikaatsoojustussüsteeme kasutades. Et vältida külmakahjustusi vanas sisekrohvis (ning "kapillaaraktiivsete" süsteemide puhul ka kapillaarsidemete katkemist) tuleks see enne seespoolse lisasoojustuse paigaldust eemaldada. Soojustusetagused hallitusindeksid olid kõrged kõigi lahenduste puhul – paigaldustöödel tuleb jälgida, et soojustusekiht jääks õhutihe vältimaks hallituseoste kandumist soojustuse taha ning võimaliku hallitusekasvu puhul ka mükotoksiinide jõudmist siseõhku. Kuigi seespoolse lisasoojustuse kasutamisel on suur tõenäosus saavutada toimiv lahendus, on kriitiliste kombinatsioonide vältimiseks vajalik juhtumipõhine lähemine.

Märksõnad: seespoolne lisasoojustus, soojus- ja niiskustehniline modelleerimine, ajalooline müüritis, mõõtmised

Appendix

Original Article

Hygrothermal performance of internally insulated brick wall in cold climate: A case study in a historical school building

Paul Klõšeiko, Endrik Arumägi and Targo Kalamees

Abstract

Interior thermal insulation is frequently one of the only possible solutions for thermal upgrade of the building envelope where the external appearance cannot be changed. In this study, four insulation materials were used in a case study in a historical school building in in situ test walls. The indoor climate in the test room was controlled to simulate the typical dwelling with high moisture load. The temperatures, relative humidity, and heat flows were monitored over 9 months to analyze the hygrothermal performance of four different insulation materials. The hygrothermal performance of insulation materials during drying and wetting periods are presented. Moisture test reference year was used in working out possible energy-renovation solutions. The results show that timing of the renovation works is a matter of consideration to avoid the hygrothermal risks inside the renovated wall assemblies. The results show that in all the cases, thermal comfort can be improved by increasing the inner surface temperature and decreasing thermal conductivity. However, in some cases, the risks of mold growth and interstitial condensation were present inside the retrofitted wall assemblies. Computer simulations of the wall assemblies with moisture reference years under different humidity loads concluded that all solutions are suitable for future analysis.

Chair of Building Physics and Energy Efficiency, Department of Structural Design, Faculty of Civil Engineering, Tallinn University of Technology, Tallinn, Estonia

Corresponding author:
Paul Klõšeiko, Chair of Building Physics and Energy Efficiency, Tallinn University of Technology, Ehitajate tee 5, 19086 Tallinn, Estonia.
Email: paul.kloseiko@ttu.ee

Introduction

During the last years, campaigns have promoted and explained the need to save energy in buildings. The improvement of existing buildings has raised people's awareness of energy consumption.

Historic buildings are forming well-preserved areas in all the larger cities in Estonia. These areas are nominated as milieu valuable areas and are protected by planning laws. The main focus is on the built-up environment, and therefore, preserving the exterior of the buildings is essential.

The simplest way to save energy in apartment buildings is to improve the building envelope by lowering the heat losses through the existing walls, ceilings, and windows. By improving the building envelope with additional thermal insulation, it is possible to save energy and increase thermal comfort. Adding insulation to the external walls is a common solution. That can be easily used to lower the heat losses through the existing exterior walls if the buildings have no restrictions because of their architectural and historical values and if the exteriors can be changed.

However, there exists a strong pressure to use internal insulation as an energy-conservation measure in historic buildings, because their architectural and historic values set limitations on the use of external thermal insulation.

Maurenbrecher et al. (1998) monitored hygrothermal performance of an internally insulated 765-mm thick masonry wall. As a result of the renovation, the thermal resistance of the wall increased by 47% to 63%. The temperature between the insulation layer and masonry drops below freezing temperature for several months in the winter. Nevertheless, the moisture levels did not seem to be a problem in the monitored wall sections.

Hens (1998) studied the hygrothermal performance of masonry walls insulated on the inside face and indicated that it increased the thermal bridging effect of the partition walls, which resulted in much lower thermal resistance than that calculated.

Today's living habits cause higher indoor air humidity and therefore building structures face larger humidity loads. Using correctly dimensioned vapor barriers can prevent the water vapor penetration to the construction. However, the quality of the installation is not always guaranteed, and therefore the risk potential remains.

In addition to limiting the water vapor diffusion into structures, there is also the possibility of using capillary-active insulation materials. With these materials, it is possible to decrease the initiation of moisture problems and upgrade the thermal resistance of the existing walls (Scheffler and Grunewald, 2003). Stopp et al. (2001) found that with new materials and new technologies inside, insulation can be a viable method. The authors preferred calcium silicate because this material can distribute the liquid moisture content in the structures, and, therefore, accelerate the

drying-out process. Häupl et al. (2003, 2004) demonstrated the function of the insulation systems by presenting the measurement results of several internal insulation systems at a number of different outside wall constructions. The application of capillary-active inside insulation materials proved advantageous for the drying process of potential built-in moisture as well as for the limitation of the condensation amount during winter. The thermal transmittance of the building walls could approximately be halved in the presented cases without the necessity of vapor barriers. Toman et al. (2009) presented long-term on-site assessment of hydrophilic mineral wool insulation system without water vapor barrier. The reconstructed building envelope exhibited very good hygrothermal performance. Nevertheless, Morelli et al. (2010) performed a computational analysis of the internal insulation solution of masonry walls with wooden floor beams in northern humid climate and showed that the solution would almost halve the heat loss through the wall section compared to the original one but the internal insulation reduces the drying potential of the wall, which can lead to moisture problems.

Scheffler (2011) introduced an innovative and sustainable internal insulation system based on a lightweight autoclaved aerated concrete. The results showed that though the moisture content inside the masonry structure increased, the overall moisture level was kept below critical value.

Vereecken and Roels (2011) made a hygrothermal comparison between capillary-active and traditional vapor-tight interior insulation system. The performance of the capillary-active system is shown to be more sensitive to the different parameters (wind-driven rain load, orientation, catch ratio, finishing coat, thickness of the wall, etc). Additionally, there exists a large number of uncertainties concerning internal insulation (Nielsen et al., 2012; Zhao et al., 2011).

Most of these computational and experimental studies have focused on wall structures in Central European climatic conditions. In cold climate, external thermal insulation is hygrothermally a much safer solution than internal thermal insulation. Frequently, in hygrothermal performance, risks arise. To avoid the possible mold growth and condensation problems, special attention should be paid during the design and installation phase of the renovation solution.

A better understanding of the hygrothermal performance of the interior insulation retrofit approach in cold climate is needed. In this study, four solutions of internal thermal insulation for the brick wall are tested. An analysis was carried out to assess the impact of an interior insulation retrofit on the hygrothermal performance of a brick wall. The article describes the test wall setup, presents measurement results over one year period, calibration of numerical simulation models and computational analysis with various humidity loads.

Methods

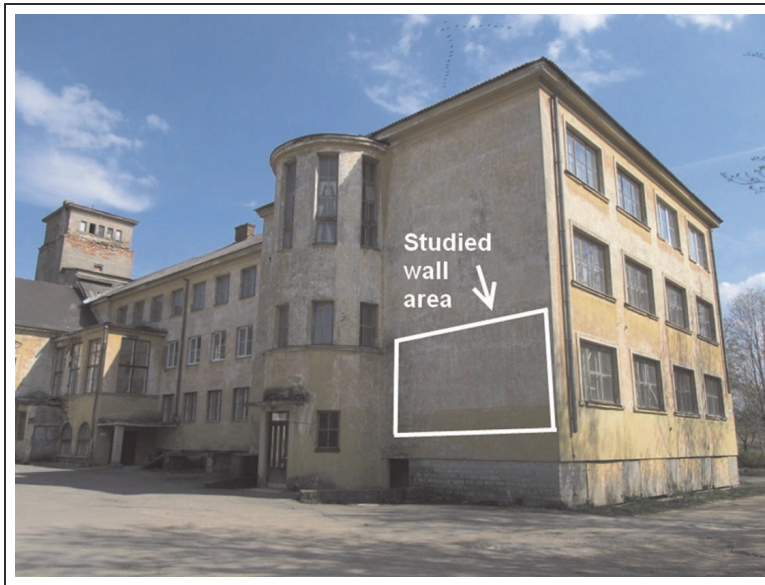Field measurements on a school building (Figure 1) and computer simulations were used in this study.

Figure 1. View of the studied school building.

Field measurements

To compare the hygrothermal performance of different internal insulation materials and to work out energy-renovation solutions for a historic school building, the exterior wall was insulated with four materials (Figure 2). Materials were selected so that diffusion open, capillary-active, and vapor-tight materials were used:

- calcium silicate (CaSi): capillary-active material with very high open porosity and low vapor diffusion resistance;
- aerated concrete (AAC) with high open porosity, lower capillary activity and thermal conductivity;
- polyurethane board with capillary-active channels (IQ-T)—combines low thermal conductivity and a certain capillary activity;
- polyisocyanurate (PIR) board with closed pores: low thermal conductivity and relatively high vapor diffusion resistance forming a vapor barrier in itself.

The original brick wall was 73–75 cm thick, composed of three layers of brick with two air and insulation (peat) layers between them. The thickness of the insulation layer was selected to represent typical products and to avoid large thermal transmittance differences between the walls.

Each test wall was equipped with two temperature and relative humidity (*RH*) sensors between insulation and the original wall (Ø 5 mm, Rotronic HC 2 SC05) and heat flow plates (Hukseflux HFP01) on the internal surface of insulation. Internal and external surface temperatures were also measured.
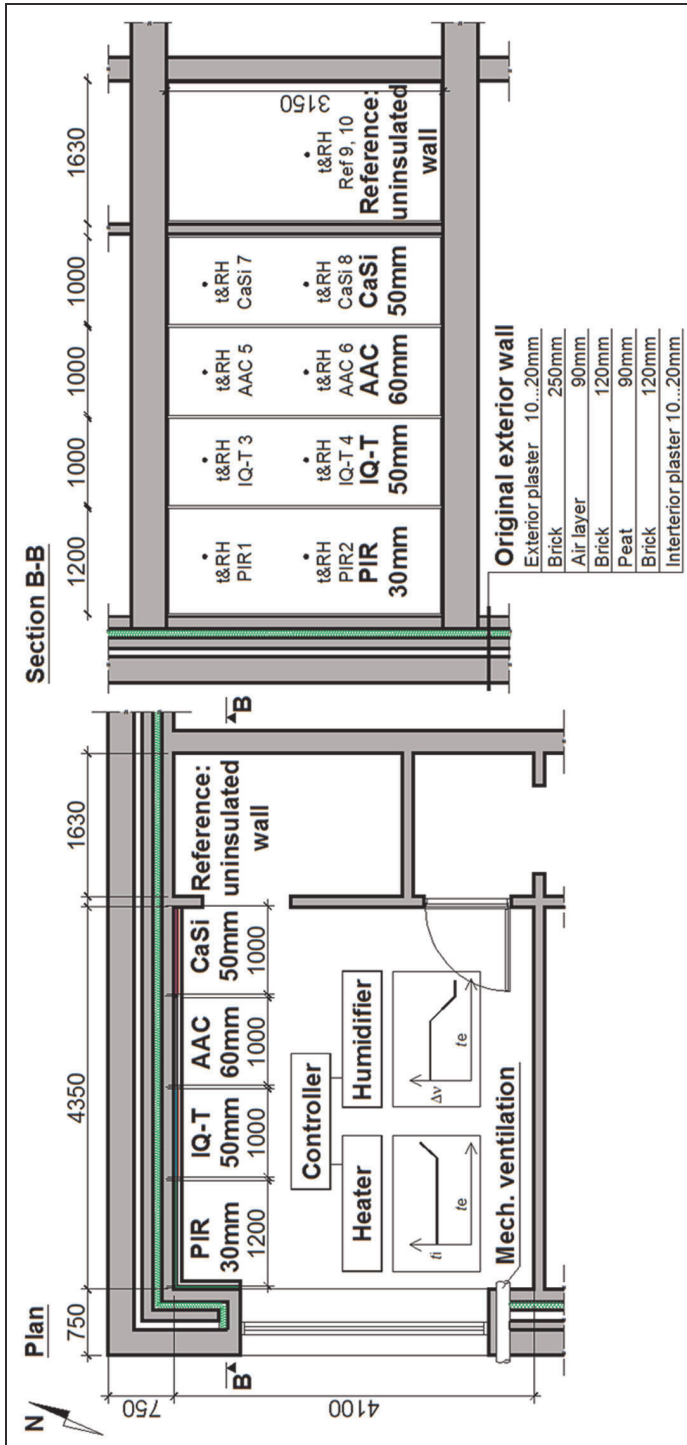
Figure 2. Plan and section/view of the studied test walls.
PIR: polyisocyanurate board.

Indoor climate was heated with the set point of thermostat $+21°C$ and humidified to keep the moisture excess of $+2.3$ to $+4.4$ g/m^3, to represent the average conditions in dwellings with high humidity loads (Kalamees, 2006).

The climatization of the test room was started by an attempt to imitate a typical renovation process:

- Period 1 (P1): internal insulation works and starting to heat the room: 27 March 2012; $\Delta\nu + 0.1$ g/m^3
- Period 2 (P2): starting to humidify $\sim$3 months after installation (4 July 2012) to represent time period between the renovation and moving back in, high humidity load; $\Delta\nu + 2.3$ g/m^3 (humidified)
- Period 3 (P3): humidifying period to see the influence of different humidity loads on hygrothermal performance of test walls, medium high humidity load: 4 July 2012 to 8 October 2012; $\Delta\nu + 2.9$ g/m^3
- Period (P4): medium humidity load, 8 October 2012 to 14 December 2012; $\Delta\nu + 4.2$ g/m^3 (humidified)
- Period 5 (P5): with low humidification (from 14 December 2012) to see drying-out potential of different walls; $\Delta\nu + 2.5$ g/m^3 (humidified according to indoor *RH*)

To assess the conditions favorable for mold growth, the Finnish mold growth model (Viitanen et al., 2010; Viitanen and Ojanen, 2007) was used. Critical *RH* levels, namely, $RH_{\text{crit}} > 80\%$ and $RH_{\text{crit}} > 95\%$ depending on substrate category were used. $RH_{\text{crit}} > 80\%$ in case of PIR was used, because the side which is in contact with the original wall is covered with paper. $RH_{\text{crit}} > 95\%$ for stone materials (CaSi and AAC) and IQ-T were used.

Computer simulations

The results of temperature and humidity measurements from test walls were compared in a one-dimensional (1D) model with a commercial hygrothermal simulation program DELPHIN 5.8.1 (Grunewald, 1997; Nicolai et al., 2008). There were three main reasons for this comparison:

- to acquire a better understanding of the hygrothermal performance of the internally insulated brick walls;
- to validate the simulation model for future simulations with different initial and climatic conditions as well as with different dimensions of the building envelope;
- to test the suitability of internal insulation solutions for that specific historic school building.

The material producer's data and simulation program's (DELPHIN) material libraries were used to provide material properties. In addition, several properties of

the original brick (open porosity, absorption coefficient of water, density) were measured in laboratory. Although an exact equivalent was not found from the database, several bricks with similar properties were tested and the best match was chosen for further fine-tuning. Vapor diffusion and liquid water conduction curves were scaled to match the measured material properties and in situ test results.

The hygrothermal properties for the peat layer were based on literature (Jürgenson, 1942; Kuts and Sheiman, 1965; Mikk, 1977; Vinha et al., 2005).

The dependency of hygrothermal properties on the environmental conditions was taken into account: water vapor permeability, liquid water conductivity, and thermal conductivity dependent on water content of a material. The main properties of materials used in the study are shown in Table 1.

To test the hygrothermal performance of energy-renovation solutions, Estonian moisture test reference year (Kalamees and Vinha, 2004) was used for outdoor climate. For indoor climate, three different humidity load levels were used: $\Delta\nu +$ 2 g/m^3 (school, office), $+4$ g/m^3 (low humidity load in dwellings), and $+6$ g/m^3 (high humidity loads in dwellings).

Results

Climate conditions

Indoor and outdoor temperatures as well as temperatures between the insulation and the original wall are shown in Figure 3. Outdoor air temperatures fluctuated from $+17$°C to $+30$°C in July, with an average of $+19.4$°C. Temperature until December was rather mild, with an average temperature of $+5.4$°C in November and minimum temperatures reaching $+1$°C on a number of occasions.

According to Künzel (2011), freezing should be avoided to prevent damage to the materials. Although the outdoor air temperature stayed under -10°C for 8 days in December, none of the sensors detected temperatures below 0°C between the insulation systems and original wall.

Conditioned indoor temperature stayed the same throughout the heating period ($+21 \pm 0.5$°C). A drop (minimum of $+17.5$°C) of the indoor temperature during the cold period in December was caused by the low power setting of additional heating in the room.

Figure 4 shows the values of moisture excess plotted against exterior temperature. On the graph, different periods of humidification can be identified. Average values of moisture excess were 0.1, 2.3, 2.9, 4.2, and 2.5 g/m^3 for periods P1 to P5, respectively. Figures 8 to 11 show the duration of the periods.

Comparison of reactions to changes in climate conditions

Comparisons of relative humidities during the period without humidification (P1) of the test walls are given in Figure 5. Drying-out period finished fastest in the case of CaSi (24 days), AAC section dried to the same level in 38 days, whereas IQ-T

Table 1. Properties of used materials

Property	RH	Original wall materials				Insulation materials			
		Exterior plaster	Brick	Peat	Interior plaster	PIR	IQ-T	AAC	CaSi
Dry density, kg/m³	0%	1270	1800	150	1800	35	49	126	297
Thermal conductivity λ, W/(m·K)	0%	0.55	0.70	0.07–0.09	0.82	0.020	0.029	0.045	0.067
	33%	0.56	0.70	0.07–0.09	0.82	0.020	0.029	0.046	0.071
	75%	0.58	0.70	0.07–0.09	0.83	0.021	0.029	0.047	0.075
	⩾ 93%	0.59	0.71	0.07–0.09	0.83	0.022	0.030	0.054	0.077
Moisture content, kg/m³	33%	11	4.8	9.1	2.3	0.49	0.27	1.3	16
	75%	57	6.4	18	9.2	0.96	0.35	3.4	21
	⩾ 93%	75	13	42	25	4.4	1.4	16	26
Vapor diffusion resistance coefficient μ	0%	12	25	2	12	400	51	6	11
	33%	12	25	2	12	400	51	6	11
	75%	14	25	2	13	400	51	6	11
	⩾ 93%	14	26	2	13	400	51	6	11
Water absorption coefficient A_w, kg/(m² h$^{0.5}$)		0.0093	0.055	0.15	0.127	1.0×10^{-7}	0.013	0.0036	0.39

AAC: aerated concrete; CaSi: calcium silicate; IQ-T: capillary-active channels; PIR: polyisocyanurate board; RH: relative humidity.
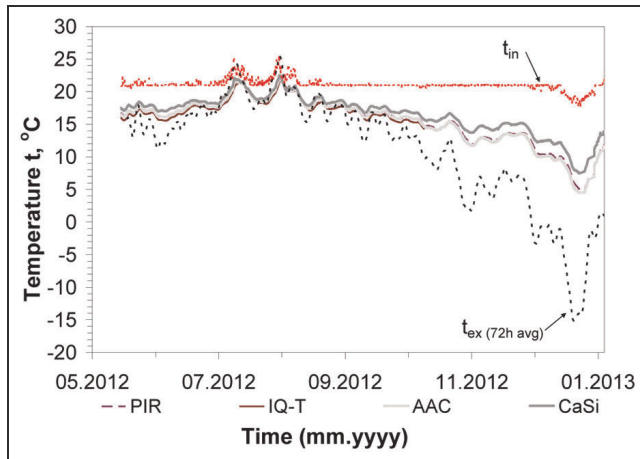
Figure 3. Temperatures between insulation systems and original wall and indoor/outdoor air temperatures.
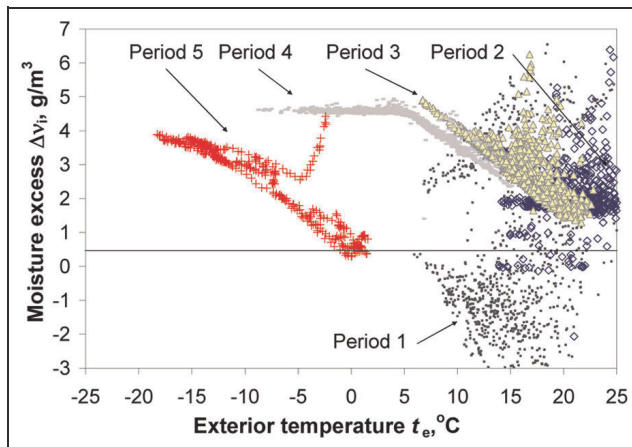AAC: aerated concrete; CaSi: calcium silicate; IQ-T: capillary-active channels; PIR: polyisocyanurate board.

Figure 4. Indoor moisture excess dependent on exterior temperature.

reached the lowest *RH* of 86% at the start of humidification (3 months after the installation).

Figure 6 shows the period of the start of humidification (transition from P1–P2). Two distinct behaviors are apparent—in the case of low vapor diffusion resistance (AAC, CaSi), the *RH* level behind the insulation follows the indoor conditions closely. PIR and iQ-T, on the other hand, reacted more slowly. Second period of drying (P5) is visible in Figure 7; permeable materials stabilize in about 5 days.
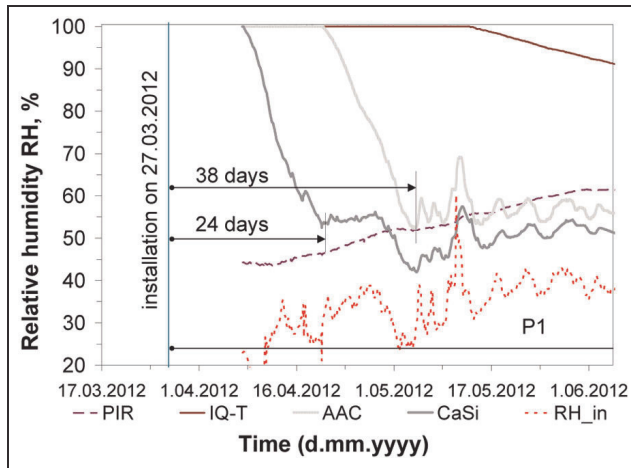
Figure 5. Drying period without humidification—relative humidities between insulation systems and original wall.

AAC: aerated concrete; CaSi: calcium silicate; IQ-T: capillary-active channels; PIR: polyisocyanurate board; RH: relative humidity.
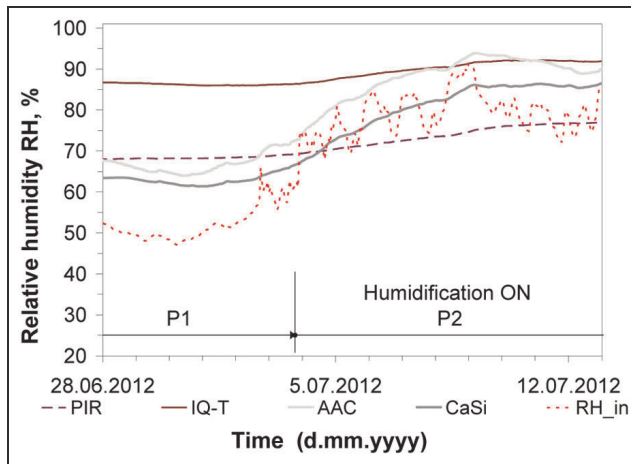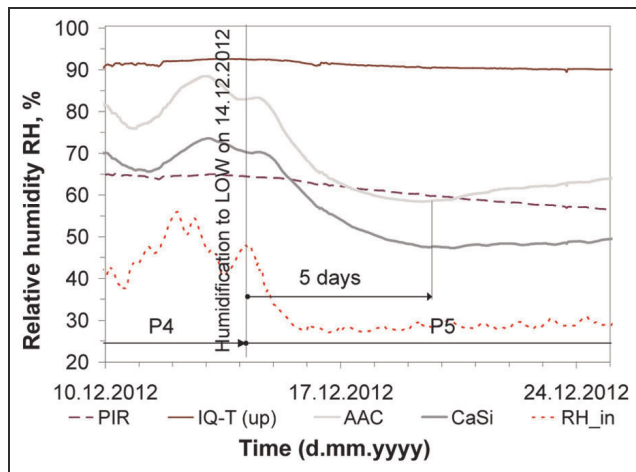

Figure 6. Start of humidification—relative humidities between insulation systems and original wall.

AAC: aerated concrete; CaSi: calcium silicate; IQ-T: capillary-active channels; PIR: polyisocyanurate board; RH: relative humidity.

Moisture performance of the test walls

Relative humidity between the insulation and the original wall. Relative humidity behind the insulating layer and the surface of the original wall from different walls are given in Figures 8 to 11. These charts also show the corresponding values of the

Figure 7. Drying period with no humidification—relative humidities between insulation systems and original wall. Time for permeable materials to reach stable level.
AAC: aerated concrete; CaSi: calcium silicate; IQ-T: capillary-active channels; PIR: polyisocyanurate board; RH: relative humidity.
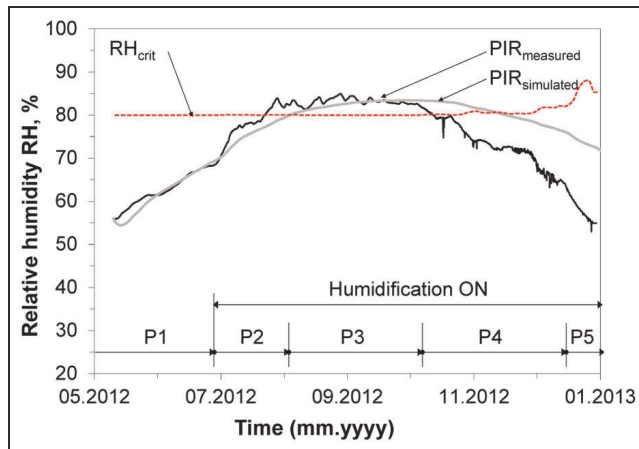

Figure 8. Relative humidity between PIR board and original wall and periods of humidification.
PIR: polyisocyanurate board; RH: relative humidity.

relative humidity as simulated in DELPHIN and the assessment criteria for proper hygrothermal performance.

Figure 8 exhibits the relative humidity of the PIR test wall. Measured values of the relative humidity exceeded the critical limit ($RH \sim 80\%$) for 78 of the 230 days of the test duration. Both the measured and simulated humidities dropped to safer levels during P4, while the lack of humidification (second half of December 2012) lowered it even further.
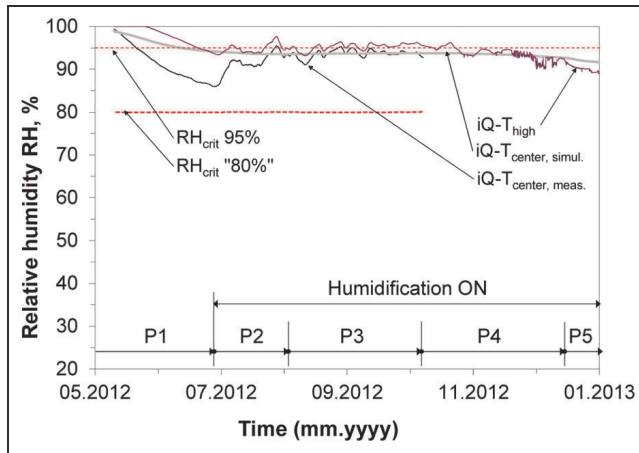
Figure 9. Relative humidity between IQ-T insulation system and original wall and periods of humidification.

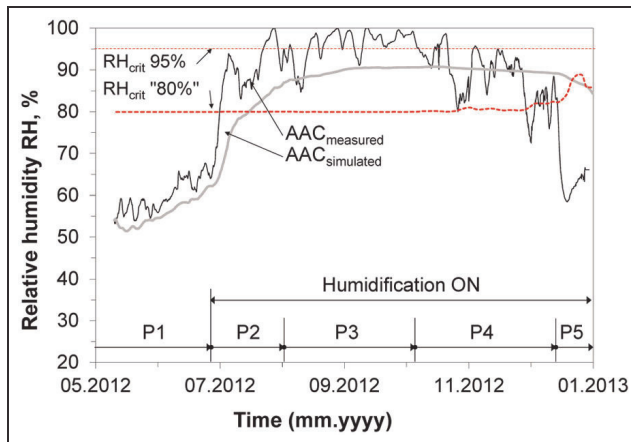IQ-T: capillary-active channels; RH: relative humidity.

Figure 10. Relative humidity between AAC insulation system and original wall and periods of humidification.

AAC: aerated concrete; RH: relative humidity.

Figure 9 shows the relative humidity behind the IQ-T insulation until the error of the measurement system. The value of *RH* stayed just below the limit of 95%, which is also the region where the capillary transport of humidity increases significantly. As a reference, the *RH* of the sensor close to the ceiling (IQ-T$_{high}$) is given.

Relative humidity behind the layer of AAC (Figure 10), due to its low water vapor diffusion resistance, reacted more quickly and drastically to the changes of
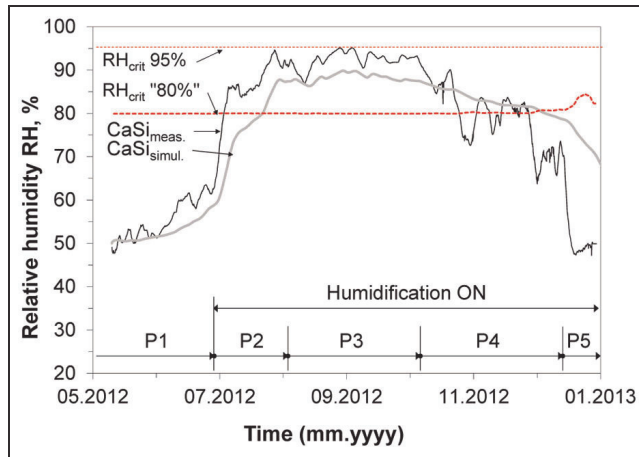
Figure 11. Relative humidity between CaSi insulation system and original wall and periods of humidification.
CaSi: calcium silicate; RH: relative humidity.

indoor humidity. The period with higher moisture excess resulted in 59 h of possible condensation.

Likewise to the AAC wall segment, the *RH* graph of CaSi (Figure 11) exhibits high fluctuations which follow the changes in the indoor relative humidity. However, the overall level stays lower, with the maximum value of 95% during P3. This is due to lower insulation thickness and higher thermal conductivity which leads to higher temperatures behind the insulation, while the absolute humidities stay practically on the same level.

As the simulated *RH* levels for both CaSi and AAC were considerably lower than measured values, a safety margin of $5\%_{RH}$–$10\%_{RH}$ should be used when analyzing future simulation results.

Thermal conductivity and surface temperature. Thermal transmittance was calculated based on heat flow and surface temperature measurements for the period from 1 September 2012 to 28 December 2012. This period was chosen because of low temperature fluctuations and solar radiation. The average values for thermal transmittance are given in Figure 12.

Higher water vapor content was found to have an inconsiderable effect on the thermal transmittance, as the moist values of all materials dropped ~3% during the period without humidification. This is quite unexpected, as the reduction of the moisture content of the vapor-permeable materials was more significant than on the PIR.

The average values of surface temperature in November stayed within 19.2°C–19.8°C and the average for the uninsulated reference wall was 17.3°C (average indoor temperature 20.9°C). During the cold period in December, the surface temperature of the reference wall dropped to an average of 13.1°C, while the sections
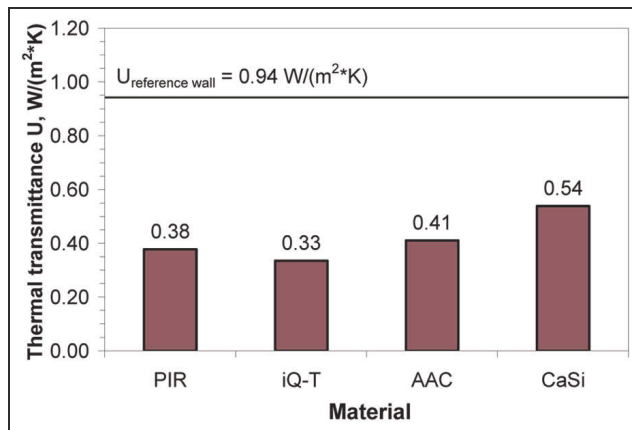
Figure 12. Average thermal transmittances calculated from measured heat fluxes of reference and insulated walls during the period 1 September 2012 to 28 December 2012.
AAC: aerated concrete; CaSi: calcium silicate; IQ-T: capillary-active channels; PIR: polyisocyanurate board.

with insulation stayed 3°C–4°C higher (average indoor temperature 19.0°C), depending on the material.

Hygrothermal performance of the internally insulated wall during moisture reference year. The moisture reference years (MRYs; Kalamees and Vinha, 2004) were used to test the hygrothermal performance of the internally insulated brick wall. The internal moisture loads were chosen according to different use of the rooms: $\Delta\nu +$ 2 g/m^3 as a school or office room; $\Delta\nu +$ 4 g/m^3 as a dwelling with the low humidity load; and $\Delta\nu +$ 6 g/m^3 as a dwelling with the high humidity load.

Figures 13 and 14 present *RH* results between original wall and additional interior thermal insulation calculated with calibrated wall models and MRYs for mold growth under different moisture loads.

Table 2 gives the overview about *RH* results between original wall and additional interior thermal insulation in case of different indoor and outdoor climate conditions. The percentage of the time when the $RH > RH_{crit}$ (RH_{crit} 80% for PIR and RH_{crit} for other materials 95%) is also presented in Table 2.

Discussion

The hygrothermal performance of four internally insulated test walls was compared in field conditions. Sections of thermal insulation systems that were 1000 mm wide were installed on the same wall in the test room. Because of the possible moisture and heat flux between the test wall sections the different parts were separated by 50-mm wide joints. In the existing wall the ~50-mm deep grooves were cut and cleaned. Afterward, the joints in the existing wall and between the different insulation sections were completed with aluminum foil and polyurethane foam.
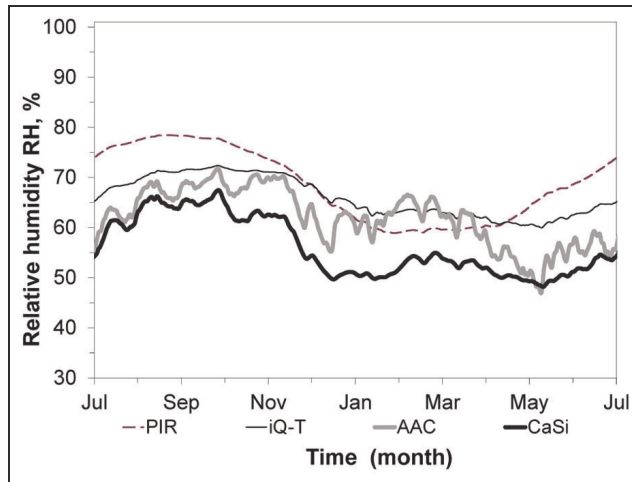
Figure 13. Relative humidity behind the insulation layer during 1 year after equilibrium has been reached, $\Delta\nu = 2$ g/m^3, mold moisture reference years (MRYs).
AAC: aerated concrete; CaSi: calcium silicate; IQ-T: capillary-active channels; MRYs: moisture reference years; PIR: polyisocyanurate board; RH: relative humidity.

Figure 14. Relative humidity behind the insulation layer during 1 year after equilibrium has been reached, $\Delta\nu = 6$ g/m^3 mold MRYs.
AAC: aerated concrete; CaSi: calcium silicate; IQ-T: capillary-active channels; MRYs: moisture reference years; PIR: polyisocyanurate board; RH: relative humidity.
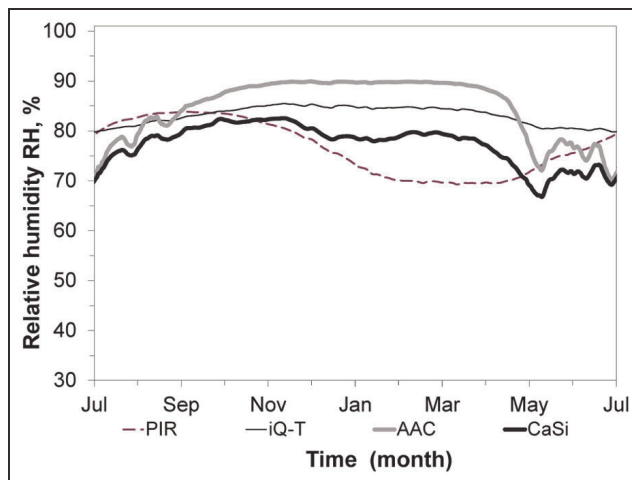
Although there may have been some minor leaks between the test walls, the potential for the vapor diffusion and heat conduction was low and possible heat and moisture movement between the test walls was probably minor. Another factor influencing the accuracy of direct comparison between the wall sections could be

Table 2. Results of the simulations: minimum and maximum RH levels under different climate conditions and percentage of hours of the calculated MRY exceeding the RH_{crit} level in the wall

Insulation material	MRY	Moisture excess $\Delta\nu$, g/m^3	RH min	max	$RH{>}RH_{crit}$ % $RH > RH_{crit}$
PIR, 30 mm	Mold	+2	59	79	0
		+4	64	82	19
		+6	69	84	36
	Condensate	+2	55	79	0
		+4	61	81	10
		+6	66	83	30
IQ-T, 50 mm	Mold	+2	61	73	0
		+4	72	79	0
		+6	80	86	0
	Condensate	+2	53	73	0
		+4	66	78	0
		+6	78	84	0
AAC, 60 mm	Mold	+2	47	72	0
		+4	58	84	0
		+6	70	90	(cond.[a])
	Condensate	+2	37	76	0
		+4	57	85	0
		+6	72	90	(cond.[a])
CaSi, 50 mm	Mold	+2	49	68	0
		+4	57	76	0
		+6	67	83	0
	Condensate	+2	37	69	0
		+4	51	76	0
		+6	64	83	0

AAC: aerated concrete; CaSi: calcium silicate; IQ-T: capillary-active channels; MRYs: moisture reference years; PIR: polyisocyanurate board; RH: relative humidity.
[a]Possible underestimation of RH levels in computational models—condensation could take place.

non-uniform distribution of insulation in the existing wall and air flows in cavities. This may be considered as a general limitation of the field study.

The temperatures measured in all the different insulation material sections and in reference wall section of the brick facade were uniform. Facade temperature is mainly influenced by the outdoor temperature. The test wall faces north, and therefore the solar heat absorption was minimal. The uniform temperature can be explained by the relatively thick wall construction (typical thickness of external brick walls is 43–51 cm) and the different layers inside the wall that equalize the temperature distribution. The bigger temperature differences were on the surface of the inner face of the existing masonry wall. The largest temperature drop in the added insulation material was in the case of IQ-T and lowest in the case of CaSi, because of the difference in thermal transmittance. This result coincides with expected results.

Freeze–thaw damage mechanism can occur at temperatures well below freezing when the wall construction is essentially saturated. With brick walls, the limit for freezing can be lower than 0°C because of the dissolved salts in the brick pores. The temperature limit can be from 0°C to −5°C (Vesikari, 1998). The temperatures inside the wall assemblies were measured between the added insulation material and existing wall. In all the cases the temperature did not drop below the freezing temperature between the insulation and existing wall. During the first year, no freeze–thaw cycles were observed directly behind the insulation even if the limit was set to 0°C.

The lowest *RH* is with the PIR (dry installation) and the highest with the AAC (wet installation and vapor-permeable material). During the installation of PIR, no extra moisture was added to the wall, and the *RH* between the insulation material and existing wall reflects the built-in moisture of the existing wall. All the other materials were installed using glue mortar and additional moisture was added to the construction, which contributed to a higher *RH* level.

As all wet materials had ˜5-mm layer of glue mortar according to installation instructions, the amount of water added to the wall was largely the same. With IQ-T, the topmost plaster level was thicker than on the others (10–15 mm vs 2 mm with the CaSi and 5 mm with AAC). The moisture added during the retrofit works can cause long periods of high *RH*, if the renovation works are done during the period when the outdoor and indoor conditions are not suitable for the drying out or the moisture is not dried out before the rooms are taken into use again. The results show that timing of the renovation works or the start point of the reuse needs to be taken into account. The time after the renovation works is most critical for the IQ-T; for the CaSi and AAC, it is considerably shorter. It is also significant, that although more resistant to vapor diffusion, humidification also increases the *RH* behind the PIR layer (probably caused by outdoor climate/rain).

To simulate the use of the room as a living space, the humidifier and ventilation systems were switched on 3 months after the installation of the insulation material layers. After switching on and off the humidifier, a much quicker response of the vapor-open materials to the change than that of vapor-tight materials was observed. Also, there is a difference in drying rate of the materials if two time periods are compared (P1 and P5). The drying is accelerated because of the lowered moisture load and mechanical ventilation during P5.

The measurement results show high humidity levels in all the cases. In the case of AAC, possible condensation occurred. The conditions suitable to initiate the mould growth are described in Viitanen and Ojanen (2007) and Viitanen et al. (2010). The measured temperature and *RH* results show that the conditions suitable for the mould growth were fulfilled during most of the time period. The most critical are the conditions in case of the PIR ($RH_{crit} > 80\%$) and AAC ($RH_{crit} > 95\%$).

The important aspect of any retrofit is the increase in thermal resistance of the building envelope. This results in reduced energy usage and improved thermal comfort for inhabitants. The thermal resistance was calculated using measured

temperature difference across the brick wall, the insulation layers, and the heat flow through the wall. Regarding the wall construction, the additional insulation resulted in a decrease of the thermal transmittance of the wall by 40% to 65%. The highest thermal resistance was achieved with IQ-T. There was evident temperature difference on the surface of the wall on the room side. During the winter period, the temperature of the inner surface of the IQ-T wall was almost 3°C higher than that of the reference wall. In all the cases, the temperature was higher than that of the reference wall and the thermal comfort was improved.

The simulation models of four internally insulated brick walls were used to analyze the hygrothermal performance of the renovated wall with the different indoor and outdoor humidity loads.

In all cases, the temperature directly behind the added insulation did not drop below 4°C—frost avoidance criteria is thus fulfilled.

Under low moisture load (office, school: $\Delta \nu = + 2$ g/m^3), all wall assemblies functioned satisfactorily. Under low moisture loads, the PIR exhibited higher RH levels during most of the year than other materials, except for the spring period during the mold MRY (see Figure 13).

Because the PIR insulation board was covered with paper, the critical RH for it was lower: $RH_{crit} > 80\%$. This makes wall assembly with PIR problematic in dwellings ($\Delta \nu > +4$ g/m^3). The critical period is from late summer to early winter. This could be due to the outdoor climate since the original wall assembly is moistened during summer and autumn and the indoor direction drying is limited because of the higher water vapor diffusion resistance of PIR. In case of the more open materials, the critical period exists during the winter and spring time due to the higher moisture flux through the insulation. The use of paper in the production of PIR should be critically analyzed and, if possible, more durable material for the surface of PIR board should be found.

Taking into account the results derived from model calibration, the RH_{crit} for the AAC and CaSi was lowered to 85%–90%. Consequently, the risk of condensate was present in the wall assembly insulated with AAC at high moisture excess ($\Delta \nu > +6$ g/m^3).

Conclusion

In upgrading of energy performance for historic buildings, the use of internal thermal insulation should be always carefully analyzed. In this study, the use of four different materials was studied by field measurements and computer simulations.

The results show that the built-in moisture during installation can cause high RH levels in a wall for a long period that can lead to interstitial condensation. The temperature and RH condition inside the wall between the added insulation and brick wall favoring mold growth were fulfilled during most of the time period.

As PIR board exceeded the $RH_{crit"80"}$ convincingly, it cannot be recommended to be used in its current form in high humidity loads—for example, using a product

without the paper layer on the "cold" side to increase the critical *RH* criterion could be considered. Furthermore, possible problems caused by moisture diffusion flux toward the interior will have to be evaluated.

IQ-T behaved similarly to PIR, however, the thicknesses differed. Thus, the materials could not be compared directly, and the effect of its capillary-active channels will need further assessment.

AAC and CaSi exhibited almost equal absolute humidity behind the insulation, with the difference in *RH* due to lower thermal transmittance of the AAC layer. To reduce the *RH* levels, lower thicknesses of insulation (in both AAC and IQ-T cases) should also be evaluated.

The temperature on the inner surface was increased compared to the existing wall, and thermal transmittance was halved almost in all the cases.

Based on the measurements and simulation results, all analyzed insulation materials are suitable for future analysis (two-dimensional (2D) details, different brick wall constructions, and climate conditions) to work out internal insulation solutions for historic buildings. Nevertheless, hygrothermal performance of exterior wall solutions does not depend only on insulation materials, as the properties and dimensions of original wall are important and have to be taken into account.

References

Grunewald J (1997) *Diffusiver und konvektiver Stoff-und Energietransport in kapillarporösen Baustoffen*. PhD Thesis, TU Dresden, Dresden.
Häupl P, Fechner H and Petzold H (2004) Interior retrofit of masonry wall to reduce energy and eliminate moisture damage: comparison of modeling and field performance. In: *Proceedings of the thermal performance of the exterior envelopes of buildings IX*, Clearwater Beach, FL, 5–10 December 2004.
Häupl P, Jurk K and Petzold H (2003) Inside thermal insulation for historical facades. In: *Proceedings of the 2nd international conference on building physics*, Antwerpen, 14–18 September, pp. 463–469. Antwerpen, Belgium: AA Balkema Publishers.

Hens H (1998) Performance predictions for masonry walls with inside insulation using calculation procedures and laboratory testing. *Journal of Thermal Envelope and Building Science* 22: 32–48.

Jürgenson L (1942) *Elamu soojapidavus*. Tartu: Tartu Eesti kirjastus, p. 203.

Kalamees T (2006) Indoor hygrothermal loads in Estonian dwellings. In: *Proceedings of the 4th European conference on energy performance and indoor climate in buildings and the 27th conference of the Air Infiltration and Ventilation Centre*, Lyon, 20–22 November, pp. 541–546. Lyon, France: Air Infiltration and Ventilation Centre.

Kalamees T and Vinha J (2004) Estonian climate analysis for selecting moisture reference years for hygrothermal calculations. *Journal of Thermal Envelope and Building Science* 27(3): 199–220.

Künzel HM (2011) Bauphysik der Innendämmung und Bewertungsverfahren. In: *Proceedings of the 1. Internationaler Innendämmkongress*, Dresden, 20–21 May, pp. 9–16. Dresden: TU Dresden.

Kuts PS and Sheiman VA (1965) Investigation of the hygroscopic properties of peat insulating slabs. *Journal of Engineering Physics* 9(5): 394–396.

Maurenbrecher AHP, Shirtliffe CJ, Rousseau MZ, et al. (1998) Monitoring the hygrothermal performance of a masonry wall with and without thermal insulation on its interior surface. In: *Proceedings of the 8th Canadian masonry symposium*, Jasper, AB, Canada, 31 May–3 June.

Mikk I (1977) *Soojustehnika käsiraamat*. Tallinn: Valgus, p. 85.

Morelli M, Scheffler GA, Nielsen TR, et al. (2010) Internal insulation of masonry walls with wooden floor beams in northern humid climate. In: *Proceedings of thermal performance of the exterior envelopes of whole buildings XI* (U.S. Department of Energy, Oak Ridge National Laboratory), Clearwater Beach, FL, 5–9 December, pp. 89–100. Atlanta, GA: ASHRAE.

Nicolai A, Scheffler GA, Grunewald J, et al. (2008) *An efficient numerical solution method and implementation for coupled heat, moisture and salt transport: The Delphin program*, (Research Report on Priority Program DFG SPP 1122) (ed L Franke, G Dekkelmann and R Espinosa-Marzal). Göttingen: Cuilliver Verlag, pp. 85–100.

Nielsen A, Möller EB, Rasmussen TV, et al. (2012) Use of sensitivity analysis to evaluate hygrothermal conditions in solid brick walls with interior insulation. In: *Proceedings of the 5th international building physics conference (IBPC)—NSB 2011*, Kyoto, Japan, 28–31 May, vol. 1, pp. 377–384. Japan: Department of Architecture and Architectural Engineering of Kyoto University.

Scheffler GA and Grunewald J (2003) Material development and optimisation supported by numerical simulation for capillary-active inside insulation material. In: *Proceedings of the 2nd international conference on building physics*, Antwerpen, 14–18 September, pp. 77–85. Antwerpen, Belgium: AA Balkema Publishers.

Scheffler G (2011) Hygric performance of internal insulation with light-weight autoclaved aerated concrete. In: *Proceedings of 5th International Conference on Autoclaved Aerated Concrete*, Bydgoszcz, 15–16 September, pp. 323–335.

Stopp H, Strangeld P, Fechner H, et al. (2001) The hygrothermal performance of external walls with inside insulation. In: *Proceedings of the thermal performance of the exterior envelopes of buildings VIII*, Clearwater Beach, FL, 2–7 December.

Toman J, Vimmrová A and Černý R (2009) Long-term on-site assessment of hygrothermal performance of interior thermal insulation system without water vapour barrier. *Energy and Buildings* 41(1): 51–55.

Vereecken E and Roels S (2011) A numerical study of the hygrothermal performance of capillary active interior insulation systems. In: *Proceedings of the 9th Nordic symposium on building physics (NSB 2011)*, Tampere, 29 May–2 June, vol. 1, pp. 365–372. Tampere: Department of Civil Engineering, Tampere University of Technology.

Vesikari E (1998) *Prediction of service life of concrete structures by computer simulation.* Licentiate's Thesis, Helsinki University of Technology, Espoo, 131 pp.

Viitanen H and Ojanen T (2007) Improved model to predict mold growth in building materials. In: *Proceedings of the thermal performance of the exterior envelopes of buildings X*, Clearwater Beach, FL, 2–7 December.

Viitanen H, Vinha J, Salminen K, et al. (2010) Moisture and bio-deterioration risk of building materials and structures. *Journal of Building Physics* 33(3): 201–224.

Vinha J, Valovirta I, Korpi M, et al. (2005) *Rakennusmateriaalien rakennusfysikaaliset ominaisuudet lämpötilan ja suhteellisen kosteuden funktiona.* Tampere: Tampere University of Technology.

Zhao J, Plagge R and Grunewald J (2011) Performance assessment of interior insulations by stochastic method. In: *Proceedings of the 9th Nordic symposium on building physics (NSB 2011)*, Tampere, 29 May–2 June, vol. 1, pp. 465–472. Tampere: Department of Civil Engineering, Tampere University of Technology.

Publication II
Klõšeiko, P.; Kalamees, T. (2016). Case Study: In-situ Testing and Model Calibration of Interior Insulation Solution for an Office Building in Cold Climate. CESB 2016 - Central Europe Towards Sustainable Building 2016: Innovations for Sustainable Future; Prague; Czech Republic; 22 June 2016 through 24 June 2016. Prague: Czech Technical University in Prague, 159–166.

CASE STUDY: IN-SITU TESTING AND MODEL CALIBRATION OF INTERIOR INSULATION SOLUTION FOR AN OFFICE BUILDING IN COLD CLIMATE

Paul KLÕŠEIKO[a], Targo KALAMEES[a]

[a] *Chair of Building Physics and Energy Efficiency, Tallinn University of Technology, Ehitajate tee 5, 19086 TALLINN, Estonia, paul.kloseiko@ttu.ee*

Abstract

Interior insulation is one of the options to provide thermal upgrade to buildings with culturally valuable facades. However, cold climate in Northern Europe is more critical to the hygrothermal behaviour of the interior insulation and most solutions currently used in Central Europe are considered risky and remain untested there.

This paper discusses the development of an interior insulation solution for a 7-story office building in Tallinn, Estonia (brick façade, concrete frame). First, variations of the solution were tested in-situ for a period of 1 year. Measurements and opening of the wall structure provided the essential background information for numerical simulations in HAM software Delphin. 1D and 2D HAM models were calibrated and finally, the models were tested against moisture reference years to assess the functioning of the system in more critical hygrothermal boundary conditions.

Keywords: *hygrothermal behaviour, interior insulation, cold climate, case study*

1 Introduction

Energy efficiency requirements, better understanding of moisture safety and higher demands by the users have created the need to find solutions to upgrade the envelope of heritage brick buildings. If the façades are valuable, exterior insulation is not an acceptable. At the same time, traditional interior insulation solutions using mineral wool with or without vapour barrier are risky due to possible mould hazard and moisture accumulation caused by wind driven rain.

During the last 15 years, so-called capillary active insulation materials have been used in Central Europe to mitigate these risks. Recently the approach has been also investigated in Scandinavia: Knarud et al [1] used Wufi to analyze different interior insulation solutions in different Norwegian regions with varying wind driven rain conditions. Preliminary studies by Odgaard et al [2], Bjarløv et al [3] showed the potential for energy savings and also underlined the effect and possible risks of wind driven rain. However, these studies have been based on calculations and not on field tests. Previous study in Estonia [4] showed that in the case of capillary active insulation materials, correlating measurement and simulation data can be difficult and in this case the error was nonconservative. This illustrates the need for in-situ testing.

Main problems caused by interior insulation are: a) reduction of temperature of the original wall – which, depending on the used materials, may cause mould growth and

condensation on the interior surface; and increased risk of frost damage on the exterior surface; b) increased effect of thermal bridges; c) reduction of thermal mass of the interior layer.

When interior insulation is planned (and even more so in the case of historic buildings) these risks and effects should be considered and a thorough study is required to investigate the actual hygrothermal behavior of the insulation system. This study describes such design and monitoring process of an interior insulation solution for a historic office building.

2 Methods

2.1 Description of the studied building

Current study concentrates on a 7-storey office building built in 1932 (**Fig. 1**). As it is listed by heritage protection, alterations to the façade are forbidden.

During preliminary studies, the wall structure was opened, its design was specified (**Fig. 4**) and material samples were collected. Due to the wall structure being complex and previous experience showing the need for caution, a field study was carried out.
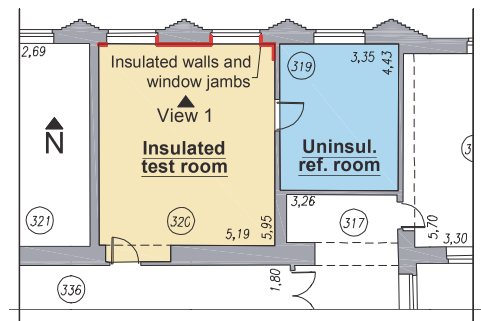

Fig. 1   Façade of the studied building

Fig. 2   Plan of the test rooms

2.2 Test setup

Field study consists of monitoring an insulated test room (**Fig. 1** and **Fig. 2**) and its neighbouring uninsulated reference room. Both are situated on the 3rd floor and are orientated to the north.

Based on initial hygrothermal simulations a 50mm layer of autoclaved aerated concrete (AAC) insulation Ytong Multipor was chosen to cover the the walls and one of the two radiator niches. Due to space restrictions, window jambs were insulated with t=12.5mm and 20mm XPS insulation boards (Tycroc TWP). **Fig. 3** and **Fig. 4** show the insulation and measurement setup. Insulation and monitoring equipment were installed during the period of 2–8.07.2014. The following measurement devices were used in monitoring of the hygrothermal performance of the building: T&RH probes: Rotronic HygroClip HC2-C05 (accuracy ±0.3°C, ±1%RH); heat flux plates: Hukseflux HFP01 (accuracy ±5%); data logger Grant Squirrel SQ2020 1F8 (accuracy ±0.05% of readings ± 0.025% of range); data logger Grant Squirrel SQ2010 (accuracy ±0.1% of readings ± 0.1% of range); temperature probes: Onset Hobo TMC6-HD (accuracy ±0.15°C); T&RH data loggers: Onset Hobo U12 and UX100 (accuracy ±0.21°C, ±2.5-3.5%RH). Measurement interval of 1h was used.
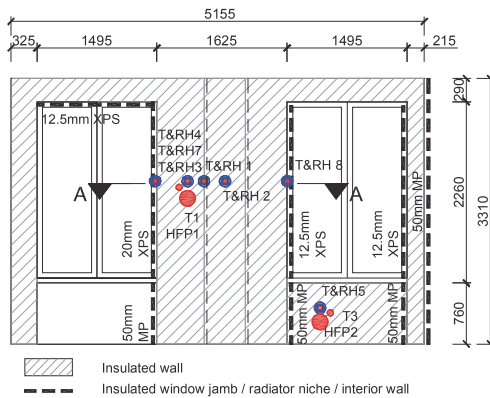
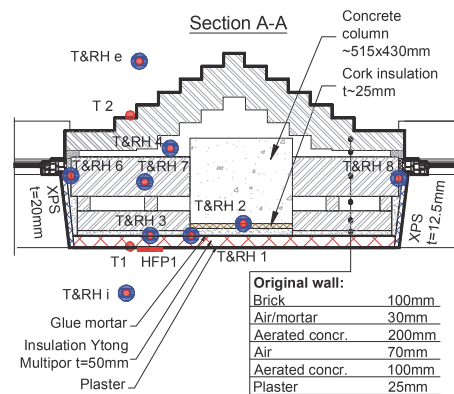**Fig. 3** *View 1: insulated test wall – placement of sensors and insulation scheme*

Fig. 4 *Section A-A: middle part of the test wall – wall structure, placement of sensors*

2.3   Performance criteria

High moisture levels can cause **mould growth**. VTT mould growth model [5, 6] gives the temperature dependent **critical relative humidity** above which mould growth is possible. As the model was developed for mould sensitive pine sapwood, it can be considered conservative for many other materials. On the other hand, it is more flexible and gives a more realistic assessment than a fixed $80\%_{RH}$ criterion. If the critical *RH* was exceeded, the severity of the situation was assessed using **mould index** [7, 8]. The results of the model range from "0 – No growth" to "6 – Heavy and tight growth".

In the case of **mineral capillary active insulation systems** where insulation is glued to the wall in full plane mould risk can be considered low. Künzel [9] suggests to **avoid condensation** in the glue layer and $RH_{crit.}=95\%_{RH}$ is proposed. In addition, **frost avoidance** in the pores is advised. Taking into account the capillary pressure and salts in the pore water, the frost should be avoided if the temperature is above -5°C. WTA Merkblatt 6-5 [10] proposes assessment according to **saturation degree** – maximum of $30\%_{sat}$ is allowed to avoid frost damage. Scheffler [11] concluded that in most cases in German climate Ytong Multipor can be considered frost resistant and frost avoidance dropped. However, this conclusion has not been further analysed in Nordic climate.

2.4   Hygrothermal modelling

To test the suitability of the insulation solution in more critical conditions than occurred during the measurement period, hygrothermal modelling in commercial 2D HAM software DELPHIN 5.8.1 [12, 13] was used. First, the models were calibrated against measured temperature, relative humidity and heat flux data; then, moisture reference years were used to assess the performance of the solutions.

In this paper, study of the middle part of the wall (**Fig. 4**) is presented. Although more were used in development, 2 hygrothermal models are described here: **2D model** spanning from the window to the center axis of the column and **1D model** representing cross section of the wall along sensors HFP1-TRH3-TRH7.

2.4.1 Material properties

Where possible simulation program's (DELPHIN) material libraries and material producers' data were used to provide material properties. Basic properties (density, porosity, thermal conductivity, water uptake, water vapour diffusion resistance) of the aerated concrete were measured and similar materials in Delphin's database were sought for. "Lightweight concrete" and „Blast furnace slag concrete" were chosen as a basis and during calibration process its properties were altered to find best correlation with measurement results. **Tab. 1** lists the interrelationship between the materials in the measured wall and in Delphin database.

Tab. 1   Materials in the measured wall and respective materials in Delphin database that were used in the hygrothermal simulations.

Material	Equivalent in Delphin database
Brick	Old Building Clinker Hamburg Holstenkamp
Aerated concrete	Based on "Lightweight concrete" and "Blast furnace slag concrete"
Plaster	Lime plaster
AAC insulation board (Ytong Multipor)	Mineral Foam Multipor (from 2011)
Glue mortar/plaster for AAC insulation (Ytong Leichtmörtel)	Glue Mortar (For Mineral Insulation Board)
Glue foam for XPS (Ceresit CT84)	Polyurethane-foam
XPS insulation board (Tycroc TWP)	Polystyrene Board – Extruded
Wood	Spruce SW Radial
Concrete	Concrete
Cork	Insulation-Clay-Cork-FW

2.4.2 Climatic conditions

During the calibration process following climatic boundary conditions were used: indoor and outdoor temperature and relative humidity – as measured on site; precipitation, wind speed, wind direction – as measured at Tallinn-Harku weather station of Estonian Weather Service; diffuse and direct radiation – as measured at Tõravere weather station of Estonian Weather Service. Time step for the data was 1 hour.

Later, Estonian moisture reference years (MRY) [14] were used as outdoor climate. Condensate and Mould MRYs are used for hygrothermal design and represent the critical years for the risk of water vapour condensation and risk of mould growth respectively [14]. Indoor moisture load was characterized by moisture excess of $\Delta v = +4g/m^3$ in low and $\Delta v = +1g/m^3$ in warm outdoor temperatures, indoor temperature was based on ICC II according to EN15251 (both chosen according to measured indoor climate of the building). Indoor and outdoor climate based on MRYs were repeated for 5 years to take longer processes into account.

3   Results and discussion

3.1   Measurement results and model calibration

3.1.1   Climatic conditions during the measurement period

Fig. 5 gives the indoor and outdoor temperatures as measured on site. Minimum outdoor temperature during the winter of 2014/2015 was -11.1°C with an average of +1.5°C (1.11.2014…1.03.2015), which is significantly higher than usual. Average indoor temperature

in the test rooms was 21.5°C. Due to intermittent heating scheme the indoor temperature had a daily amplitude of <4°C.

Moisture loads can be described using moisture excess (*Δv*; difference between indoor and outdoor air moisture contents). **Fig. 6** gives the moisture excess in the studied rooms and shows that moisture load during the measurement period was relatively low.
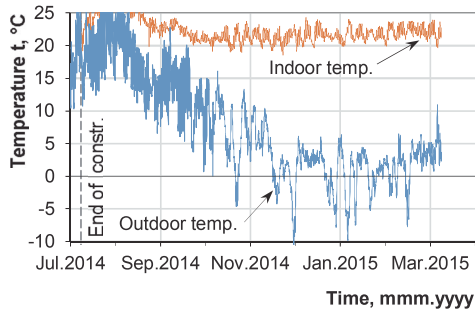

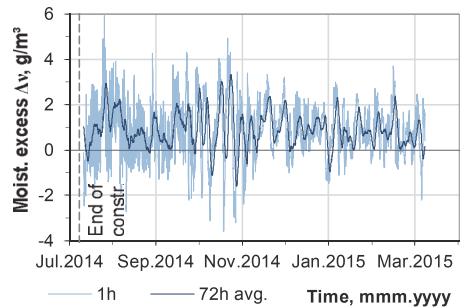**Fig. 5** *Indoor and outdoor temperatures at the tested building during the measurement period*

Fig. 6 *Moisture excess in test room during the measurement period*

3.1.2 Monitoring of the middle section of the wall and calibration results

Data from all sensors show that hygrothermal conditions during the measurement period stayed well below the safe performance limits of the system. On one hand this can be attributed to relatively low thermal conductivity of the historic aerated concrete (when compared to other masonry structures) and air cavity between outer brick leaf and interior layers, which reduces the ingress of driving rain. However, it has to be noted that winter was very mild and moisture load in the test room was low. Comparison of heat flux data from HFP1 and similarly placed sensor on reference wall revealed over twofold reduction of thermal transmittance (U_{HFP1}=0.50 W/(m²·K) vs U_{ref}=1.13 W/(m²·K)) showing potential for energy savings.

Because monitoring sensors cover the axis HFP1-TRH3-THR7 best, this paper gives measurement and simulation results (**Fig. 7** to **Fig. 10**) from the position of TRH3. Different types (temp., rel. hum., heat flux) of data allow for finer assessment of the simulation accuracy.

Calibration process mainly consisted of iteratively fine-tuning the historic aerated concrete's properties while comparing simulation results with measurements from all relevant sensors. While good agreement was mostly found, larger discrepancies exist in measured and modelled heat flux data. Although opening of the structure and data from TRH4 gives ground to belief that some ventilation took place in the air cavities, they were modelled as unventilated. This and uncertainties of the original wall material properties could cause the differences. Comparison of 2D and 1D models, showed that in this position (TRH3) results from the models differed only slightly. Temperature error of both models at TRH3 was non-conservative (~3°C at Δt≈30°C boundary conditions) and should be taken into account when doing frost avoidance assessment. Water vapour pressure and relative humidity errors were conservative.

At a hygrothermally more critical position TRH1, humidity and temperature coincided better with measurement results and both errors were found to be conservative. Between cork insulation and r/c column (TRH2) underestimation of temperature and overestimation of water vapour pressures occurred. This resulted in RH modelling error of +10%$_{RH}$ during the winter period and making calculation in this position conservative. Possible cause for errors at TRH2 could be unreliable material data for existing cork insulation.
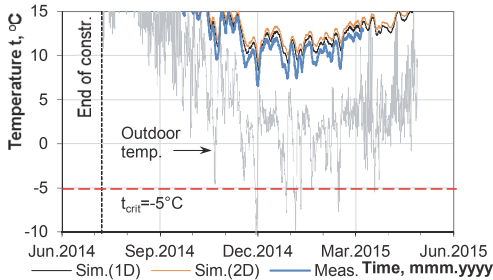
Fig. 7   *Measured (TRH3) and simulated temperatures betw. Insul. And aerated concrete*
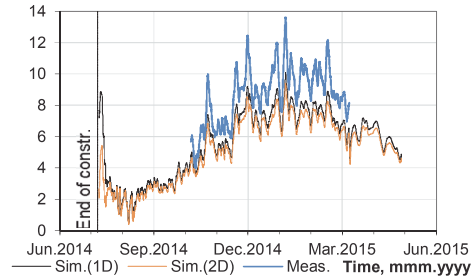

Fig. 8   *Measured (HFP1) and simulated 24h average heat fluxes on interior surface*
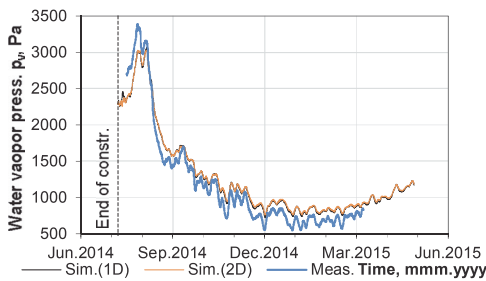

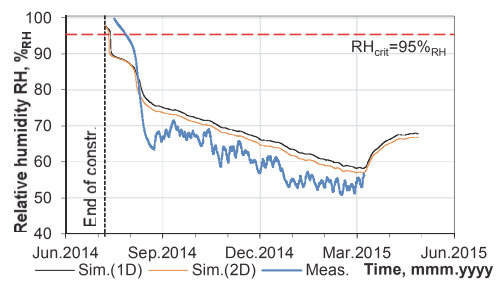**Fig. 9**   *Measured (TRH3) and simulated water vap. pressures betw. insul. and aerated concrete*

Fig. 10   *Measured (TRH3) and simulated rel. humidity betw. insul. and aerated concrete*

3.2   Calculations with Estonian moisture reference years (MRYs)

As expected, simulations with calibrated 2D model using Estonian MRY's as boundary conditions gave hygrothermally more severe results. As position TRH1 gives lowest temperatures in glue layer, the situation there is most critical in terms of capillary active insulation performance limits. **Fig. 11** to **Fig. 13** give the modelling results and their respective performance criteria for TRH1. While being closer to the limits, they are not exceeded and in case of RH and saturation degree, there is still headroom.
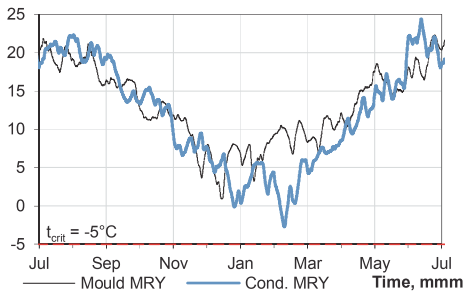

Fig. 11   *Temperature behind insulation at column-wall intersection (TRH1), Estonian MRYs, 5th year of calculations*
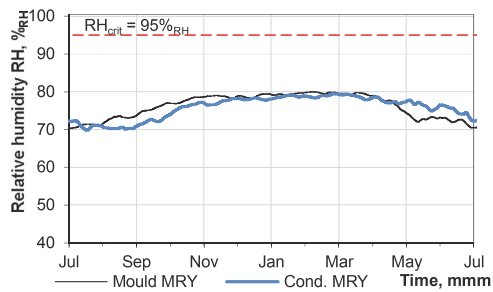

Fig. 12   *Relative humidity behind insulation at column-wall intersection (TRH1), Estonian MRYs, 5th year of calculations*
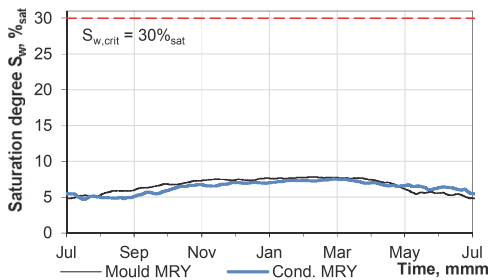
Fig. 13   Saturation degree in plaster layer at column-wall intersection (TRH1), Estonian MRYs, 5th year of calculations
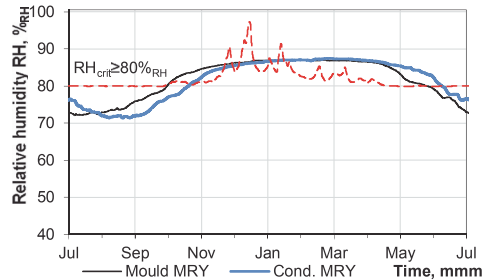

Fig. 14   Relative humidity in cork layer (TRH2), Estonian MRYs, 5th year of calculations

In terms of mould prevention, most critical position is between existing cork insulation and r/c column (TRH2). Both mould and condensate MRYs exceeded critical limit above which mould growth is possible (**Fig. 14**). Analysis of mould index (C_{mat}=0.25; material sensitivity class: "sensitive") revealed that yearly fluctuations were between 0.7…1.2 (mould MRY) and 0…0.5 (condensate MRY). Given that hygrothermal model overestimated RH levels in this position, maximum mould index stayed close to 1 ("Initial stages of growth"), and cork layer being separated from indoor air, the risks for mould damage can be considered relatively low.

4   Conclusion

From an energy efficiency point of view of the insulated wall functioned well – measured thermal transmittance in aerated concrete section of the wall was reduced over 2 times. Measurement results from the period of summer 2014…spring 2015 were hygrothermally favorable in all measured positions and critical limits were not exceeded. While on one hand the structure was suitable for insulation, the climatically very mild winter and low indoor moisture load might have left possible problems uncovered by the measurements.

To overcome this, hygrothermal modelling was used to assess the performance of the insulation solution during more critical boundary conditions (Estonian moisture reference years). HAM models were calibrated against measurement data; mostly good correlation was found with discrepancies possibly caused by uncertainties in material data and ventilation occurring in air cavities in the wall. Calculations with MRYs gives ground to belief that the insulated wall will perform within acceptable limits.

Next, suitable solutions for different details (interior wall-exterior wall and exterior wall-floor slab intersections etc) will be developed with the aid of HAM models. Also, as measurements are still ongoing, analysis of long term data will be carried out. Further research into the frost avoidance criteria might allow the use of more efficient insulation layers.

Overall, the study gave encouraging results, especially when considering interior insulation of office buildings with similar wall structure. However, research to determine the existing structure and its properties, moisture loads and thorough hygrothermal calculations are necessary in design stage. In-situ measurements are strongly advised in cases where higher moisture loads, unknown materials/wall structures and special details (e.g. wooden beam-ends) are concerned.

Acknowledgement

References

[1]   KNARUD, J.I.B., GEVING, S., et al., *Hygrothermal simulations of internally insulated massive masonry walls exposed to driving rain in cold climate*, Proceedings of the 10th Nordic Symposium on Building Physics (NSB 2014), Grafisk gruppen AB, Lund 2014.

[2]   ODGAARD, T., BJARLØV, S.P., et al., *Building renovation with interior insulation on solid masonry walls in Denmark – A study on the building segment and possible solutions*, Energy Procedia, 2015.

[3]   BJARLØV, S.P., FINKEN, G., et al., *Retrofit with Interior Insulation on Solid Masonry Walls in Cool Temperate Climates – An Evaluation of the influence of Interior Insulation Materials on Moisture Condition in the Building Envelope*, Energy Procedia, 2015.

[4]   KLÕŠEIKO, P., ARUMÄGI, E., et al., *Hygrothermal performance of internally insulated brick wall in cold climate: A case study in a historical school building*, Journal of Building Physics, 2015, *38*, pp.444–464.

[5]   HUKKA, A., VIITANEN, H., *A mathematical model of mould growth on wooden material*, Wood Science and Technology, 1999, *33*, pp.475–485.

[6]   VIITANEN, H., OJANEN, T., *Improved Model to Predict Mold Growth in Building Materials*, Thermal Performance of the Exterior Envelopes of Buildings X, 2007, p. 8.

[7]   OJANEN, T., VIITANEN, H., et al., *Mold Growth Modeling of Building Structures Using Sensitivity Classes of Materials*, Thermal Performance of the Exterior Envelopes of Buildings XI, 2010.

[8]   VIITANEN, H., OJANEN, T., et al., *Mould growth modelling to evaluate durability of materials*, Freitas, V.P. de, Corvacho, M.H., Lacasse, M. (Eds.), Proceedings of the 12DBMC – International Conference on Durability of Building Materials and Components, Porto 2011.

[9]   KÜNZEL, H.M., *Bauphysik der Innendämmung und Bewertungsverfahren*, 1. Internationaler Innendämmkongress 2011, TU Dresden, Dresden 2011, pp. 9 – 16.

[10]   KÜNZEL, H., WORCH, A., et al., *Innendämmung nach WTA II: Nachweis von Innendämmsystemen mittels numerischer Berechnungsverfahren (Merkblatt 6-5)*, 2012.

[11]   SCHEFFLER, G.A., *Frostempfindlichkeit kapillaraktiver Innendämmung*, Grunewald, J., Plagge, R. (Eds.), 2. Internationaler Innendämmkongress. Tagungsunterlage, TU Dresden, Dresden 2013.

[12]   GRUNEWALD, J., *Diffusiver und konvektiver Stoff- und Energietransport in kapillarporösen Baustoffen*, TU Dresden, 1997.

[13]   NICOLAI, A., SCHEFFLER, G.A., et al., *An efficient numerical solution method and implementation for coupled heat, moisture and salt transport: The Delphin Simulation Program*, Simulation of Time Dependent Degradation of Porous Materials, 2009.

[14]   KALAMEES, T., Hygrothermal criteria for design and simulation of buildings, Tallinn University of Technology, 2006.

Publication III

Klõšeiko, P.; Kalamees, T. (2018). Long term measurements and HAM modelling of an interior insulation solution for an office building in cold climate. 7th International Building Physics Conference (IBPC2018); Syracuse, NY, USA; September 23-23 2018. Syracuse CoE, 1423–1428. DOI: 10.14305/ibpc.2018.ps23

Long term measurements and HAM modelling of an interior insulation solution for an office building in cold climate

Paul Klõšeiko[1,*], Targo Kalamees[1]

[1]Tallinn University of Technology, Estonia

*Corresponding email: paul.kloseiko@ttu.ee

ABSTRACT

Excessive mould damage was detected in an office building in Northern Europe and thus a renovation need was established. This paper studies a renovation solution using measurements and heat, air & moisture (HAM) modelling. Polyurethane (PUR) foam was used to fill the air gap in masonry while capillary active calcium silicate (CaSi) insulation was used on the interior surface at thermal bridges. During renovation works temperature and relative humidity (*t&RH*) and heat flux sensors were installed throughout the wall.

Nearly 3 years of measurements are presented. Average thermal transmittance (*U*) of the wall was reduced around 3 times. While the climate was probably not critical during the monitoring, the measured values stayed within hygrothermally safe limits.

The paper also compares the measurement data to 2D HAM modelling and discusses the discrepancies. Calibrated models were used to model the wall using real 42-year weather data and give a more thorough assessment of the hygrothermal performance. Although the original wall stayed fairly moist, no performance limits were exceeded and the interior surface became safer in terms of mould risk.

KEYWORDS

interior insulation, HAM modelling, capillary active, cold climate, case study

INTRODUCTION

Interior insulation has usually been disapproved in Northern Europe as a hygrothermally risky solution. However, "capillary active" insulation has gained ground in Central Europe and become a compelling choice by taking a different approach to mitigating the risks caused by insulation on the interior side (compared to traditional mineral wool + vapour barrier solution). This study took place on the last floor of an 8-storey office building (built in 1936; cultural heritage). Existing interior insulation (gypsum board, PE foil, min. wool) exhibited excessive mould damage and a renovation solution had to be found. Main challenges were: low surface temperatures, high thermal transmittance and avoidance of future biological decay. Preliminary HAM modelling showed that "closed cell" PUR foam injected into air cavities of the masonry and "capillary active" CaSi on the surface of the wall could perform well. This paper discusses the monitoring and modelling of the chosen solution.

METHODS

Measurement setup

Vertical and horizontal sections of the studied wall are given in Figure 1. The wall structure, renovation solution and sensor placement are also shown. Sensors and their positions were selected both to assess the hygrothermal situation after the insulation and to have enough reference points to calibrate the HAM models.

The following measurement devices were used: T&RH probes: Rotronic HygroClip HC2-C05 (accuracy ±0.3°C, ±1%RH); heat flux plates: Hukseflux HFP01 (accuracy ±5%); data logger Grant Squirrel SQ2020 1F8 (accuracy ±0.05% of readings ± 0.025% of range); temp. probes & logger: Onset Hobo UX120-006M & TMC6-HD (accuracy ±0.15°C); T&RH data loggers: Onset Hobo U12 and UX100 (accuracy ±0.21°C, ±2.5-3.5%RH). Measurement interval: 1h.
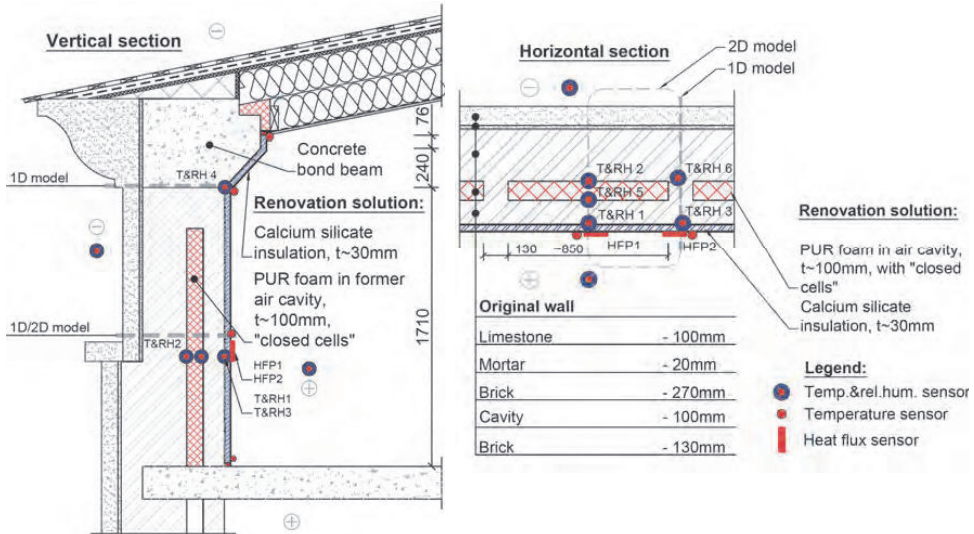

Figure 1. Vertical and horizontal sections of the wall showing sensor placement and wall layers.

Performance criteria

WTA Merkblatt 6-5 (Künzel et al. 2012) proposes to avoid frost and condensation in insulation and glue. Assessment according to saturation degree should be carried out – maximum of 30%$_{sat}$ is allowed to avoid frost damage. However, our previous research (Klõšeiko et al. 2017) showed that freeze-thaw cycling affected tensile strength of capillary active insulation material even though saturation degree stayed below the 30%$_{sat}$ limit. Therefore, slightly stricter limits of $RH_{crit.}$= 95 %$_{RH}$ and t_{crit} = -5 °C (Künzel 2011) are used in this study. Minimizing freeze-thaw cycles of the limestone cladding was not a criterion as conversion to ventilated façade is planned for the building.

Hygrothermal modelling

IBK Delphin 5.9.0 (Grunewald 1997; Nicolai et al. 2009) was used to model the hygrothermal performance of the exterior wall. Modelling consisted of 2 steps: 1) model calibration and 2) modelling with 42-year weather data. 1D and 2D models of the masonry section were created (while brickwork was treated as a homogenous material for both). Concrete bond beam was modelled as a 1D case. Model geometry is given in Figure 1.

During calibration, measured (t, RH (+ calculated vapour pressure), heat flux) and modelled data were compared. Then the HAM models were iteratively changed within plausible extents to achieve a better match between the two. Different bricks and concrete types from Delphin material database were tested (finally settling with ID 543 and 569 for brick and concrete respectively), PUR foam properties were fine-tuned according to limits given in its datasheet (based on ID 195; following changes were made: ρ = 39 kg/m³, μ = 39, λ = 0.022 W/(m·K)). Rest of the material IDs from Delphin database used in models were 464, 143, 424, 21, 230.

Boundary conditions for model calibration were: *t&RH* (measured on site); wind, rain (measured 10km away) and solar radiation (measured 165km away). 42-year weather data (*t*, *RH*, wind, rain, solar radiation; all measured 165km away) was used to assess the performance in more critical conditions. As the indoor humidity load in the test room was very low, more critical indoor *t* & moisture excess profiles were used for 42-year modelling (roughly moisture class 2 given in EN ISO 13788 Table/Figure A.2). They were based on an earlier study in a similar building (Klõšeiko & Kalamees 2016).

RESULTS & DISCUSSION
Measurement results
Temperatures behind CaSi (Figure 2 top, sensors TRH1, 3, 4) were closest to limits during the winter of the first year. At sensor TRH4 (concrete section) they fell to as low as -2.5°C, but not reaching the critical -5°C. In masonry section the temperatures were higher due to PUR insulation adding further thermal resistance. Consequently, sensors on the exterior side of PUR (TRH2 shown here) measured far lower temperatures than between CaSi and concrete bond beam. Figure 2 (bottom) gives the measured relative humidities. Dryout of the built-in moisture to stable levels took about 2.5…3 months. *RH* values between exterior brick leaf and PUR (sensor TRH2) were quite stable (fluctuating about 5%$_{RH}$ throughout the year) after the dryout of CaSi built-in moisture.
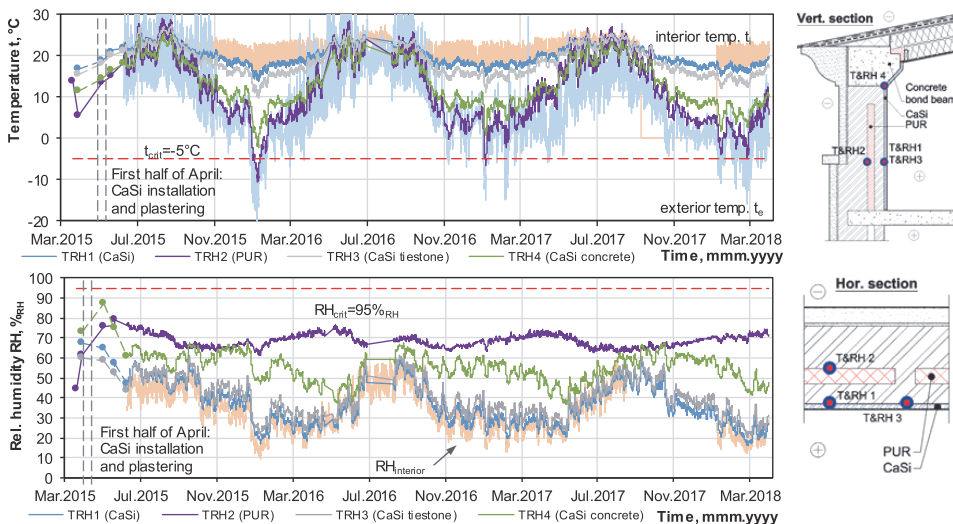

Figure 2. Measured temperatures (top) and relative humidities (bottom) throughout the monitoring period.

Moisture excess during the measurement period in the test room was very low (close to moisture class 1 according to EN-ISO 13788 A.2), as a well-functioning HVAC system was installed. Analysis of measured data hints that moisture contents of air in the pores of exterior masonry leaf are governed by outdoor climate while lagging about half a week. A ~ 4 g/m³ rise in moisture contents compared to indoor and outdoor air in autumn (mid-Aug...Oct.) is pronounced, possibly due to rain. However, moisture does not seem to be accumulating in the wall over time, which could be the case with vapour tight interior insulation and heavy wind

driven rain loads. Sensors behind CaSi insulation measured moisture contents quite close to that of the indoor air throughout the year. A lag of a couple of days was detected.

Temperature indexes (f_{Rsi}) were calculated from surface temperatures to assess mould and condensate risk on the wall surface. The worst situation was detected at wall-floor intersection (f_{Rsi} = 0.79) and at concrete bond beam (f_{Rsi} = 0.83). None of those results should indicate a risk, however, as indoor moisture load was low. f_{Rsi} values at the rest of the intersections were also considerably higher (i.e. safer).

Average heat flux and temperature data from 1. Nov. 2015… 29. Feb. 2016 was used to calculate the thermal transmittances (U) of the insulated wall (see Figure 1 for placement of the sensors). At tie bricks (HFP2) U = 0.52 W/(m²·K) was measured and between tie bricks (HFP1) the value was U = 0.31 W/(m²·K). 2D thermal transfer modelling of the insulated structure results in average thermal transmittance of U = 0.39 W/(m²·K), which is ~ 3-fold reduction compared to the uninsulated case (U = 1.14 W/(m²·K)).

Calibration of HAM models
Results from the models which achieved the best fit and positions that are most relevant to the assessment criteria are presented here. Figure 3 shows data from TRH2 (between CaSi and tie brick) and TRH4 (between CaSi concrete bond beam). Relative humidity is given as it integrates the errors in thermal and moisture calculations.

Agreement of calculated and measured temperatures (TRH3 2D model; TRH4 1D model) was within ±1°C for most of the year with overestimation of temperatures by 2…3°C taking place in summer (possibly due to deficiencies in solar modelling of the south facing wall). TRH3 1D model exhibits too low temperatures which results in higher than measured *RH*. Modelled *RH* values exhibit less fluctuation in all cases, however, that seems to be the characteristic of the Delphin program (Klõšeiko et al. 2015; Klõšeiko & Kalamees 2016; Klõšeiko et al. 2017). 24h avg. heat fluxes in masonry section achieved less than ±1 W/m² (~5…10%) difference for most of the heating period using 2D model; in case of 1D models, the errors were 4…8 times higher. Possible sources of errors could be: material data (limestone as location specific and inhomogeneous material; only basic parameters were measured for brick), unknows concerning the actual wall structure, wind driven rain modelling, solar radiation modelling.
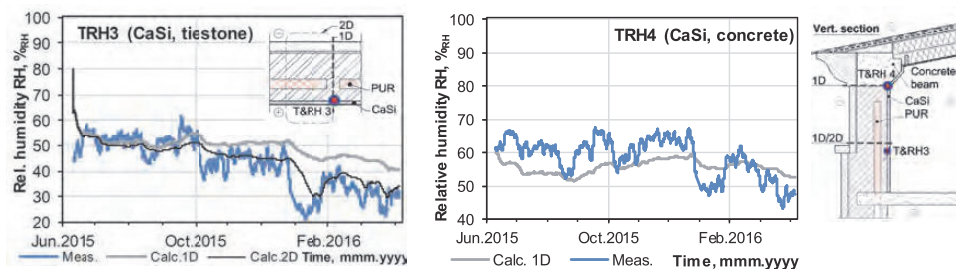

Figure 3. Comparison of measured and modelled relative humidities at TRH3 (between CaSi and tie brick; left) and TRH4 (CaSi insulation on top of concrete; right).

The correlation between measurements and modelling was deemed satisfactory. For performance assessment of CaSi insulation the 1D model of the masonry section might be good enough as the errors on that part were conservative. However, as wind driven rain could cause accumulation of moisture in the exterior masonry leaf, 2D model is also necessary.

Modelling with 42-year weather data
Due to limited space only the most critical point in the wall (TRH4 behind CaSi on concrete bond beam) is discussed here. Modelled $t\&RH$ values are given in Figure 4. Yearly minimum temperatures and maximum relative humidities are shown so the most critical year can be highlighted. In the case of TRH4, the 1986/1987 season was the harshest and is shown in Figure 4 (right). Yearly maximum relative humidities are much more stable than temperatures. "Flattening" the peaks of the RH graphs is possibly due to relatively high moisture capacity and redistribution of moisture in both concrete and CaSi.

Figure 4 also illustrates that 42-year modelled $t\&RH$ are far more critical than measured values. While lower t is largely the result of colder outdoor climate, the significantly higher modelled RH are caused by using higher indoor moisture load.

During 10 out of 42 years (~24%) t behind the insulation fell below critical -5°C. Still, RH was far below the 95%$_{RH}$ limit. Thus, according to the modelling data, frost damage in insulation system will not be a problem and the solution could be approved for use in the rest of the building. However, as previous research (Binder et al. 2013; Klõšeiko et al. 2017) has shown, the modelling results of "capillary active" materials can also be non-conservatively skewed, especially when higher moisture contents are concerned and values are closer to the performance limits. To overcome that, development of improved liquid and vapour conductivity curves for CaSi as well measurements of limestone and brick properties are in progress.
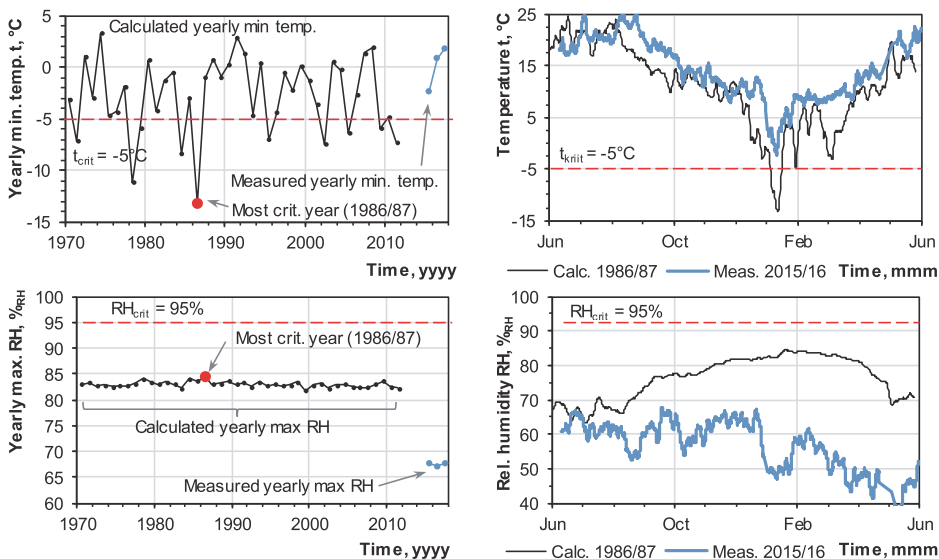

Figure 4. Most critical point in the wall (TRH4 – betw. CaSi insulation and concrete beam): yearly min. temperatures (top left) and max. rel. humidities (bottom left) of the 42-year HAM modelling and hourly values for the most critical year (right) compared to the measured values.

CONCLUSIONS

Measurements show that interior insulation can perform well at least if HVAC systems function nominally. Wind driven rain did not cause a notable accumulation of moisture on the exterior side of "vapour tight" PUR foam. Comparison of modelled and measured data shows that 2D modelling should be used for this type of structure. If interior insulation layers are thin, the HAM models can still fairly adequately portray the processes behind the insulation even if detailed material data for existing wall is unavailable.

Modelling results suggest that even in the case of increased moisture load, the CaSi boards are quite a robust solution and provide an extra layer of safety thanks to quite high moisture capacity and lack of biological decay. Modelling with long-term weather data gives an increased confidence in the results. For example, if test reference years are used, the principle of their selection might not always match that of the current modelling aim. Also, the measured data was far on non-conservative side compared to 42-year modelling results, partly due to current winters being quite mild. To test an experimental structure in more critical boundary conditions, modelling with historic data and calibrated model can be a viable option.

ACKNOWLEDGEMENT

REFERENCES

Binder, A., Künzel, H.M. & Zirkelbach, D., 2013. A new approach to measure liquid transport in capillary active interior insulation. In *Proceedings of 2nd Central European Symposium on Building Physics*. Vienna.

Grunewald, J., 1997. *Diffusiver und konvektiver Stoff- und Energietransport in kapillarporösen Baustoffen*. TU Dresden.

Klõšeiko, P., Arumägi, E. & Kalamees, T., 2015. Hygrothermal performance of internally insulated brick wall in cold climate: A case study in a historical school building. *Journal of Building Physics*, 38(5), pp.444–464.

Klõšeiko, P. & Kalamees, T., 2016. Case study: In-situ testing and model calibration of interior insulation solution for an office building in cold climate. In *CESB 2016 - Central Europe Towards Sustainable Building 2016: Innovations for Sustainable Future*.

Klõšeiko, P., Varda, K. & Kalamees, T., 2017. Effect of freezing and thawing on the performance of "capillary active" insulation systems: a comparison of results from climate chamber study to HAM modelling. *Energy Procedia*, 132, pp.525–530.

Künzel, H. et al., 2012. Innendämmung nach WTA II: Nachweis von Innendämmsystemen mittels numerischer Berechnungsverfahren (Merkblatt 6-5).

Künzel, H.M., 2011. Bauphysik der Innendämmung und Bewertungsverfahren. In *1. Internationaler Innendämmkongress 2011*. Dresden: TU Dresden, pp. 9–16.

Nicolai, A. et al., 2009. An efficient numerical solution method and implementation for coupled heat, moisture and salt transport: The Delphin Simulation Program. In *Simulation of Time Dependent Degradation of Porous Materials*.

133

11th Nordic Symposium on Building Physics, NSB2017, 11-14 June 2017, Trondheim, Norway

Effect of freezing and thawing on the performance of "capillary active" insulation systems: a comparison of results from climate chamber study to HAM modelling

Paul Klõšeiko*[a], Kadi Varda[a], Targo Kalamees[a]

[a] Department of Civil Engineering and Architecture, Tallinn University of Technology, Ehitajate tee 5, 19086, Tallinn, Estonia

Abstract

A climate chamber test was carried out to study the effects of freezing and thawing on strength and hygrothermal performance of three interior insulation systems: autoclaved aerated concrete, calcium silicate and expanded perlite insulation. Wall assemblies were monitored for temperature, relative humidity, moisture content and heat flux during dryout, preconditioning and freeze-thaw cycling. Pull-off strength was tested to detect changes in the material structure caused by freeze-thaw cycles.
Significant drop in strengths was detected for most of the setups. Comparison of measurement and hygrothermal modelling (IBK Delphin) results illustrates that even if state-of-the-art material data is available for HAM modelling, the reality may turn out to be vastly different, especially in the range of high moisture contents.

© 2017 The Authors. Published by Elsevier Ltd.
Peer-review under responsibility of the organizing committee of the 11th Nordic Symposium on Building Physics.

Keywords: interior insulation, frost resistance, hygrothermal modelling, HAM, climate chamber, capillary active

1. Introduction

High thermal conductivity and low surface temperatures are the sources of concern in historic masonry buildings resulting in high heating costs and mould risk. Interior insulation can be one solution should the exterior insulation be ruled out due to facades that are worth preserving. While the application of "capillary active" insulation can lessen some of the problems inherent to interior insulation, there too are its own risks. As the interface of original wall and

_____

* Corresponding author. Tel.: +372-620-2402; fax: +372-620-2405.
  E-mail address: paul.kloseiko@ttu.ee

insulation can be wet and cold, frost might be an issue. According to Künzel [1] freezing temperatures behind interior insulation system should be avoided. Thus, temperature at insulation-original wall interface should be above -5°C and relative humidity should be stay below 95%$_{RH}$. This very much restricts the thickness of interior insulation that can be applied, especially so in colder climates on walls with high thermal transmittance.

WTA Merkblatt 6-5 [2] recommends taking saturation degree of the material pores into account, it should stay below 30%$_{sat}$. That allows more freedom comparing to the previous criterion. However, authors' previous field measurements of capillary active interior insulation [3] showed considerably higher relative humidity levels when compared to Delphin model with same climate conditions. Thus the authors feel that a certain level of caution is required when interpreting the modelling results.

Research conducted by Scheffler [4] shows, that Ytong Multipor as a material is not sensitive to freeze-thaw cycles, however, the testing was limited to hygroscopic range and did not take into account other elements of the insulation system (e.g. glue mortar).

The aim of the study is to clarify the topic using hard data and research the possibility of mitigating the freezing criterion and therefore being able to install thicker insulation while having higher confidence in the interior insulation systems.

2. Methods

2.1. Test setup

In this study 3 different "capillary active" insulation systems are tested: Ytong Multipor autoclaved aerated concrete in 50mm and 60mm thicknesses (designated as MP50 and MP60 respectively), 50mm Knauf Tectem expanded perlite (TT) and 50mm Epasit Epatherm calcium silicate (ET). All of the insulation boards were attached to the base structure using system-specific glue mortar and covered with plaster and paint. The goal of the was not to imitate the exterior wall exactly as it would appear in real life but to achieve similar moisture contents in the insulation systems and test them for frost resistance. Thus, to shorten the duration of the cycle, a base structure with low thermal mass was selected. This consisted of timber framing, wood particleboard, PE foil and Knauf Aquapanel cement fiberboard. The view and section of the wall are given in Fig. 1. The materials in the test wall were selected so that majority of them would be represented in Delphin database to reduce uncertainties.

Boundary conditions for the study were selected based hygrothermal modelling. They were meant to achieve similar moisture contents as a 380mm brick wall with 100mm autoclaved aerated concrete or calcium silicate interior insulation modelled with 43-year real climatic data from Tartu, Estonia.

Temperature, relative humidity, moisture content and heat flux sensors were installed in the wall (Fig. 1 top left and top right). The following sensors and devices were used: 1) temp. sensors (inside the wall and on surfaces): Onset Hobo TMC15-HD & logger UX120-006M (accuracy ±0.15°C); 2) t&RH sensors (boundary conditions in chambers and inside the wall): Rotronic Hygroclip HC2-C05 (accuracy ±0.3°C, ±1%RH) & A/D converter: Siemens SM331 6ES7331-1kf02-0ab0 (accuracy ±0.004V); 3) heat flux sensors: Hukseflux HFP01 (accuracy ±5%), logger: Grant Squirrel SQ2020 1F8 (accuracy ±0.05% of readings, ± 0.025% of range); 4) backup t&RH sensors for int. and ext. chamber climate: Onset Hobo UX100-023; 5) balance: Vibra AJH-2200CE (e=0.1g, d=0.01g); 6) oven Venticell 111. Also, gravimetric measurement of moisture contents from different drill core layers were used (see Fig. 1 bottom right). Samples were dried at 70°C until constant mass had been achieved.

2.2. Freeze-thaw resistance assessment

At 0, 11, 26 and 53 freeze-thaw cycles 10 test samples of each insulation system were tested. A Ø92 mm core-drill was used for the separation of the samples (resulting in Ø85mm specimens) and adhesion/tensile strength was tested with Proceq DYNA Z Pull-Off tester. Although other methods have also been used for frost resistance assessment (e.g. compressive strength [4], dilatometry [5], dynamic elasticity modulus [6], mass loss, visual inspection etc), tensile strength was deemed suitable as the whole system was under study.
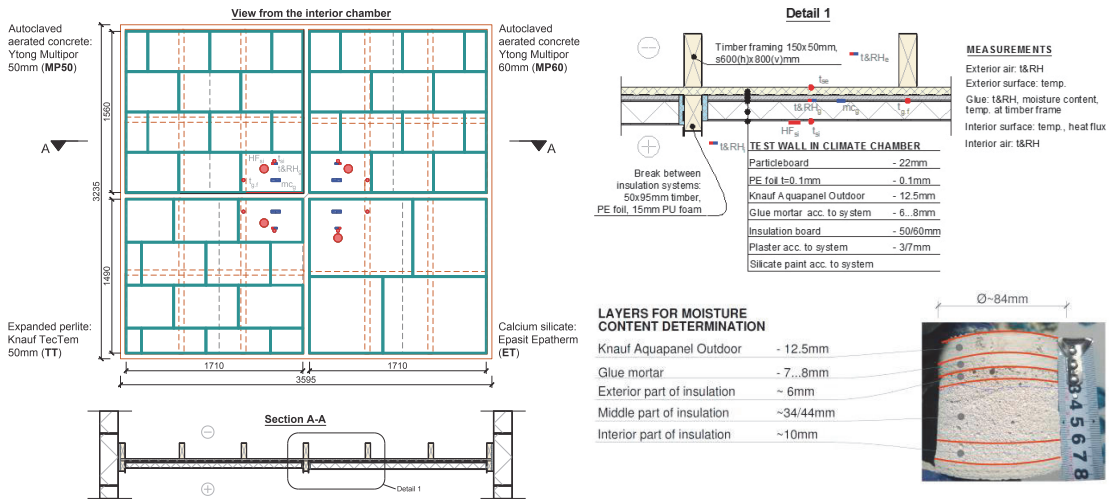
Fig. 1   View to the test wall from the interior chamber (top left), horizontal section (bottom left), detail of the layers (top right) and a typical drill core from which moisture contents were gravimetrically measured (bottom right).

2.3. Hygrothermal modelling

For modelling purposes IBK Delphin 5.8.3 [7,8] was used with ice model [9] turned "on". 1D model was used for comparison to the measurements, as prior 2D modelling deemed the thermal and hygric effect of framing >10…15cm from the edges insignificant. Boundary conditions for the modelling were for a) heat conduction: measured interior & exterior surface temperatures; and b) vapour diffusion: measured t&RH in air of interior and exterior chambers. Initial temperature and RH for the wall layers were 23°C and 60%$_{RH}$ respectively, while the glue and plaster layers were presumed to be saturated.

Material properties were taken from Delphin database. Exact matches existed for all materials except for the Epasit Epatherm glue and plaster layers, which were selected based on basic parameters (ρ, ψ, λ, μ, A_w). Also, exact properties of 0.1mm PE foil and 22mm particleboard are not yet known. The effect of particleboard on the insulation systems is largely thermal and its properties in the models were adjusted using the heat fluxes and temperatures. The thicknesses of the layers were based on measurements of the drill cores. Based on manufacturer's data, an additional vapour resistance of s_d=0.18m was added to the interior surface to take the silicate paint into account.

3. Results and discussion

Temperature and relative humidity in interior and exterior chamber throughout the test are given in Fig. 2. A typical freeze-thaw cycle in exterior chamber consisted of freezing period (t ~ -29°C, duration ~25h) and thawing period (t ~ -20°C, duration ~11h), while interior chamber temperature was kept constantly at 20°C. During the freezing period the temperature inside the glue layer dropped to as low as -15…-10°C depending on the insulation system (see Fig. 2 (right)). Due to relatively high moisture content, the effect of freezing and thawing is evident on temperature chart. It can be said that freezing starts at nearly 0°C for MP50 and MP60 and at around -1…-2°C for TT and ET systems. This is higher than -5°C temperature limit for frost avoidance derived from thermodynamics in [1] and suggests that larger pores are filled with water. Using porosities and densities from Delphin database, the saturation degrees were calculated from the measured moisture contents at the end of the test (Fig. 4). The saturation degree in insulation reached the highest in ET (24%$_{sat}$) and stayed the lowest in MP and TT insulations (9…11%$_{sat}$). In the case of the substrate (cement fiberboard), the trend was reversed – the lowest saturation degree was in ET and TT sections (25…29%$_{sat}$) vs MP (34…35%$_{sat}$). Highest saturation degree in the glue was in TT (41%$_{sat}$) and lower in MP and ET sections (25…32%$_{sat}$).
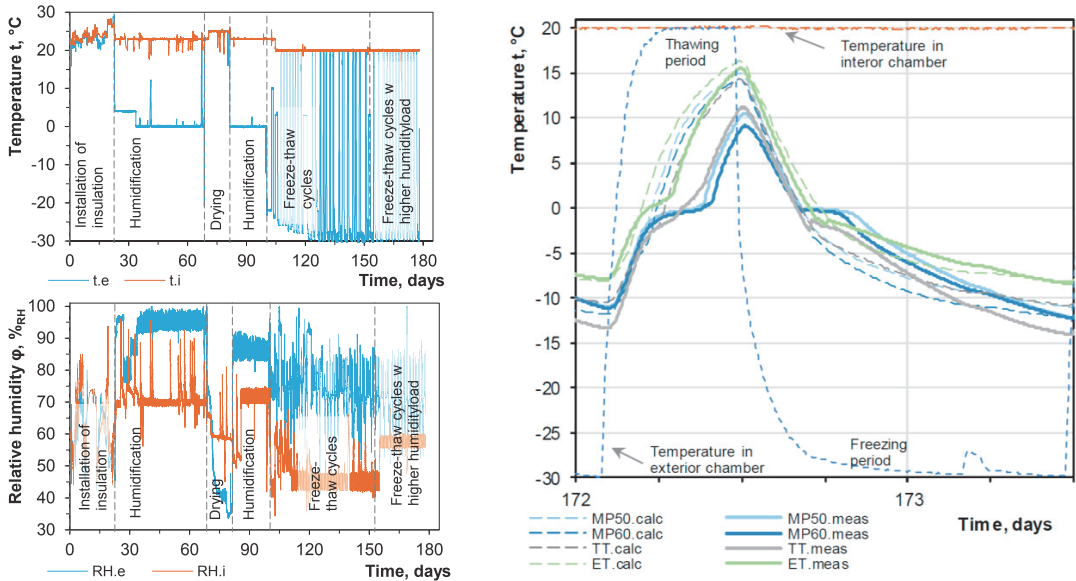
Fig. 2   Boundary conditions: temperature (top left) and relative humidity (bottom left) in interior and exterior chamber for the whole test and temperatures in the chambers and inside wall assemblies (measured and modelled) for a typical freeze thaw cycle (right). Also note the effect of freezing and thawing.
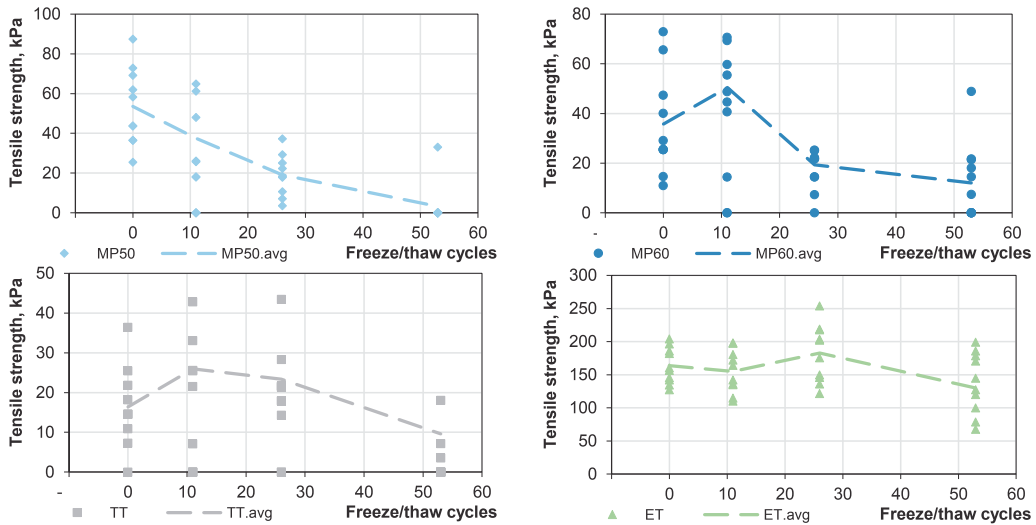
Fig. 3   Tensile strengths of drill cores: sample and mean values of 50mm Multipor (MP50, top left), 60mm Multipor (MP60, top right), 50mm Tectem (TT, bottom left) and 50mm Epatherm (ET, bottom right).

Tensile strengths of the insulation systems before and after freeze-thaw cycling are given in Fig. 3. Testing showed quite high spread. In TT & ET systems the rupture appeared in insulation layer near the glue in all cases. With MP50 and MP60 the break occurred in the middle of insulation layer during the base (0 cycles) and 11 cycle cases. However, in cases of 26 and 53 cycles (especially with MP50), the drill cores mostly separated from the base structure (cement fiberboard) from the glue layer.

Comparing the base cases to the tensile strengths at 53 cycles, independent samples 1-tailed t-tests showed statistically significant drop in tensile strengths for all insulation systems (p<0.05) except for ET. In case of MP50 and MP60, the deterioration was significant already at 26 cycles too. However, as statistical equivalence of the results from different cycles was not tested for, it cannot be said that ET is frost resistant.

Comparison of measurements to modelling. Gravimetric measurements give a more accurate indication of moisture content of the material compared to RH measurements. Almost all hygrothermal models underestimated the moisture contents during humidification periods. Typically, 1.5…3-fold differences occurred in glue and exterior part of insulation layers. The exception was cement fiberboard (Fig. 4 top left), where TT and ET models achieved best correlations. Theory of underestimated moisture contents is asserted by freeze thaw-cycling where delay in temperature drops and rises is not apparent in modelled data (see Fig. 2 right). It has to be born in mind that for ET insulation system the detailed glue and plaster material data was not available and influences the modelling results.

As the relative humidity inside glue layer was over range for RH sensors for most of the study, the comparison can be given for the initial phases (Fig. 4 bottom right). The trend coincides with authors' previous studies [3] where measured rel. humidities exceeded the modelled values in higher rel. humidities and when sharp rises were concerned.
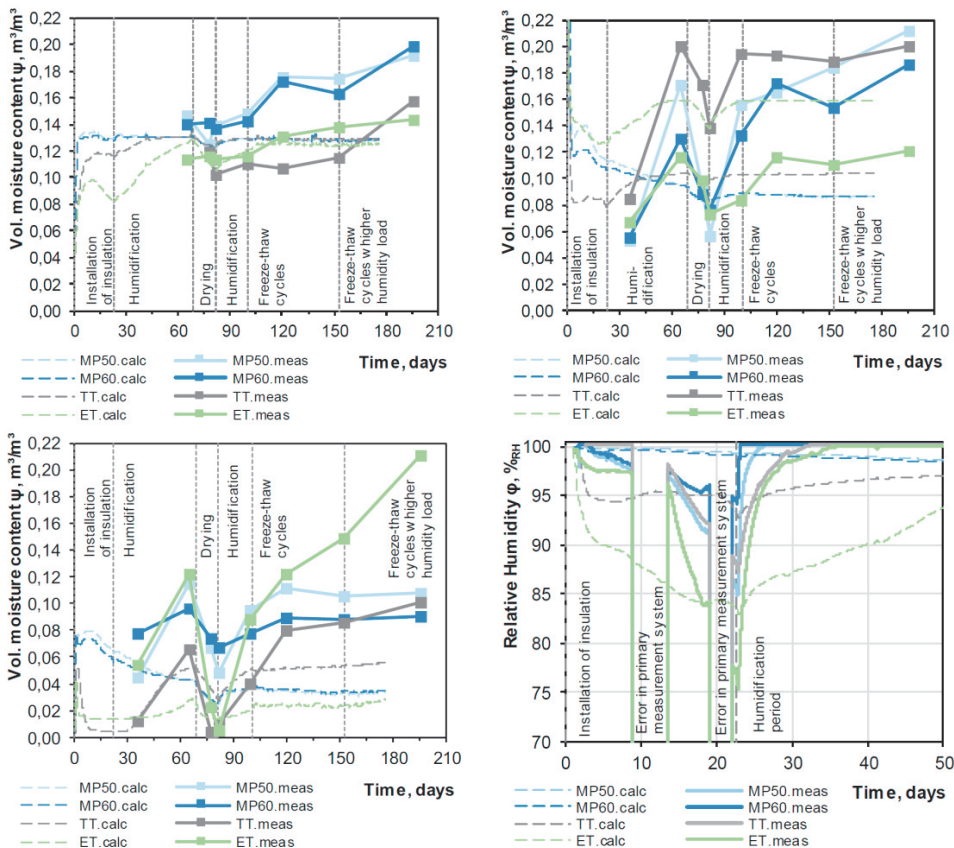
Fig. 4   Gravimetrically measured volumetric moisture contents in different parts of drill cores and comparison to modelling results: cement fiberboard (top left), glue mortar (top right) and exterior part of insulation (bottom left). Bottom right: measured and modelled relative humidities inside the wall (glue layer) during the first stages of the test. NB1: vol. moisture contents were calculated using respective densities from Delphin database; NB2: detailed hygrothermal material data for ET glue and plaster layers was not available and their modelling results should be treated with caution.

Sources of deviations. It is certain that errors were made sampling the data during this study (sensor errors, flaws in cutting, weighing, drying, etc). However, as large deviations, repeated sampling, duplicated sensors and previous studies show, the trend is probably still the same. Beside measurement errors, the other possibility is that the model might have its weaknesses. Deviations in material production might induce errors. Janssen et al [10] have raised questions about the low-capillarity approach in Delphin's handling of over-capillary moisture range. Also, the methods for deriving the moisture dependent liquid conductivity (K_l) function from measured material data might be the cause of inconsistencies. Dynamic effects too have been identified influencing on hygrothermal processes [11], but are not yet reliably described by the models.

4. Conclusion

Pull-off testing of drill cores from the insulation systems during different stages of the study showed that statistically significant changes in tensile strength occurred in MP50, MP60 and TT insulation systems. As the frost resistance cannot be ruled out as an assessment criteria based on current study, the correct modelling of moisture contents inside the wall is necessary to calculate the saturation degree and possible freeze-thaw cycles.

The hygrothermal models used to compare to the measurements were composed under best assumptions. They represent what engineers and consultants may use without conducting any further time- and resource-intensive studies. Comparison of measurement results to hygrothermal modelling revealed that even if thoroughly studied state-of-the-art material data is available for HAM modelling, the reality may turn out to be vastly different. This seems to hold true especially in high moisture content range.

These results suggest that further studies are necessary before safe functioning of "capillary active" interior insulation with higher thicknesses in cold climate can be warranted.

Acknowledgements

References

[1]   Künzel HM. Bauphysik der Innendämmung und Bewertungsverfahren, in: 1. Int. Innendämmkongress 2011, Dresden: TU Dresden, 2011: pp. 9–16.
[2]   Künzel H, Worch A, et al. Innendämmung nach WTA II: Nachweis von Innendämmsystemen mittels numerischer Berechnungsverfahren (Merkblatt 6-5). 2012.
[3]   Klõšeiko P, Arumägi E, et al. Hygrothermal performance of internally insulated brick wall in cold climate: A case study in a historical school building. J. Build. Phys. 38; 2015. p. 444–464.
[4]   Scheffler GA. Frostempfindlichkeit kapillaraktiver Innendämmung, in: J. Grunewald, R. Plagge (Eds.), 2. Int. Innendämmkongress. Tagungsunterlage, Dresden: TU Dresden, 2013
[5]   Mensinga P, De Rose D, et al. A Test Method to Identify the Onset of Freeze-Thaw Deterioration in Masonry. Sel. Tech. Pap. STP 1577. 2014; 2014. p. 197–217.
[6]   CEN. EN 14146:2004 Natural stone test methods - Determination of the dynamic modulus of elasticity (by measuring the fundamental resonance frequency). 2004.
[7]   Grunewald J. Diffusiver und konvektiver Stoff- und Energietransport in kapillarporösen Baustoffen. TU Dresden. 1997.
[8]   Nicolai A, Scheffler GA, et al. An efficient numerical solution method and implementation for coupled heat, moisture and salt transport: The Delphin Simulation Program, in: Simul. Time Depend. Degrad. Porous Mater., 2009
[9]   Sontag L. Implementation of an efficient numerical solution method to simulate freezing processes in porous media, in: Proc. 2nd Cent. Eur. Symp. Build. Phys., Vienna: 2013
[10]   Janssen H, Vereecken E, et al. A confrontation of two concepts for the description of the over-capillary moisture range: Air entrapment versus low capillarity. Energy Procedia. 78; 2015. p. 1490–1494.
[11]   Janssen H, Scheffler GA, et al. Experimental study of dynamic effects in moisture transfer in building materials. Int. J. Heat Mass Transf. 98; 2016. p. 141–149.

Publication V

Klõšeiko, P.; Freudenberg, P. (2019). Generative reverse-modelling approach to hygrothermal material characterization. MATEC Web of Conferences, 282: 4th Central European Symposium on Building Physics (CESBP 2019), Prague, Czech Republic, September 2-5, 2019. Ed. Černý, R.; Kočí, V.; Kočí, J. EDP Sciences,. DOI: 10.1051/matecconf/201928202088

Generative reverse-modelling approach to hygrothermal material characterization

Paul Klõšeiko[1]*and *Peggy* Freudenberg[2]

[1] Tallinn Univ. of Technology, Dept. of Civil Engin. and Arch., Ehitajate tee 5, Tallinn, Estonia
[2] TU Dresden, Institute for Building Climatology, Zellescher Weg 17, 01069 Dresden, Germany

Abstract. Reliable hygrothermal modelling depends on the quality of material characterization, especially so when higher moisture contents are concerned. Previous research has shown that adding additional material tests (e.g. capillary condensation redistribution (CCR) test) to the experimental dataset brings improvements to the modelling accuracy, but also adds to the workload of characterization process. This paper discusses a generative optimization workflow to increase the speed of the characterization and quality of the result. The proposed workflow incorporates optimization tool GenOpt and hygrothermal modelling software IBK Delphin to search for best fit of the water vapour and liquid conductivity curves of interior insulation materials based on modelling the CCR, drying and wet cup tests. Finally, models using material data from the proposed workflow and from the software database are compared to measurement results from two studies on interior thermal insulation. The results suggest that the generative optimization shows promise on the grounds of reducing tedious work analysing material tests. Also, a wider experimental dataset is shown to be useful when characterizing the vapour and liquid conductivity functions in over-hygroscopic region.

1 Introduction

Interest in interior insulation has grown year-by-year in the Nordic countries as the need to combat high heating costs and mould risk in historic buildings increases. "Capillary active" insulation could be one solution, but the possibility of frost damage in cold climate necessitates deeper studies into the topic – also through hygrothermal modelling.

According to Künzel [1], temperature behind the insulation should be above -5°C and relative humidity should be stay $\leq 95\%_{RH}$ to avoid frost damage. Hygrothermal modelling tools and material data have shown good correlation in this range and in experienced hands, the results can be considered reliable. However, these limit values restrict the thickness of interior insulation that can be applied, especially so in colder climates on walls with high thermal transmittance and where the need for thicker insulation is more pressing.

As stated in WTA Merkblatt 6-5 [2], a lot milder performance criterion can be used: the saturation degree inside the material pores should be below $30\%_{sat}$. Previous research [3, 4] has indicated that in high moisture content range, the modelling results can indicate much

---

* Corresponding author: paul.kloseiko@taltech.ee

lower humidity than there actually is – thus making the error non-conservative. Usually, water uptake and drying test are used to determine the water vapour and liquid conductivity curves in higher moisture content range [5, 6]. Assessing the share between the flows in these cases is based on assumptions as both have the same direction and are subjected to rather extreme conditions (water contact and full saturation). To gain more information on this, Binder et al [3, 7, 8] proposed a capillary condensation redistribution (CCR) test. There, a condensation plane inside a material sample is caused by temperature difference while mass change and moisture profile are monitored.

Taking the CCR test results into account has been so far been a step-by-step iterative process [8], which adds to the already existing high work load when doing the material characterization. This paper investigates the application of a generative optimization tool GenOpt to counter that and increase the quality of the results.

2 Methods

The proposed workflow incorporates optimization tool GenOpt [9] and hygrothermal modelling software IBK Delphin [10, 11] to search for best fit of the water vapour and liquid conductivity curves of interior insulation materials based on experimental data from material tests. This work is a further development of the tool [12] used to calibrate hygrothermal simulations according to measurements.

The operating principle of the optimization tool is given in Fig. 1. Moisture dependent water vapour ($\log(K_v(\psi))$) and liquid water conductivity ($\log(K_l(\psi))$) curves are defined by having a certain number of points at fixed moisture content values while GenOpt varies their conductivities. As GenOpt handles all optimizable variables independently, the Python script checks if the liquid conductivity curve is monotonically increasing. In the case of vapour conductivity, the curve should increase until point i and is expected to fall since point j (both can be defined). Penalties are applied if previous conditions are not met.
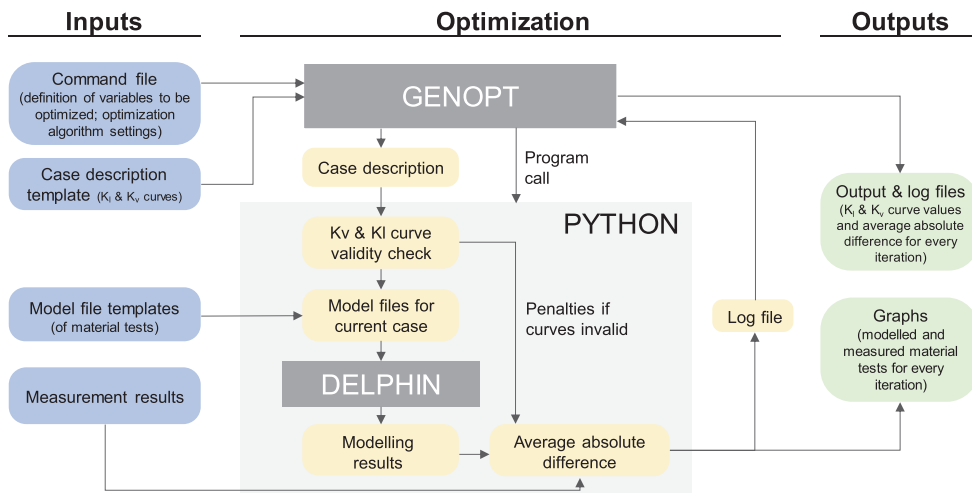
Fig. 1. Operating principle of the optimization tool based on GenOpt, Python and Delphin 5.9.

This paper presents optimization cases with autoclaved aerated concrete (AAC; mostly large macropores and fine capillaries) and calcium silicate (CaSi; mostly fine capillaries) insulation materials as an example. The tests currently incorporated in the optimization tool are: capillary condensation redistribution (CCR; moisture content profile at final time step; avg. moisture content over time), drying (avg. moisture content over time) and wet cup tests (moisture flux at wet cup boundary conditions). The CCR test data for CaSi is taken from

[7] and for AAC from [8], the rest of the material tests are based on TU Dresden IBK lab data. First point of the K_v curve was fixed to conductivity determined from dry cup measurements. Optimization limits were selected wide enough to keep the process unbiased. Average absolute difference between measured and modelled data is used as a cost function that GenOpt tries to minimize using Particle Swarm Optimization combined with Generalized Pattern Search method implementation of Hooke-Jeeves algorithm (GPSPSOOCCHJ)[13]. A weighting factor of 0.4 was applied to CCR m/c profile assessment (reducing its importance in overall average absolute difference) to take its larger scale into account and keep the optimization balanced. Finally, both the optimized material properties and unchanged material files from Delphin database are used to model 2 different case studies [4, 14] and are compared to the measurement results.

3 Results and discussion

3.1 Optimization results

In the case of CaSi, 2 different curve resolutions were tested (high resolution (hires): 10p on K_v and 15p on K_l curve; low resolution (lowres): 5p on both K_v and K_l curves). For all materials, 3 initial curves were set: 1) existing Delphin curve; 2) min. limit curve; 3) max. limit curve. The 0…0.15 m³/m³ part of the curves are shown in Fig. 2. Compared to Delphin versions, the optimized curves tend to have lower liquid conductivity and higher vapour conductivity. Table 1 gives an overview of final assessment value and time consumption of the optimization cases. Fig. 3 shows the results of material tests that the optimization was based upon. The drying test is modelled well with all material properties. The biggest differences are in CCR test results – optimized materials manage to reproduce the high moisture content at cold side of the sample. Optimized CaSi has problems reaching the "dynamic equilibrium" when comparing the average m/c of CCR test.
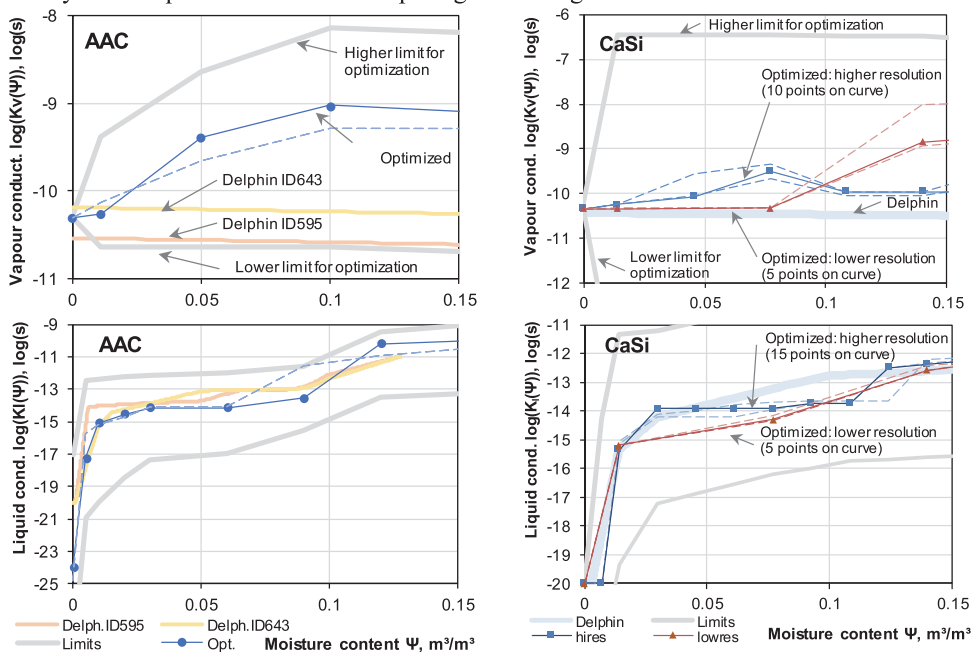
Fig. 2. Comparison of optimized and Delphin versions of liquid (top row) and vapour conductivity curves (bottom row). Dashed lines represent cases where initial values of the variables were different.

Table 1. Optimization cases and their properties. Cases chosen for further use have been underlined.

Case	Initial curves	Avg. abs. diff.	Iterations	Run time, h
CaSi highres	based on Delphin mat. file	2.72	7000	18
CaSi highres.min	min. limit	2.72*	6541	16
CaSi highres.max	max. limit	2.80*	6315	16
CaSi lowres	based on Delphin mat. file	2.74	2260	6
CaSi lowres.min	min. limit	2.81	2988	5
CaSi lowres.max	max. limit	2.74	2991	6
AAC	based on Delphin mat. file	1.72	2685	6
AAC.min	min. limit	2.21	1948	6
AAC.max	max. limit	2.21	1951	6

* – curve not conforming to the set rules in 1 point
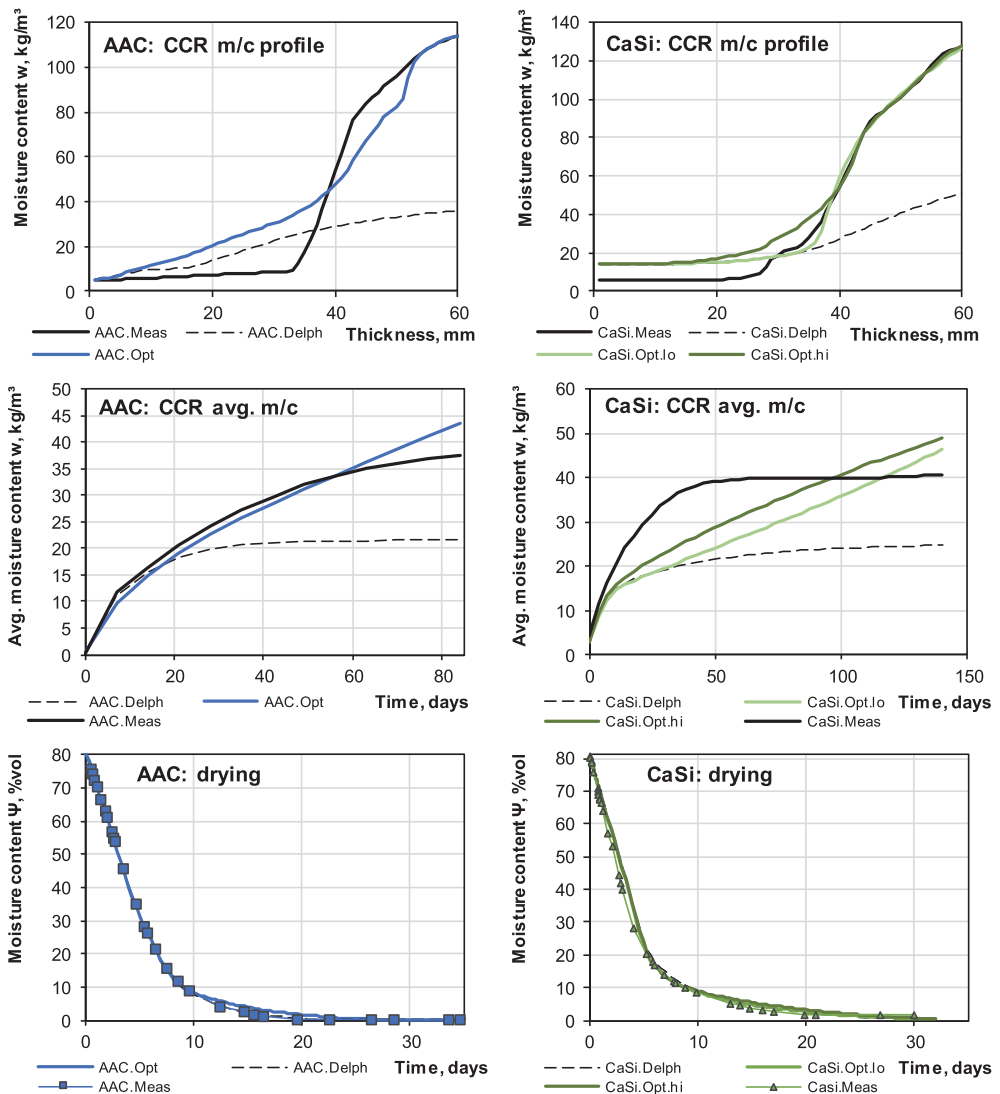
Fig. 3. Comparison of measured and modelled material test results for AAC (left) and CaSi (right).

3.2 Comparison to case studies

Two case studies were used to compare how the optimized material properties behaved against their unchanged versions and the measurement results. The first one [4] took place in a climate chamber and is characterized by high moisture contents. Also, during the second half of the study, ~50 freeze-thaw cycles take place. Fig. 4 gives the modelled and measured moisture content of ~7mm layer on the cold side of insulation. Moisture contents of AAC and CaSi are both underestimated by the Delphin database versions of the material data, while the optimized version of AAC is remarkably closer to measured results.
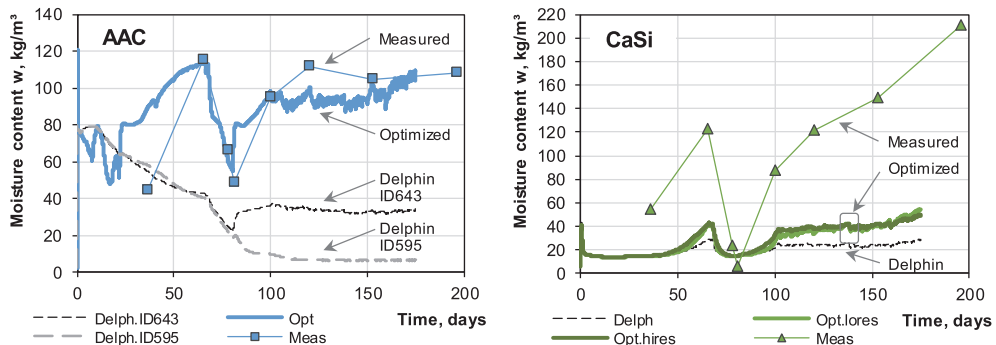
Fig. 4. Case study 1 (high moisture content; climate chamber): comparison of measurement results to modelling with optimized and unchanged material properties for AAC (left) and CaSi (right).

The second case study [14] was based on an exterior brick wall of a historic school building with added interior insulation and a humidification system. The moisture load mimicked an unventilated apartment. Moisture was measured using relative humidity sensors. Fig. 5 shows that the the optimized and database versions of material properties result in similar RH values for both AAC and CaSi.
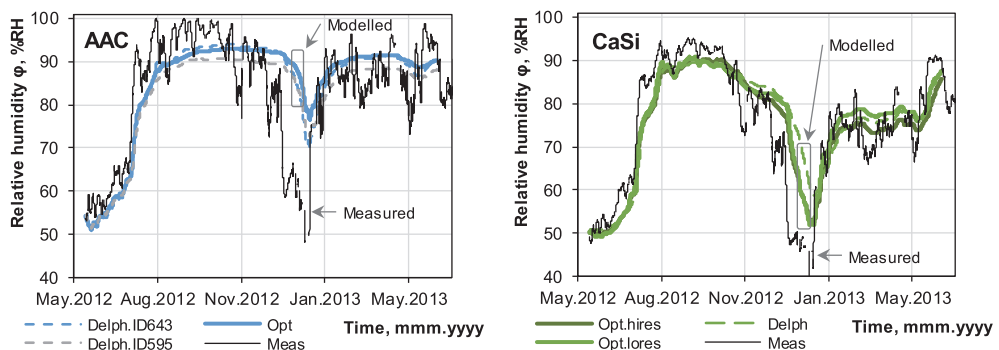
Fig. 5. Case study 2 (medium moisture content; real building): comparison of measurement results to modelling with optimized and unchanged material properties for AAC (left) and CaSi (right).

4 Conclusions

As a study on developing a material characterization tool, the results can be considered good. Although the variation limit boundaries were kept large and different initial values and curve resolutions were used for optimization, the resulting optimized curves were in a relatively similar range and in most part matched the curves in Delphin database. However, optimized liquid conductivity tended to be lower and vapour conductivity higher in the range of 0.05…0.1 m³/m³ moisture content. This could be explained by the liquid island

effect. Still, as the CCR test data was taken from literature and the exact tested products and boundary conditions were not disclosed, it is quite possible that the CCR and rest of material data were measured from different products. This brings along mismatches in moisture retention curves and the optimization algorithm trying to compensate for it through conductivity curves.

Comparison to case study results show that for both AAC and CaSi, the optimized materials show better correlation to measured data in high moisture content range (especially so for AAC), hinting at the value of CCR test. In hygroscopic range, the optimized properties perform similarly to their default counterparts – as Delphin has shown to be quite reliable in that range, it could be considered a good result for the algorithm. These results underline that there are still many unknowns when dealing with overhygroscopic moisture contents – caution is advised when drawing far-reaching conclusions from modelling results in that region.

Future work could include developing a wider experimental base for optimization and defining stricter rules/boundaries for the conductivity curves. Currently, the results show quite high spread at moisture contents above CCR test – the share of liquid and vapour transfer is hard to determine. Also, the CCR test could be enhanced with relative humidity sensors in the samples to gain more reference data from the hygroscopic region.

References

1. H. M. Künzel, in *1. Internationaler Innendämmkongress 2011*, 2011, 9–16.
2. H. Künzel *et al.*, 2012.
3. A. Binder, D. Zirkelbach, and H. M. Künzel, in *Thermal Performance of the Exterior Envelopes of Whole Buildings XI*, 2010.
4. P. Klõšeiko, K. Varda, and T. Kalamees, Energy Procedia **132**, 525–530 (2017).
5. G. a. Scheffler and R. Plagge, Int. J. Heat Mass Transf. **53**, 286–296 (2010).
6. M. Krus, *Moisture transport and storage coefficients of porous mineral building materials. Theoretical principles and new test methods*. Stuttgart: Fraunhofer IRB Verlag, 1996.
7. A. Binder, H. M. Künzel, and D. Zirkelbach, in *Proceedings of 2nd Central European Symposium on Building Physics*, 2013.
8. A. Binder, D. Zirkelbach, and H. M. Künzel, in *NSB 2014, 10th Nordic Symposium on Building Physics: 15-19 June 2014, Lund, Sweden*, 2014, 1061–1068.
9. M. Wetter, in *Seventh International IBPSA Conference*, 2001.
10. A. Nicolai, G. A. Scheffler, J. Grunewald, and R. Plagge, in *Simulation of Time Dependent Degradation of Porous Materials*, 2009.
11. J. Grunewald, TU Dresden, 1997.
12. P. Freudenberg, U. Ruisinger, and E. Stöcker, Energy Procedia **132**, 405–410 (2017).
13. M. Wetter, *GenOpt® User Manual v3.1.1*. Berkeley: LBNL, 2016.
14. P. Klõšeiko, E. Arumägi, and T. Kalamees, J. Build. Phys. **38**, 444–464 (2015).

Publication VI

Klõšeiko, P.; Kalamees, T. (2021). Hygrothermal performance of a brick wall with interior insulation in cold climate: vapour open vs vapour tight approach. Journal of Building Physics. DOI: 10.1177/17442591211056067

Accepted manuscript

Hygrothermal performance of a brick wall with interior insulation in cold climate: vapour open vs vapour tight approach

Paul Klõšeiko, Targo Kalamees

Acknowledgement

Funding

1

Abstract

Interior insulation of historic buildings is well-studied in Central Europe; however, their conclusions might not be directly applicable to colder climates. Heat, air, and moisture (HAM) modelling can be a valuable tool for studying those solutions in different conditions. Recently, incorporating the capillary condensation redistribution (CCR) test into the material characterization process has shown to cause dramatic improvement in correlating hygrothermal modelling results to measurements in certain situations. It is also noteworthy, that the HAM modelling errors made using material data from conventional characterization process can be severely non-conservative.

In this article a parametric study of a 51 cm thick mass masonry wall is undertaken to determine the effect of the improved material properties on the reliability of a vapour open "capillary active" autoclaved aerated concrete (AAC) and calcium silicate (CaSi) interior insulation solutions and to compare them to a vapour tight insulation system. A 49-year real weather dataset from Estonia is used.

The results show that compared to conventionally characterized material properties the CCR-optimized material data causes more critical conditions directly behind the interior insulation, while having a similar performance in the exterior part of the masonry. The differences occur close to the performance limits and highlight the importance of using the CCR test in material characterization process.

The vapour tight and vapour open systems showed a very similar impact on the freeze-thaw cycles and on the maximum ice saturation of the exterior part of the masonry. The vapour open solutions perform better than the vapour tight PIR in terms of frost damage and possible mould growth behind the insulation – even though the advantage has been reduced when using the CCR-optimized material data. Regardless of the insulation solution, a case-specific approach is still required to avoid damaging the original wall and/or the added insulation system.

Keywords

1 Introduction

To erect energy efficient, moisture safe and thermally comfortable buildings the modern masonry structures offer a wide variety of solutions – a review of which is presented by Ismaiel et al. (2021). However, the need for a thermal upgrade also affects existing buildings where the inherently safer exterior insulation may not be desirable or possible.

There, interior insulation – although a hygrothermally riskier concept – is often seen as a solution. This has been further encouraged by the introduction of vapour open "capillary active" insulation systems that are promoted to solve some of issues that make the more "traditional" vapour tight approach risky – mould growth risk at the old wall-insulation interface, moisture accumulation in the original wall etc.

In recent decades the accessibility and use of hygrothermal modelling tools (e.g. IBP Wufi, IBK Delphin) has grown noticeably. Compared to calculations made using the Glaser method (Glaser, 1959) / EN ISO 13788, complex problems involving dynamic boundary conditions and combined vapour and liquid water transfer can be solved. Design decisions can be made without expensive and time-consuming in-situ or laboratory tests.

Numerous studies by different research groups as well as engineers and architects have employed such tools to analyse the impact of interior insulation on the hygrothermal performance of building enclosures. Häupl et al. (2005) modelled the performance of a 600 mm masonry wall in Amsterdam and concluded that the use of vapour tight cellular glass insulation would lead to moisture buildup and the destruction of the structure while the impact of "capillary active" calcium silicate would be much more tolerable. Modelling results of several interior insulation solutions in Norwegian climate by Knarud et al. (2014) show that CaSi has lower relative humidity behind insulation than vapour tight systems. Vereecken et al. (2015) conducted a probablilistic modelling study of a 15–50 cm-thick brick wall using outdoor climate data from Germany. They concluded that of the studied solutions the vapour open calcium silicate is preferable for buildings which are sensitive to frost damage and with wooden beam ends, whilst vapour tight solutions are more appropriate in those buildings where these aspects are not important. A modelling study using Swedish climate data (Abdul Hamid and Wallentén, 2017) exhibits the risk of microbiological growth and an increased corrosion rate of reinforcement if vapour tight solutions are used. At the same time, calcium silicate shows a lower mould risk and can even reduce the corrosion rate and its combination with hydrophobation is reported to perform best. In recent years, the RIBuild project has made valuable contributions to the field through experiments and modelling alike. For example Jensen, Bjarløv, et al. (2020) determined that of the studied solutions, only CaSi and CaSi+PUR systems with hygrophobic treatments would be robust enough to withstand the future climate.

However, the accuracy of hygrothermal modelling is – among correct boundary conditions, properly specifying the structure, etc. – largely dependent on the reliability of the material properties. Conventionally, water uptake and drying tests are used to determine the water vapour and liquid conductivity curves in the higher moisture content range (Krus, 1996; Scheffler and Plagge, 2010). Assessing the share between the flows in these experiments is based on assumptions as both have the same direction and are subjected to rather extreme conditions (water contact and full saturation). To gain more

Accepted manuscript

information on this, Binder et al (2010, 2013, 2014) proposed a capillary condensation redistribution (CCR) test, where vapour and liquid flows are in opposite directions. In this test, a temperature difference causes a condensation plane inside a material sample while mass change and moisture profile are monitored.

Klõšeiko & Freudenberg (2019) suggest a method for generically optimizing the vapour and liquid conductivity curves by remodelling the material tests also involving the CCR test. Autoclaved aerated concrete (AAC) and calcium silicate (CaSi) were used as an example for this process. The CCR-optimization notably improved the correlation of AAC when the modelling results were compared to measurements from Klõšeiko et al. (2017).

Hirsch et al. (2020) described a slightly modified CCR test setup, presented measurement results and inverse modelling results to identify the vapour and liquid conductivity functions. Using the dataset from Klõšeiko et al. (2017), they demonstrated that modelling with newly CCR-optimized CaSi material data now had good agreement between modelling and measurements.

In their preliminary example comparisons Binder et al (2014), Klõšeiko & Freudenberg (2019) and Hirsch et al. (2020) indicated that the errors made by using conventional material characterization were non-conservative, especially near the performance limits which might not be reached in laboratory or in-situ tests that have been used to calibrate the HAM models. This raises the question whether the conclusions drawn from previous modelling in high moisture range while using conventional material characterization are still valid.

By using a parametric study of different interior insulation solutions and a long-term real weather dataset (a preferable choice over Reference Years or mean years, that are usually used in previous studies), this article has two main aims:

- To quantify the difference in modelling results caused by conventional and CCR-optimized material characterization processes.
- To assess the suitability of vapour open and vapour tight insulation approaches in cold climate and to determine if the "capillary active" vapour open materials with corrected liquid conductivity curves still have the advantages as described in the literature.

Accepted manuscript

2 Methods

2.1 Modelling

2.1.1 Calculation models

IBK Delphin 5.9.6 (Grunewald, 1997; Nicolai et al., 2009) was used for HAM modelling. Delphin uses the implementation of the ice model by Sontag (2013) to take the phase change enthalpies and freezing point depression (model by (Häupl and Xu, 2001)) into account.

A 51 cm thick masonry wall was selected to represent a typical Estonian mass masonry structure. Thinner walls would have a lower thermal resistance and moisture capacity (hence making them more critical), however, they are not common. Thicker walls, in contrast, are less critical and usually have an air cavity, which further reduces the effect of wind driven rain.

Figure 1 describes the structure of models used in the current study as modelled in Delphin. Two 1-dimensional base models were created: a section through brick layer, intersected with a vertical mortar joint (base model B), and a section through a horizontal mortar joint itself (base model M). Two 1-dimensional models were chosen instead of a single 2D model due to modelling speed, which also allowed more variations in parameters to be included. Preliminary modelling showed that the difference in results between the 1D and 2D models was small, which corroborates the findings of Vereecken and Roels (2013).

Two different insulation approaches were considered – vapour open capillary active autoclaved aerated concrete (AAC) & calcium silicate (CaSi) and a more vapour tight polyisocyanurate (PIR) insulation with a 9 mm gypsum board on top of it as a finishing layer. The vapour open systems were presumed to have hydraulic contact with the original wall as glue mortar is used for installation, while a 3 mm air cavity was assigned between the original wall and the PIR insulation system (to account for unevenness of the original wall). According to the manufacturer's guidelines (Heße et al., 2018), the old interior plaster was retained under the insulation layer.

The thicknesses of the insulation layers (30 mm PIR, 60 mm AAC and 90 mm CaSi) were selected to represent real products available on the market while achieving similar thermal resistance. The largest differences were between CaSi and PIR: the thermal resistance of the PIR system was ca 1/10 higher than that of the CaSi one, while thermal transmittances of the whole walls differed by ca. 5%. To minimize the frost risks in cold climates, the layers were intentionally thin.
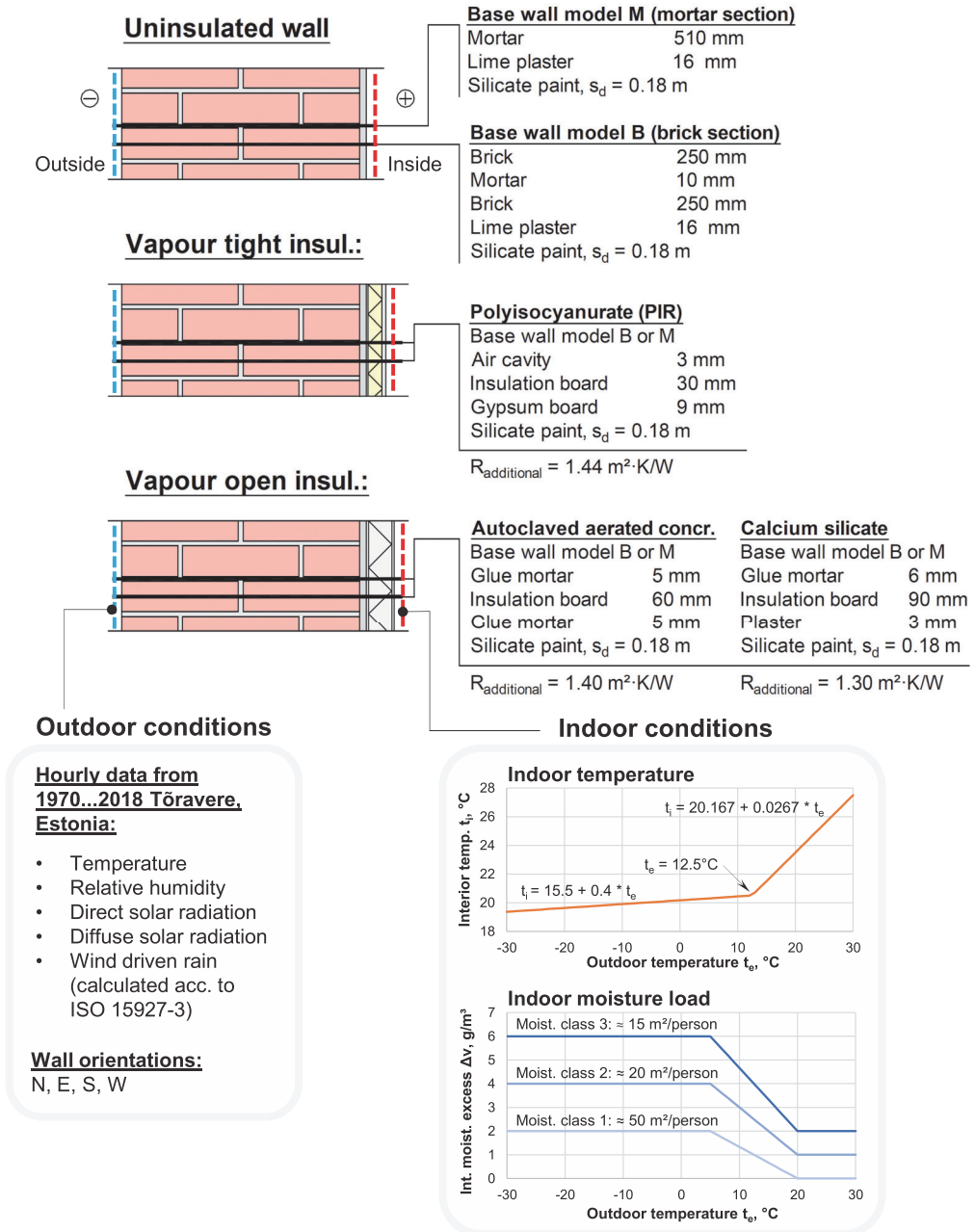
Figure 1   Schematic of the 1D wall models and their boundary conditions used in Delphin.

2.1.2   Material properties

2.1.2.1   CCR-optimized conductivity functions

The liquid and vapour conductivity curves were created using the tool described in Klõšeiko & Freudenberg (2019). However, for this publication, new material characterizations were done compared to the ones in the aforementioned paper. The main changes are monotonically decreasing vapour conductivity functions and the inclusion of CCR test data for CaSi boards from Hirsch et al (2020) – now the whole CaSi dataset is measured using the same material. Furthermore, to eliminate the effect of different material characterization methodologies and source data, the "conventional" material characterization was done using the same tool while leaving the CCR test out. These material files resulted in similar hygrothermal performance as the respective files in the Delphin database.

The optimized material data (Figure 2 row 1) shows notably reduced liquid conductivity in the moisture content range of 0.01–0.15 m³/m³ compared to the conventionally acquired material data. Similarly to Binder et al. (2014) and Hirsch et al. (2020) an ideal combination of material functions that would fit the reference tests (Figure 2 rows 2–4) could not be found – the main contradiction being between the CCR and drying tests and, in the case of slightly hydrophobic dry AAC, water uptake too. Here, more emphasis was put on achieving a better correlation with the CCR test and as it describes the behaviour in actual usage scenarios and at performance limits better.

Accepted manuscript
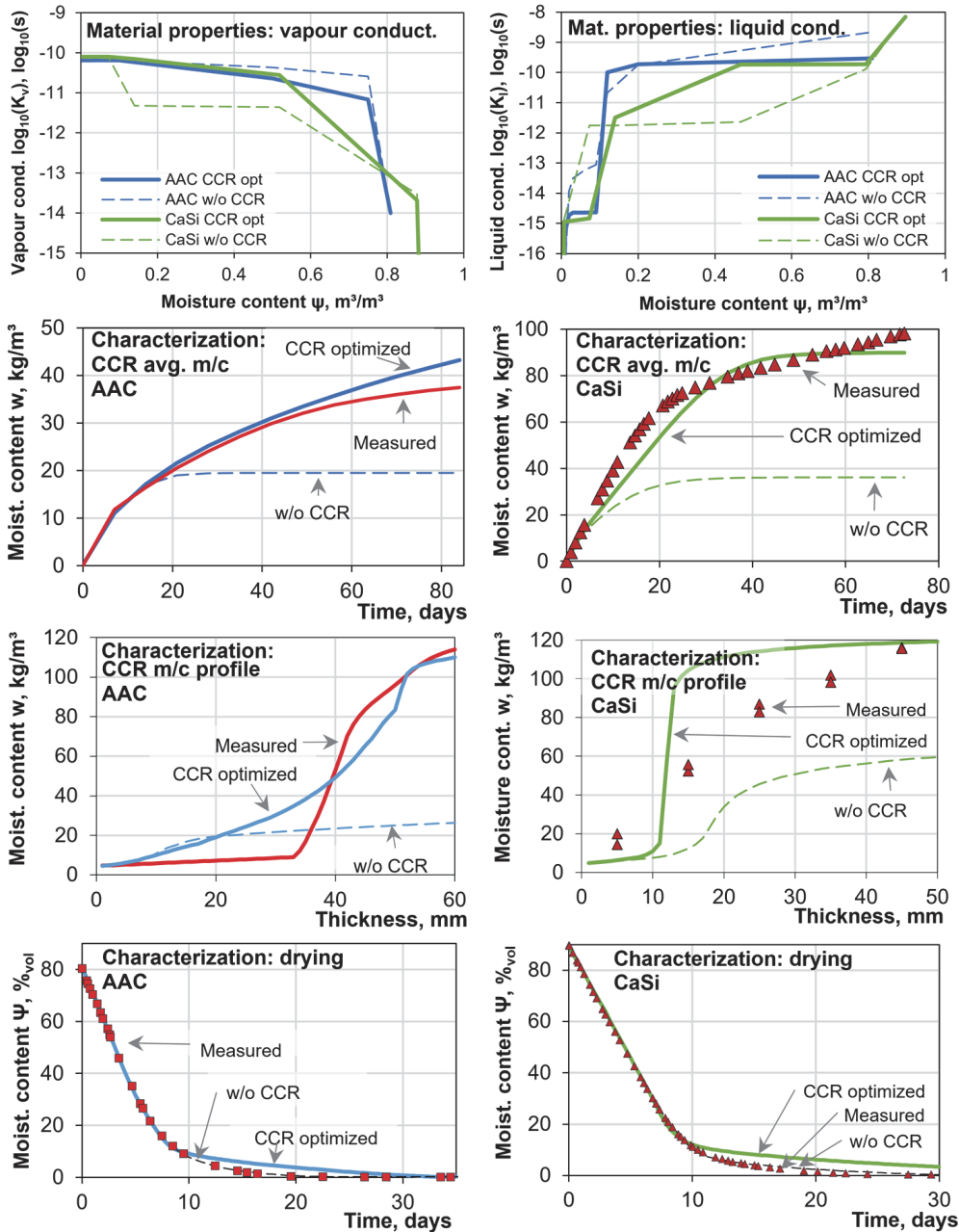
Figure 2 CCR optimized and conventionally characterized material properties ("w/o CCR") used in this study (top row) and some of the material tests used as a reference for optimization (bottom 3 rows). (Based on Klõšeiko and Freudenberg, 2019)

Klõšeiko and Freudenberg (2019) also discussed the difference in modelling results caused by the changes to material properties on the basis of two studies – they are presented here again using the updated material data. In a laboratory study with a high moisture load (Klõšeiko et al., 2017), the moisture content in the cold (exterior) part of the AAC and CaSi insulation boards increased about 2.5–3 times and therefore dramatically improved the correlation with measurement data (see Figure 3). In case of more realistic moisture loads in a real building (Case study 2 (Klõšeiko et al., 2015), see Figure 4), the difference of RH on the cold side of the insulation was small (conventional vs CCR-optimized properties) and did not improve nor worsen the correlation between measured and modelled data noticeably. The discrepancies in Case study 2 can be attributed to a lack of detailed material data, but also the dynamic effects (Janssen et al., 2016) in ad- and desorption processes.
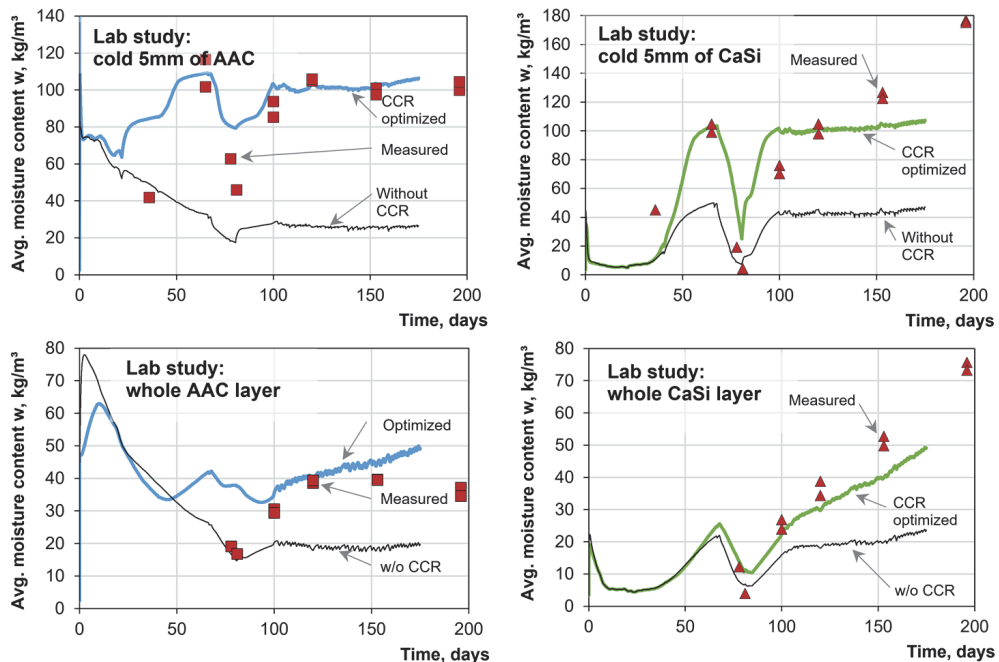
Figure 3   Comparison of measurement results to modelling with optimized ("CCR optimized") and conventionally characterized material properties ("w/o CCR"). Case study 1 (high moisture content; climate chamber), moisture content of cold side of insulation (top row) and the whole insulation layer (bottom row). The CCR-optimized material shows about 2…3-fold increase in maximum moisture content and coincides better with measurement data. Measurement data from Klõšeiko et al. (2017).

Accepted manuscript
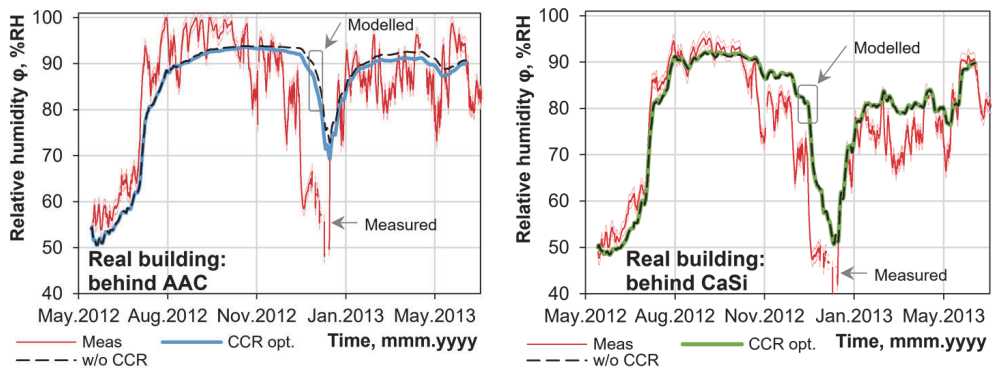
Figure 4   Case study 2 (medium moisture content; real building), relative humidity in cold side of insulation: comparison of measurement results to modelling with optimized and conventionally characterized material properties. No notable differences between modelling results. Measurement data from Klõšeiko et al. (2015).

2.1.2.2   Summary of material properties used in the study

Table 1 gives the overview of basic material properties used for modelling in different combinations. Three different bricks were selected from the Delphin database to represent historic Estonian bricks based on in-house measurements of basic parameters (type, porosity, vapour conductivity and water uptake coefficient). The selection of 3 lime-cement mortars covered different historic mortars in the Delphin database.

Three interior insulation solutions with different approaches were selected:

- 2 vapour open solutions advertised as "capillary active":
    - Autoclaved aerated concrete (based on data for material ID 643).
    - Calcium silicate (based on data for material ID 571).
  Both had 2 versions: one with conventional material characterization and one which included capillary condensation redistribution test in the calibration of liquid and vapour conductivity functions.
- "Vapour tight" material without liquid conductivity: polyisocyanurate (PIR) board (without diffusion tight coatings) with a gypsum board applied on top (id 599). The insulation material was based on material id 194 with a modified vapour diffusion resistance coefficient $\mu = 60$ and thermal conductivity of $\lambda_{dry} = 0.023$ W/(m·K).

Table 1 Basic material properties of materials used in modelling.

Name	ID in Delphin	Density ρ, kg/m³	Thermal conductivity λ_{dry}, W/(m·K)	Porosity ψ_{por}, m³/m³	Water vap. diffusion resistance factor μ, -	Water uptake A_w, kg/(m²·s⁰·⁵)
Brick Bernhard	97	2060	1.00	0.25	19	0.100
Historical Brick (Cluster 4)	33	1710	0.80	0.33	8.3	0.278
Lime Sand Brick (traditional)	153	1810	1.00	0.34	40	0.052
Lime cement mortar	143	1570	0.70	0.41	11	0.176
Lime cement mortar	717	1878	0.80	0.29	37	0.036
Lime cement mortar (low cement ratio)	718	1739	1.05	0.34	28	0.494
Lime Plaster (historical)	148	1800	0.82	0.30	12	0.127
Glue Mortar	407	1472	0.92	0.44	38	0.008
Inside Plaster	656	1279	0.31	0.52	10	0.082
CaSi insulation		270	0.069	0.91	2.5	1.13
Glue Mortar	77	830	0.16	0.69	13	0.003
AAC insulation		99	0.044	0.96	3	0.006
PIR insulation		32	0.023	0.95	60	-
Gypsum Board	599	745	0.18	0.72	11	0.179
Air gap (3mm)	13	1.3	0.03	1	1	-

Unless explicitly defined by a function in the material file, Delphin assumes the moisture dependent thermal conductivity according to (1) and discards the temperature dependency of thermal conductivity. (Vogelsang et al., 2013)

$$\lambda(\psi) = \lambda_{dry} + \psi \cdot 0.56 \frac{W}{m \cdot K} \qquad (1)$$

2.1.3 Interface contact resistances

Derluyn et al. (2011) obtained the interface resistances R_{if} of $1.25 \cdot 10^{10}$ m/s (dry cured mortar) and $2.5 \cdot 10^{10}$ m/s (wet cured mortar), while Vereecken & Roels (2013) used $2.5 \cdot 10^{10}$ m/s and $5 \cdot 10^{10}$ m/s respectively in their simulations. Later, Vereecken and Roels (2015a) studied the hydraulic contact resistances in case of capillary active insulation glue and concluded that constant resistances do not represent measurements very well and recommended values depending on moisture content. Calle et al. (2019) determined that hydraulic lime-brick interface resistances are an order of magnitude lower than the cement mortar-brick ones available in literature. Zhou et al. (2020) conducted an experiment on the water uptake of a masonry section and determined that the interface

Accepted manuscript

resistances between brick and mortar were in the range of $3.5 \cdot 10^9$–$8 \cdot 10^{10}$ m/s – this shows that the interface resistances can vary by several orders of magnitude even on different interfaces of the same masonry.

In this study, in order to simplify the modelling, interface resistance of $R_{if} = 2.5 \cdot 10^{10}$ m/s is compared to perfect hydraulic contact ($R_{if} = 0$ m/s). Resistances are applied to brick-mortar and brick-plaster interfaces. The choices made here are meant to reflect the impact of different parts of the interface resistance spectrum and should not be considered as the only possibilities.

2.1.4 Boundary conditions

A 49-year period of historical weather data from Tõravere, Estonia was used as **outdoor climate**. According to the Köppen-Geiger classification, Estonia belongs to humid continental climatic zone (Dfb). Outdoor temperature, relative humidity, wind speed, wind direction, short-wave radiation and wind driven rain were assigned as climate conditions. The overview of them is given in Figure 5 and Figure 6.

Hourly values of wind driven rain (WDR) imposed on the wall were calculated according to ISO 15927-3 (2009). The parameters for WDR calculations were mostly fixed – height: 7 m, terrain category: III (suburban and industrial areas), topography coefficient CT: 1 (building not on an uphill slope), obstruction factor O: 0.8 (obstacles of similar size 80–100 m from the building, no wind funnelling). Wall factor W was varied as 0.5 (top part of a multi-storey building without eaves) and 0.75 (local maxima). Yearly mean wind driven rain rose (W = 0.5) is given in Figure 6 (center). If the air temperature was below -2°C, the precipitation was deemed as snow and discarded.

The climate data used for the modelling starts on the 1st of January 1970. The initial temperature of the wall was 12°C and 80%$_{RH}$ was assigned on all layers.

Indoor climate model was based on the analysis of 190 apartments with central heating (Ilomets et al., 2018). The indoor temperature model was based on indoor climate of Estonian brick apartments and it corresponds to the lower limit of Fig. 7 in Ilomets et al. (2018). The indoor temperature and moisture excess dependence on outdoor temperature is given in Figure 1 (bottom right). 3 different moisture excess (moisture load) levels based on Figure NA.3 from (EVS EN ISO 13788 2012) were varied and are shown in Figure 1 (bottom right). Figure 1 (bottom right) also gives the corresponding average occupancy rates based on Fig. 9 in Ilomets et al. (2018).
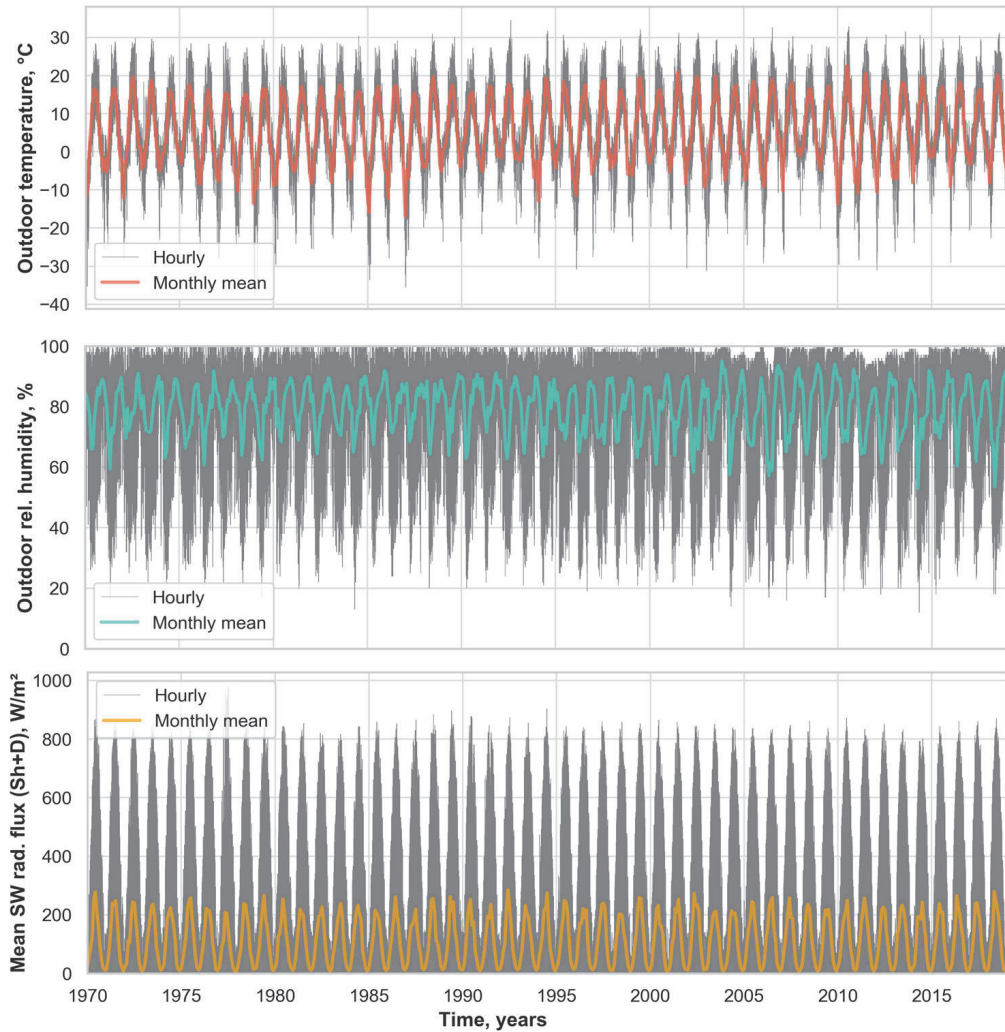
Figure 5   Outdoor boundary conditions: hourly and monthly mean temperature (top), relative humidity (middle) and total shortwave (direct + diffuse) radiation on a horizontal surface (bottom).

Accepted manuscript
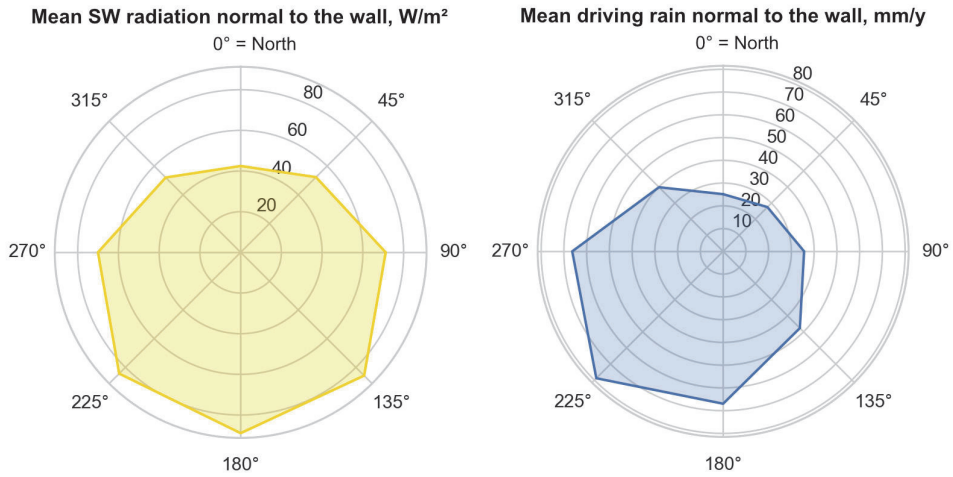
Figure 6   Mean shortwave radiation (direct + diffuse; left) and yearly mean wind driven rain (calculated according to ISO 15927-3:2009, wall factor W = 0.5; right) roses.

2.1.5   Summary of variations

The summary of all varied parameters is given in Table 2. Combinations of them resulted in 3455 different models. No weighting of the variations was done as the distribution of the parameters in real life is not known.

Accepted manuscript

Table 2   Variations of parameters used in this study.

Parameter	Variations
Brick	• Historical brick (id 97) • Brick Bernhard (id 33) • Lime sand brick (id 153)
Lime-cement mortar	• Lime cement mortar (id 143) • High cement ratio (id 717) • Low cement ratio (id 718)
Interface resistances (brick-mortar and mortar-insulation)	• Perfect hydraulic contact • $2.5 \cdot 10^{10}$ m/s
Wall factor W in ISO 15927-3 (rain exposure)	• 0.5 • 0.75
Wall orientations	• North • East • South • West
Indoor air moisture excess	• Moisture class 1 (≈ 50 m²/person) • Moisture class 2 (≈ 20 m²/person) • Moisture class 3 (≈ 15 m²/person)
Interior insulation solution	• Uninsulated • AAC (CCR-optimized) • AAC (without CCR) • CaSi (CCR-optimized) • CaSi (without CCR) • PIR on paper backing + gypsum board

2.2   Performance assessment

Figure 7 shows the sections and parameters assessed in these locations. The greatest number of freeze-thaw cycles and the highest ice contents occurs near the exterior surface. The exact location of the critical section depends on the combination of material properties, insulation solution and saturation degree used to count the freeze-thaw cycles, etc., all of which varied from case to case. Based on preliminary modelling, the layers between 5–135 mm from the exterior surface were used to judge the magnitude

Accepted manuscript

of changes caused by different parameters and the result from most critical layer of each case is presented as "exterior masonry".
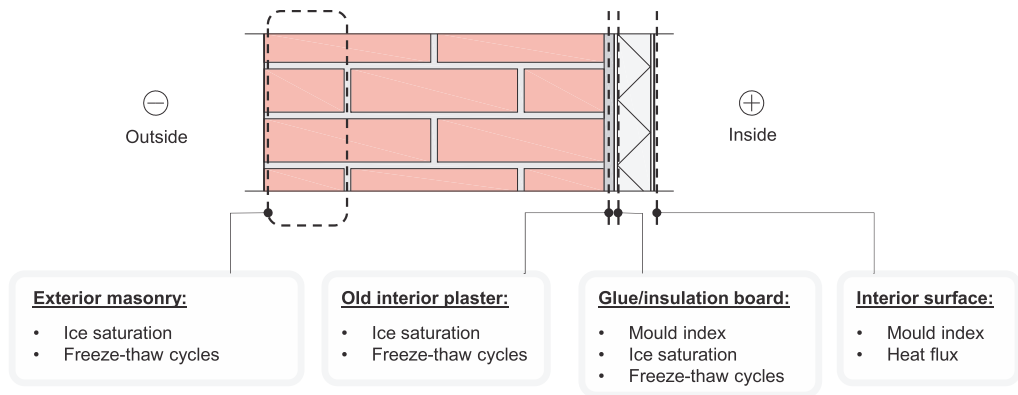
Figure 7   Sections and parameters used for performance assessment.

Freeze-thaw cycles were counted if the ice saturation (ratio between ice and pore volumes) rose above a certain level and was then reduced to zero. Unfortunately, the exact damage criteria for used materials were unknown. To overcome this, the freeze-thaw cycles are presented in 2 ways:

- Curves of freeze thaw cycles as a function of different ice saturation threshold levels are given to get an overview of the cycle counts independent of a specific criterion.
- Boxplots of freeze-thaw cycles counted based on the threshold of 1% ice saturation (default setting in Delphin 5). While the limit is very low, it allows for the assessment of changes in that end of the spectrum.

WTA Merkblatt 6-5 (Künzel et al., 2012) suggested a maximum moisture saturation degree of $30\%_{sat}$ to prevent frost damage. Study on Canadian bricks by van Straaten (2014) corroborated that most of the bricks had their critical saturation degree above $30\%_{sat}$. Experiences from a previous study (Klõšeiko et al., 2017) suggested that the AAC insulation system can also fail below that level.

Based on a study by Feng et al. (2019), the critical saturation degree is a function of temperature – the lower the frost temperature, the lower the maximum allowable saturation degree. Experiments conducted by Feng et al. (2019) and Al-Omari et al. (2015) suggest that the main damage to the material takes place during the first freeze-thaw cycles with additional cycles being less significant.

Therefore, **maximum ice saturation** is also assessed based on:

- curves of maximum ice saturation as a function of temperature;
- boxplots of maximum ice saturation.

Mould growth was analysed using the Finnish mould model (Hukka and Viitanen, 1999; Ojanen et al., 2010; Viitanen et al., 2011). The interior surface and surfaces behind the insulation layer were concentrated on (due to the possibility of air gaps). The parameters for mould index calculation are given in Table 3, the choice of which was based on the documentation of the Finnish mould model calculation file (VTT and TTY, 2018). According to that, the AAC has separate sensitivities for mould growth and M_{max}.

The recommendations by the developers of the mould model suggest that if the analysed surface is in contact with indoor air, the mould index values 1–2 correspond to the upper limits of safe functioning of the structure (Viitanen et al., 2015). Previous experience in real buildings has shown that despite the aim for gapless installation, air cavities will still be present behind the insulation boards (Klõšeiko and Kalamees, 2016; Morelli and MØller, 2019). In this study mould index 1 (corresponding to the start of mould growth) was considered as the performance criterion for interior surfaces and for walls where air cavities behind the insulation and possibility for convection exist. Higher mould indexes behind the insulation are an indication that cavities and convection must be avoided.

Table 3   Surface properties used for mould index calculation according to the Finnish mould model.

Surface	Parameter	Surface properties			
		Uninsul.	AAC	Calcium silicate	PIR (paper coated)
Interior surface	material	wallpaper	plaster + paint	plaster + paint	gypsum board + paint
	sensitivity	sensitive	medium resistant	medium resistant	sensitive
	C_{mat}	0.25	0.25	0.25	0.25
Behind insulation	material		AAC	CaSi	paper coated PUR
	sensitivity		sensitive (mould growth), med. resistant (M_{max})	medium resistant	sensitive
	C_{mat}		0.25	0.25	0.25

Changes in **heat fluxes** were assessed based on modelling results on the interior surface. As the thermal boundary conditions were the same for different insulation solutions, the heat flux also reflected the thermal transmittance.

Accepted manuscript

2.3 Data analysis and presentation of results

The analysis of modelling results was done using Python 3.7.2 and pandas 1.0.1 library (Mckinney, 2010; Reback et al., 2020). Seaborn 0.10.1 library (Waskom et al., 2020) was used for creating the figures. A variation of Tukey's boxplots (see Figure 8 for explanation) are used to help sum up the results from all the models. Annexes 1.1–1.3 given in supplementary material (Klõšeiko and Kalamees, 2021) to this article present the boxplots of the outputs grouped by variables to help identify the significant parameters.
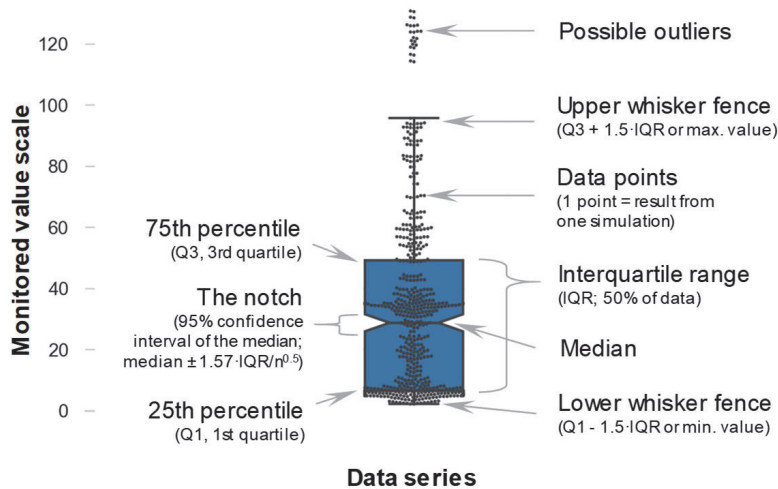
Figure 8   Explanation of elements of the boxplot figures. Adopted from Doyle (2016).

Annex 2.1 in the supplementary material (Klõšeiko and Kalamees, 2021) presents the combination-wise comparison between different insulation solutions and the respective uninsulated cases – absolute values, absolute difference and relative difference are given. Annexes 2.2 and 2.3 do the same for CCR-optimized material data vs conventional characterization and vapour open vs PIR insulation respectively.

As exemplified by Calle and Van Den Bossche (2021), decision trees can also be used to assess the parameters and the combinations of them that potentially contribute to failures or, on the contrary, help avoid them. They are class discriminators that reclusively partition the dataset until each partition consists entirely or dominantly of examples from one class (Shafer et al., 1996) – in the current case, "pass" or "fail". At each junction the pass/fail ratios are shown. The trees are given in Annexes 3.1–3.5 (Klõšeiko and Kalamees, 2021) and were generated from modelled data using the KNIME platform (Berthold et al., 2007).

3   Results and discussion

3.1   Frost and moisture in exterior layers of masonry

3.1.1   Results

The depth of the harshest location in the exterior masonry varies between models and observed quantities. For each case, the layers between 5–135 mm from exterior surface are analysed and the most critical result is presented.

The maximum **ice saturations** (Figure 9 left) of insulated cases are nearly all higher than uninsulated ones (median relative increase ranged between 7–8%, maximum up to 93% – see Annex 2.1 (Klõšeiko and Kalamees, 2021)). However, the difference between the studied insulation solutions (vapour tight and vapour open both in CCR-optimized and conventional form) is small. The median relative increase of mean ice ratios (Figure 10 left) of the insulated walls was ≈ 150%, but could also reach a 35-fold increase, hinting at a longer time the walls stay frozen compared to the uninsulated cases.

Figure 9 (right) helps to analyse the modelling results based on the concept that the combination of high ice saturation levels and low temperatures contribute to the destruction of the material (Feng et al., 2019). The figure adds the temperature dimension to the boxplot in Figure 9 (left) while the area between 25th and 75th percentiles is given between dashed lines. In general, the insulated models were colder and more saturated with ice, but the difference between insulation types, and optimized and conventional material characterization is negligible. The mean moisture contents of the whole masonry layers (Figure 10 right) increased due to the insulation 15–600%; the vapour tight PIR caused ca 1.4x higher median increase than those of vapour open insulation types (see Annex 2.1 (Klõšeiko and Kalamees, 2021)).
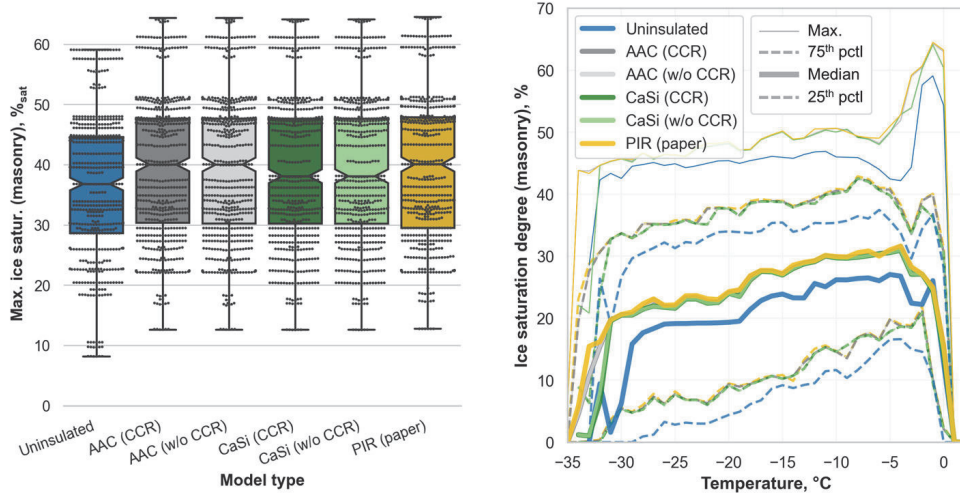
Figure 9   The most critical results from exterior layers of masonry: boxplots of maximum ice saturation (left) and maximum ice saturation at different temperatures (right).
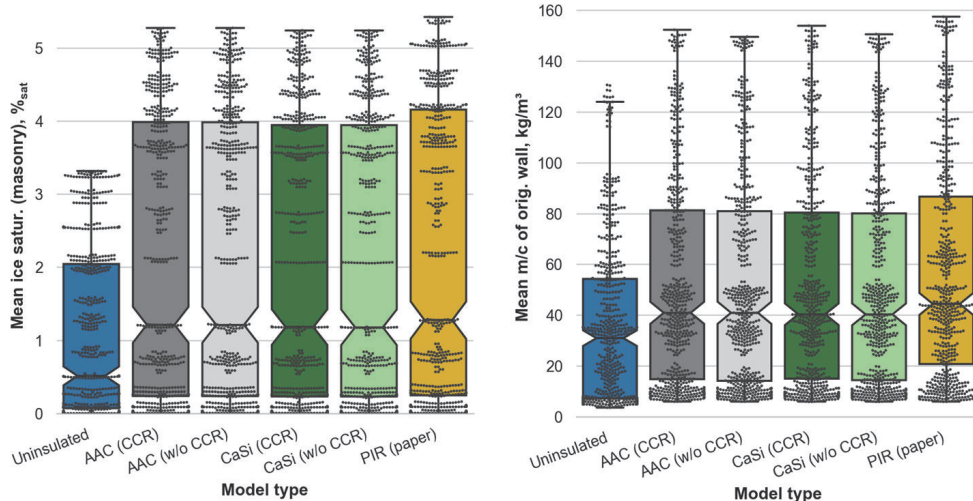
Figure 10 The highest mean ice ratios from exterior layers of masonry (left) and mean moisture content of the original wall (right).

Regardless of the insulation solution, the number of **freeze-thaw cycles** (Figure 11 left) increased significantly, with a median relative increase of ≈ 55% compared to uninsulated walls. Figure 11 (right) shows the number of freeze thaw cycles dependent on the ice saturation limit that is used to count them. The relative increase in FTC caused by interior insulation was greater at higher limiting saturation degrees, while CaSi performed slightly better than AAC and PIR in the top quartile if medium ice saturations are used as the FTC threshold.

Accepted manuscript
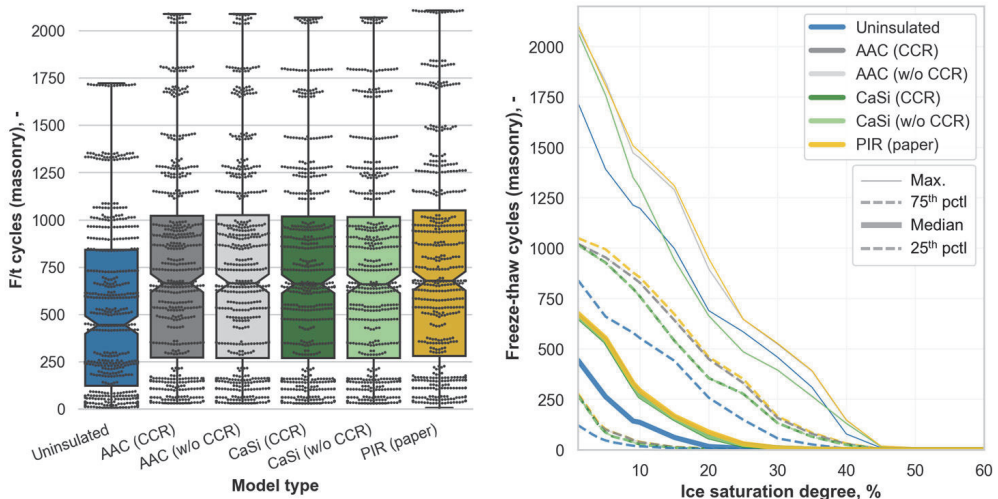
Figure 11 The most critical results from exterior layers of masonry: freeze thaw cycles (1% ice saturation used as limit, left) and freeze thaw cycles dependent on the ice saturation degree limit (right).

3.1.2   Discussion

The main factors contributing to both maximum ice saturation and freeze thaw cycles (see Annexes 1.1–1.3, 2.1 and 3.1 in Klõšeiko and Kalamees, 2021) in the exterior layer were the brick type and wind driven rain load (dependent on orientation and rain exposure coefficient). Compared to them, the effects of indoor moisture load, hydraulic contact resistances and even the type of insulation (whether it is "capillary active" or "vapour tight", and the specifics of material characterization) are minute. This means that the impact of interior insulation probably stems mainly from its additional thermal resistance.

An aspect not dealt with in detail in this study is imperfections of masonry – while the influence of contact resistances is explored, the additional water infiltration due to cracking is not. Based on experiments, Calle et al. (Calle et al., 2020; Calle and Van Den Bossche, 2021) suggested leakage rates to be applied as sources inside the wall. Gutland et al. (2021) proposed a methodology to model the cracks as separate material thus accounting for both accelerated wetting and drying through the imperfections. In Calle et al. (2020; 2021) the wall with imperfections resulted in being wetter, while in Gutland et al. (2021) drier in long-term than regular baseline model. However, the latter method would benefit from experimental validation and requires simplification to make it applicable to large modelling campaigns.

Unfortunately, the performance limits of the modelled bricks are not known. The conservative 30% ice saturation limit was exceeded in about half of the uninsulated cases and in 2/3 of the insulated cases (regardless of the insulation solution; see Annex 3.1 in

Accepted manuscript

(Klõšeiko and Kalamees, 2021)). Should the 30% limit prove to be true, the bricks of a historic building would probably be damaged even before any thermal upgrade and the insulation works would only worsen the situation.

The critical saturation degrees (tested at -15 °C) of various bricks from North America were presented in Figure 5 in a paper by van Straaten (2014). Most of the bricks tested there were able to endure higher saturation degrees than those reached in this study. However, as Figure 9 (right) shows, the temperature in this study can be far lower and thus more critical.

On one hand, increase in ice saturation due to insulation is not very dramatic and if the results about the North American bricks are representative of Estonian ones too, it could be deduced that if the façade has survived until now without frost damage, the interior insulation should not be a major problem. On the other hand, if the main cause of the damage is the high number of freeze-thaw cycles at higher ice saturation degrees, the distinction is clear – insulation causes higher cycle counts and hence accelerated degradation.

3.2   Frost between interior insulation and original wall

3.2.1   Results

Maximum ice saturation levels in plaster on the interior surface of the original wall behind the insulation are given in Figure 12. The lower 3 quartiles perform similarly in vapour open solutions. As Annex 2.3 (Klõšeiko and Kalamees, 2021) shows, the PIR insulation is mostly more critical and can cause up to 75%$_{sat}$ higher ice saturation than a similar case using the vapour open approach. The tentative 30% ice ratio threshold was exceeded in 31% of PIR cases, while when using CaSi and AAC insulation the rate was much lower at 2% and 8% respectively (also see Annex 3.2 in (Klõšeiko and Kalamees, 2021)). The CCR optimization caused more severe conditions in the majority of the cases compared to material characterization without the CCR data. Furthermore, the number of cases exceeding the tentative 30% ice ratio increased by ≈ 2 times when using optimized material properties.

The outcome was mainly determined by the wind-driven rain load (wall orientation and exposure coefficient) and the material of the original wall – see Annex 1.1–1.3 and 3.2 in (Klõšeiko and Kalamees, 2021). Of the walls with optimized material characterization exceeding the 30% ice saturation ca 1/10 were oriented to the west. Walls made of sand-lime bricks fared best: they did not exceed the limit in vapour open cases and had a 2% failure rate when PIR insulation was used. The other two brick types were more susceptible to higher ice saturations.

The trend and the contributing factors were similar when **freeze-thaw cycles** (ice saturation > 1%) were considered (Figure 13, left). In the top quartile, the number of freeze-thaw cycles was roughly 1.5–2 times higher using PIR insulation compared to vapour open insulation. Figure 13, right exposes the vastly higher number of freeze-thaw cycles in PIR's top quartile if higher ice limits are used.
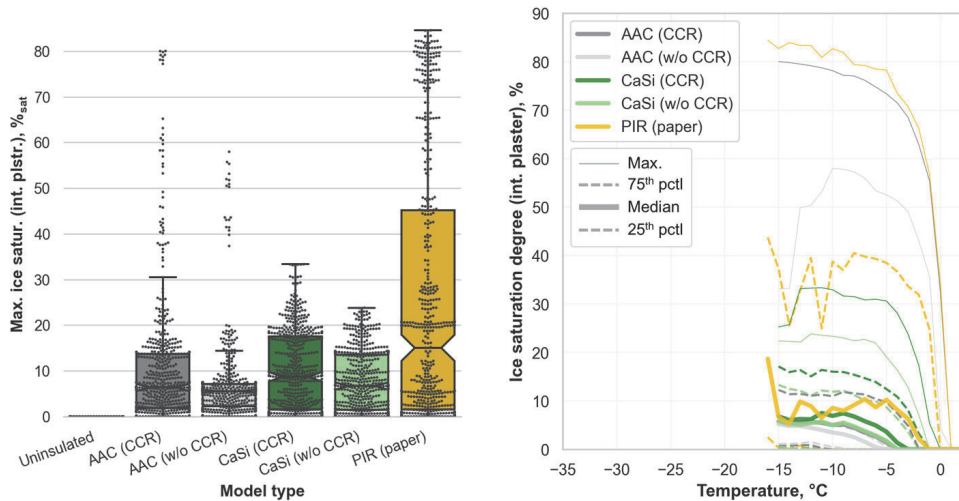

Figure 12 Boxplots of maximum ice saturation (left) and isopleths of temperature and maximum ice saturation degrees (right) in the old interior plaster layer behind the insulation.
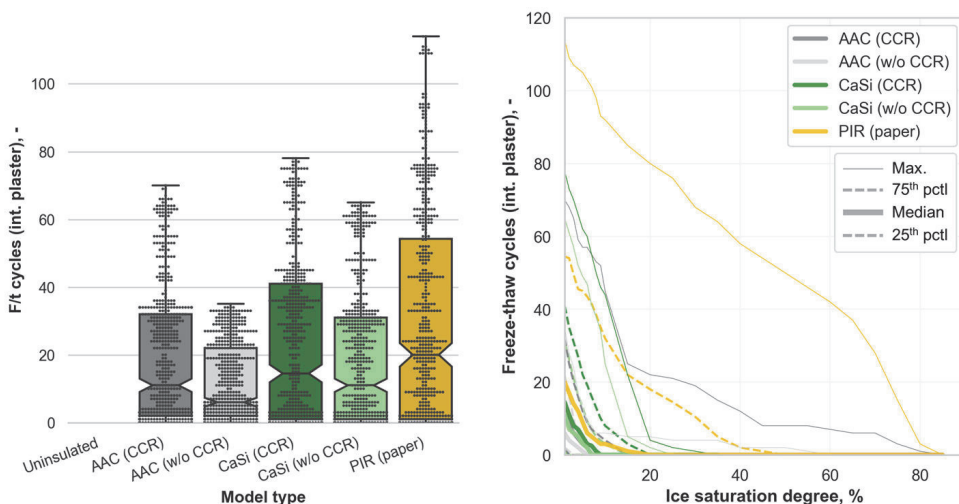

Figure 13 Freeze thaw cycles (1% ice saturation used as limit, left) and freeze thaw cycles dependent on the ice saturation degree limit (right) in the old interior plaster layer behind the insulation.

3.2.2   Discussion

Vereecken and Roels (2016) suggested that in severe climate conditions, the insulation material and glue mortar should be able to handle the freezing and thawing; according to the current study, this applies to the old interior plaster too.

High ice ratio and the number of freeze-thaw cycles imply that if PIR insulation is applied on top of existing interior plaster, gluing the insulation to the plaster may not be enough and a mechanical fastening to the masonry layer should also be used. This will possibly cause issues with high surface humidity at the fasteners and is further discussed in section 3.4.

While the number of freeze-thaw cycles using vapour open materials was lower compared to PIR, the extreme cases of AAC still caused ice saturation well above the $30\%_{sat}$ limit – some even on par with PIR (albeit subjected to fewer cycles). Should the damage occur, it would have an impact on the hydraulic contact with the original wall and possibly hamper the intended functioning of the capillary active insulation (Vereecken and Roels, 2015a).

It must be noted that only one plaster type was modelled in this study, however, it is doubtful that the interior plasters would have been designed to endure repeated high ice saturation levels that the extreme cases of the AAC and PIR insulation solutions cause. Therefore, the safe option would be the removal of the existing interior plaster.

3.3   Frost in the cold side of the insulation

3.3.1   Results

Due to a more realistic moisture distribution (higher moisture content on the cold side of insulation), the CCR-optimized materials showed an increase in both the maximum ice saturation (Figure 14) and in freeze-thaw cycles (Figure 15). While the median increase was rather low at $0.2\%_{sat}$ and 1 cycle for both AAC and CaSi, the change was greater in the top quartile as the increase could reach $5\%_{sat}$ and $7\%_{sat}$ and 45 and 28 cycles respectively in some cases (see Annex 2.2 in (Klõšeiko and Kalamees, 2021)). Similarly to the interior plaster layer, the high values were caused by a high indoor moisture load and a wind-driven rain load (orientation and rain exposure) – see Annexes 1.1 and 3.4 (Klõšeiko and Kalamees, 2021). The type of brick also had an impact here. While maximum moisture saturation degrees in the exterior layer of PIR insulation reached over $80\%_{sat}$ in extreme cases, no ice was detected there due to high moisture content coinciding with warm temperatures.

Accepted manuscript

Figure 14 Maximum ice to pore volume ratios (left) and isopleths of temperature and maximum ice saturation degrees (right) on the cold side of the interior insulation.
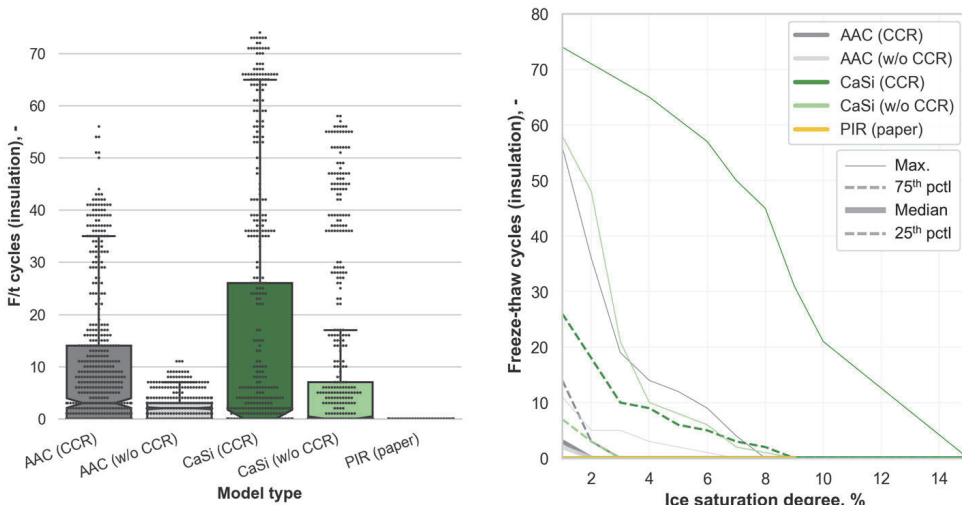
Figure 15 Cold/exterior side of the interior insulation: freeze thaw cycles (1% ice saturation used as limit; left) and freeze thaw cycles dependent on various ice saturation degree limits (right).

3.3.2 Discussion

Although the maximum ice saturation in the insulation layer was well below the tentative $30\%_{sat}$ limit, a previous study (Klõšeiko et al., 2017) suggested that the AAC insulation system can still fail below that level. Significant reduction of tensile strength of the AAC insulation system was detected at glue saturation of $15–20\%_{sat}$ and insulation saturation of $\approx 10\%_{sat}$. The rupture occurred in either the cold side of the insulation, at the glue-insulation interface or the glue-substrate interface. The loss of strength progressed over

Accepted manuscript

the duration of the experiment (concluding at 53 freeze-thaw cycles). In the current study, similar ice saturation levels were modelled in extreme cases in the glue layer using CCR-optimized AAC material, suggesting that damage could occur. In the same study (Klõšeiko et al., 2017) CaSi fared better, as damage occurred in saturated samples, while no statistically significant changes in tensile strength were detected during the test at 10-18%$_{sat}$.

Scheffler (2013) also tested AAC for frost damage and found that no loss of strength occurred in samples conditioned at 97.4%$_{RH}$ and frozen at -15°C for 20 cycles. This humidity corresponds to ≈ 4%$_{sat}$ and the minimum temperatures in the insulation in current study were ≈ -15°C too. Stemming from the moisture content where damage did *not* occur, the ice saturation limits of 4%$_{sat}$ (AAC) and 10%$_{sat}$ (CaSi) can be conservatively used to compare the results of optimized and conventionally characterized materials (see Annex 3.4 (Klõšeiko and Kalamees, 2021)). The failure rate of the optimized AAC models was about 7 times higher than the conventional ones (9.5% vs 1.5% of all models using the respective material data), while 16% of the optimized CaSi cases failed in contrast to 0% without CCR. According to these results, keeping the indoor humidity within Moisture class 1, and reducing the wind driven rain wall factor to 0.5 will mitigate frost damage risks in the insulation layer.

3.4   Mould indexes behind the insulation and on the interior surface

3.4.1   Results

The risk of mould growth is assessed using mould indexes with values above 1 being undesirable and indicating mould growth. The surface parameters used for mould index calculation and the choice of the performance criterion are discussed in sections 2.2 and 3.4.2.

Figure 16 (left) gives the **maximum mould indexes** over the whole modelling period for the surface **between the insulation and the original wall**. The median maximum mould indexes were well above the safe threshold of 1 for all insulation solutions except the CaSi without CCR optimization (also see Annex 3.3 in (Klõšeiko and Kalamees, 2021)). Median maximum mould indexes for both AAC materials were ca 2, which corresponds to "several local mould growth colonies" that are detectable using a microscope. The median levels were lower in CaSi walls, however, similarly to AAC, the top quartile was at the maximum possible value according to their sensitivity class (mould index = 3). Paper-coated PIR performed far worse as the majority of models indicated moderate to plenty of visually detectable growth, the median increase compared to vapour open insulation solutions was ca. 2 units on the mould index scale (see Annex 2.3 in (Klõšeiko and Kalamees, 2021)).

Accepted manuscript

Based on Annexes 1.2 and 3.3 (Klõšeiko and Kalamees, 2021), the mould index behind insulation is mainly determined by the indoor humidity load. About 15% of the optimized CaSi cases in the mildest indoor moisture class 1 ($\Delta v_{t_e < 5°C}$ = 2 g/m³, 53 m² / person) had a maximum mould index above the acceptable threshold of 1, while in the case of AAC, it was roughly twice of that. The failure rate of the PIR models at a low humidity load was a further ≈ 2 times higher than those of the AAC ones (ca 70% of the cases). Virtually all cases with indoor humidity loads in moisture classes 2 ($\Delta v_{t_e < 5°C}$ = 4 g/m³, 20 m² / person) and 3 ($\Delta v_{t_e < 5°C}$ = 6 g/m³, 15 m² / person) failed regardless of the insulation solution, with the exception being CaSi, where at MC2, the failure rate was 43%. Wind driven rain load was also important with northerly and easterly walls faring better than others.

The higher mould index of PIR insulation can be explained by its higher sensitivity to mould growth and by higher humidity occurring also in warm periods, which is more favourable for mould growth. The opposite is true for the AAC and CaSi – their sensitivity class is lower and their higher vapour conductivity allows for drying out during the summer, while the indoor moisture load causes wetting during cold periods.

The maximum **mould indexes on the interior surface** are given in Figure 16 (right) and the failure decision tree in Annex 3.5 in (Klõšeiko and Kalamees, 2021). Uninsulated walls are most at risk with 9% of the cases failing to stay below the critical threshold of mould index 1 and at some combinations showing serious mould growth. All the failed walls were oriented to the west with a high rain exposure coefficient, a high indoor moisture load and good hydraulic contact in masonry further contributing to the failure. The majority (≈ 95%) of the failures occurred in walls made of burnt bricks (id 33 and 97) while sand-lime brick (id 153) walls fared better – the latter had a lower water uptake coefficient A_w, which caused less wind driven rain to be absorbed into the masonry.

The PIR insulation did not cause problems with mould index on the interior surface, while in CaSi and unoptimized AAC walls some combinations existed above the mould index 1. None of the AAC walls with CCR-optimized material data failed and the failure rate was reduced 2-fold in CCR-optimized CaSi – this can be attributed to their lower liquid conductivity and reduced redistribution of moisture towards the interior surface.
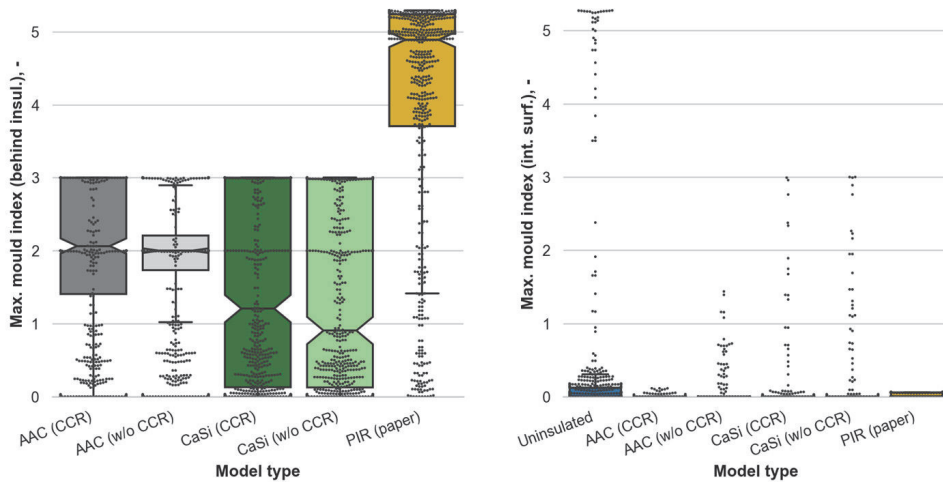
Figure 16 Maximum mould indexes behind the insulation (left) and on the interior surface (right).

3.4.2 Discussion

The modelled mould indexes behind the insulation were high for all insulation solutions. However, the VTT mould model was developed to predict mould growth on exposed surfaces, while by design, the AAC and CaSi systems should be glued in whole plane, and the PIR boards sealed around the board perimeter. According to Künzel (2011) gluing on the whole surface of the insulation should prevent mould growth and contaminants reaching the indoor air. This depends on the quality of the workmanship, as it is possible to leave air pockets behind the insulation (too dry mortar, uneven subsurface, etc), and unfortunately has occurred in practice (Klõšeiko and Kalamees, 2016; Morelli and Møller, 2019). The instructions of one AAC producer (Heße et al., 2018) state that "the high alkalinity of the product effectively inhibits mould growth.", which (at least to some degree) is taken into account in the mould index calculation by a lower sensitivity parameter. The producer also suggests filling the joints between the insulation and floors/ceilings/interior walls with hemp felt – creating an air cavity and introducing biodegradable material into the moist zone. The latter, in light of the current modelling results, is a very questionable recommendation.

In a recent field study Jensen et al. (2020) detected mould growth on the masonry-AAC insulation interface and inside the AAC material itself too. The growth inside the AAC was even higher than on the interface and the authors presume it to be due to the lower pH than on the glue mortar. In contrast, mould growth in CaSi systems stayed below the detection levels both on the interface and inside the material, although subjected to similar conditions and pH values, and the Finnish/VTT mould model predicting growth for both CaSi and AAC.

In a laboratory study Jensen et al. (2021) further tested the mould growth on the masonry-insulation interface. It was determined that when the pH of the surface is high, the existing mould growth is inactivated. However, 12 months from the start of the experiment, the spores on the interface were still viable and could become active as the pH declines over time.

A RIBuild project report (Johansson et al., 2019) compared the VTT mould modelling results to measurements and detected a high number (61%) of false-negatives in borderline cases, while in low humidity and extreme cases the model agreed with the results.

Also, questions can be raised about the PIR insulation. According to the installation instructions of one product (Kingspan Insulation OÜ, 2017), PU foam caulk is applied around the perimeter of the boards, probably leaving an air gap behind the insulation. The insulation is also penetrated by mechanical fasteners. Metal screws or wall plugs are usually used to affix the PIR + a gypsum board system to the wall causing surface temperatures much lower than the 1D models in this article predict. This was also demonstrated in-situ in a previous study (Klõšeiko et al., 2013), where condensation and rust occurred on the fasteners. This means that the mould index when using PIR insulation could actually be higher in both studied sections – behind the insulation and on the interior surface.

Overall, while the mould index calculated here does not directly describe the exact situation behind the insulation in 1D wall (as the air cavities should not be a rule, but an exception to be avoided), it can reveal what happens in borderline cases (bad workmanship, air leakages, joints tightened with biodegradable hemp wool etc). Due to the higher modelled mould indexes it also shows that risks associated with such cases in the PIR insulation are much higher than those of the AAC insulation.

3.5   Heat flux on the interior side

Figure 17 (left) gives the mean heat fluxes for main model types. All insulation solutions present a ≈ 65% median reduction of mean heat fluxes compared to the uninsulated cases. In case of the vapour open insulation, the spread of the results is larger due to the higher variability of the moisture content of the insulation (Figure 17 (right)).

Leaving aside the differences in thermal conductivities of the original wall, moisture content and heat flux in the vapour open systems are primarily dependent on the indoor moisture load and wind driven rain (see Annex 1.3 in Klõšeiko and Kalamees, 2021). As the PIR insulation itself is fairly vapour tight, the variations in its heat flux are caused by changes in the moisture content of the original wall and its thermal resistance. As long as

Accepted manuscript

the thermal resistances are similar, the authors do not see a reason to prefer one system to another based on their slightly different thermal behaviour alone.
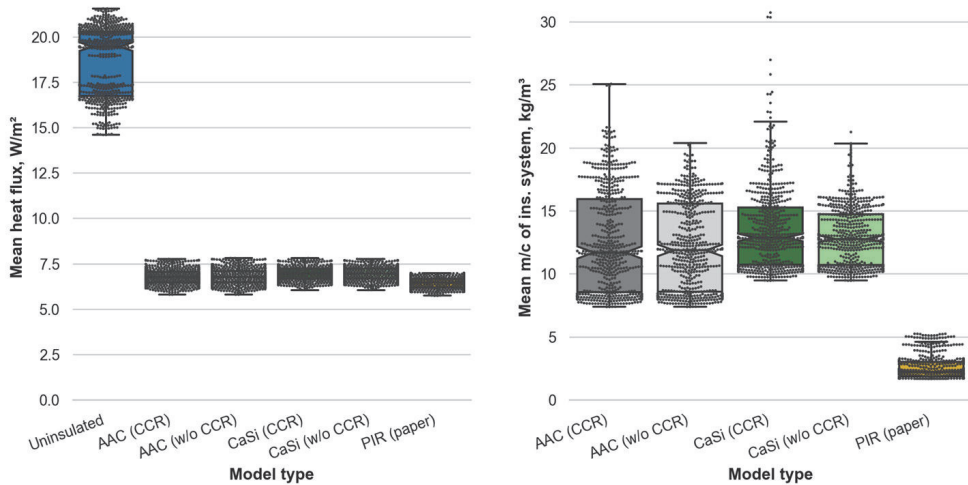
Figure 17 Mean heat fluxes on the interior surface (left) and mean moisture contents of the whole insulation system (right).

4   Conclusion

Based on the modelling done with AAC and CaSi in this study it can be stated that the material characterization process using a capillary condensation redistribution test causes more critical results. The **CCR-optimized material data** resulted in the following changes **compared to the result of the conventional material characterization**:

- Increased moisture content, maximum ice ratios and freeze-thaw cycles in the cold side of the insulation;
- higher maximum ice ratios and more freeze-thaw cycles in the interior plaster and glue mortar;
- the increases coincide with high indoor (moisture class 3) and outdoor moisture loads (West-oriented walls, higher rain exposure coefficient), which cause more critical conditions;

The CCR-optimized materials performed worse especially near their tentative performance limits, which, for example, in the cold side of the insulation layer resulted in a 7-fold increase in failure rate due to frost in the case of AAC, and caused previously unexpected failures when using CaSi. Although not studied here, the damper conditions behind the insulation would also have an impact on mould and rot risks of wooden beam ends. While the results only describe the effect of CCR-optimization on specific CaSi and AAC materials, it is probable that similar results also occur when other insulation materials

Accepted manuscript

with notable liquid conductivity are accounted for and it makes sense to incorporate the CCR test into the material characterization procedures.

When **comparing the "capillary active" vapour open insulation to "vapour tight" PIR insulation**, no significant differences were found in freeze-thaw cycles and in the maximum ice saturation of the exterior part of the masonry, however, the increase of mean moisture content of the whole wall was ca. 1.4 times higher using PIR than vapour open solutions. Nevertheless, AAC and CaSi insulations bring some benefits over PIR: maximum ice volumes and freeze-thaw cycles and mould indexes behind the insulation are significantly reduced. The results suggest that PIR insulation would require mechanical fastening to the underlying structure as the original interior plaster will be at risk of frost damage. The mould risk on top of those fasteners will probably be higher than the current 1D modelling suggests. Still, in extreme cases AAC insulation can also cause the ice saturations in the original interior plaster to reach ≈ 70% – thereby hinting at frost damage risk. This would have an impact on the hydraulic contact with the original wall and possibly hamper the intended functioning of the capillary active insulation (Vereecken and Roels, 2015a). It is therefore necessary to detect and avoid those extreme cases in the design process. Calculated mould indexes behind the insulation using the paper-backed PIR product were very high and in 89% of the cases above the safe threshold. Therefore, until further research into actual mould growth inside such structures has been conducted or gapless installation can be absolutely assured, the application of such products on mass masonry walls open to wind driven rain cannot be recommended.

In general, the vapour open materials with CCR-optimized data still have their specific advantages over the vapour tight solution, although the gap is smaller than before. Furthermore, the mass masonry wall is probably the best showcase for the vapour open approach – for example, should the original wall have air cavities, the wind driven rain loads would be reduced and the vapour tight approach might then turn out to be more favourable (presuming the issues with fasteners and unintentional defects can be mitigated).

The overall impact of interior insulation can be summarized by the following:

- a 65% median reduction of mean heat fluxes (30 mm PIR, 60 mm AAC or 90 mm CaSi on top of a 52 cm-thick mass masonry wall);
- a reduction of interior surface mould indexes: 7% of the uninsulated walls failed to stay below the threshold value, while the failure rate was 1.9% of all CaSi cases and 0 when using AAC or PIR;

- maximum mould indexes between masonry and insulation ranged from high using CaSi (median ≈ 1.2) and AAC (median ≈ 2.1) to very high using PIR (median ≈ 4.9). This hints that whole-surface gluing is required for AAC & CaSi and an airtight installation for all insulation solutions;
- the exterior layer of the original wall must tolerate higher ice saturation levels (median relative increase ≈ 8%) and freeze-thaw cycles (median relative increase ≈ 50%) regardless of the type of insulation;
- the old interior plaster will become moist and susceptible to frost damage – unless it is certain that the plaster can endure that, its removal is recommended.

Nonetheless, a criterion with high failure rate could be found for all systems. As the real distribution of currently varied parameters was not exactly known, even the outlier cases should be considered carefully. Thus, as Vereecken and Roels (2015b, 2016) have also stated, the "capillary active" interior insulation is no miracle cure and still needs case-specific approach.

Frost and mould risk inside and directly behind both insulation approaches are governed by the indoor air moisture load and can be at least to some degree mitigated by lowering it. The hygrothermal conditions in the exterior layer of the original wall can be mainly improved by reducing the wind driven rain loads. Hydrophobization can help here (Jensen, Bjarløv, et al., 2020) but accounting for it in modelling also depends on the availability of material data and literature shows that the treatment can also worsen the situation (Calle and Van Den Bossche, 2021; Janssen et al., 2020; Metavitsiadis et al., 2017). Further determination of the exact frost damage limits of CaSi and AAC systems themselves will probably show these results in better light as the current limiting criteria were selected rather conservatively.

While it can be currently stated that the exterior brick layer will be at a worse state after the insulation, the question whether the risks of accelerated frost damage would be realized needs to be answered based on further material studies, for example, by determining the critical saturation degrees and their temperature dependencies of these materials.

This study only dealt with 1D modelling: 2D and 3D modelling are also required, as corners, exterior wall - interior wall details, wooden beam ends, etc. – also in future climate – can result in more critical situations.

Declaration of conflicting interests

The Authors declare that there is no conflict of interest.

Annexes given in supplementary material

Available at: https://zenodo.org/record/5078138 (Klõšeiko and Kalamees, 2021)

Annex 1: Boxplots of the outputs grouped by variables

Annex 1.1   CCR-optimized vs conventional material characterization

Annex 1.2   Vapour open vs PIR interior insulation

Annex 1.3   Uninsulated walls vs insulation solutions

Annex 2: Boxplots of combination-wise comparison

Annex 2.1   Uninsulated wall as reference

Annex 2.2   CCR-optimized vs conventional material characterization

Annex 2.3   Vapour tight insulation as reference

Annex 3: Decision trees of failure in different layers

Annex 3.1   Outer 135mm of the brick wall: failure due to maximum ice saturation (failure: $s_{ice} \geq 30\%_{sat}$).

Annex 3.2   Old interior plaster behind the insulation: failure due to maximum ice saturation (failure: $s_{ice} \geq 30\%_{sat}$).

Annex 3.3   Between insulation and original wall: failure due to mould index (failure: $M_{ind} \geq 1$).

Annex 3.4   Exterior/cold part of the insulation: failure due to maximum ice saturation (failure: $s_{ice} \geq 4\%_{sat}$).

Annex 3.5   Interior surface: failure due to mould index (failure: $M_{ind} \geq 1$).

References

Abdul Hamid A and Wallentén P (2017) Hygrothermal assessment of internally added thermal insulation on external brick walls in Swedish multifamily buildings. *Building and Environment* 123: 351–362.

Al-Omari A, Beck K, Brunetaud X, et al. (2015) Critical degree of saturation: A control factor of freeze-thaw damage of porous limestones at Castle of Chambord, France. *Engineering Geology* 185: 71–80.

Berthold MR, Cebron N, Dill F, et al. (2007) KNIME: The Konstanz Information Miner. In: *Studies in Classification, Data Analysis, and Knowledge Organization (GfKL 2007)* (eds C Preisach, H Burkhardt, L Schmidt-Thieme, et al.), Freiburg, 2007, pp. 319–326. Springer, Berlin, Heidelberg.

Binder AB, Zirkelbach DM and Künzel HM (2010) Test Method to Quantify the Wicking Properties of Insulation Materials Designed to Prevent Interstitial Condensation. In: *Thermal Performance of the Exterior Envelopes of Whole Buildings XI*, Clearwater Beach, Florida, 2010, pp. 1–12. ASHRAE.

Binder AB, Künzel HM and Zirkelbach DM (2013) A new approach to measure liquid transport in capillary active interior insulation. In: *Proceedings of 2nd Central European Symposium on Building Physics (CESBP2013)* (eds A Mahdavi and B Martens), Vienna, 2013, pp. 393–400. ÖKK-Editions.

Binder AB, Zirkelbach DM and Künzel HM (2014) Keeping risks at bay – improving a test method to reliably quantify the capability of capillary active interior insulation. In: *Proceedings of 10th Nordic Symposium on Building Physics (NSB2014)* (eds J Arfvidsson, L-E Harderup, A Kumlin, et al.), Lund, 2014, pp. 1061–1068. Building Physics, LTH, Lund University.

Calle K and Van Den Bossche N (2021) Sensitivity analysis of the hygrothermal behaviour of homogeneous masonry constructions: Interior insulation, rainwater infiltration and hydrophobic treatment. *Journal of Building Physics* 44(6): 510–538.

Calle K, De Kock T, Cnudde V, et al. (2019) Liquid moisture transport in combined ceramic brick and natural hydraulic lime mortar samples: Does the hygric interface resistance dominate the moisture transport? *Journal of Building Physics* 43(3): 208–228.

Calle K, Coupillie C, Janssens A, et al. (2020) Implementation of rainwater infiltration measurements in hygrothermal modelling of non-insulated brick cavity walls. *Journal of Building Physics* 43(6): 477–502.

Derluyn H, Janssen H and Carmeliet J (2011) Influence of the nature of interfaces on the capillary transport in layered materials. *Construction and Building Materials* 25(9): 3685–3693.

Doyle D (2016) Notched Box Plots. Available at: https://sites.google.com/site/davidsstatistics/home/notched-box-plots (accessed 14 January 2020).

EVS, CEN and ISO (2009) EVS-EN ISO 15927-3:2009 Hygrothermal performance of buildings - Calculation and presentation of climatic data — Part 3: Calculation of a driving rain index for vertical surfaces from hourly wind and rain data.

EVS, CEN and ISO (2012) EVS-EN ISO 13788:2012 Hygrothermal performance of building components and building elements - Internal surface temperature to avoid critical surface humidity and interstitial condensation - Calculation methods.

Feng C, Roels S and Janssen H (2019) Towards a more representative assessment of frost damage to porous building materials. *Building and Environment*: 106343.

Glaser H (1959) Grafisches Verfahren zur Untersuchung von Diffusionsvorgénge. *Kältetechnik* 11(10): 345–349.

Grunewald J (1997) *Diffusiver und konvektiver Stoff- und Energietransport in kapillarporösen Baustoffen*. Technische Universität Dresden.

Gutland M, Bucking S and Santana Quintero M (2021) A methodology for hygrothermal modelling of imperfect masonry interfaces. *Journal of Building Physics* 44(6): 485–509.

Häupl P and Xu Y (2001) Numerical Simulation of Freezing and Melting in Porous Materials under the Consideration of the Coupled Heat and Moisture Transport. *Journal of Thermal Envelope and Building Science* 25(1): 4–31.

Häupl P, Grunewald J and Ruisinger U (2005) Hygrothermal analysis of external walls within the reconstruction of the Rijksmuseum Amsterdam. In: *Proceedings of Structural Studies, Repairs and Maintenance of Heritage Architecture IX* (eds CA Brebbia and A Torpiano), Southampton, 2005, pp. 345–354. WIT Press.

Heße M, Griebel H, Georgi F, et al. (2018) Multipor Insulation Guide. 1st ed. Duisburg: Xella Baustoffe GmbH.

Hirsch H, Heyn R and Klõšeiko P (2020) Capillary condensation experiment for inverse modelling of porous building materials. Kurnitski J and Kalamees T (eds) *E3S Web of Conferences* 172: 17003.

Hukka A and Viitanen H (1999) A mathematical model of mould growth on wooden material. *Wood Science and Technology* 33(6): 475–485.

Ilomets S, Kalamees T and Vinha J (2018) Indoor hygrothermal loads for the deterministic and stochastic design of the building envelope for dwellings in cold climates. *Journal of Building Physics* 41(6): 547–577.

Ismaiel M, Chen Y, Cruz-Noguez C, et al. (2021) Thermal resistance of masonry walls: a literature review on influence factors, evaluation, and improvement. *Journal of Building Physics*.

Janssen H, Scheffler GA and Plagge R (2016) Experimental study of dynamic effects in moisture transfer in building materials. *International Journal of Heat and Mass Transfer* 98: 141–149.

Janssen H, Deckers D, Vereecken E, et al. (2020) *RIBuild D2.3: Impact of water repellent agents on hygric properties of porous building materials*. Available at: https://www.ribuild.eu/s/RIBuild_D23_final.pdf.

Jensen NF, Odgaard T, Bjarløv SP, et al. (2020) Hygrothermal assessment of diffusion open insulation systems for interior retrofitting of solid masonry walls. *Building and Environment* 182(107011): 1–17.

Jensen NF, Bjarløv SP, Rode C, et al. (2020) Hygrothermal assessment of four insulation systems for interior retrofitting of solid masonry walls through calibrated numerical simulations. *Building and Environment* 180(107031): 1–15.

Jensen NF, Bjarløv SP, Rode C, et al. (2021) Laboratory-based investigation of the materials' water activity and pH relative to fungal growth in internally insulated solid masonry walls. *Indoor Air*: ina.12796.

Johansson P, Lång L, Capener C-M, et al. (2019) *RIBuild D2.2: Threshold values for failure, linked to types of building structures and failure modes*. Available at: https://www.ribuild.eu/s/RIBuild_D22_v10_1.pdf.

Kingspan Insulation OÜ (2017) Kingspan Therma TW56 Anselmi paigaldusjuhised / installation instructions. Available at: https://www.kingspan.com/ee/et-ee/tooted/soojustus/materjalid/projekteerimisjuhendid/kingspan-therma-tw56-anselmi-illustreeritud-paigal (accessed 14 January 2020).

Klõšeiko P and Freudenberg P (2019) Generative reverse-modelling approach to hygrothermal material characterization. Černý R, Kočí J, and Kočí V (eds) *MATEC Web of Conferences* 282: 02088.

Klõšeiko P and Kalamees T (2016) *Vabaduse väljak 10 seespoolse lisasoojustuse konsultatsioon, lahenduste väljatöötamine ja niiskustehnilise toimivuse uuring. Lõpparuanne / Consultation, design and performance an interior insulation solution of Vabaduse väljak 10 office building*. Tallinn. Available at: https://uuringud.tallinn.ee/uuring/vaata/2016/Vabaduse-valjak-10-seespoolse-lisasoojustuse-lahenduse-valjatootamine-ja-niiskustehnilise-toimivuse-uuring.

Klõšeiko P and Kalamees T (2021) Supplementary material to article 'Hygrothermal performance of a brick wall with interior insulation in cold climate: vapour open vs vapour tight approach'. Zenodo. DOI: 10.5281/zenodo.5078138.

Klõšeiko P, Arumägi E and Kalamees T (2013) Hygrothermal performance of internally insulated brick wall in cold climate: field measurement and model calibration. In: *Proceedings of 2nd Central European Symposium on Building Physics (CESBP2013)* (eds A Mahdavi and B Martens), Vienna, 2013, pp. 185–192. ÖKK-Editions.

Klõšeiko P, Arumägi E and Kalamees T (2015) Hygrothermal performance of internally insulated brick wall in cold climate: A case study in a historical school building. *Journal of Building Physics* 38(5): 444–464.

Klõšeiko P, Varda K and Kalamees T (2017) Effect of freezing and thawing on the performance of "capillary active" insulation systems: a comparison of results from climate chamber study to HAM modelling. *Energy Procedia* 132: 525–530.

Knarud JIB, Geving S and Kvande T (2014) Hygrothermal simulations of internally insulated massive masonry walls exposed to driving rain in cold climate. In: *Proceedings of the 10th Nordic Symposium on Building Physics (NSB 2014)* (eds J Arfvidsson, L-E Harderup, A Kumlin, et al.), Lund, 2014, pp. 1141–1148.

Krus M (1996) *Moisture Transport and Storage Coefficients of Porous Mineral Building Materials. Theoretical Principles and New Test Methods*. Stuttgart: Fraunhofer IRB Verlag.

Künzel H, Worch A, Bäumler S, et al. (2012) Innendämmung nach WTA II: Nachweis von Innendämmsystemen mittels numerischer Berechnungsverfahren (Merkblatt 6-5).

Künzel HM (2011) Bauphysik der Innendämmung und Bewertungsverfahren. In: *1. Internationaler Innendämmkongress 2011*, Dresden, 2011, pp. 9–16. TU Dresden.

Mckinney W (2010) Data Structures for Statistical Computing in Python. In: *Proceedings of the 9th Python in Science Conference (SciPy 2010)* (eds S van der Walt and J Millman), Austin, Texas, 2010, pp. 51–56.

Metavitsiadis V, Soulios V, Janssen H, et al. (2017) Wall hydrophobization and internal insulation: the impact of impregnation strength and depth on moisture levels and moisture damages. In: *Proceedings of Hydrophobe VIII* (eds J-G Dai, H Yokota, TJ Zhao, et al.), Hong Kong, 2017, pp. 69–76. The Hong Kong Polytechnic University.

Morelli M and Møller EB (2019) Energy savings and risk of mold growth in apartments renovated with internal insulation. *Science and Technology for the Built Environment* 25(9): 1199–1211.

Accepted manuscript

Nicolai A and Sontag L (2013) Implementation of an efficient numerical solution method to simulate freezing processes in porous media. In: *Proceedings of 2nd Central European Symposium on Building Physics (CESBP2013)* (eds A Mahdavi and B Martens), Vienna, 2013. ÖKK-Editions.

Nicolai A, Scheffler GA, Grunewald J, et al. (2009) An efficient numerical solution method and implementation for coupled heat, moisture and salt transport: The Delphin Simulation Program. In: Franke L, Deckelmann G, and Espinosa-Marzal R (eds) *Simulation of Time Dependent Degradation of Porous Materials*. Göttingen: Cuvillier Verlag, pp. 85–100.

Ojanen T, Viitanen H, Peuhkuri R, et al. (2010) Mold Growth Modeling of Building Structures Using Sensitivity Classes of Materials. In: *Proceedings of Thermal Performance of the Exterior Envelopes of Buildings XI*, Clearwater Beach, Florida, 2010. ASHRAE.

Reback J, McKinney W, jbrockmendel, et al. (2020) pandas-dev/pandas: Pandas 1.0.1.

Scheffler GA (2013) Frostempfindlichkeit kapillaraktiver Innendämmung. In: *2. Internationaler Innendämmkongress. Tagungsunterlage* (eds J Grunewald and R Plagge), Dresden, 2013. TU Dresden.

Scheffler GA and Plagge R (2010) A whole range hygric material model: Modelling liquid and vapour transport properties in porous media. *International Journal of Heat and Mass Transfer* 53(1–3): 286–296.

Shafer J, Mehta M, Agrawal R, et al. (1996) SPRINT: A Scalable Parallel Classifier for Data Mining. In: *VLDB '96: Proceedings of the 22th International Conference on Very Large Databases* (eds TM Vijayaraman, AP Buchmann, C Mohan, et al.), Mumbai, India, 1996, pp. 544–555. Morgan Kaufmann Publishers Inc.

van Straaten R (2014) Improving Access to the Frost Dilatometry Methodology for Assessing Brick Masonry Freeze Thaw Degradation Risk. In: *Proceedings of the 14th Canadian Conference on Building Science and Technology*, Toronto, 2014, pp. 79–88.

Vereecken E and Roels S (2013) Hygric performance of a massive masonry wall: How do the mortar joints influence the moisture flux? *Construction and Building Materials* 41: 697–707.

Vereecken E and Roels S (2015a) A numerical study of the influence of the hydraulic interface contact on the hygric performance of a multi-layered system. In: *XIII Conference on Durability of Building Materials and Components - XIII DBMC* (eds M Quattrone and VM John), 2015, pp. 512–519. RILEM Publications SARL.

Vereecken E and Roels S (2015b) Capillary active interior insulation: do the advantages really offset potential disadvantages? *Materials and Structures* 48(9): 3009–3021.

Vereecken E and Roels S (2016) Capillary Active Interior Insulation Systems for Wall Retrofitting: A More Nuanced Story. *International Journal of Architectural Heritage* 10(5): 558–569.

Vereecken E, Van Gelder L, Janssen H, et al. (2015) Interior insulation for wall retrofitting – A probabilistic analysis of energy savings and hygrothermal risks. *Energy and Buildings* 89: 231–244.

Accepted manuscript

Viitanen H, Ojanen T and Peuhkuri R (2011) Mould growth modelling to evaluate durability of materials. In: *Proceedings of the XII DBMC: 12th International Conference on Durability of Building Materials and Components* (eds VP de Freitas, MH Corvacho, and M Lacasse), Porto, 2011. FEUP Edições.

Viitanen H, Krus M, Ojanen T, et al. (2015) Mold Risk Classification Based on Comparative Evaluation of Two Established Growth Models. *Energy Procedia* 78: 1425–1430.

Vogelsang S, Fechner H and Nicolai A (2013) *Delphin 6 Material File Specification, Version 6.0.* Dresden. Available at: https://nbn-resolving.org/urn:nbn:de:bsz:14-qucosa-126274.

VTT and TTY (2018) Suomalainen homemalli / Finnish mould model calculation file (version 11.05.2018). Available at: https://research.tuni.fi/uploads/2019/01/suomalainen_homemalli_11052018.xlsx (accessed 14 January 2020).

Waskom M, Botvinnik O, Ostblom J, et al. (2020) seaborn: statistical data visualization v0.10.1. DOI: 10.5281/zenodo.3767070.

Zhou X, Desmarais G, Vontobel P, et al. (2020) Masonry brick–cement mortar interface resistance to water transport determined with neutron radiography and numerical modeling. *Journal of Building Physics* 44(3): 251–271.

Curriculum vitae

Personal data

Name:	Paul Klõšeiko
Date of birth:	14.01.1987
Place of birth:	Tallinn, Estonia
Citizenship:	Estonian

Contact data

E-mail:	paul.kloseiko@taltech.ee

Education

2014–2022	Tallinn University of Technology, PhD
2006–2014	Tallinn University of Technology, MSc
1994–2006	Tallinn Järveotsa Gymnasium, Basic and secondary education

Language competence

Estonian	native language
English	fluent
Russian	basic
German	basic
Finnish	basic

Professional employment

2012–…	Tallinn University of Technology, researcher
2012–2013	Civen OÜ, structural engineer/draftsman

Elulookirjeldus

Isikuandmed

Nimi: Paul Klõšeiko
Sünniaeg: 14.01.1987
Sünnikoht: Tallinn, Eesti
Kodakondsus: Eesti

Kontaktandmed

E-post: paul.kloseiko@taltech.ee

Hariduskäik

2014–2021 Tallinna Tehnikaülikool, PhD
2006–2014 Tallinna Tehnikaülikool, MSc
1994–2006 Tallinna Järveotsa Gümnaasium, üldharidus

Keelteoskus

eesti keel emakeel
inglise keel kõrgtase
saksa keel algtase
vene keel algtase
soome keel algtase

Teenistuskäik

2012– Tallinna Tehnikaülikool
2012–2013 Civen OÜ, konstruktor/tehnik

Publications / Teaduspublikatsioonid

Articles in peer-reviewed journals indexed in reputable databases (1.1)
Artiklid teadusajakirjades, mis on tunnustatud andmebaasides indekseeritud (1.1)

Klõšeiko, P.; Kalamees, T. (2021). Hygrothermal performance of a brick wall with interior insulation in cold climate: vapour open vs vapour tight approach. Journal of Building Physics. DOI: 10.1177/17442591211056067.

Kalamees, T.; Põldaru, M.; Ilomets, S.; **Klõšeiko, P.**; Kallavus, U.; Rosenberg, M.; Õiger, K. (2020). Failure analysis of a spray polyurethane foam roofing system. Journal of Building Engineering, 32, #101752. DOI: 10.1016/j.jobe.2020.101752.

Klõšeiko, P.; Arumägi, E.; Kalamees, T. (2015). Hygrothermal performance of internally insulated brick wall in cold climate: A case study in a historical school building. Journal of Building Physics, 38 (5), 444–464. DOI: 10.1177/1744259114532609.

Papers in peer-reviewed conference proceedings indexed in reputable databases (3.1):
Artiklid konverentsikogumikes, mis on tunnustatud andmebaasides indekseeritud (3.1):

Kiil, M.; Käärid, M.-S.; **Klõšeiko, P.**; Võsa, K.-V.; Simson, R.; Sarevet, H.; Thalfeldt, M.; Kurnitski, J. (2020). PCSP's Diagonal Tie Connectors Thermal Bridges Impact on Energy Performance and Operational Cost: Case Study of a High-Rise Residential Building in Estonia. In: E3S Web of Conferences: 12th Nordic Symposium on Building Physics (NSB 2020) (#08006). EDP Sciences. DOI: 10.1051/e3sconf/202017208006.

Klõšeiko, P.; Piir, R.; Jeltsov, M.; Kalamees, T. (2020). Thermal bridge effect of vertical diagonal tie connectors in precast concrete sandwich panels: an experimental and computational study. E3S Web of Conferences: 12th Nordic Symposium on Building Physics (NSB 2020), 172: 12th Nordic Symposium on Building Physics (NSB 2020). Ed. Kurnitski, J.; Kalamees, T. EDP Sciences. DOI: 10.1051/e3sconf/202017208001.

Hirsch, H.; Heyn, R.; **Klõšeiko, P.** (2020). Capillary condensation experiment for inverse modelling of porous building materials. E3S Web of Conferences, 172: 12th Nordic Symposium on Building Physics (NSB 2020). Ed. Kurnitski, J.; Kalamees, T. EDP Sciences. DOI: 10.1051/e3sconf/202017217003.

Kalamees, T.; Ilomets, S.; Põldaru, M.; **Klõšeiko, P.**; Kallavus, U.; Rosenberg, M.; Õiger, K. (2020). Analysis of causes of the end of service life of a spray polyurethane foam and polyurea roof. E3S Web of Conferences: 12th Nordic Symposium on Building Physics (NSB 2020), 172: 12th Nordic Symposium on Building Physics (NSB 2020). Ed. Kurnitski, J.; Kalamees, T. EDP Sciences. DOI: 10.1051/e3sconf/202017215002.

Klõšeiko, P.; Freudenberg, P. (2019). Generative reverse-modelling approach to hygrothermal material characterization. MATEC Web of Conferences, 282: 4th Central European Symposium on Building Physics (CESBP 2019), Prague, Czech Republic, September 2-5, 2019. Ed. Černý, R.; Kočí, V.; Kočí, J. EDP Sciences. DOI: 10.1051/matecconf/201928202088.

Klõšeiko, P.; Varda, K.; Kalamees, T. (2017). Effect of freezing and thawing on the performance of "capillary active" insulation systems: a comparison of results from climate chamber study to HAM modelling. Energy Procedia, 132: 11th Nordic Symposium on Building Physics, NSB2017, 11-14 June 2017, Trondheim, Norway. Ed. Geving, S.; Time, B. Elsevier, 525−530. DOI: 10.1016/j.egypro.2017.09.714.

Klõšeiko, P.; Kalamees, T. (2016). Case Study: In-situ Testing and Model Calibration of Interior Insulation Solution for an Office Building in Cold Climate. CESB 2016 - Central Europe Towards Sustainable Building 2016; Prague; Czech Republic; 22 June 2016 through 24 June 2016. Prague: Czech Technical University in Prague, 159−166.

Klõšeiko, P.; Kalamees, T. (2016). Overview of Damage to Medieval Rural Churches in Estonia. In: João M.P.Q. Delgado (Ed.). Case Studies of Building Pathology in Cultural Heritage (47−68). Springer. (Building Pathology and Rehabilitation; 7). DOI: 10.1007/978-981-10-0639-5_3.

Ilomets, S.; Kalamees, T.; Lahdensivu, J.; **Klõšeiko, P.** (2016). Impact of ETICS on corrosion propagation of concrete facade. Energy Procedia, 96: SBE16 Tallinn and Helsinki Conference; Build Green and Renovate Deep, 5-7 October 2016, Tallinn and Helsinki. Ed. J. Kurnitski. Scopus: Elsevier, 67−76. DOI: 10.1016/j.egypro.2016.09.101.

Klõšeiko, P.; Kalamees, T.; Arumägi, E.; Kallavus, U. (2015). Hygrothermal Performance of a Massive Stone Wall with Interior Insulation: an In-Situ Study for Developing a Retrofit Measure. Energy Procedia, 78: 6th International Building Physics Conference (IBPC 2015), 14-17.06.2015. Elsevier, 195−200. DOI: 10.1016/j.egypro.2015.11.139.

Klõšeiko, P.; Arumägi, E.; Kalamees, T. (2013). Hygrothermal performance of internally insulated brick wall in cold climate: field measurement and model calibration. Proceedings of the 2nd Central European Symposium on Building Physics 9-11 September 2013, Vienna, Austria: 2nd Central European Symposium on Building Physics, Vienna, Austria, September 9-11, 2013. Ed. Mahdavi, A.; Martens, B. Vienna, Austria: Vienna University of Technology, 185−192.

Peer-reviewed conference proceedings not indexed in listed databases (3.2 & 3.4):
Artiklid indekseerimata konverentsikogumikes (3.2 & 3.4):

Klõšeiko, P.; Kalamees, T. (2018). Long term measurements and HAM modelling of an interior insulation solution for an office building in cold climate. 7th International Building Physics Conference (IBPC2018); Syracuse, NY, USA; September 23-23 2018. Syracuse CoE, 1423−1428. DOI: 10.14305/ibpc.2018.ps23.

Klõšeiko, P.; Kalamees, T. (2015). Overview of damage to facades and interior surfaces of medieval rural churches in Estonia. ISBP 2015 Conference Proceedings: 1st International Symposium on Building Pathology (ISBP-2015), 24th to 27th March 2015 in Porto, Portugal. Ed. N. Peixoto de Freitas, E. de Angelis, H. Corvacho, J. Delgado, A. Sofia Guimarães. Porto, Portugal: FEUP Edições

Kalamees, T; Arumägi, E; Thalfeldt, M; Ilomets, S; **Klõšeiko, P.**; Alev, Ü. (2012). The analysis of indoor hygrothermal loads based on measurements in multi-storey wooden apartment buildings. Proceedings of 5th IBPC: International Building Physics Conference, The Role of Building Physics in Resolving Carbon Reduction Challenge and Promoting Human Health in Buildings. Kyoto, Japan, May 28-31, 225–232.

Klõšeiko, P.; Agasild, T.; Kalamees, T. (2011). Deterioration of building envelope of wooden apartment buildings built before 1940 based on external survey. 9th Nordic Symposium on Building Physics - NSB 2011: Tampere, Finland 29 May – 2 June, 917–924.

Chapters in books, project reports:
Raamatupeatükid, projektiaruanded:

Kalamees, T.; **Klõšeiko, P.**; Väli, A.; Kurik, L.; Kallavus, U.; Tooming, L.; Raado, L-M.; Hain, T.; Napp, M.; Larsen, P.K.; Wessberg, M.; Broström, T. (2013). Sustainable management of rural churches. The final report of of the project, WP 3. Tallinn-Visby, Estonia-Sweden: Tallinn University of Technology.

Kalamees, T.; **Klõšeiko, P.**; Väli, A.; Napp, M.; Kurik, L.; Kallavus, U.; Tooming, K.; Raado, L-M.; Hain, T.; Larsen, P-K.; Wessberg, M.; Broström, T. (2013). The final research report of the project "Sustainable Management of Historic Rural Churches in the Baltic Sea Region (SMC). Tallinn: Tallinn University of Technology.

Kalamees, T; Ilomets, S; Liias, R; Raado, L-M; Kuusk, K; Maivel, M; Ründva, M; **Klõšeiko, P**.; Liho, E; Paap, L; Mikola, A; Seinre, E; Lill, I; Soekov, E; Paadam, K; Ojamäe, L; Kallavus, U; Mikli, L; Kõiv, T-A. (2012). Eesti eluasemefondi ehitustehniline seisukord – ajavahemikul 1990–2010 kasutusele võetud korterelamud. Tallinn Technical University Press.

Kalamees, T.; Ilomets, S.; Liias, R.; Raado, L.-M.; Kuusk, K.; Maivel, M.; Ründva, M.; **Klõšeiko, P.**; Liho, E.; Paap, L.; Mikola, A.; Seinre, E.; Lill, I.; Soekov, E.; Paadam, K.; Ojamäe, L.; Kallavus, U.; Mikli, L.; Kõiv, T.-A. (2012). Eesti eluasemefondi ehitustehniline seisukord - ajavahemikul 1990-2010 kasutusele võetud korterelamud: uuringu lõpparuanne. Tallinn: Tallinn Technical University Press.

Kalamees, T.; Arumägi, E.; Just, A.; Kallavus, U.; Mikli, L.; Thalfeldt, M.; **Klõšeiko, P.**; Agasild, T.; Liho, E.; Haug, P.; Tuurmann, K.; Liias, R.; Õiger, K.; Langeproon, P.; Orro, O.; Välja, L.; Suits, M.; Kodi, G.; Ilomets, S.; Alev, Ü.; Kurik, L. (2011). Eesti eluasemefondi puitkorterelamute ehitustehniline seisukord ning prognoositav eluiga: uuringu lõpparuanne. Tallinn: Tallinn Technical University Press.

Kalamees, T; Kõiv, T-A; Liias, R; Õiger, K; Kallavus, U; Mikli, L; Ilomets, S; Kuusk, K; Maivel, M; Mikola, A; **Klõšeiko, P**.; Agasild, T; Arumägi, E; Liho, E; Ojang, T; Tuisk, T; Raado, L-M; Jõesaar, T. (2010). Eesti eluasemefondi telliskorterelamute ehitustehniline seisukord ning prognoositav eluiga. Uuringu lõpparuanne. Tallinna Tehnikaülikool.